

TECHNICAL REPORT STANDARD PAGE

1. Report No. FHWA/LA.14/531		2. Government Accession No.	3. Recipient's Catalog No.
4. Title and Subtitle The Rideability Of A Deflected Bridge Approach Slab (LTRC Project 02-2GT Continuation: Phase II)		5. Report Date October 2014	
		6. Performing Organization Code	
7. Author(s) Mark Martinez, P.E.		8. Performing Organization Report No. LTRC Project No: 11-3P SIO No: 30000160	
9. Performing Organization Name and Address Louisiana Transportation Research Center 4101 Gourrier Avenue Baton Rouge, LA 70808		10. Work Unit No.	
		11. Contract or Grant No.	
12. Sponsoring Agency Name and Address		13. Type of Report and Period Covered Final Report (2011-2014)	
		14. Sponsoring Agency Code	
15. Supplementary Notes Conducted in Cooperation with the U.S. Department of Transportation, Federal Highway Administration			
16. Abstract <p>This report presents the findings associated with an effort to develop a complementary pavement roughness indexing system that utilizes the 25 ft. Moving Baseline Length Roughness Index (IRI_{25-ft}) alongside the posted speed localized roughness index (LRI_{PS}) to find, index, and detect the types of bumps that appear on Louisiana highways. Currently established pavement roughness indices, such as ride number (RN), profile index (PI), and international roughness index (IRI), cannot effectively locate the position of bumps on the pavement due to inherent limitations. The complimentary index being proposed is intended to overcome these limitations.</p> <p>The IRI_{25-ft} represents a methodology that the pavement indexing community has begun to utilize to evaluate bumps. For the purposes of this research, it is to be employed to index bump magnitude. The LRI_{PS} was developed in a previous study carried out at the Louisiana Transportation Research Center (LTRC). For the purposes of this research, it is to be employed to locate the position of bumps on roadways and to identify bump type like faults and angle changes.</p>			
17. Key Words Bridge Bump, Joint Fault, Ride Quality, LRI, LRI _{PS} , RN, IRI, Roughness, Inertia, Index, Localized Roughness, 25-ft Moving Baseline Length Roughness Index, ProVAL		18. Distribution Statement Unrestricted. This document is available through the National Technical Information Service, Springfield, VA 21161.	
19. Security Classif. (of this report) N/A	20. Security Classif. (of this page) N/A	21. No. of Pages 145	22. Price N/A

Project Review Committee

Each research project has an advisory committee appointed by the LTRC Director. The Project Review Committee (PRC) is responsible for assisting the LTRC Administrator or Manager in the development of acceptable research problem statements, requests for proposals, review of research proposals, oversight of approved research projects, and implementation of findings.

LTRC appreciates the dedication of the following Project Review Committee members in guiding this research study to fruition.

LTRC Administrator

Zhongjie “Doc” Zhang, Ph.D., P.E.

Members

Mark Chenevert

Jeff Lambert

Masood Rasoulia

Melinda Braud

Kelly Kemp

Christophe Fillastre

Chris Abadie

Hector Santiago (FHWA)

Michael B. Boudreaux

Jason Chapman

Directorate Implementation Sponsor

Richard Savoie

Chief Engineer, DOTD

The Rideability of a Deflected Bridge Approach Slab

by

Mark Martinez, P.E.

Louisiana Transportation Research Center
4101 Gourrier Avenue
Baton Rouge, LA 70808

LTRC Project No. 11-3P
State Project No. 30000160

conducted for

Louisiana Department of Transportation and Development
Louisiana Transportation Research Center

The contents of this report reflect the views of the author/principal investigator who is responsible for the facts and the accuracy of the data presented herein. The contents do not necessarily reflect the views or policies of the Louisiana Department of Transportation and Development, the Louisiana Transportation Research Center, or the Federal Highway Administration. This report does not constitute a standard, specification, or regulation.

October 2014

ABSTRACT

This report presents the findings associated with an effort to develop a complementary pavement roughness indexing system that utilizes the 25 ft. Moving Baselength Roughness Index ($IRI_{25\text{-ft}}$) alongside the posted speed localized roughness index (LRI_{PS}) to find, index, and detect the types of bumps that appear on Louisiana highways. Currently established pavement roughness indices, such as ride number (RN), profile index (PI), and international roughness index (IRI), cannot effectively locate the position of bumps on the pavement due to inherent limitations. The complimentary index being proposed is intended to overcome these limitations.

The $IRI_{25\text{-ft}}$ represents a methodology that the pavement indexing community has begun to utilize to evaluate bumps. For the purposes of this research, it is to be employed to index bump magnitude. The LRI_{PS} was developed in a previous study carried out at the Louisiana Transportation Research Center (LTRC). For the purposes of this research, it is to be employed to locate the position of bumps on roadways and to identify bump type like faults and angle changes.

ACKNOWLEDGMENTS

This research was underwritten by the Louisiana Department of Transportation and Development (DOTD) and carried out by its research division at the Louisiana Transportation Research Center (LTRC). The author would like to thank his colleagues at LTRC's Pavement Research Group, which include Zhongjie Zhang, Ph.D., who supervised project development and contributed to the Final Report layout; Leticia Courville, Ph.D., who helped flowchart and investigate both the standard IRI and IRI_{25-ft} algorithms; and Mitchell Terrell, Shawn Elisar, Glen Gore, and Terrell Gorham who carried out field testing and preliminary data development.

IMPLEMENTATION STATEMENT

The LRI_{PS} indexing system should be used as a supplement to traditional roughness indexing systems (IRI_{25-ft}, IRI, and RN). IRI and RN should continue to be used to rate steady-state roughness (roads) as the LRI_{PS} is intended only for use in rating localized roughness (bridge approach slabs, joint faults, potholes, etc.). IRI_{25-ft} should continue to be used to quantify the magnitude of localized roughness. However, it should not be used to identify longitudinal position of localized roughness phenomena because of inherent problems. Rather the LRI_{PS} should be used to accomplish location finding.

Although IRI_{25-ft} is able to index localized roughness, it has been observed that grinding according to its suggestions has not been consistently effective in reducing roughness. The LRI_{PS} appears to overcome the problem in that it appears to better isolate problem locations. Developing a proper indexing methodology is necessary because there is currently no method available that can consistently and accurately rate localized roughness. As such, there is no way to assess the condition of the Department's bridge approach inventory as it relates to such distresses. It has been observed that Louisiana's highway structures have often achieved high states of localized distress before they have come to the attention of pavement management. The combined IRI_{25-ft}/LRI_{PS} indexing system, it is expected, will provide a window onto the mechanism of such failure and, thereby, help to formulate design and rehabilitation strategies that can minimize the effect.

TABLE OF CONTENTS

ABSTRACT	iii
ACKNOWLEDGMENTS	v
IMPLEMENTATION STATEMENT	vii
TABLE OF CONTENTS	ix
LIST OF TABLES	xi
LIST OF FIGURES	xiii
INTRODUCTION	1
OBJECTIVE	3
SCOPE	5
METHODOLOGY	7
Calculation of IRI _{25-ft} and LRI _{PS} from Accelerometer and Laser Data.....	8
Comparison of IRI _{25-ft} and LRI _{PS} Results	9
Using the LRI _{PS} to Detect Distress Type on Vehicles Other than the HSLP	10
DISCUSSION OF RESULTS	13
Collection of Accelerometer and Laser Data in the Field.....	13
Calculation of IRI _{25-ft} and LRI _{PS} from Accelerometer and Laser Data.....	18
Backcalculation of Road Profile from Laser and Accelerometer Signal.....	18
Calculation of IRI _{25-ft} Using ProVAL 2.7.....	19
Calculation of LRI _{PS} from Accelerometer Data	19
Comparison of IRI _{25-ft} and LRI _{PS} Results	20
AREA 1: Distress Magnitude Assessment	20
AREA 2: Distress Location Assessment.....	27
AREA 3: Distress Type Assessment.....	36
Results from Golden Car Model.	36
Results from Field Data.....	41
Using the LRI _{PS} to Detect Distress Type on Vehicles Other Than the HSLP	44
CONCLUSIONS.....	49
RECOMMENDATIONS.....	51
ACRONYMS, ABBREVIATIONS, AND SYMBOLS	53
REFERENCES	55
APPENDIX A: RSP Data File and RSP Data File Convention	57
APPENDIX B: IRI _{25-ft} and LRI _{PS} Curve Summaries.....	67

LIST OF TABLES

Table 1	Suspension systems evaluated	11
Table 2	Bridges tested along Louisiana’s I-10 corridor using LTRC’s HSLP	14
Table 3	IRI _{25-ft} vs. LRI _{PS} delay summary.....	34
Table 4	IRI _{25-ft} step-fault curve summary	39
Table 5	IRI _{25-ft} ramp-fault curve summary.....	39

LIST OF FIGURES

Figure 1 ProVAL (Version 2.7) settings used to develop IRI _{25-ft} curves	9
Figure 2 Bridges IRI _{25-ft} and LRI _{PS} tested using LTRC's HSLP	13
Figure 3 Typical HSLP accelerometer and laser outputs: (I-10 BB 450-08 EB Bridge 3) ...	17
Figure 4 HSLP generated road profile (I-10 BB 450-08 EB Bridge 3)	18
Figure 5 IRI _{25-ft} plot (I-10 BB 450-08 EB Bridge 3)	19
Figure 6 LRI _{PS} plot (I-10 BB 450-08 EB Bridge 3)	20
Figure 7 I-10 BB 450-11 EB BRIDGE 1 plots: IRI _{25-ft} (top) and LRI _{PS} (bottom)	22
Figure 8 I-10 BB 450-08 WB BRIDGE 3 plots: IRI _{25-ft} (top) and LRI _{PS} (bottom)	24
Figure 9 I-10 BB 450-11 WB BRIDGE 9 plots: IRI _{25-ft} (top) and LRI _{PS} (bottom)	26
Figure 10 LRI _{PS} leading edge and peak (I-10 BB 450-08 EB Bridge 3)	28
Figure 11 IRI _{25-ft} leading edge and peak (I-10 BB 450-08 EB Bridge 3)	29
Figure 12 I-10 BB 450-11 EB BRIDGE 1 plots: IRI _{25-ft} (top) and LRI _{PS} (bottom)	31
Figure 13 I-10 BB 450-11 EB BRIDGE 10 plots: IRI _{25-ft} (top) and LRI _{PS} (bottom)	33
Figure 14 IRI _{25-ft} response to a ± 1 in. fault	37
Figure 15 IRI _{25-ft} response to a $\pm 1^\circ$ slope	37
Figure 16 LRI _{PS} response to a ± 1 in. fault	38
Figure 17 LRI _{PS} response to a $\pm 1^\circ$ slope	38
Figure 18 IRI _{25-ft} for profile with series of 1 in. step faults (Golden Car Model)	40
Figure 19 IRI _{25-ft} for profile with series of 1° ramps (Golden Car Model)	40
Figure 20 LRI _{PS} for 2 in. faults separated by 7 ft.	41
Figure 21 I-10 BB 450-11 EB BRIDGE 1 plots: IRI _{25-ft} (top) and LRI _{PS} (bottom)	43
Figure 22 LRI _{PS} for step profile (Golden Car Model)	45
Figure 23 LRI _{PS} for ramp profile (Golden Car Model)	45
Figure 24 LRI _{PS} curves for 2 in. step profile (Models A thru F)	47
Figure 25 LRI _{PS} curves for 3° slope change profile (Models A thru F)	47

INTRODUCTION

Localized bumps have been known to appear at bridge transitions in Louisiana because of differential settlement taking place where approach embankments meet bridge abutments. DOTD recognizes that such distresses must be systematically identified and indexed in order to assess the extent of the problem across the state. Doing so would mean that DOTD could develop remediation strategy that the Department could use to mitigate the problem.

About 10-15 years ago, DOTD made attempts to use standard IRI to index bridge bumps. However, it was discovered that IRI has problems indexing localized roughness due to inherent problems with the standard index both in terms of theory and application in that it requires 328 ft. of road profile data to make a fully accurate assessment. Typically, highly localized forms of roughness were not picked up by the standard IRI algorithm because they can be overshadowed by the non-localized distresses that exist in the 328 ft. adjacent to them. The more localized the roughness, the less the standard IRI algorithm is able to isolate it.

A research effort was undertaken by DOTD, completed in 2009, that attempted to investigate if there might be a means to overcome the aforementioned problem [1]. As a result of this effort, DOTD was able to develop the Posted-Speed Localized Roughness Index (LRI_{PS}) which attempted to overcome the problems by returning to a response-type road roughness measuring systems (RTRRMS) approach. It was discovered that the LRI_{PS} was able to isolate the positions of localized roughness phenomena very well. However, it being an RTRRMS, it did suffer from “transportability” and “suspension degradation” problems which prevented it from being a tool adequate for measuring distress magnitude.

Details elaborating on LRI_{PS} development along with a treatment of the “transportability” and “suspension degradation” issue is provided in the LTRC Research Project 02-2GT [1]. Transportability and suspension degradation prevents the LRI_{PS} from being able to give a repeatable index value from one vehicle to the next. Despite this being a problem, preliminary indications showed that the LRI_{PS} did accurately locate the position of a bump, fault or pothole independent of the vehicle being used.

The profiling community also recognized that the standard IRI has problems coping with localized roughness [2]. Through their efforts, the so-called 25-ft. moving base-length method of evaluating localized roughness (IRI_{25-ft}) was developed. This methodology attempts to index localized roughness by taking a 25-ft. moving average of a road profile’s continuous standard IRI signal. The approach has been found to be effective on many forms of localized roughness and, as such, the road-profiling community has generally accepted it as the favored

means to index localized roughness. Louisiana's attempts to use the system have met with some difficulty, however. The IRI_{25-ft} methodology indexes bumps adequately. However, DOTD has had difficulty using it to locate the position of bumps on the pavement.

Each index has a different strength. The LRI_{PS} can be used to determine the precise locations of a localized roughness phenomenon on the road and to assess distress type while the IRI_{25-ft} can be used to assess magnitude. Both indexes are derived from the same ride so they are compatible; the LRI_{PS} output is derived from the High Speed Laser Profiler's (HSLP) accelerometer signal and the IRI_{25-ft} output is derived from the HSLP's accelerometer and laser signal. Because this is so, there is the potential that they can be used together in a complementary fashion. This study sets out the details as to how this could be done.

OBJECTIVE

This research was initiated in order to determine the means by which the IRI_{25-ft} and LRI_{PS} localized roughness testing methodologies might be employed in combination so as to take advantage of their respective strengths and to overcome their respective weaknesses in localized roughness testing. That is to say, the objective of this research was to attempt using the LRI_{PS} methodology to fix the longitudinal locations at which localized roughness phenomena appear on Louisiana highways and to utilize the IRI_{25-ft} methodology to arrive at an index magnitude once a localized phenomenon has been found. It was also an objective to use the LRI_{PS} to determine distress types (bridge bump, fault, pot-hole, etc.).

SCOPE

For this research, 40 bridges along I-10 located across six parishes including five control sections were analyzed using DOTD's HSLP. Data collected was analyzed using both the IRI_{25-ft} and LRI_{PS} methodologies. A series of synthesized profiles were then developed in order to parametrically investigate IRI_{25-ft} and LRI_{PS} reaction to special profile cases not available in the field so as to better refine and understand the combined index. These synthesized profiles included a series of simple ramps (positive and negative 1-, 2-, 3-, 4-, and 5-degree slopes) and a series of simple faults (positive and negative 0.5-, 1-, 2-, 3-, and 6-in. steps). All real and synthesized profiles were processed using ProVAL 2.7 so as to evaluate IRI_{25-ft}. The Golden Car model along with a tunable model that could be used to investigate suspension characteristics other than the Golden Car was developed in order to evaluate alternate suspension system impact on LRI_{PS}.

METHODOLOGY

When a vehicle transverses a pavement, there are two qualities that can be observed. The first is the road profile that the vehicle is driving over and the second is the vehicle's response to that profile. The IRI_{25-ft} is designed to record the profile while the LRI_{PS} is designed to record the vehicular response. In both cases, the methodologies are tuned to look specifically at localized roughness. An HSLP equipped with the proper lasers and accelerometers is able to record the raw data that can be used to calculate both the IRI_{25-ft} and LRI_{PS} during a single ride. In order to explore the strengths and weaknesses of the LRI_{PS} and the IRI_{25-ft} , and to determine how they can be used in a complementary fashion to meet DOTD needs, four steps were followed:

- 1) Collection of accelerometer and laser data in the field.
- 2) Calculation of IRI_{25-ft} and LRI_{PS} from accelerometer and laser data.
- 3) Comparison of IRI_{25-ft} and LRI_{PS} results.
- 4) Using the LRI_{PS} to detect distress type on vehicles other than the HSLP.

The data collection phase of research involved carrying out HSLP data collection on forty bridges along Louisiana's I-10 corridor, spanning six parishes and including five control sections. The bridges utilized were selected because they were on a major corridor that is heavily trafficked, suggesting that they would be reasonably distressed, and because the concentration of bridges along this corridor was large enough to get a reasonable sampling.

It was necessary to ensure that bumps seen in the collected data corresponded to actual locations on the ground. To accomplish this, the HSLP was first synchronized to the Control Section Log Mile (CSLM) of the pavement/bridges being tested. In this way, the CSLM of bridge transitions, as recorded in the DOTD structural inventory, would match up with the CSLM being reported by the HSLM during testing. To add a measure of redundancy, the HSLM operator also used a feature made available on the HSLM that allowed him to manually insert an event marker in the HSLM's data stream that showed up in the HSLP's output file at bridge transitions.

The specific HSLP used in this study was a Dynatest 5051 Mach III with two Selcom wing lasers, two Selcom wheelpath lasers, one texture laser, and a single long reach laser for bump detection. The long reach laser was a Selcom SLS 5000. To deal with localized roughness, a specially modified laser had to be retrofitted to the HSLP (the long reach laser). This was because the standard devices delivered by the OEM were seen to clip when encountering more extreme bumps [1].

Calculation of $IRI_{25\text{-ft}}$ and LRI_{PS} from Accelerometer and Laser Data

Producing $IRI_{25\text{-ft}}$ and LRI_{PS} plots is a three step process:

Step 1: Backcalculation of road profile from laser and accelerometer signal:

On-board equipment housed in the HSLP first takes the laser and accelerometer signals and uses it to backcalculate the road profile.

Step 2: Calculation of $IRI_{25\text{-ft}}$ using ProVAL 2.7:

ProVAL 2.7 is used to produce $IRI_{25\text{-ft}}$ curves from the backcalculated road profile. Figure 1 shows the ProVAL settings that are required to generate the $IRI_{25\text{-ft}}$ curves. The “Continuous Short Interval (ft)” entry in Figure 1 is set to 25 ft. in ProVAL 2.7 to ensure that the type of IRI that will be calculated will be the $IRI_{25\text{-ft}}$.

Step 3: Calculation of LRI_{PS} from accelerometer data

LRI_{PS} plots are created using only the accelerometer signal. HSLP accelerometer readings are collected at the highest sample rate available (10 readings per foot) so signal resolution can be maximized. To eliminate random noise in the signal, all raw accelerometer data are first filtered using a 6-in. median filter. Once filtered, the LRI_{PS} for any given point along the pavement is tabulated as the squared variance of accelerometer readings collected within the 1.52 m. (5 ft.) of pavement immediately following the point. This 1.52-m. (5-ft.) window is selected because it best delineates bridge bumps. The result is then divided by 10,000. This division by 10,000 is required because it was observed that extremely distressed bumps often produced LRI_{PS} scores in the millions. Dividing by 10,000 ensures that scores are manageable. The LRI_{PS} curve is the resulting output. LTRC Research Project 02-2GT gives a more comprehensive account of LRI_{PS} development [1].

The screenshot displays the 'Smoothness Assurance' window in ProVAL software. It features a blue header and several tabs: 'Inputs', 'Analysis', 'Grinding', 'Grinding Results', and 'Warnings'. The 'Inputs' tab is selected. The interface is organized into several sections:

- Input Set:** A dropdown menu set to 'User-Defined'.
- Smoothness Specifications:** Includes a dropdown for 'Ride Quality Index' set to 'IRI', a text input for 'Ride Quality Threshold (in/mi)' at 350, and a text input for 'Continuous Short Interval (ft)' at 25. There are two radio button options: 'Fixed Interval Report' (unselected) and 'Continuous Long Interval Report' (selected). Under 'Fixed Interval Report', there is a text input for 'Fixed Interval (ft)' at 528. Under 'Continuous Long Interval Report', there is a text input for 'Ride Quality Threshold (in/mi)' at 50 and a text input for 'Continuous Long Interval (ft)' at 340.
- Profile Selection:** Includes a dropdown for 'File' set to 'I-10 BB 450-07 EB BRIDGE' and a dropdown for 'Channel' set to 'Right Wheel Path'. There are two checkboxes: 'Use Point Reset' (unchecked) and 'Apply 250mm Filter' (checked).
- Histogram:** Includes text inputs for 'Lower Bound (in/mi)' at 80, 'Upper Bound (in/mi)' at 150, and 'Class Interval (in/mi)' at 10.
- Comparison:** Includes a dropdown for 'Analysis Type' set to 'Raw Profile', a dropdown for 'Pre-Processor Filter' set to 'None', and three text inputs for 'Short Cutoff Wavelength', 'Long Cutoff Wavelength', and 'Straightedge Wheelbase (ft)' at 10. There is a button labeled 'Wheel Offsets...'.
- Analyze:** A large button at the bottom right of the window.

Figure 1
ProVAL (Version 2.7) settings used to develop IRI_{25-ft} curves

Comparison of IRI_{25-ft} and LRI_{PS} Results

IRI_{25-ft} and LRI_{PS} plots for the forty bridges were then compared side by side in order to assess the strengths and weaknesses of the IRI_{25-ft} and LRI_{PS} methodologies. Special note was taken of instances where the IRI_{25-ft} and LRI_{PS} methodologies complemented each other (i.e., cases where LRI_{PS} plots could be used to reveal distress magnitude, location, or type wherein the IRI_{25-ft} plots could not and vice versa). Three areas of assessment were examined:

1. Distress Magnitude: Ability of index to produce consistent, repeatable results that clearly index the magnitude of the localized distress
 - a. IRI_{25-ft} and LRI_{PS} both register bumps similarly
 - b. LRI_{PS} registers significant bumps where the IRI_{25-ft} does not
 - c. IRI_{25-ft} registers significant bumps where the LRI_{PS} does not
2. Distress Location: Ability of the index to produce consistent, repeatable results that clearly and accurately determine the location of the distress on the road

- a. Distress location could be clearly discerned in both the IRI_{25-ft} and LRI_{PS} plot
 - b. Distress location could be clearly discerned in the LRI_{PS} alone
 - c. Distress location could be clearly discerned in the IRI_{25-ft} alone
3. Distress Type: Ability of the index to produce consistent, repeatable results that identifies distress type such as fault, rut, bump, etc...
- a. Distress Type could be discerned in both the IRI_{25-ft} and LRI_{PS} plot
 - b. Distress Type could be discerned in the LRI_{PS} alone
 - c. Distress Type of distress could be discerned in the IRI_{25-ft} alone

Because of the complexity of the field data collected on the faulted bridges, the Golden Car model was first used on simple fabricated profiles in order to “fingerprint” how IRI_{25-ft} and LRI_{PS} respond to a single fault and a single slope. The Golden Car is detailed in Gillespie and Sayers (1980) [3]. Only faults and slopes needed to be examined because other types of localized roughness like potholes, joint faults, cracks, etc. can be composed of faults and slopes. Positive and negative faults with 0.5-, 1-, 2-, 3-, and 6-in. steps and positive and negative ramps with 1-, 2-, 3-, 4-, and 5-degree slope changes were used in this regard. Field data was then compared accordingly.

Using the LRI_{PS} to Detect Distress Type on Vehicles Other Than the HSLP

All LRI_{PS} calculations up to this stage of the research were based on the unique suspension characteristics associated with the HSLP. For the LRI_{PS} to be useful in determining bump type, it needed to be proved that the LRI_{PS} shapes would be maintained on vehicles other than HSLP. To investigate this, a mathematical model was developed that could be used to test vehicles with different suspension characteristics.

The model consisted of two mass-spring-dashpot modules arranged in the same geometry as the Golden Car. The model had six variables:

- M1 - Quarter car mass (kg)
- M2 - Axle and tire mass (kg)
- k1 - Shock absorber spring constant (N/m)
- k2 - Inflated tire spring constant (N/m)
- b1 - Shock absorber damping factor [(N*s)/m]
- b2 - Inflated tire damping factor [(N*s)/m]

Seven different suspension systems were tested using the model by tuning the variables to the values shown in Table 1. The Golden Car was used as the reference. Models A through F

were based on taking one of the Golden Car’s variables and dividing it by two. The exception was the b2 parameter that was increased to 350 (N*s)/m given that the Golden Car was initially set to zero.

Table 1
Suspension systems evaluated

Model No.	M1 (kg)	M2 (kg)	k1 (N/m)	k2 (N/m)	b1 ((N*s)/m)	b2 ((N*s)/m)
Golden Car	250	37.5	15825	163250	1500	0
Model A	125	37.5	15825	163250	1500	0
Model B	250	18.75	15825	163250	1500	0
Model C	250	37.5	7912.5	163250	1500	0
Model D	250	37.5	15825	81625	1500	0
Model E	250	37.5	15825	163250	750	0
Model F	250	37.5	15825	163250	1500	350

Fault and slope change profiles were used to excite the model for the same reasons discussed in the methodology. The same 20 fabricated profiles defined in that section were used here as well.

DISCUSSION OF RESULTS

Collection of Accelerometer and Laser Data in the Field

A map showing the locations of the forty bridges tested is provided in Figure 2. Table 2 provides a summary of the bridge details for all bridges tested. Most, but not all, bridges consisted of a paired eastbound and a westbound structure. ‘I-10 BB 450-07 EB BRIDGE 4’ and ‘I-10 BB 450-07 WB BRIDGE 1’ serve as an example.

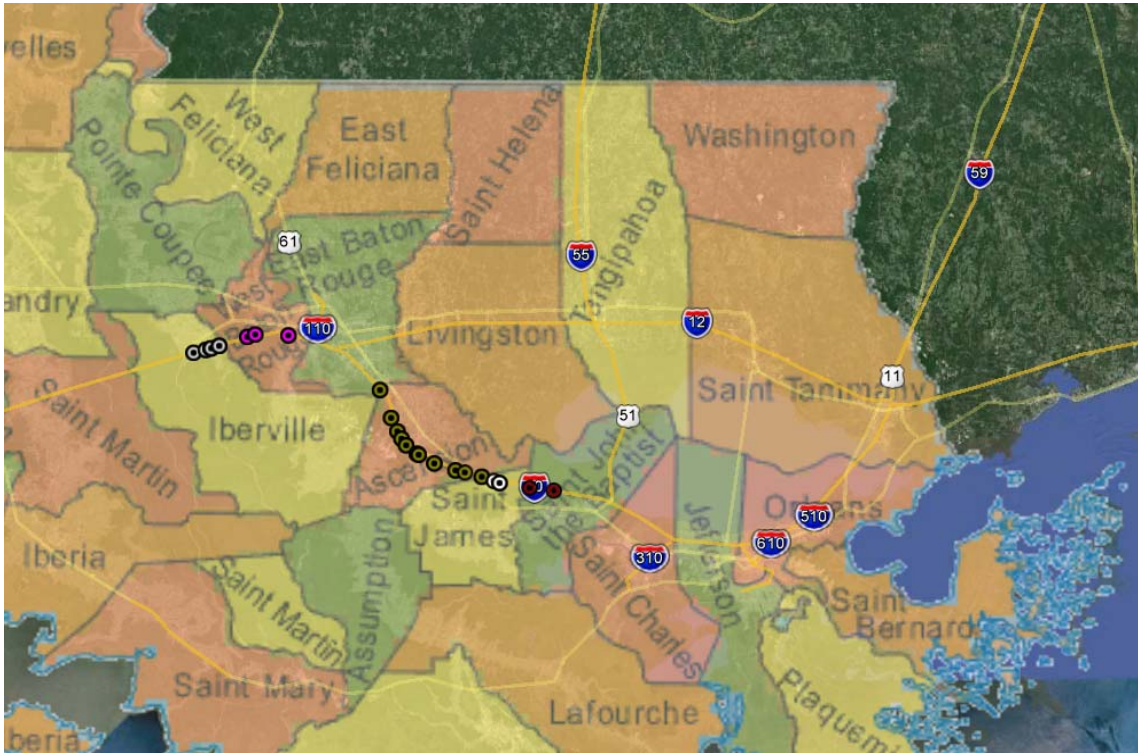


Figure 2

Bridges IRI_{25-ft} and LRI_{PS} tested using LTRC's HSLP

Table 2
Bridges tested along Louisiana's I-10 corridor using LTRC's HSLP

Ctrl. Sect.	Log Mile	Bridge ID	Latitude	Longitude	Structure Number	Mile post	Crossing	Length (ft.)	Year Built
450-07	10.25	I-10 BB 450-07 EB BRIDGE 1	30.4077	-91.4810	4500710251	136.93	Trinity Drainage Canal	140	1971
	12.13	I-10 BB 450-07 EB BRIDGE 2	30.4142	-91.4504	4500712131	138.81	M.P. R.R.	2026	1972
	12.99	I-10 BB 450-07 EB BRIDGE 3	30.4178	-91.4366	4500712993	139.67	Bayou Grosse Tete	200	1972
	14.23	I-10 BB 450-07 EB BRIDGE 4	30.4232	-91.4168	4500714231	140.91	Bridge 250 Ebl	147	1974
	14.23	I-10 BB 450-07 WB BRIDGE 1	30.4232	-91.4168	4500714232	140.91	Br 250 Westbound	147	1974
	12.99	I-10 BB 450-07 WB BRIDGE 2	30.4178	-91.4366	4500712994	139.67	Bayou Grosse Tete	200	1972
	12.13	I-10 BB 450-07 WB BRIDGE 3	30.4142	-91.4504	4500712132	138.81	M.P. R.R.	2026	1972
	10.25	I-10 BB 450-07 WB BRIDGE 4	30.4077	-91.4810	4500710252	136.93	Trinity Drainage Canal	140	1971
450-08	3.83	I-10 BB 450-08 EB BRIDGE 1	30.4432	-91.3469	4500803831	145.29	Bayou Choctaw	240	1974
	5.06	I-10 BB 450-08 EB BRIDGE 2	30.4484	-91.3272	4500805061	146.52	Bridge 290 Ebl	159	1973
	10.11	I-10 BB 450-08 EB BRIDGE 3	30.4471	-91.2440	4500810111	151.57	I-10 Over LA 415-Westover	966	1969
	10.11	I-10 BB 450-08 WB BRIDGE 1	30.4471	-91.2440	4500810112	151.57	I-10 Over LA 415-Westover	963	1969
	5.08	I-10 BB 450-08 WB BRIDGE 2	30.4485	-91.3269	4500805082	146.54	Bridge 290 Wbl	159	1973
	3.83	I-10 BB 450-08 WB BRIDGE 3	30.4432	-91.3469	4500803832	145.29	Bayou Choctaw	240	1974
450-11	0	I-10 BB 450-11 EB BRIDGE 1	30.3300	-91.0140	4501100001	168.52	Bayou Manchac	200	1970
	4.6	I-10 BB 450-11 EB BRIDGE 2	30.2698	-90.9858	4501104601	173.12	I-10 Over LA 73	289	1975
	6.81	I-10 BB 450-11 EB BRIDGE 3	30.2408	-90.9700	4501106811	175.33	I-10 Over La429/New River	297	1975
	8.08	I-10 BB 450-11 EB BRIDGE 4	30.2248	-90.9595	4501108081	176.6	Smith Bayou	120	1975
	9.27	I-10 BB 450-11 EB BRIDGE 5	30.2108	-90.9479	4501109271	177.79	I-10 Over LA 30	307	1975

Table 2 (continued)
Bridges tested along Louisiana's I-10 corridor using LTRC's HSLP

Ctrl. Sect.	Log Mile	Bridge ID	Latitude	Longitude	Structure No.	Mile post	Crossing	Length (ft.)	Year Built
450-11 (cont.)	11.32	I-10 BB 450-11 EB BRIDGE 6	30.1926	-90.9214	4501111321	179.84	I-10 Over LA 44	286	1979
	11.65	I-10 BB 450-11 EB BRIDGE 7	30.1903	-90.9166	4501111651	180.17	Bayou Conway	120	1979
	14.3	I-10 BB 450-11 EB BRIDGE 8	30.1719	-90.8777	4501114301	182.82	I-10 Over LA 22	260	1979
	17.62	I-10 BB 450-11 EB BRIDGE 9	30.1572	-90.8249	4501117621	186.14	Bayou Conway	120	1969
	21.72	I-10 BB 450-11 EB BRIDGE 10	30.1436	-90.7596	4501121721	190.24	Panama Canal	175	1975
	21.72	I-10 BB 450-11 WB BRIDGE 1	30.1436	-90.7596	4501121722	190.24	Panama Canal	175	1975
	19.06	I-10 BB 450-11 WB BRIDGE 2	30.1527	-90.8015	4501119066	187.58	I-10 Under Ramp	1920	1975
	17.62	I-10 BB 450-11 WB BRIDGE 3	30.1572	-90.8249	4501117622	186.14	Bayou Conway	140	1969
	14.3	I-10 BB 450-11 WB BRIDGE 4	30.1719	-90.8777	4501114302	182.82	I-10 Over LA 22	260	1979
	11.65	I-10 BB 450-11 WB BRIDGE 5	30.1903	-90.9166	4501111652	180.17	Bayou Conway	120	1979
	11.32	I-10 BB 450-11 WB BRIDGE 6	30.1926	-90.9214	4501111322	179.84	I-10 Over LA 44	286	1979
	9.27	I-10 BB 450-11 WB BRIDGE 7	30.2108	-90.9479	4501109272	177.79	I-10 Over LA 30	307	1975
	8.08	I-10 BB 450-11 WB BRIDGE 8	30.2248	-90.9595	4501108082	176.6	Smith Bayou	120	1975
	6.81	I-10 BB 450-11 WB BRIDGE 9	30.2408	-90.9700	4501106812	175.33	I-10 Over La429/New River	292	1975
	4.6	I-10 BB 450-11 WB BRIDGE 10	30.2698	-90.9858	4501104602	173.12	LA 73 Under I-10	289	1975
0	I-10 BB 450-11 WB BRIDGE 11	30.3300	-91.0140	4501100002	168.52	Bayou Manchac	200	1970	
450-12	1.9	I-10 BB 450-12 EB BRIDGE 1	30.1345	-90.7296	8470206501	192.26	I-10 Under LA 641	290	1981
	2.79	I-10 BB 450-12 EB BRIDGE 2	30.1303	-90.7156	4501202791	193.15	Blind River	1805	1975
	2.79	I-10 BB 450-12 WB BRIDGE 1	30.1303	-90.7156	4501202792	193.15	Blind River	1805	1975
450-13	0.54	I-10 BB 450-13 EB BRIDGE 1	30.1196	-90.6409	4501300541	197.74	Hope Canal	155	1975
	4.15	I-10 BB 450-13 EB BRIDGE 2	30.1142	-90.5809	4501304151	201.35	Mississippi Bayou	125	1975

Figure 3 illustrates typical laser and accelerometer outputs as collected by the HSLP. In the laser plot on the top of Figure 3, a spike can be clearly seen at about milepost 10.01. This spike shows that the distance from the bumper to the road has increased rapidly and significantly. It also indicates that the bumper to road distance is restored in an equally rapid fashion. The spike being positive shows that the localized roughness is likely a sharp negative fault followed by a sharp positive fault.

The accelerometer signal on the bottom of Figure 3 shows the vehicular response to this fault. In this plot, the suspension can be seen to be going into rapid oscillation starting at a position slightly further down the road from where the fault occurred. The accelerometer signal initially goes negative during this oscillation as a reaction to the negative fault. The signal then becomes highly excited at about milepost 10.015 because of the positive fault.

The laser and accelerometer signals shown in Figure 3 are typical of what was seen on all the bridges tested. Raw laser and accelerometer data for all the bridges tested were outputted by the HSLP in ASCII file format with an RSP file extension. An example of an .RSP data file along with a record of the .RSP data file convention is contained in Appendix A

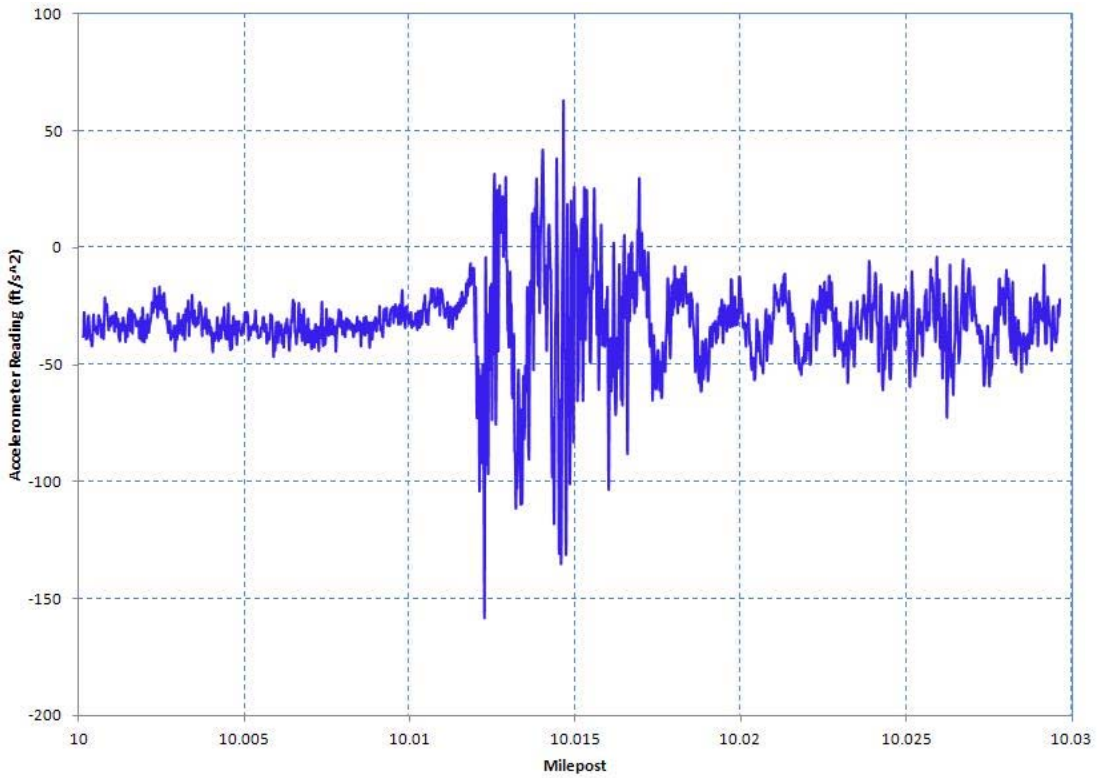
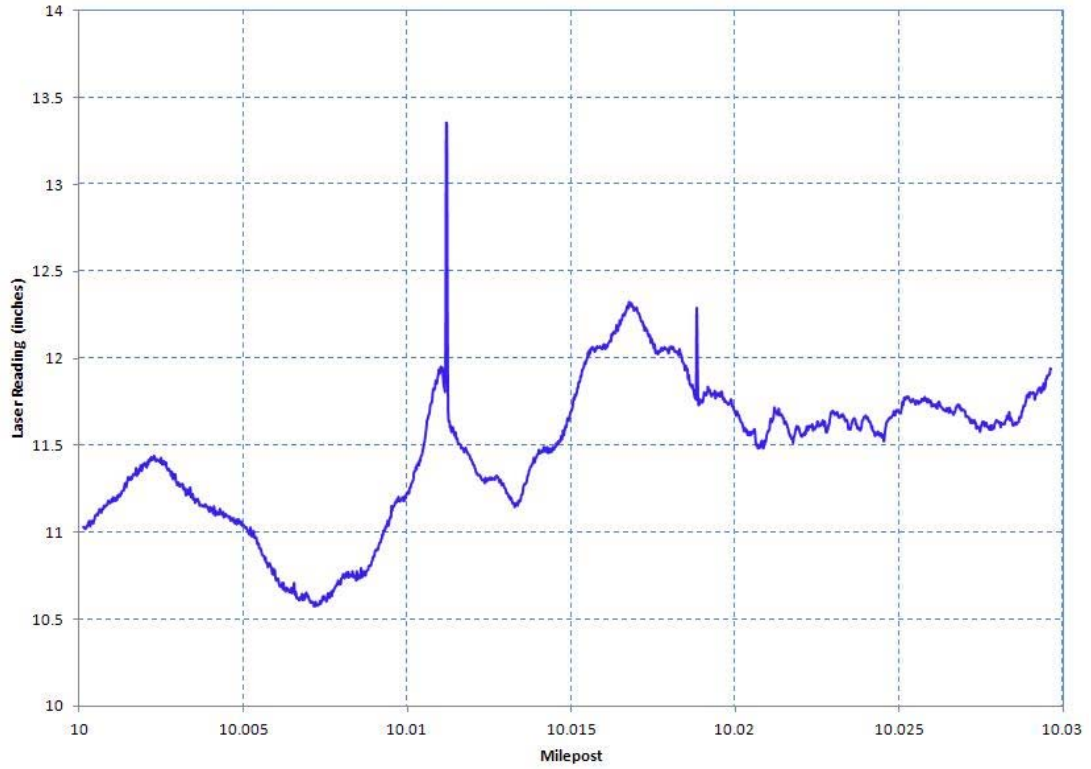


Figure 3
Typical HSLP accelerometer and laser outputs: (I-10 BB 450-08 EB Bridge 3)

Calculation of IRI_{25-ft} and LRI_{PS} from Accelerometer and Laser Data

Backcalculation of Road Profile from Laser and Accelerometer Signal

The road profile shown in Figure 4 is an example of a backcalculated road profile. It was backcalculated from the laser and accelerometer signals shown in Figure 3. The suspected negative and positive faults discussed in the previous section do appear in the Figure 4 profile at about milepost 10.0112. The inset closeup shows them in greater detail wherein the negative fault is shown having a magnitude of about 1.5 in. and the positive fault is shown with a magnitude of about 2.5 in.

All bridges listed in Figure 2 and Table 2 had profiles recorded in this manner by the HSLP. That is to say, the HSLP's onboard equipment backcalculated profiles for each bridge (like the one in Figure 4) using the laser and accelerometer data it collected.

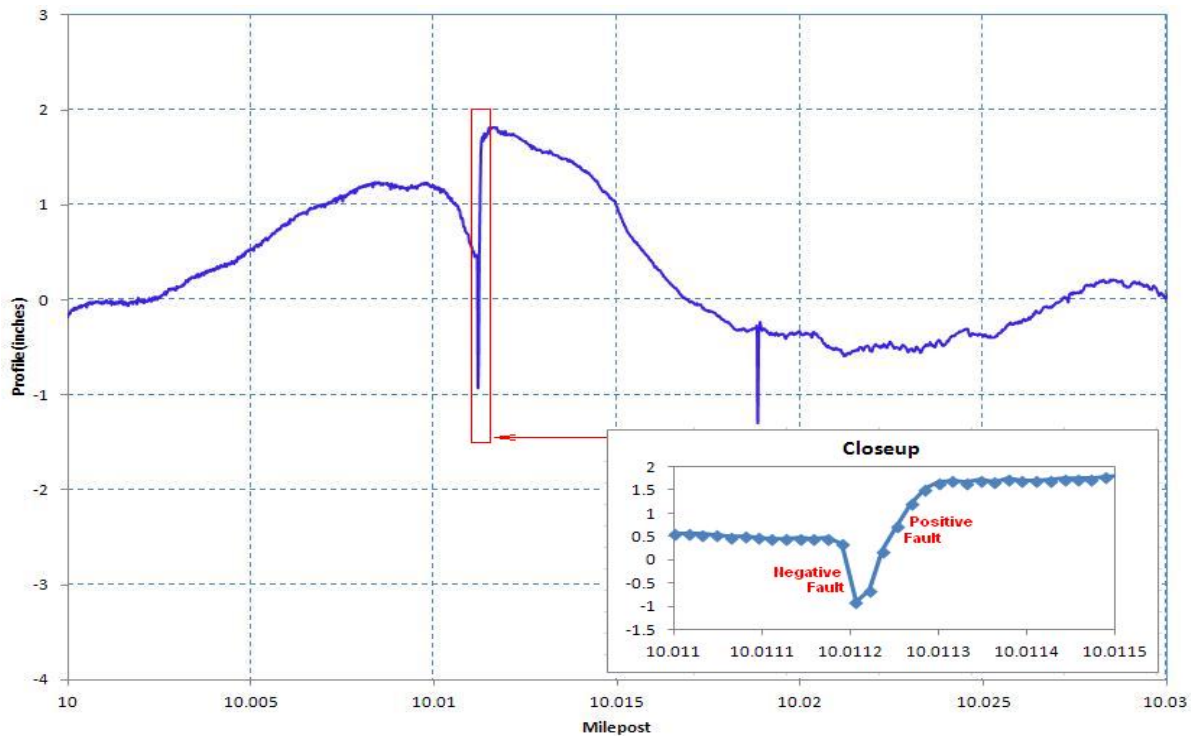


Figure 4

HSLP generated road profile (I-10 BB 450-08 EB Bridge 3)

Calculation of IRI_{25-ft} Using ProVAL 2.7

Figure 5 shows the IRI_{25-ft} curve that was produced when the Figure 4 profile was processed using ProVAL. In Figure 5, the fault at milepost 10.0112 can be seen to cause an IRI_{25-ft} peak of about 850 in/mi. This peak occurs at about milepost 10.015. Thus, there is a slight delay. ProVAL 2.7 was used in this manner to create IRI_{25-ft} curves for all the bridges that were tested. Copies can be found in Appendix B.

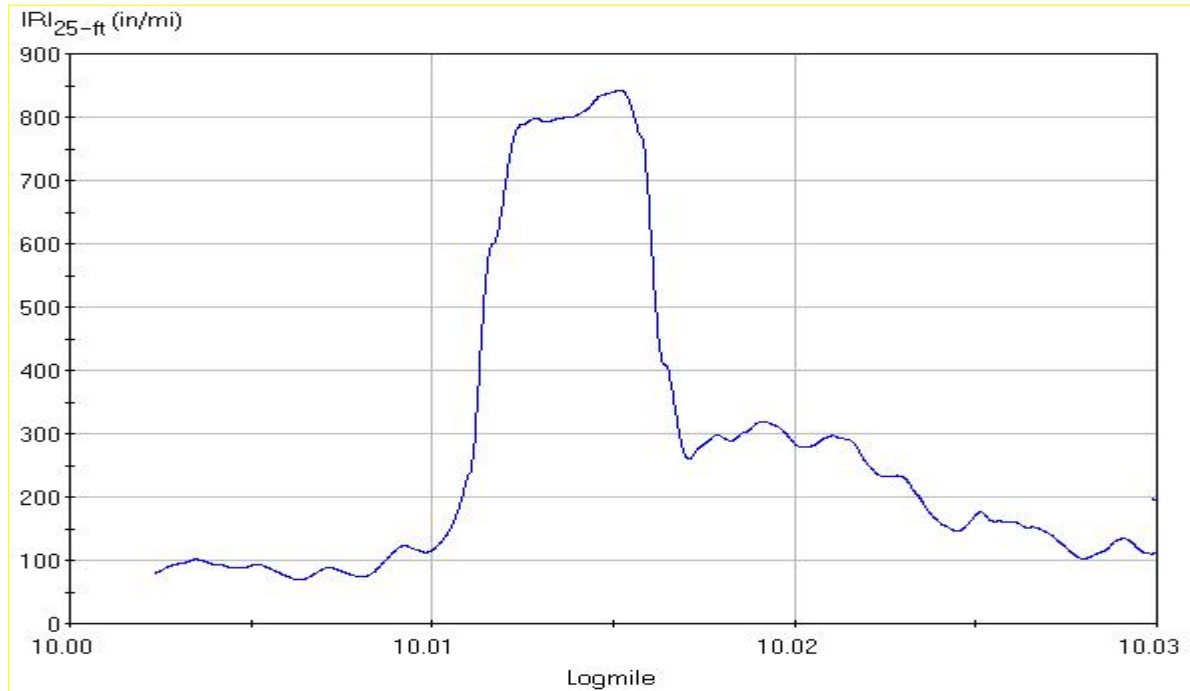


Figure 5
IRI_{25-ft} plot (I-10 BB 450-08 EB Bridge 3)

Calculation of LRI_{PS} from Accelerometer Data

Figure 6 shows the LRI_{PS} curve that was produced when the accelerometer signal in Figure 3 was processed using the LRI_{PS} algorithm. In Figure 6, the LRI_{PS} curve can be seen to rise and fall more quickly than was the case in the IRI_{25-ft} curve. Figure 6 begins to rise at about milepost 10.011, peaks at about milepost 10.013, and has largely recovered by milepost 10.015. By comparison, the IRI_{25-ft} output, shown in Figure 5 began rising at about milepost 10.01, peaked around milepost 10.015, and didn't recover until around milepost 10.017.

Appendix B presents all LRI_{PS} plots that were produced on the tested bridges. To allow for easy comparison, the IRI_{25-ft} plots for the bridges are plotted alongside of each bridge's

respective LRI_{PS} plot. IRI_{25-ft} plots are on the even pages of Appendix B and LRI_{PS} plots are on the odd pages of Appendix B.

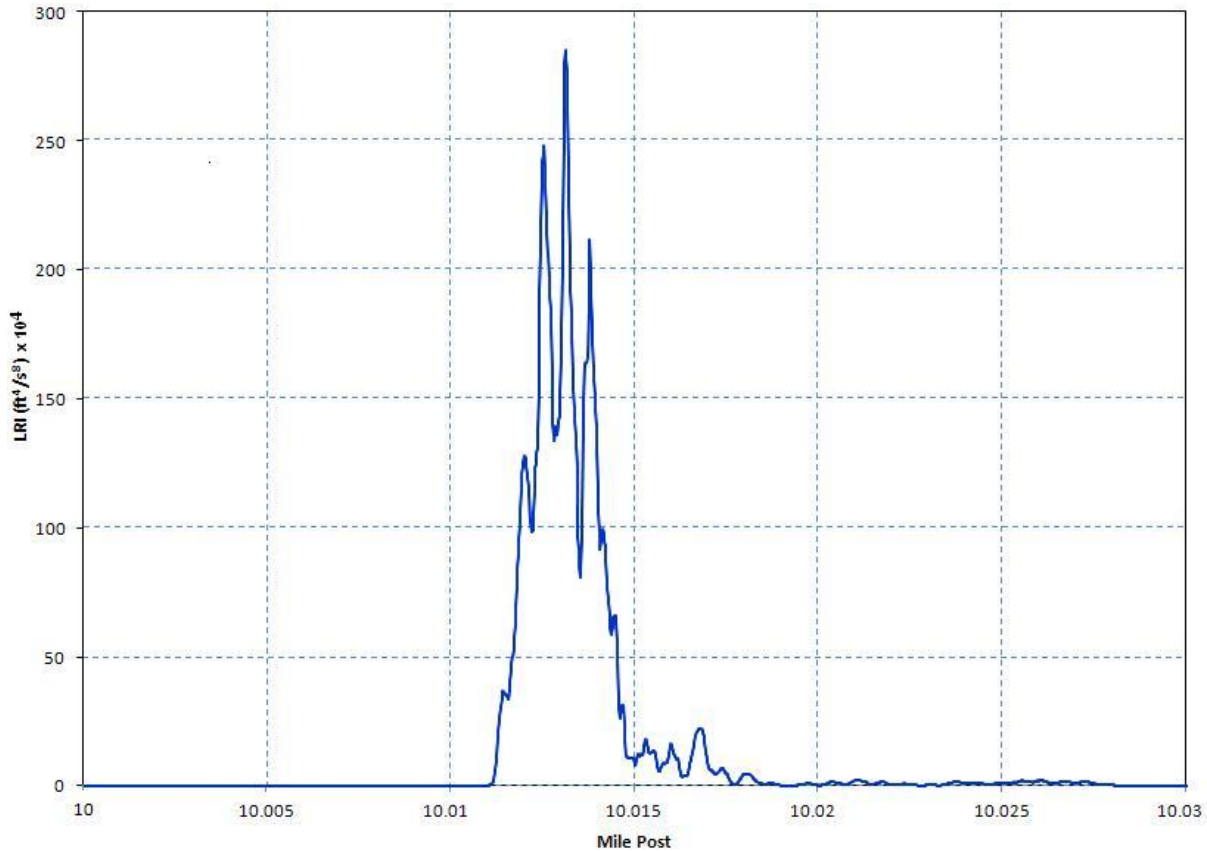


Figure 6
 LRI_{PS} plot (I-10 BB 450-08 EB Bridge 3)

Comparison of IRI_{25-ft} and LRI_{PS} Results

IRI_{25-ft} and LRI_{PS} plots for the forty bridges were compared side by side in order to carry out a comparative analysis and to assess how the IRI_{25-ft} and LRI_{PS} methodologies can be used in a complementary fashion. Three areas of assessment were examined.

AREA 1: Distress Magnitude Assessment

To carry out a proper distress magnitude comparison, it was necessary to rank the 43 worst case bridge bumps of the forty Table 2 bridges by IRI_{25-ft} and by LRI_{PS} separately. In each case, the bump with the greatest magnitude would be given a ranking of one and the bump

with the lowest magnitude would be given a ranking of 43. Ranking the bumps in this manner allowed the indexes (IRI_{25-ft} and LRI_{PS}) to be compared to each other despite the differences in units (in/mi and ft^4/s^8).

Being a profile based methodology, it was already known that the IRI_{25-ft} would produce repeatable results. IRI_{25-ft} could only fail the Area 1 assessment if there were instances where the LRI_{PS} recorded a distress that the IRI_{25-ft} algorithm did not catch at all (a special case of Modality-b). This did not occur for any of the bumps examined. Thus, the IRI_{25-ft} was shown at the outset to be suitable for bump indexing.

Despite this, all three modalities were still examined so as to gain insights and in order to determine if the LRI_{PS} might be used to obtain both magnitude and location (i.e., IRI_{25-ft} would not be needed). This turned out not to be the case. LRI_{PS} , it was discovered, could not be used to index distress magnitude.

a. IRI_{25-ft} and LRI_{PS} both register bumps similarly

The IRI_{25-ft} and LRI_{PS} curves for a bump appearing on ‘I-10 BB 450-11 EB BRIDGE 1,’ shown in Figure 7, are an example of this modality. This bump had similar rankings. For IRI_{25-ft} , the ranking was 1. For LRI_{PS} , the ranking was 4. The upper plot in Figure 7 depicts the IRI_{25-ft} output for this bump and the lower plot in Figure 7 depicts the LRI_{PS} output. Both Figure 7 plots show the bump as the same tall roughness feature running from near milepost 0.055 to about milepost 0.060. Both plots similarly show additional smaller localized bumps spread out between mileposts 0.030 and 0.055. In their general characteristics, both plots in Figure 7 register the same localized distresses. The only notable difference is that the localized distresses are somewhat more defined in the LRI_{PS} plot. This example shows that there were cases where the indexes were compatible. However, even if all bumps produced compatible outputs like this, it still would not indicate that IRI_{25-ft} and the LRI_{PS} could be used interchangeably to index localized distress magnitude due to the limitations of LRI_{PS} .

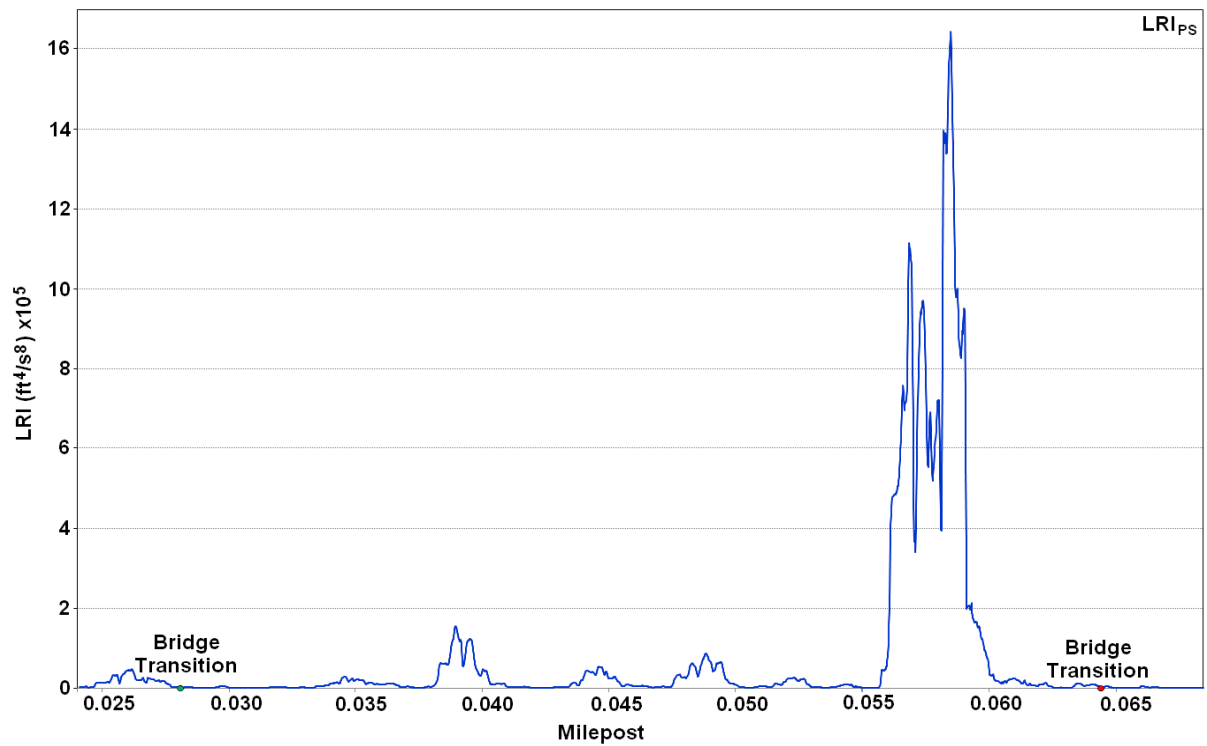
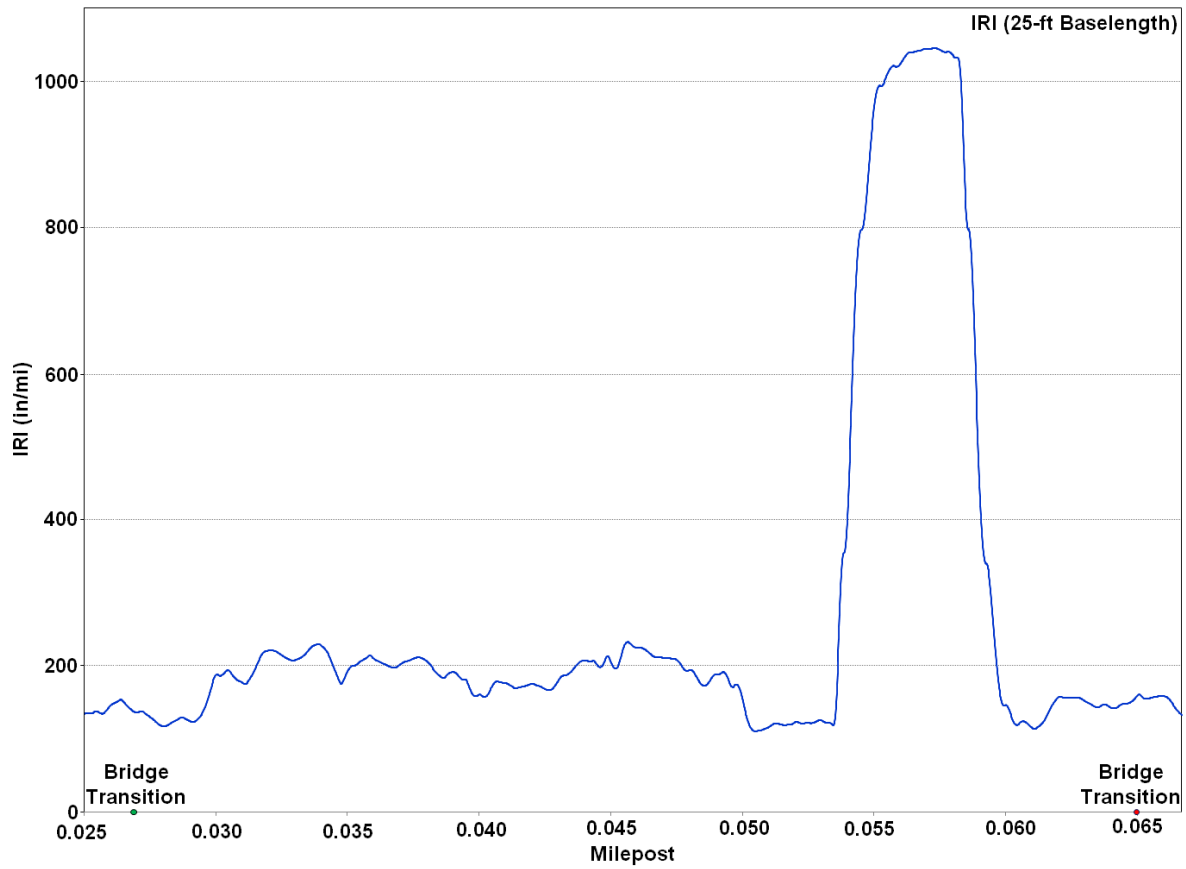


Figure 7

I-10 BB 450-11 EB BRIDGE 1 plots: IRI_{25-ft} (top) and LRI_{PS} (bottom)

b. LRI_{PS} registers significant bumps where the IRI_{25-ft} does not

Figure 8 is an example of a case where the LRI_{PS} curve peaked many orders of magnitude more than the IRI_{25-ft} curve did. In Figure 8, which shows the LRI_{PS} and IRI_{25-ft} curves for a bump on ‘I-10 BB 450-08 WB BRIDGE 3,’ it can be seen that the LRI_{PS} at about milepost 3.78 is very large (peak: 943,899 ft⁴/s⁸). This is indicative of high accelerometer activity and a comparatively rough ride. This is reflected in the LRI_{PS} ranking, which shows the bump was the 8th most distressed out of the 43 bumps tested. By comparison, the IRI_{25-ft} ranking for the bump in Figure 8 was very low (peak: 363 in/mi). It ranked 41st out of the 43 bumps examined in terms of IRI_{25-ft}.

This disparity is relevant because it shows that there was some factor that was throwing the LRI_{PS} magnitude off. The likely cause is the RTRRMS approach that lies at the heart of the LRI_{PS} methodology (i.e., transportability or system degradation likely influenced the LRI_{PS} magnitude). What is believed to have occurred is that the suspension system of the HSLP test vehicle was, by coincidence, uniquely tuned such that it became highly excited upon encountering the ‘I-10 BB 450-08 WB BRIDGE 3’ bump. By contrast, this unique profile did not overly excite the Golden Car model that is integral to the IRI_{25-ft} methodology. This supports the earlier conclusion that the LRI_{PS} should not be used to index the magnitude of localized distress because transportability and suspension degradation impacts LRI_{PS} results.

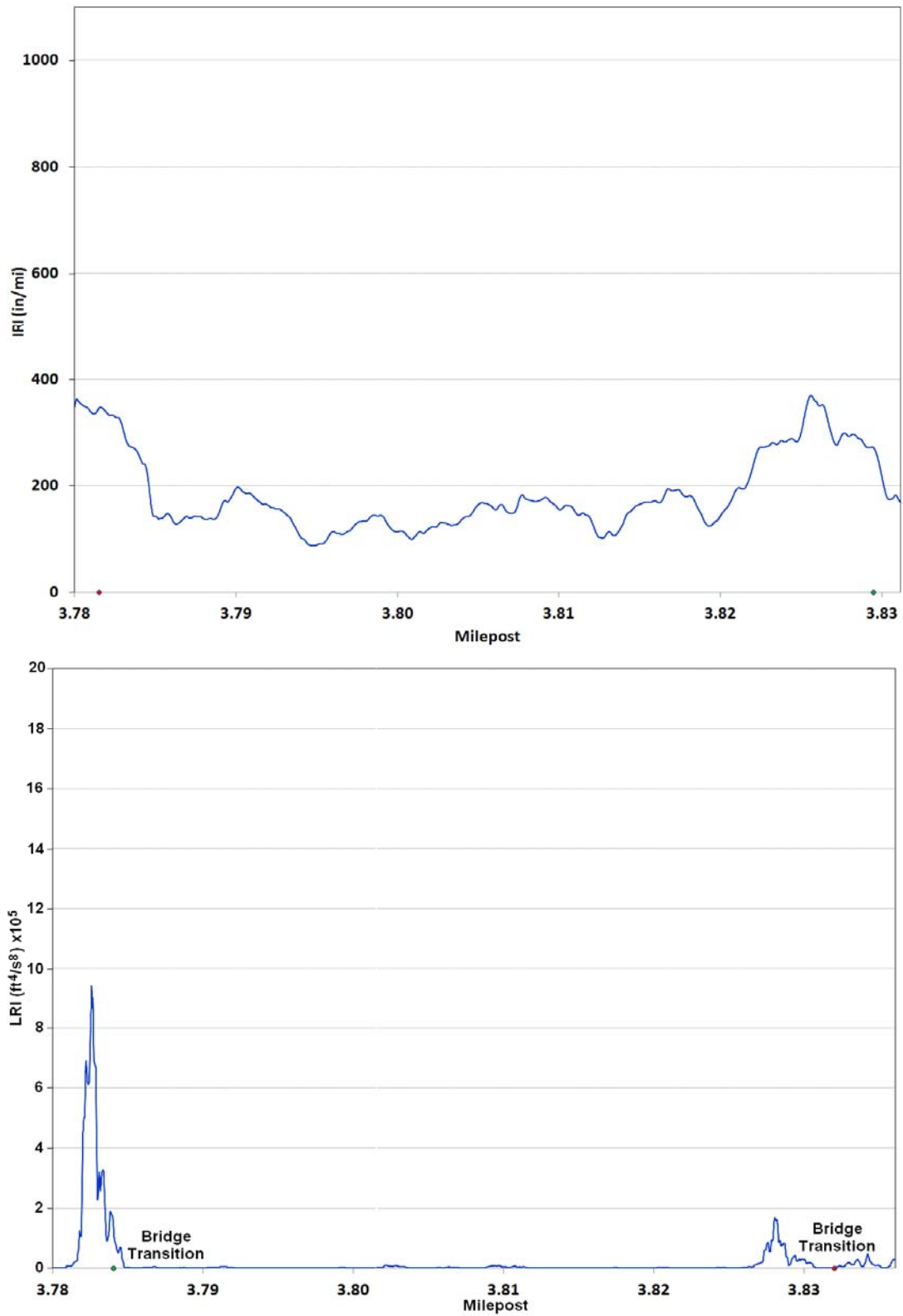


Figure 8
I-10 BB 450-08 WB BRIDGE 3 plots: IRI_{25-ft} (top) and LRI_{PS} (bottom)

c. *IRI_{25-ft} registers significant bumps where the LRI_{PS} does not*

Figure 9 is an example of a case where the IRI_{25-ft} curve peaked many orders of magnitude more than the LRI_{PS} curve did. In Figure 9, which shows the LRI_{PS} and IRI_{25-ft} curves for a bump on 'I-10 BB 450-11 WB BRIDGE 9,' it can be seen that the LRI_{PS} at about milepost 7.01 is very small (peak: 13,112 ft⁴/s⁸). This is indicative of low accelerometer activity and a comparatively smooth ride. This is reflected in the LRI_{PS} bump ranking of 41. By comparison, the IRI_{25-ft} for the bump in Figure 9 was relatively high (peak: 502 in/mi). In terms of IRI_{25-ft}, the bump ranked 18th out of 43.

This disparity is relevant, as in the previous example, because it shows that RTRRMS issues (i.e., transportability or system degradation) were likely throwing the LRI_{PS} magnitude off. Here again, it is believed that the suspension system of the HSLP test vehicle was, by coincidence, uniquely tuned such that it was only slightly excited by the 'I-10 BB 450-11 WB BRIDGE 9' bump. By contrast, the bump was able to excite the Golden Car model enough to register a significant IRI_{25-ft} reading. This, again, supports the earlier conclusion that the LRI_{PS} should not be used to index the magnitude of localized distress because transportability and suspension degradation impacts LRI_{PS} results.

Although the disparity was likely caused by the LRI_{PS} problems mentioned, there is the possibility that there were no bumps and IRI_{25-ft} is in error. In theory, application of the 25-ft. filter to the IRI algorithm is supposed to eliminate all non-localized roughness. This has not been fully proven, though. Further research must be conducted to determine how and when this may happen. In the meantime, the combined index (IRI_{25-ft} used together with LRIPS) can be used to flag where this may be happening so that caution can be used when carrying out bump assessments.

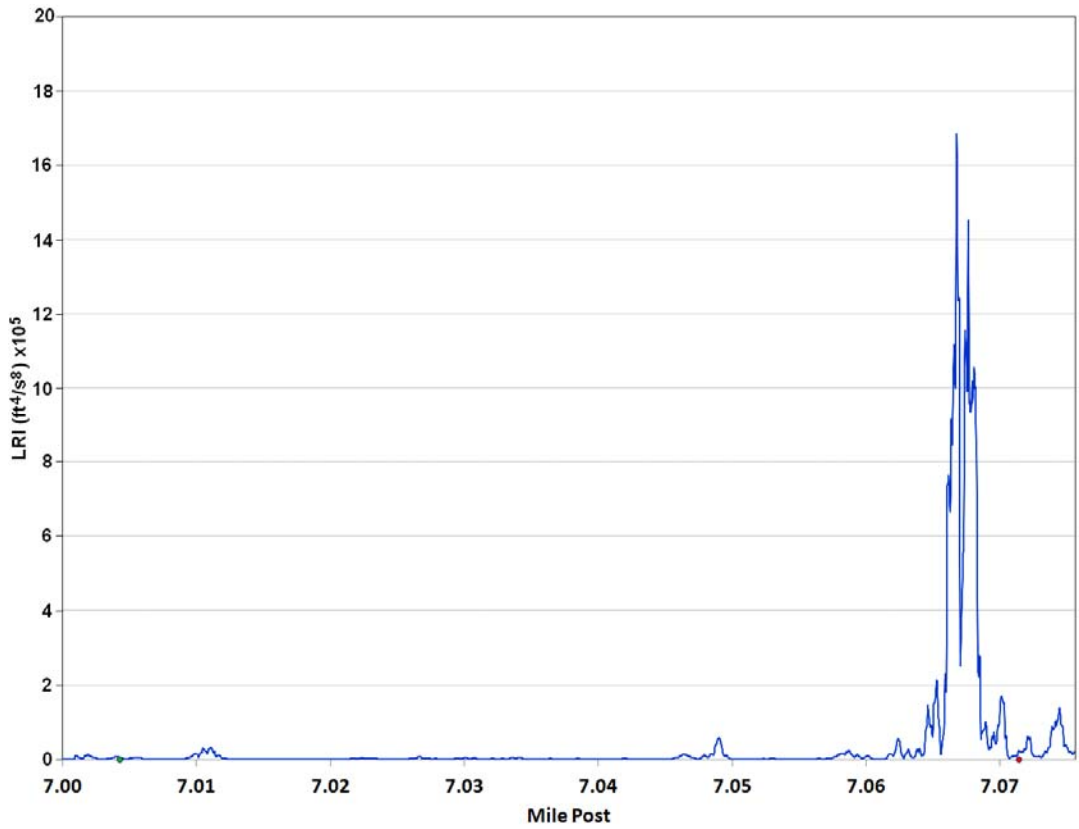
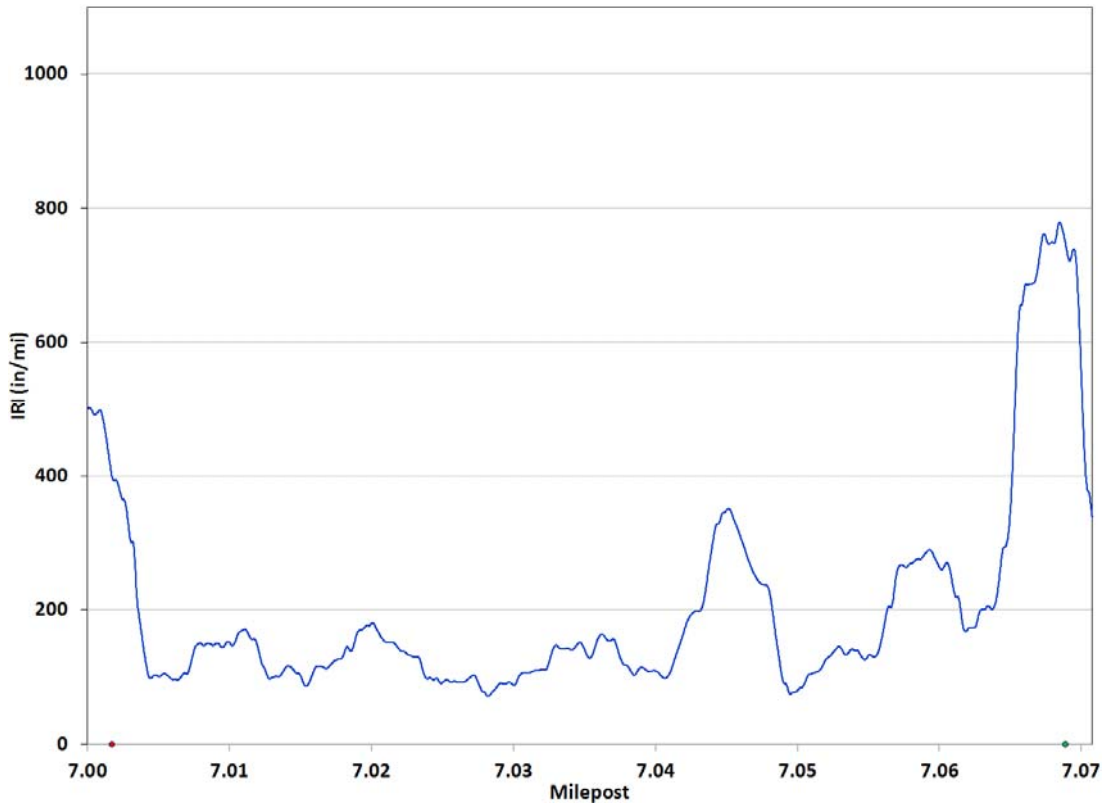


Figure 9

I-10 BB 450-11 WB BRIDGE 9 plots: IRI_{25-ft} (top) and LRI_{PS} (bottom)

The breakdown of the three Modalities associated with the Distress Magnitude Assessment was as follows:

1. Modality-a: 24 of the 43 bumps examined (55.81%) had rankings wherein the IRI_{25-ft} rank was within ± 10 points of the LRI_{PS} rank.
2. Modality-b: 9 of the 43 bumps examined (20.93%) had rankings wherein the IRI_{25-ft} was significantly rougher than the LRI_{PS} (IRI_{25-ft} rank - LRI_{PS} rank > 10).
3. Modality-c: 10 of the 43 bumps examined (23.26%) had rankings wherein the LRI_{PS} was significantly rougher than the IRI_{25-ft} (IRI_{25-ft} rank - LRI_{PS} rank < -10).

AREA 2: Distress Location Assessment

The ability of the two indexes (IRI_{25-ft} and by LRI_{PS}) to give the location of road bumps was assessed in two ways. First, the range of delays that occurred between peaks under the two index systems was noted in order to assess the extent of the problem. This was a network level assessment in that all 43 bumps were assessed together. Second, a modality assessment similar to the one carried out in the Area 1 assessment was carried out in order to appraise each index's ability to allow the user to easily locate the distress along the pavement. As in the Area 1 assessment, three modalities were used to accomplish this. Of the three modalities, only the second, "Location of a distress could be clearly discerned in the LRI_{PS} alone," could be proved.

The initial plan was to use the leading edges of the IRI_{25-ft} and LRI_{PS} curves to identify the locations of the bumps as this seemed most logical. The initial rise of the leading edge of the IRI_{25-ft} and LRI_{PS} curves should represent the suspension system's first reaction to a bump, and it is expected that this leading edge will begin very close to where the bump occurs. Peaks, by comparison, will occur where the suspension system has reached maximum excitation as a result of the bump and at a position down-road from the bump that caused them. Leading edge and peak alignments occurred as expected for the LRI_{PS} as can be seen in Figure 10 which shows the alignment for the 'I-10 BB 450-08 EB Bridge 3' bump. This was not the case for the IRI_{25-ft} plots, however. The IRI_{25-ft} 'I-10 BB 450-08 EB Bridge 3' bump alignments which can be seen in Figure 11 show this. Figure 11 had a leading edge that appears on the road before the bump occurs and a peak that appears after the bump occurs. What this shows is that the IRI_{25-ft} plots cannot be used to precisely fix bump position while the LRI_{PS} can and that the leading edge is sufficient to do so.

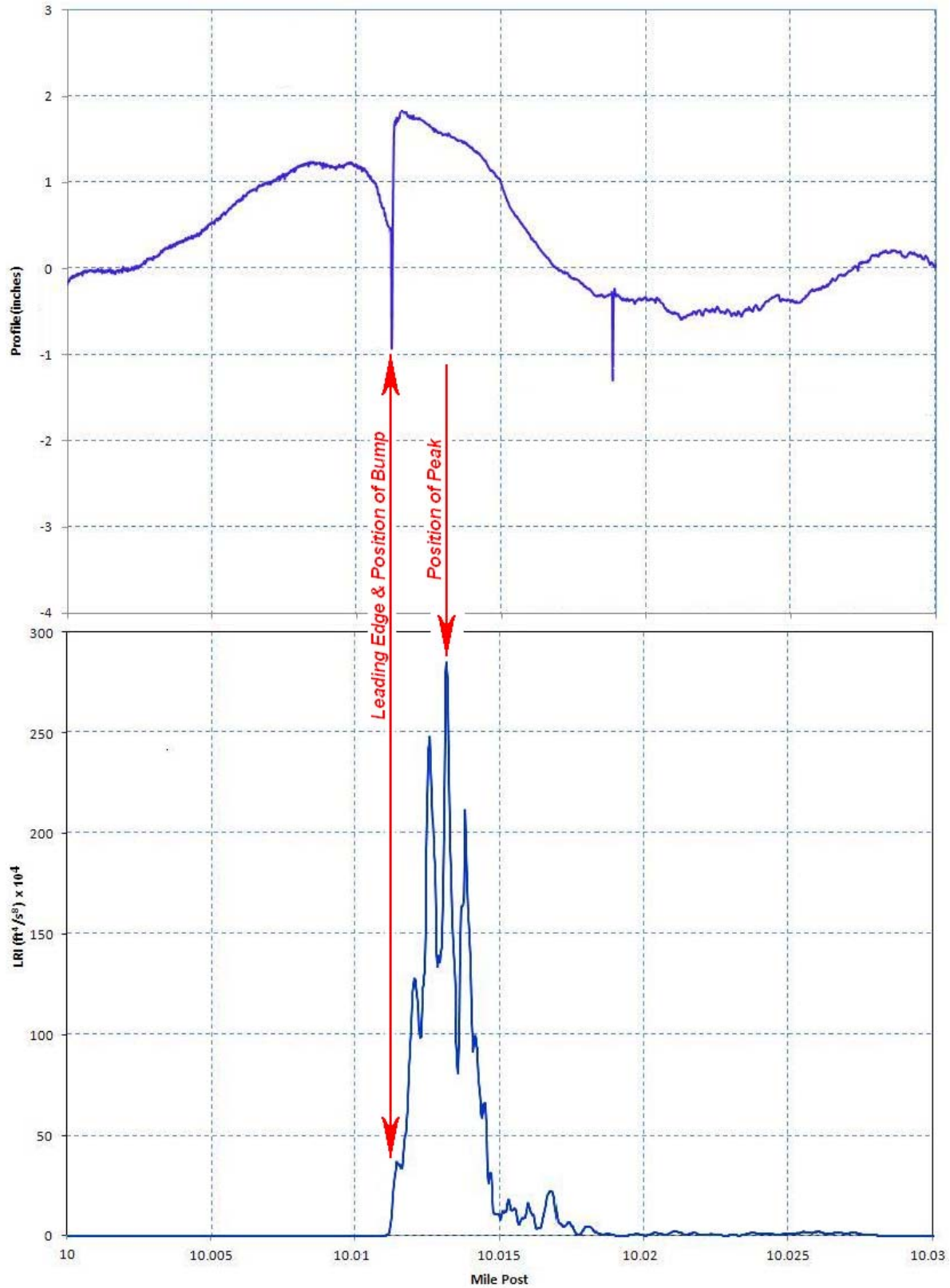


Figure 10
LRI_{PS} leading edge and peak (I-10 BB 450-08 EB Bridge 3)

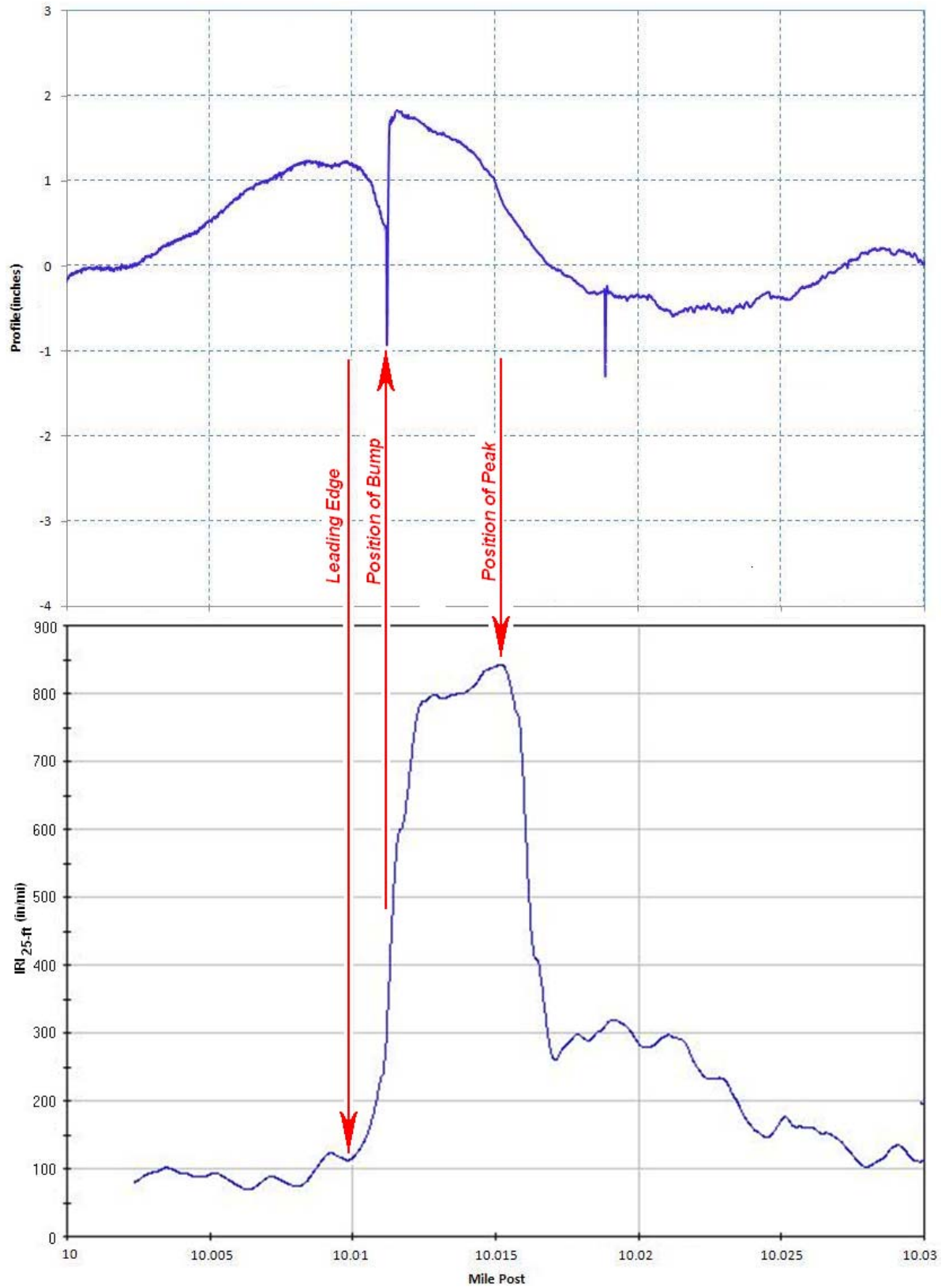


Figure 11
IRI_{25-ft} leading edge and peak (I-10 BB 450-08 EB Bridge 3)

Figure 12, which shows bumps on 'I-10 BB 450-11 EB Bridge 1,' illustrates a second reason that the leading edge method was not used to locate bumps. Figure 12 indicates that for some bumps it was not possible to find leading edges in the $IRI_{25\text{-ft}}$ plots. In the lower LRI_{PS} plot, five small equispaced bumps with clear peaks and leading edges have been delineated with arrows. Leading edges in the upper $IRI_{25\text{-ft}}$ plot, by contrast, are difficult to locate. There is some indication of peaks in the upper $IRI_{25\text{-ft}}$ plot. But, without the leading edges, it is difficult to isolate specific bumps or their locations. It should be noted that this was only a problem for $IRI_{25\text{-ft}}$. Leading edges and peaks were typically easy to locate in the LRI_{PS} plots which again supports the contention the $IRI_{25\text{-ft}}$ plots cannot be used to precisely fix bump position while the LRI_{PS} can.

The delays between peaks for the bumps studied were arrived at as follows. A peak was classified as a bump if it met one of two criteria. It had to have an $IRI_{25\text{-ft}}$ value in excess of 400 in/mi or it had to have a LRI_{PS} value in excess of $400,000 \text{ ft}^4/\text{s}^8$. Using this criterion, 43 bumps could be identified. If a bump appeared in a LRI_{PS} curve, then it was assumed that it must also be present in the corresponding $IRI_{25\text{-ft}}$ curve and vice versa.

In 25% of the 43 cases assessed, the criteria was upheld and the bump appeared in both curves. Figure 7 was an example of this. In Figure 7, the large $IRI_{25\text{-ft}}$ peak at milepost 0.055 is 1,045 in/mi, which is greater than the required 400 in/mi. The corresponding LRI_{PS} peak, which is $1,641,505 \text{ ft}^4/\text{s}^8$, is also greater than the required $400,000 \text{ ft}^4/\text{s}^8$.

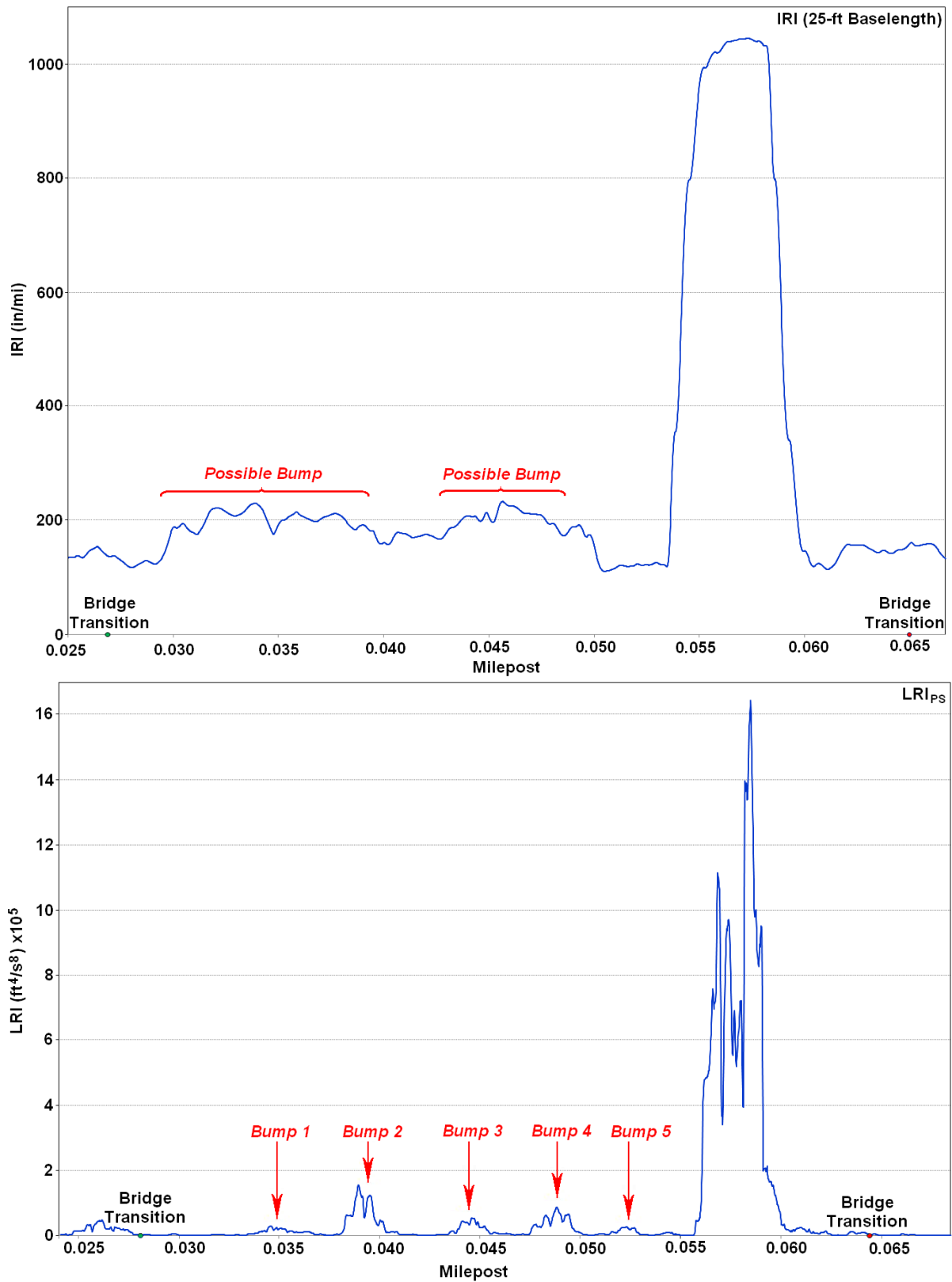


Figure 12
I-10 BB 450-11 EB BRIDGE 1 plots: IRI_{25-ft} (top) and LRI_{PS} (bottom)

Only 7% of the 43 cases assessed recorded a significant LRI_{PS} bump where there was no IRI_{25-ft} equivalent. Figure 8 is an example. In Figure 8, the IRI_{25-ft} peak near milepost 3.78 was 363 in/mi which was less than the 400 in/mi threshold. The LRI_{PS} peak, which was 943,899 ft⁴/s⁸, was greater than the 400,000 ft⁴/s⁸ threshold. The disparity between peaks was likely caused by the transportability problem. This means that the 7% of bumps that fell into this category should not be considered as significant (i.e., their IRI_{25-ft} peaks, which serve as the reference standard, were less than 400 in/mi). This detail underscores the earlier conclusion that the LRI_{PS} should not be used to index the magnitude of localized distress and IRI_{25-ft} should. It should be noted that the bumps do exist as is evidenced by their clear LRI_{PS} peaks and leading edges. They are just not significant. The fact that peaks and leading edges are easier to see in the LRI_{PS} plots suggests that LRI_{PS} should be used to locate where on the road bumps occur.

The remaining 68% of the 43 cases assessed recorded a significant IRI_{25-ft} bump where there was no LRI_{PS} equivalent. Figure 13 is an example. In Figure 13, the IRI_{25-ft} peak to the right of milepost 18.92 is 807 in/mi was greater than the 400 in/mi threshold. The LRI_{PS} peak was 272,853 ft⁴/s⁸, which is less than the 400,000 ft⁴/s⁸ threshold. The disparity between peaks was, again, likely caused by the transportability problem. As such, the bumps that fell into this category should be considered as significant and the contention is upheld that IRI_{25-ft} is better at indexing bump magnitude than LRI_{PS}. Despite this, LRI_{PS} did, as a rule, have much clearer peaks and leading edges than did IRI_{25-ft}. This fact supports the contention that LRI_{PS} should be used locate the position of bumps rather than IRI_{25-ft}.

Delay between peaks for each bump was calculated using the LRI_{PS} peak location as the reference. Delays ranged from -28.0 ft. (IRI_{25-ft} peaked 28 ft. before LRI_{PS} peaked) to +22.3 ft. (LRI_{PS} peaked 22.3 ft. before IRI_{25-ft} peaked). The range of delays provided a general sense of what the approximate margin of error is for locating a bump's position on a road.

Table 3 summarizes the delays. It shows the logmile where the peak occurred in each system (IRI_{25-ft} and LRI_{PS}), the peak value in each system (values greater than the threshold values are highlighted in red), the ranking in each peak's magnitude within each system and the delay between the peaks.

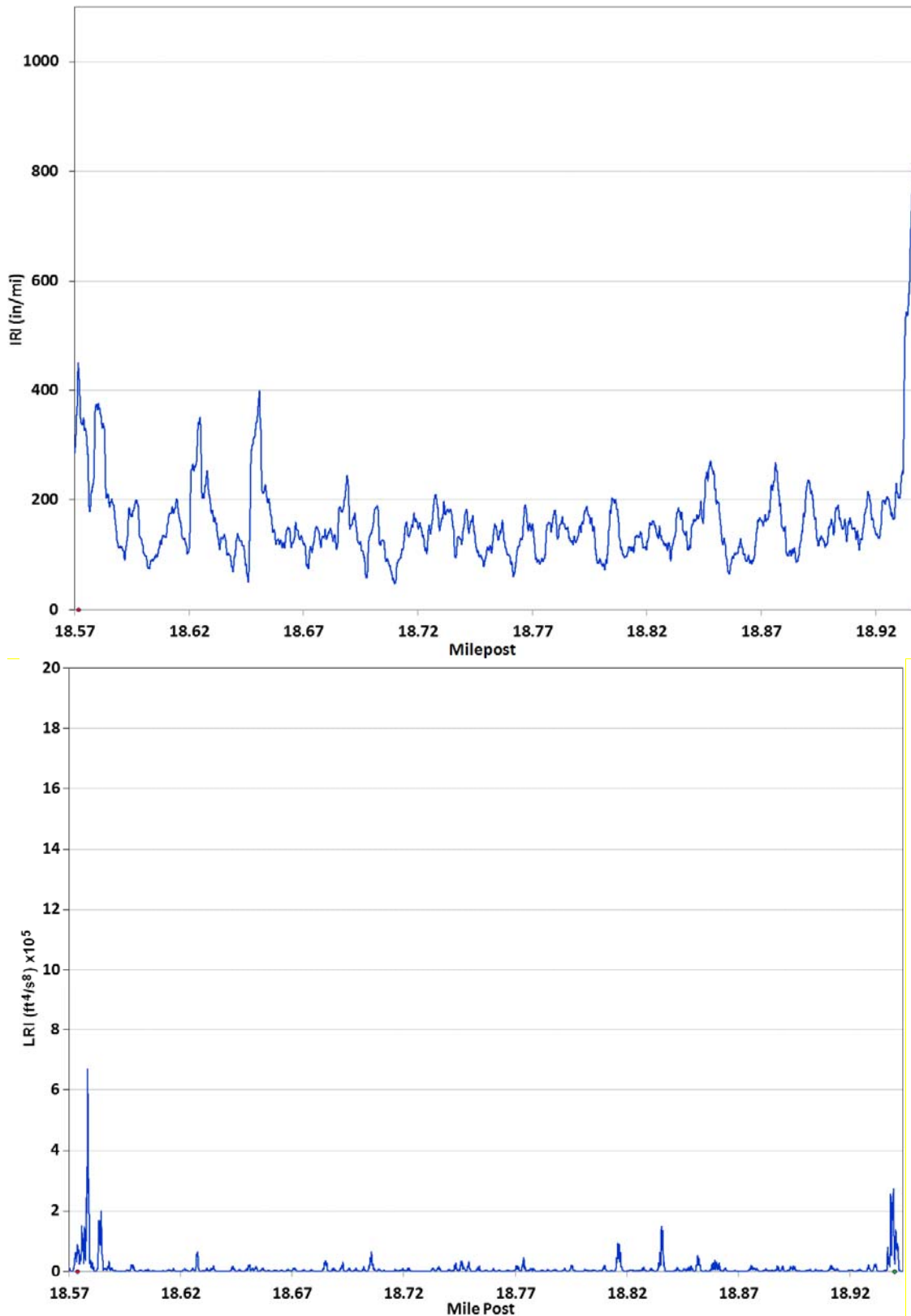


Figure 13
I-10 BB 450-11 EB BRIDGE 10 plots: IRI_{25-ft} (top) and LRI_{PS} (bottom)

Table 3
IRI_{25-ft} vs. LRI_{PS} delay summary

Bridge ID	25-ft log-mile (mi)	25-ft IRI (in/mi)	LRI log-mile (mi)	LRI (ft ⁴ /s ⁸)	25-ft IRI ranking	LRI ranking	delay (ft)
450-13 EB BRIDGE 2	4.1533	295	4.1586	501529	43	13	-28.0
450-11 WB BRIDGE 10	4.8618	426	4.8625	5632	29	42	-3.6
	4.8603	455	4.8588	22810	21	40	8.0
	4.8443	452	4.8403	347039	22	18	21.2
450-11 WB BRIDGE 9	7.0759	780	7.0717	1684528	6	3	22.3
	7.0075	502	7.0068	13112	18	41	3.9
450-11 WB BRIDGE 8	8.3068	724	8.3053	827071	8	9	7.7
450-11 WB BRIDGE 7	9.4876	402	9.4840	249784	39	21	19.1
450-11 WB BRIDGE 3	17.8576	427	17.8588	62123	28	33	-6.6
	17.8392	416	17.8396	111160	35	27	-2.1
450-11 WB BRIDGE 2	19.0308	565	19.0340	226911	13	22	-16.9
	18.6699	658	18.6689	478082	10	14	5.4
450-11 EB BRIDGE 10	18.5758	450	18.5803	670906	23	12	-23.8
	18.9410	807	18.9413	272853	4	20	-1.6
450-11 EB BRIDGE 9	17.7031	424	17.7038	37894	31	36	-3.8
	17.7055	447	17.7051	30521	24	39	2.2
450-11 EB BRIDGE 8	14.3957	457	14.3917	72709	20	29	21.0
	14.4435	582	14.4453	93222	11	28	-9.5
450-11 EB BRIDGE 6	11.4355	414	11.4365	3297	36	43	-5.3
450-11 EB BRIDGE 3	6.8551	409	6.8554	154339	37	25	-1.6
450-11 EB BRIDGE 2	4.6367	408	4.6389	57920	38	35	-11.6
	4.6395	423	4.6411	70459	32	31	-8.4
450-11 EB BRIDGE 1	0.0523	1045	0.0538	1641505	1	4	-7.8
450-08 WB BRIDGE 2	5.0392	433	5.0372	183753	27	23	10.5
450-08 WB BRIDGE 3	3.7787	363	3.7786	943899	41	8	0.6
450-08 WB BRIDGE 1	9.9977	669	9.9963	719066	9	10	7.5
450-08 EB BRIDGE 2	5.0347	349	5.0345	701093	42	11	1.4
450-08 EB BRIDGE 3	10.0113	578	10.0131	2847475	12	2	-9.5
	10.2105	994	10.2108	1225726	2	5	-1.6
450-07 WB BRIDGE 4	10.3649	419	10.3659	170604	33	24	-5.4
450-07 WB BRIDGE 3	12.6496	518	12.6471	59490	17	34	12.9
	12.3064	417	12.3049	68371	34	32	7.6
	12.2620	561	12.2606	1147050	14	7	7.5
450-07 WB BRIDGE 2	13.3005	815	13.2968	10134786	3	1	19.7
	13.0212	442	13.0198	324913	25	19	7.0
450-07 WB BRIDGE 1	14.5743	437	14.5749	145181	26	26	-3.2
450-07 EB BRIDGE 3	13.0471	789	13.0486	359025	5	16	-8.1
	13.1021	401	13.1038	355257	40	17	-8.9
450-07 EB BRIDGE 2	12.2932	541	12.2911	32518	15	38	11.2
	12.6825	521	12.6824	1165090	16	6	0.2
450-07 EB BRIDGE 1	10.3869	753	10.3909	391891	7	15	-21.0
	10.4171	486	10.4161	36325	19	37	5.2
	10.4189	424	10.4177	72636	30	30	6.4

Highlighted if:

> 400

> 400,000

The breakdown of the delays associated with the Distress Location Assessment was as follows:

1. Delay ≥ 8 ft.: 9 of the 43 bumps examined (20.93%) had delays wherein the peak was reached in the LRI_{PS} plot more than 8 ft. before it was reached in the IRI_{25-ft} plot.
2. Delay between ± 8 ft.: 24 of the 43 bumps examined (55.81%) had delays wherein the LRI_{PS} and IRI_{25-ft} peaks were within 8-ft. of each other (leading or trailing).
3. Delay ≤ -8 ft.: 10 of the 43 bumps examined (23.26%) had delays wherein the peak was reached in the IRI_{25-ft} plot more than 8 ft. before it was reached in the LRI_{PS} plot.

This array of delays was believed to be largely due to the complex nature of some of the bumps (a number of bridge approaches has a series of closely spaced slope changes) and to the inability of the analyst to often find clear leading edges or peaks in many of the IRI_{25-ft} plots. The spread largely serves to show how much the IRI_{25-ft} plots can be in error and to demonstrate why the LRI_{PS} should be used to assess a bump location on a pavement.

Three modalities were examined in the Area 2 assessment:

- a. *Distress location could be clearly discerned in both the IRI_{25-ft} and LRI_{PS} plot*

There were no cases where the distress location could be clearly discerned in both the IRI_{25-ft} and LRI_{PS} plots. There were instances where the IRI_{25-ft} plot did have clear peaks and leading edges. But this was misleading. Evidence to support this is given in Figures 10 and 11 and the related text.

- b. *Distress location could be clearly discerned in the LRI_{PS} alone*

In all 43 of the cases of significant localized distress and in the many cases of small localized distress that were seen, the LRI_{PS} , alone, was the only means in which bumps could be precisely located on the road. The case detailed in the text surrounding Figures 10 and 11 serves as an example for significant localized distress and the case detailed in the text surrounding Figure 12 serves as an example for smaller localized distresses.

- c. *Distress location could be clearly discerned in the IRI_{25-ft} alone*

There were no cases where the distress location could be clearly discerned in the IRI_{25-ft} plots alone. As in Modality-a, there were instances where the IRI_{25-ft} plot did have clear peaks and leading edges. But this was misleading for the same reasons as those discussed in the Modality-a discussion.

AREA 3: Distress Type Assessment

All of the distressed bridge transitions associated with Table 2 demonstrated sequences of closely spaced faults and/or slope changes. IRI_{25-ft} and LRI_{PS} responses to individual and isolated faults and slopes were studied first in order to simplify the problem. To do this, the Golden Car model was used to analyze a series of simple fabricated profiles. These fabricated profiles consisted of a series of positive and negative faults with 0.5-, 1-, 2-, 3-, and 6-in. steps and a series of positive and negative ramps with 1-, 2-, 3-, 4-, and 5-degree slope changes.

Results from Golden Car Model. It was discovered that the IRI_{25-ft} and LRI_{PS} responses to the assortment of fault and slope profiles fell into four unique classes as exemplified in Figures 14 through 17. These classes can be called IRI_{25-ft} (fault), LRI_{PS} (slope), LRI_{PS} (fault), and IRI_{25-ft} (slope). It was observed that the shape of the IRI_{25-ft} and LRI_{PS} curves were the same whether the underlying single fault or slope was positive or negative. Increasing or decreasing the fault height or slope angle caused no shifting in the IRI_{25-ft} and LRI_{PS} curve (i.e., location of lead-in, peak and lead-out did not change). The choice of ± 1.0 in. for the fault and $\pm 1.0^\circ$ slope for Figures 14 through 17 was arbitrary.

The uniqueness and repeatability of the four curves in Figures 14 through 17 indicated that both IRI_{25-ft} and LRI_{PS} can be used to assess distress type provided there are no other distresses nearby to pollute the signal. In isolation, the curve shape can be used to identify the type of distress. A sharp, narrow shape in the IRI_{25-ft} indicates a fault. A rectangular, blocky shape in the LRI_{PS} indicates also indicates a fault. A more gradual wavy shape indicates a slope change in both systems.

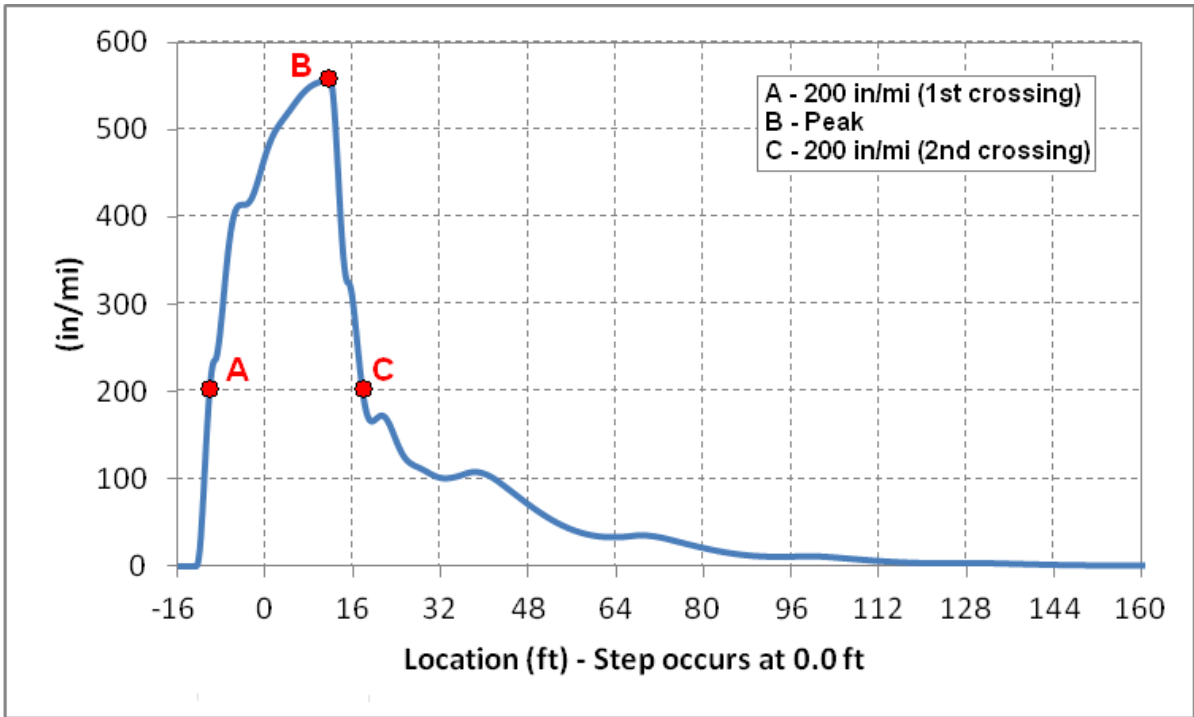


Figure 14
IRI_{25-ft} response to a ± 1 -in. fault

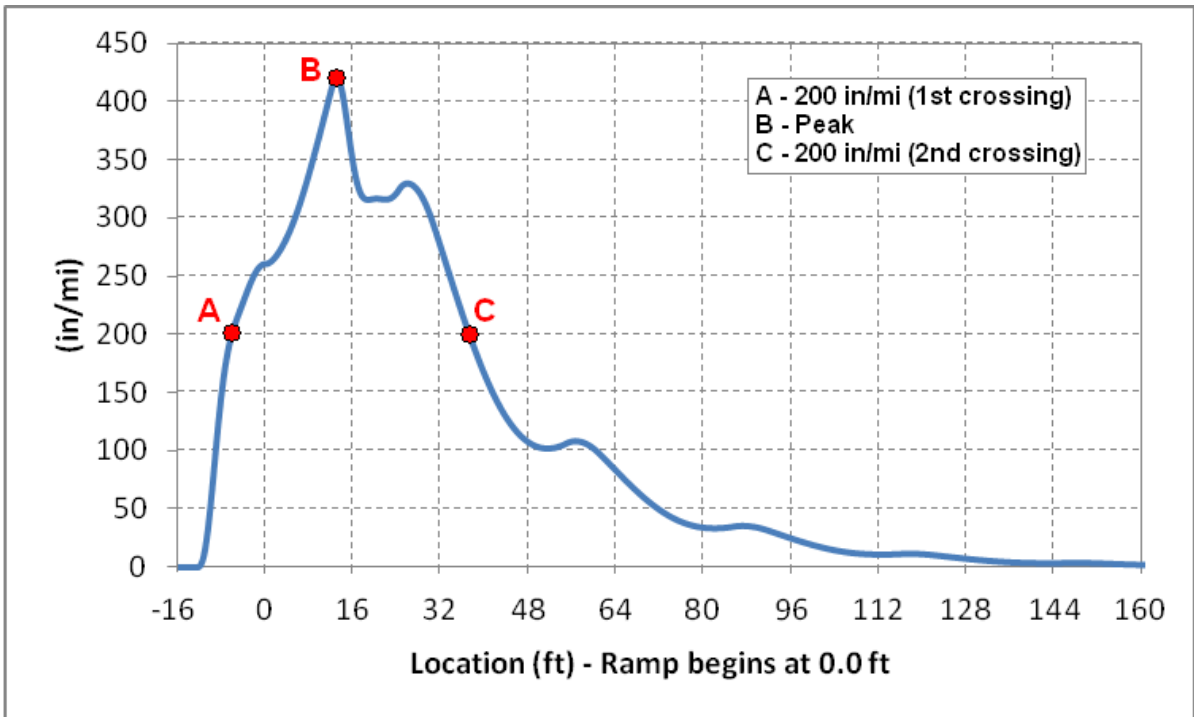


Figure 15
IRI_{25-ft} response to a $\pm 1^\circ$ slope

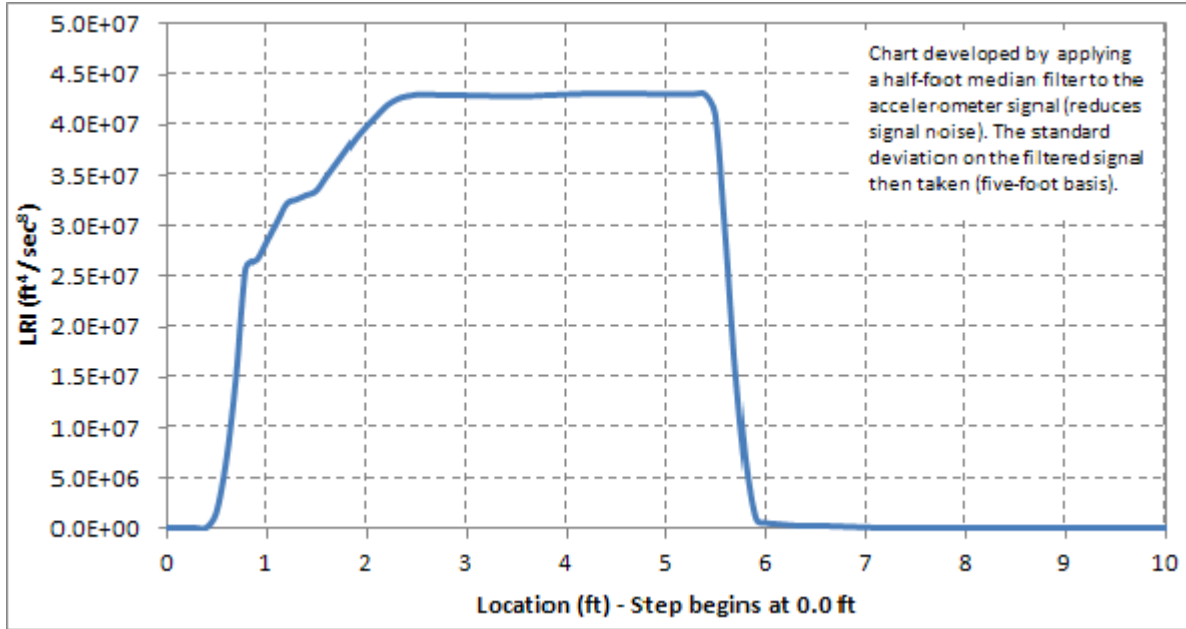


Figure 16
LRI_{PS} response to a ±1-in. fault

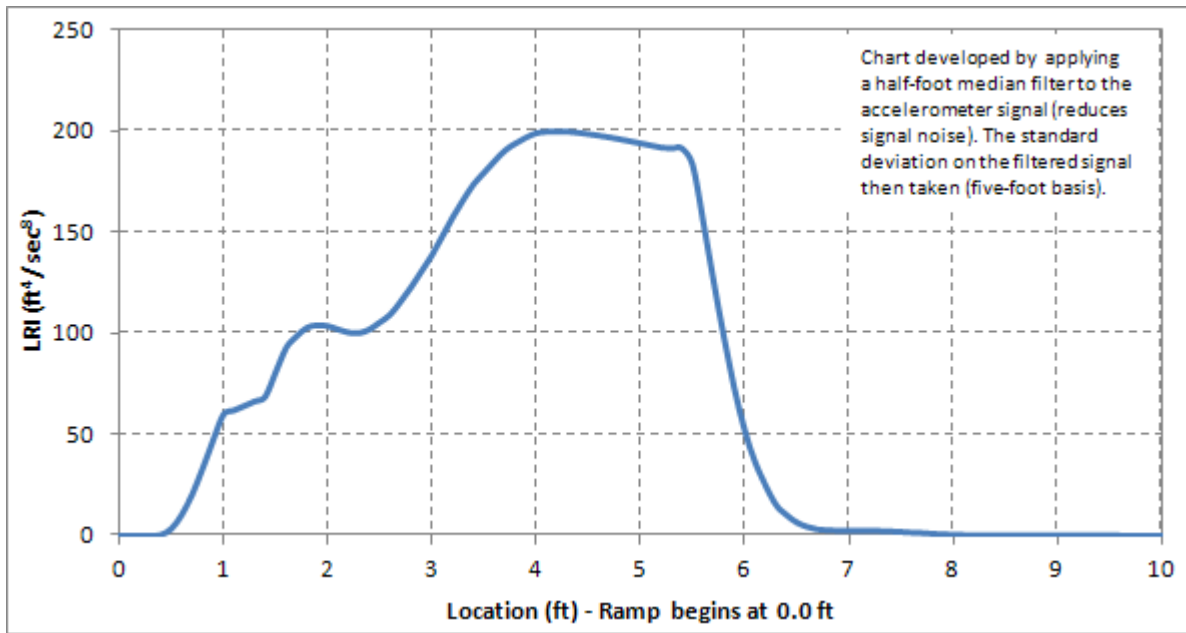


Figure 17
LRI_{PS} response to a ±1° slope

The main difference between IRI_{25-ft} and LRI_{PS}, and the reason that LRI_{PS} is better than the IRI_{25-ft} for finding distress type, is that the LRI_{PS} curve rises and falls much more quickly than IRI_{25-ft} curve does. A fast rise and fall means there is less chance for the effects of adjacent localized distresses to overlap with each other in the IRI_{25-ft} or LRI_{PS} plots. Table 4 and Table 5 show how far apart two faults or slopes would need to be for there not to be an overlap (Table 4 references Figure 14 and Table 5 references Figure 15). From these tables, it can be seen that 2 half-inch faults would have to be at least 20.3 ft. apart for overlapping to not cause a problem for the IRI_{25-ft} response. For a 1.0° slope change, the separation would need to be at least 44.4 ft. for overlap not to occur.

Table 4
IRI_{25-ft} step-fault curve summary

Fault Height (in)	Point A		Point B		Point C		Distance between Points A & C (ft)
	Location (ft)	IRI _{25-ft} (in/mi)	Location (ft)	IRI _{25-ft} (in/mi)	Location (ft)	IRI _{25-ft} (in/mi)	
±0.5	-6.0	200	12.4	281	14.3	200	20.3
±1.0	-10.3	200	12.4	561	18.4	200	28.7
±2.0	-11.3	200	12.4	1123	43.2	200	54.5
±3.0	-11.6	200	12.4	1685	50.4	200	62.0
±6.0	-11.9	200	12.4	3369	74.1	200	86.0

See Figure 14 for details on points A, B, and C

Table 5
IRI_{25-ft} ramp-fault curve summary

Ramp Angle (deg)	Point A		Point B		Point C		Distance between Points A & C (ft)
	Location (ft)	IRI _{25-ft} (in/mi)	Location (ft)	IRI _{25-ft} (in/mi)	Location (ft)	IRI _{25-ft} (in/mi)	
±1.0	-6.1	200	13.5	421	38.3	200	44.4
±2.0	-9.2	200	13.5	841	62.1	200	71.3
±3.0	-9.8	200	13.5	1262	69.4	200	79.2
±4.0	-10.2	200	13.5	1684	73.8	200	84.0
±5.0	-10.4	200	13.5	2107	77.6	200	88.0

See Figure 15 for details on points A, B, and C

The impact of this can be better seen in Figures 18 and 19. Figure 18 shows what the IRI_{25-ft} response looks like for a series of closely spaced faults (seven 1.0-in. faults spaced at 5.0-ft. intervals). Figure 19 shows what the IRI_{25-ft} response looks like for a series of closely spaced slope changes (seven 1.0° slope changes spaced at 5.0-ft. intervals). The near spacing of the

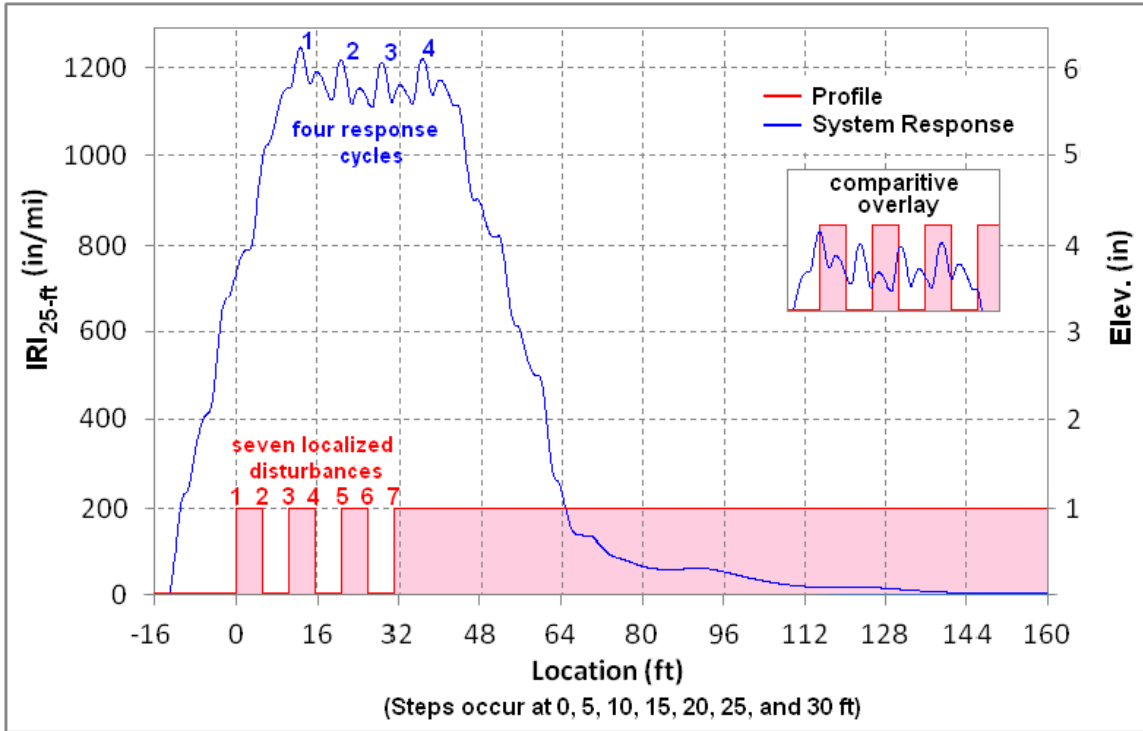


Figure 18

IRI_{25-ft} for profile with series of 1-in. step faults (Golden Car Model)

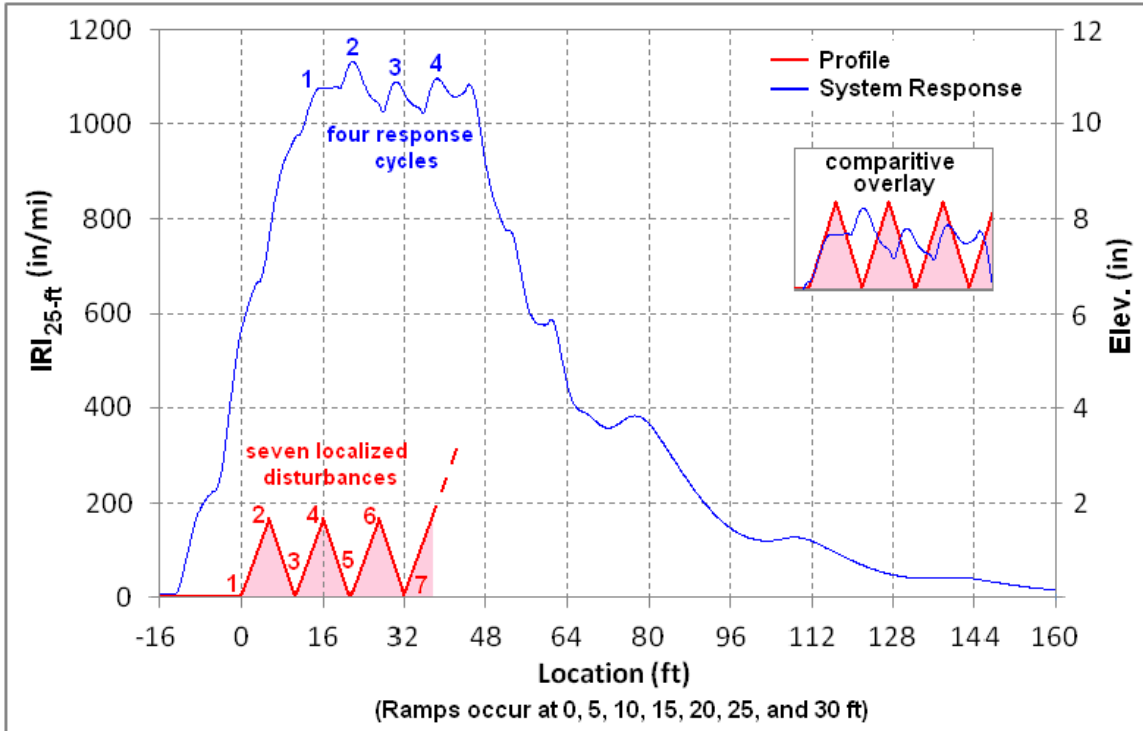


Figure 19

IRI_{25-ft} for profile with series of 1° ramps (Golden Car Model)

faults and slopes in Figures 18 and 19 (red curves) cause enough overlapping in the IRI_{25-ft} response (blue curves) as to prevent the blue curve from being useful as a tool for determining distresses type.

In terms of LRI_{PS} , localized distresses can be much closer together for overlapping not to occur. Figures 16 and Figure 17 show that for the 1.0-in. fault and the 1.0° slope change overlapping won't occur if individual localized distresses are separated by more than seven or eight feet. An example of this is depicted in Figure 20 which shows the LRI_{PS} curve generated by the Golden Car model passing over two 1.0-in. step-faults separated by 7 ft. There is no overlapping at all.

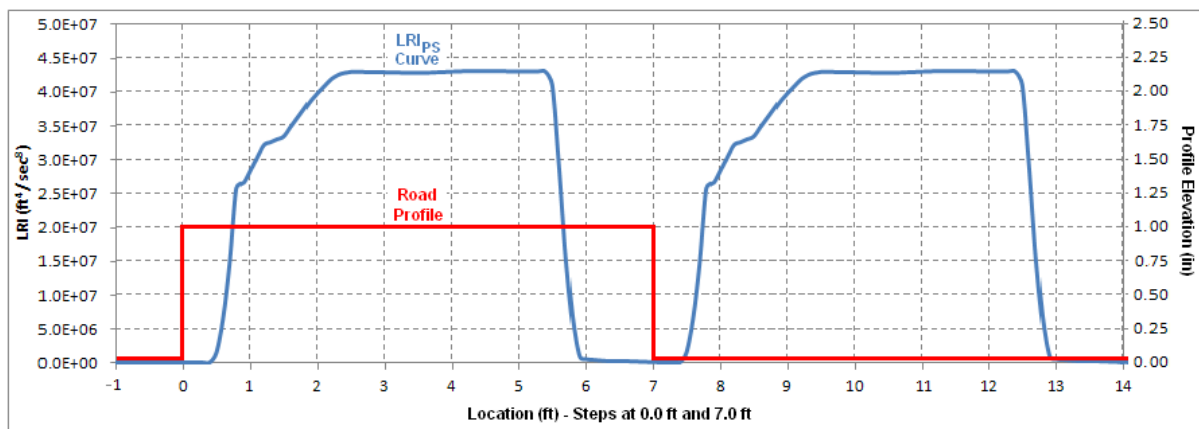


Figure 20
 LRI_{PS} for 2 1 in. faults separated by 7 ft.

Results from Field Data. Three Modalities were examined in for the Area 3 assessment:

a. Distress Type could be discerned in both the IRI_{25-ft} and LRI_{PS} plot

There were no faults or slope changes in the bridge database that were isolated enough for the “pure” distress types of Figures 14 through 17 to show up in both the IRI_{25-ft} and LRI_{PS} plots. This was more a problem related to IRI_{25-ft} than it was to LRI_{PS} . For the IRI_{25-ft} , there were typically other distresses (localized and non-localized) that were in too close a proximity to allow the IRI_{25-ft} to produce the pure curve forms.

There were a few examples in the database where Modality-a was approximated. The bump depicted in the previously detailed Figure 4 is an example of a complex profile

that has a number of faults and slope changes that occurred at exactly the same location that approximated Modality-a. For this profile, the IRI_{25-ft} and LRI_{PS} plots did not match the “pure” cases in Figures 14 through 17. But, they were very similar.

The IRI_{25-ft} curve for this profile is shown in Figure 5. In terms of distress type, this curve more closely resembles Figure 15 than it does Figure 14 which suggests that the IRI_{25-ft} is detecting the slope changes more so than it is the faulting. The Figure 5 curve does have some elements that resemble the Figure 14 faulting “fingerprint,” such as the steeper slopes at the lead-in and lead-out. So, the faulting is in evidence.

Figure 6 is the LRI_{PS} curve for the same Figure 4 profile. In terms of distress type, it more closely resembles Figure 17 than it does Figure 16. This parallels what was seen in the IRI_{25-ft} curve. It suggests that the LRI_{PS} is detecting the slope changes more so than the faulting. Also, as in the case of the IRI_{25-ft} curve, the LRI_{PS} Figure 6 curve did have some elements that resembled the Figure 16 faulting “fingerprint” such as the steeper slopes at the lead-in and lead-out. So, again, faulting was in evidence.

What was clear from the analysis was that for both indexes (IRI_{25-ft} and LRI_{PS}), it was required that the bump be isolated sufficiently enough for the patterns seen in Figures 14 through 17 to manifest. Bumps that were close together or roads that were too overly “noisy” tended to distort the IRI_{25-ft} signal.

b. *Distress Type could be discerned in the LRI_{PS} plot alone*

The segment of the previously discussed ‘I-10 BB 450-11 EB BRIDGE 1’ of Figure 21 between milepost 0.055 and 0.060 is an example of this modality. The lower LRI_{PS} plot indicates that there was a sequence of from three to five slope changes (labels 7 through 11). Three of these slope changes could be clearly discerned (bumps 7, 8, and 10). For these three, the spike pattern resembled Figure 17 more than they did Figure 18. There was some overlap. But, the pattern was clearly recognizable. Beside the three bumps mentioned, there was evidence of there being, possibly, two additional bumps (bumps 9 and 11). But, the overlapping was too pronounced to tell for certain. The direction of the slope changes associated with bumps 7, 8, and 10 could not be determined from the LRI_{PS} plots as positive and negative slope changes produce the same curve.

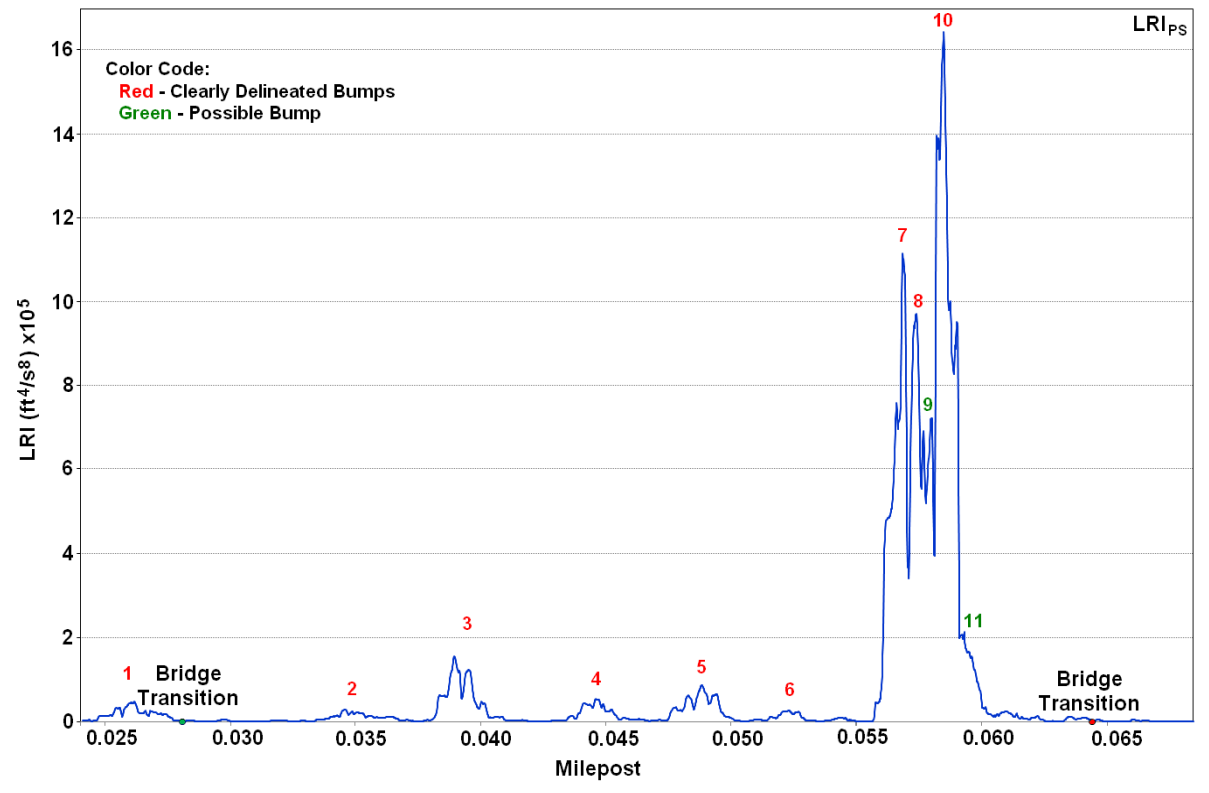
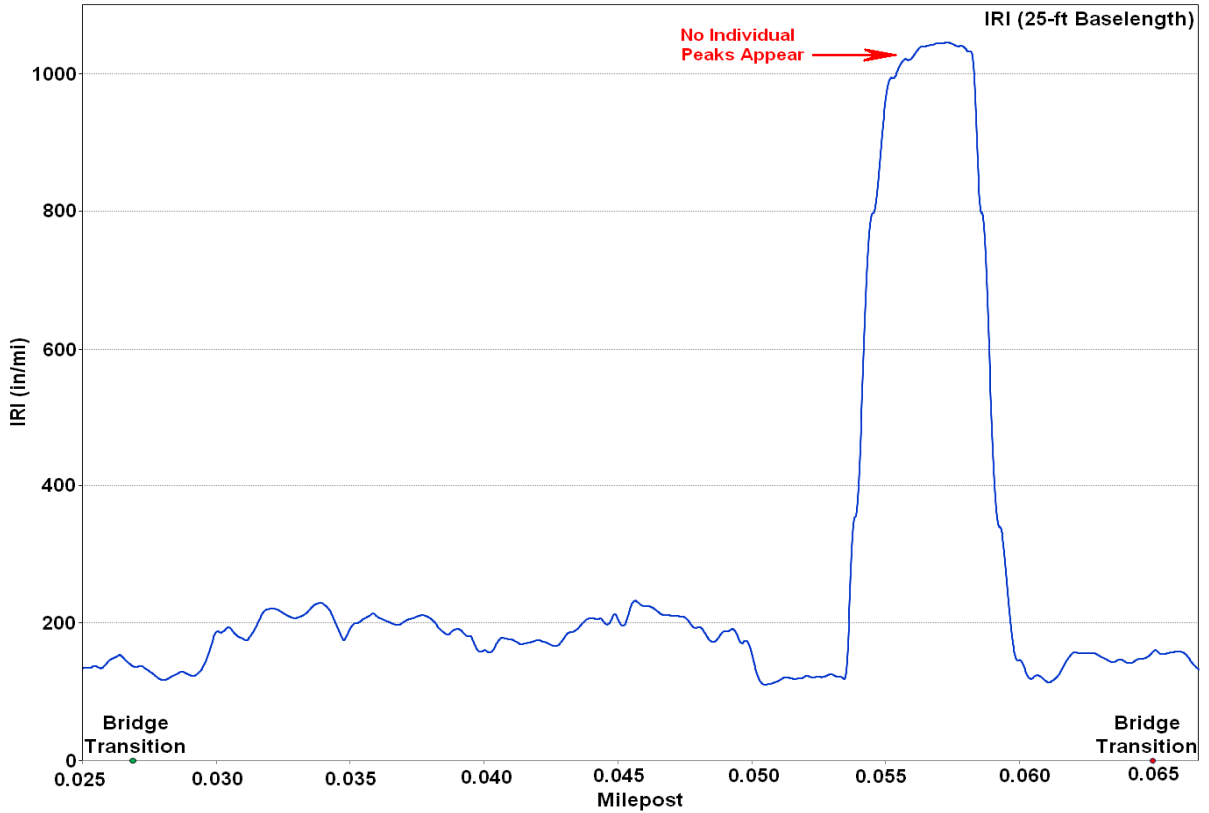


Figure 21
I-10 BB 450-11 EB BRIDGE 1 plots: IRI_{25-ft} (top) and LRI_{PS} (bottom)

By comparison, the upper IRI_{25-ft} plot of Figure 21 between milepost 0.055 and 0.060 gives no indication of separate distresses at all. All that can be seen is the single large peak. As such, it was impossible to use the IRI_{25-ft} plot to detect distress types for the three to five distresses in the sequence.

A second example of this modality can be seen in Figure 21. The LRI_{PS} plot shows a regularly repeating series of distresses (bumps 1 through 6). The shape of the LRI_{PS} curve at these locations closely matched the Figure 17 which suggested that slope changes were again present. A field assessment revealed that the bumps were at locations where bridge panels abutted each other. There was no faulting in evidence. The effect was caused by some irregularities in the panels at the joints. The effect was the introduction of some minor slope changes at the joints which caused the LRI_{PS} bumps.

By comparison, the upper IRI_{25-ft} plot gave no evidence of a regularly repeating pattern. Bump type could not be ascertained.

c. *Distress Type could be discerned in the IRI_{25-ft} plot alone*

There were no cases in evidence that suggested that distress type could be discerned from the IRI_{25-ft} plot and not the LRI_{PS} plot. This suggests that the LRI_{PS} has an advantage over the IRI_{25-ft} as it relates to identification of distress type.

Using the LRI_{PS} to Detect Distress Type on Vehicles Other Than the HSLP

Figure 22 presents the LRI_{PS} response curves based on the Golden Car reference being “driven” on the ten fault profiles. A log scale was used on the vertical axis to improve clarity. All plots in Figure 22 looked very similar (i.e., shapes are essentially the same in each curve and locations where curves rise and fall are the same). The LRI_{PS} response curves based on the Golden Car reference being “driven” on the ten slope change profiles are shown in Figure 23. All plots in Figure 23 looked very similar as well.

It is to be noted that the LRI_{PS} response to negative ramps and negative faults were exactly the same as the LRI_{PS} responses to their positive counterparts already shown (i.e., the -1.0 in. step produced the same response as the +1.0 in. step, for example). As such, the responses to negative faults and slope changes are not shown. Also, it is to be noted that the responses in Figures 22 and 23 are based on a distress (fault or ramp) that takes place on the x-axis at the plot origin (i.e., at 0.0 ft.).

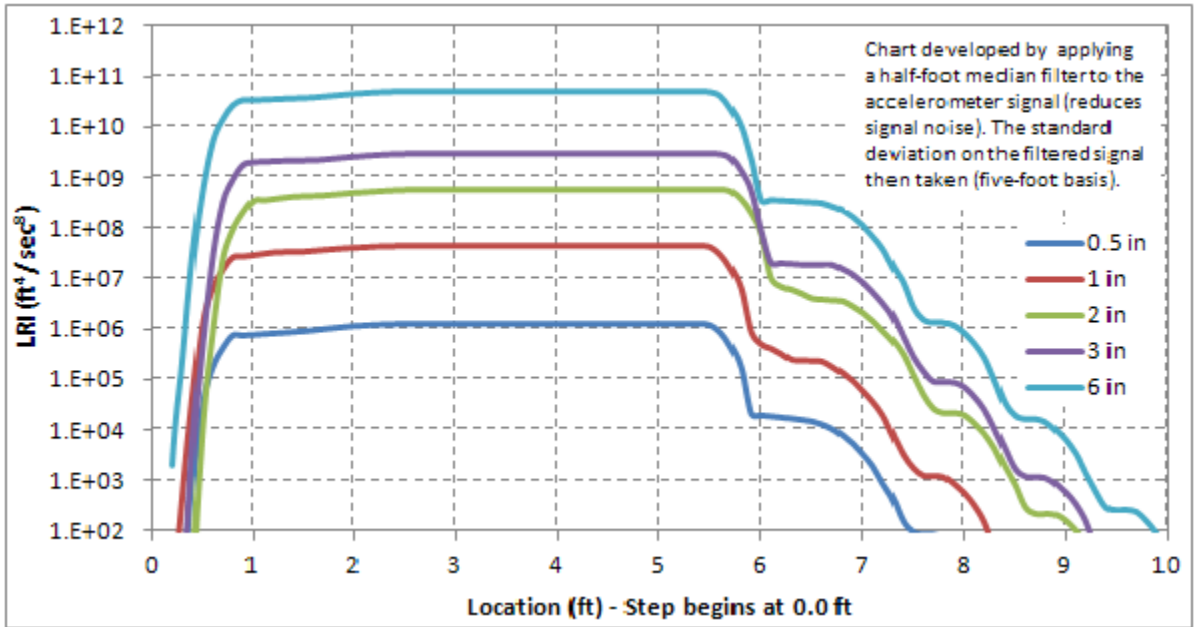


Figure 22
LRI_{PS} for step profile (Golden Car Model)

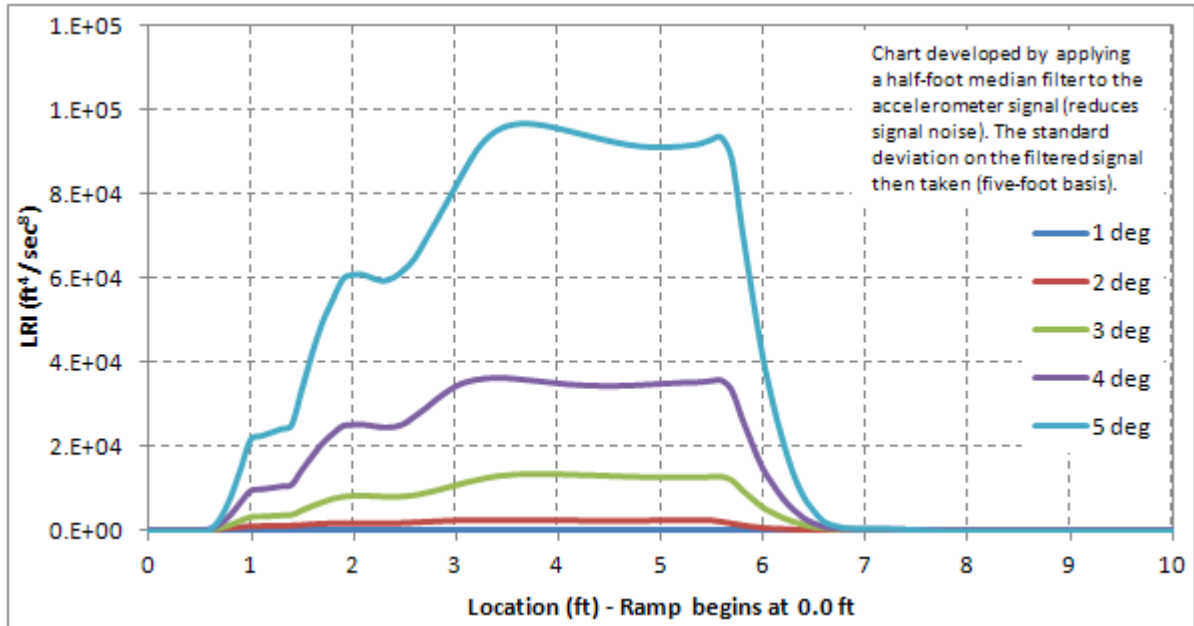


Figure 23
LRI_{PS} for ramp profile (Golden Car Model)

Similar curves to those shown in Figures 22 and 23 were developed for each of the other models presented in Table 1 (Models A through F). The results were the same. It could, therefore, be concluded that the LRI_{PS} curve shape for any given model is the same independent of distress magnitude.

The LRI_{PS} response “shapes” for each of the Table 1 models are presented in Figure 24 (fault) and Figure 25 (slope change). A log scale was used on the vertical axis of Figure 24 to improve clarity. These figures are based on the 2.0-in. fault and 3.0° slope change for convenience. As stated, changing the magnitude of the distress only has the effect of changing the magnitude of the LRI_{PS} . The curves for other distress magnitudes do not need to be presented for this reason.

Figures 24 and 25 give evidence to suggest that the LRI_{PS} 's ability to detect distress type will work independently of the suspension characteristics in most cases. All curves in Figure 24, with the exception of the Model E curve, closely resemble each other as well as the blocky shape seen in Figure 16 indicative of faulting. Likewise, all the curves in Figure 25, with the exception of the Model E curve, closely resemble each other as well as the wavier shape seen in Figure 17 indicative of a slope change. Incidentally, the locations where these curves rise in relation to where the distress occurs also closely match what is seen in Figures 16 and 17 which suggests that the LRI's ability to find the locations of distresses functions independently of model type as well.

The Model E variation is associated with a change in the shock absorber damping factor. Model E being an anomaly indicates that controls should be placed on what type of shock absorbers are allowed on HSLPs (i.e., the ratio of the HSLP's shock absorber damping factor to its sprung mass must be close to or equal to 6.0 s^{-1}). In point of fact, this requirement should be applied to current HSLPs whether LRI_{PS} is implemented or not. This is because a HSLP, being a device designed largely to report IRI (standard or otherwise), should be modeled on the Golden Car as closely as possible.

A final point can be drawn from Figures 24 and 25. From these plots, it can be seen that the six vehicles driving on the same profile will produce very different LRI_{PS} magnitudes. Model A in Figure 25, for example, has a peak value of about $27,600 \text{ ft}^4/\text{s}^8$. Model C in Figure 25, by comparison, peaks to only $4750 \text{ ft}^4/\text{s}^8$. The LRI_{PS} magnitudes are different even though the road profile is the same. These plots, therefore, show conclusively that the LRI_{PS} cannot be used to assess distress magnitude.

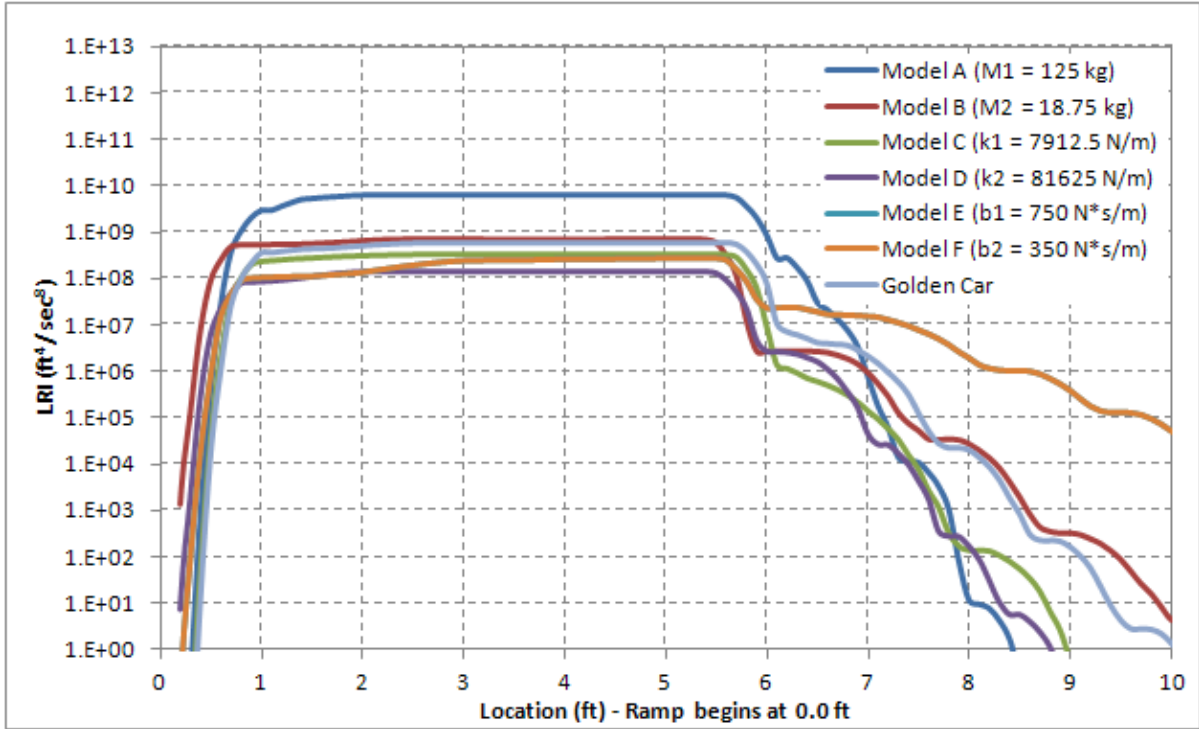


Figure 24
LRI_{PS} curves for 2 in. step profile (Models A thru F)

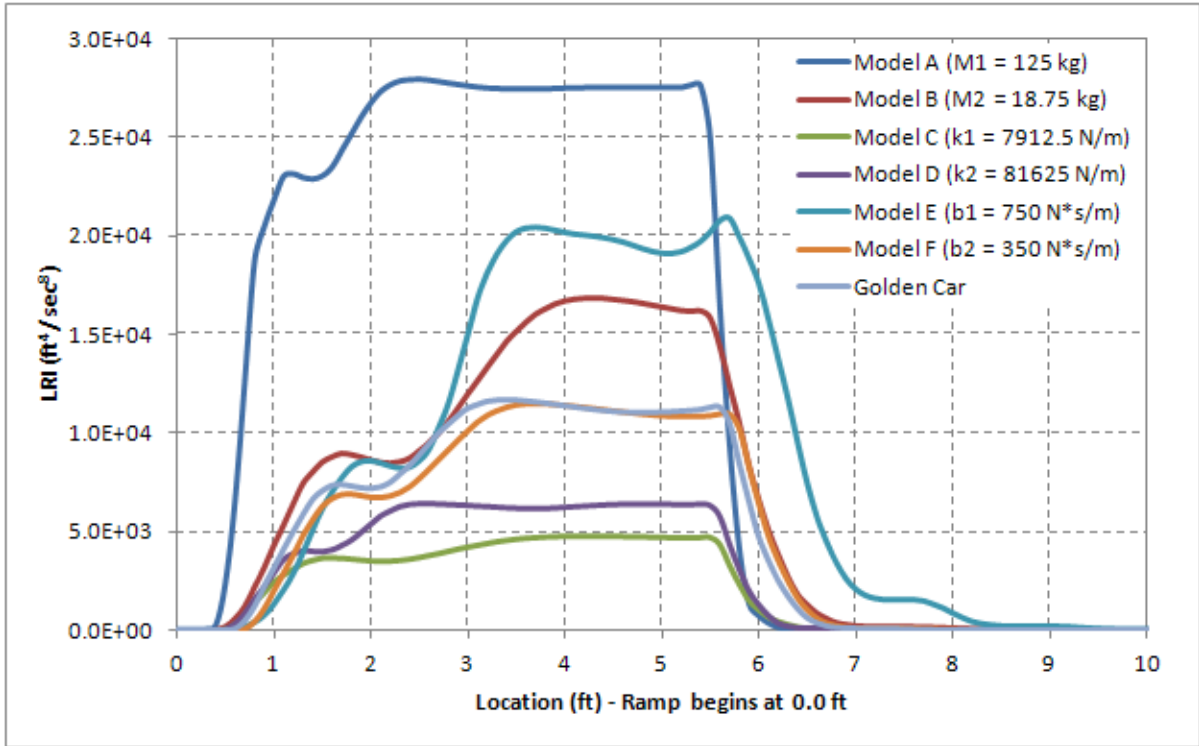


Figure 25
LRI_{PS} curves for 3° slope change profile (Models A thru F)

CONCLUSIONS

The combined index ($IRI_{25\text{-ft}}$ and LRI_{PS}) must be derived from a HSLP ride (i.e., both the $IRI_{25\text{-ft}}$ and the LRI_{PS} must be derived from the same accelerometer signal for the combined index to work).

$IRI_{25\text{-ft}}$ is better at indexing bump magnitude than LRI_{PS} . This is because the $IRI_{25\text{-ft}}$, being a profile based methodology, produces repeatable bump magnitudes independent of the HSLP's suspension characteristics. LRI_{PS} bump magnitudes vary with suspension, a fact that renders it inferior at indexing bump magnitude.

The $IRI_{25\text{-ft}}$ did not miss any localized bumps that it should have caught. Everywhere the LRI_{PS} said there was a significant bump, a corresponding bump was found by the $IRI_{25\text{-ft}}$ plots (positions were somewhat off, but, their existence was confirmed).

The $IRI_{25\text{-ft}}$ on at least one occasion *may* have seen a significant bump that the LRI_{PS} did not see (for this case, the $IRI_{25\text{-ft}}$ peaked many orders of magnitude more than the LRI_{PS}). This was likely an LRI_{PS} error caused by transportability and suspension degradation. However, it was possible that the $IRI_{25\text{-ft}}$ may have been incorrectly picking up non-localized roughness.

The LRI_{PS} was able to clearly and correctly locate the position of bumps for almost every case examined (LRI_{PS} leading edges and peaks were easy to see, even on small bumps). The only exceptions were bridge approaches that featured large closely spaced distresses (each bump within 6-ft. of next).

LRI_{PS} leading edges were adequate indicators as to where bumps were located on pavements.

LRI_{PS} was better at assessing distress types than was $IRI_{25\text{-ft}}$ because bumps could be closer together in the LRI_{PS} (Example: for 0.5-in. fault, $IRI_{25\text{-ft}}$ requires 20-ft. spacing; LRI_{PS} requires only 6-ft. spacing).

It was determined that the LRI_{PS} could identify distress type independently of the vehicle used provided that the shock absorber constant was held to a value where the ratio of the HSLP's shock absorber damping factor to its sprung mass was close to or equal to 6.0 s^{-1} .

The $IRI_{25\text{-ft}}$ often could not reliably locate the position of bumps on pavements because neither the leading edges nor the peaks, when identifiable, would line up with the bump.

IRI_{25-ft} peaks lagged or led the LRI_{PS} peaks by as much as ± 30 -ft. (as much as ± 8.0 -ft. in 44% of the cases examined). Accepting LRI_{PS} as the means of locating bump position, this shows how much IRI_{25-ft} can be off.

In many cases, the IRI_{25-ft} could not be used to locate the position of bumps because it was not possible to find clearly delineated leading edges or peaks at all.

The LRI_{PS} was not able to index bump magnitude due to transportability and suspension degradation (evidence: the six different vehicle models produced differing LRI_{PS} peaks for the same profile).

Both indexes (LRI_{PS} and IRI_{25-ft}) showed that they could be used to determine distress type *provided* there was enough separation between bumps. (Faults produced “blocky” shapes; slope changes produced “wavy” shapes).

RECOMMENDATIONS

It is recommended that the IRI_{25-ft} and LRI_{PS} indexing system should be utilized in a complementary fashion to index bumps. The IRI_{25-ft} should be used in that regard to assess bump distress magnitude and the LRI_{PS} should be used to determine where on the pavement bumps occur and to define distress type.

It is recommended that the IRI_{25-ft} and LRI_{PS} indexing system be used by DOTD's Bridge Maintenance Section to assess the Department's bridge inventory. The findings from this effort should be used to establish a bump specification.

It is recommended that the IRI_{25-ft} and LRI_{PS} indexing system be incorporated into ProVAL. At present, LRI_{PS} indexing is accomplished through a spreadsheet analysis that utilizes macros to arrive at the LRI_{PS} score.

ACRONYMS, ABBREVIATIONS, AND SYMBOLS

ARRB	Australian Road Research Board
EBR	East Baton Rouge
FVTF	Forward Vehicular Transfer Function
HSLP	High Speed Laser Profiler
ICC	International Cybernetics Corporation
IRI	International Roughness Index
DOTD	Louisiana Department of Transportation and Development
LQI	Louisiana Quality Initiative
LRI	Localized Roughness Index
LRI _{PS}	Posted Speed Localized Roughness Index
LTRC	Louisiana Transportation Research Center
NCHRP	National Cooperative Highway Research Program
PI	Profile Index
PRC	Project Review Committee
RN	Ride Number
RTRRMS	Response-Type Road Roughness Measuring Systems
RVTF	Reverse Vehicular Transfer Function
TVTF	Translational Vehicular Transfer Function
UMTRI	University of Michigan Transportation Research Institute

REFERENCES

1. Martinez, M. (2009). *The Rideability of a Deflected Bridge Approach Slab*, Louisiana Quality Initiative, Louisiana Transportation Research Center/Louisiana Department of Transportation and Development.
2. Fernando, E. G., and Bertrand, C. (2002) *Application of Profile Data to Detect Localized Roughness*. Transportation Research Record 1813, Transportation Research Board, Washington, D. C., 2002, pp. 55 – 61.
3. Gillespie, T.D., Sayers, M.W., and Segel, L. (1980). *Calibration of Response-Type Road Roughness Measuring Systems*, NCHRP Rept. No. 228.

APPENDIX A

RSP Data File and RSP Data File Convention

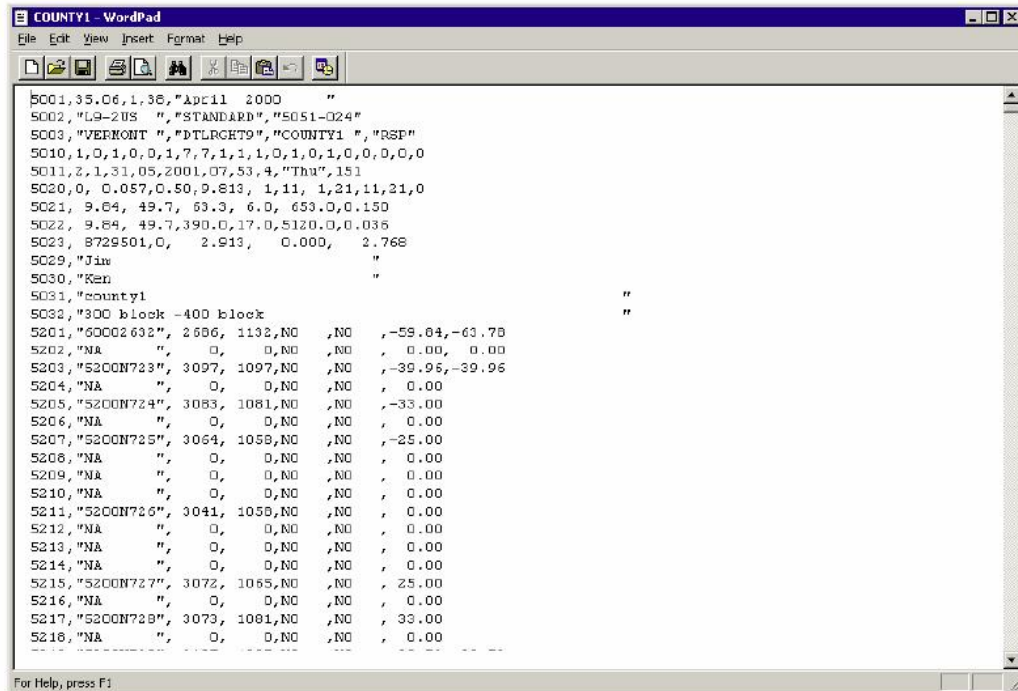
(ftp://ftp.dynatest.com/downloads/DCC/RspMan2610_RSP_MFV.pdf)

11.5 Reviewing the Data

11.5.1 RSP Data

The RSP stores its data in a comma-delimited ASCII file. This means that the file is “human readable” and that the information in each line of the file is separated by commas. This facilitates data processing and handling. The comma-delimited data can easily be imported into Microsoft Excel for ad hoc analysis and reporting.

The data file can also be reviewed in the field for completeness using Microsoft Notepad, Wordpad, or any other ASCII based text editor.



```

COUNTY1 - WordPad
File Edit View Insert Format Help
COUNTY1
5001,35.06,1.36,"Apr11 2000"
5002,"LG-2US", "STANDARD", "5051-024"
5003,"VERMONT", "DTLRCHT9", "COUNTY1", "RSP"
5010,1,0,1,0,0,1,7,7,1,1,1,0,1,0,1,0,0,0,0,0
5011,2.1,31.05,2001.07,53.4,"Thu",151
5020,0,0.057,0.50,0.813,1,11,1,21,11,21,0
5021,9.64,49.7,63.3,6.0,653.0,0.150
5022,9.64,49.7,390.0,17.0,5120.0,0.035
5023,8729501,0,2.913,0.000,2.768
5029,"Jim"
5030,"Ken"
5031,"county1"
5032,"300 block -400 block"
5201,"60002632",2606,1132,NO,NO,-59.04,-63.75
5202,"NA",0,0,NO,NO,0.00,0.00
5203,"S2CON723",3097,1097,NO,NO,-39.95,-39.95
5204,"NA",0,0,NO,NO,0.00
5205,"S2CON724",3083,1081,NO,NO,-33.00
5206,"NA",0,0,NO,NO,0.00
5207,"S2CON725",3064,1058,NO,NO,-25.00
5208,"NA",0,0,NO,NO,0.00
5209,"NA",0,0,NO,NO,0.00
5210,"NA",0,0,NO,NO,0.00
5211,"S2CON726",3041,1050,NO,NO,0.00
5212,"NA",0,0,NO,NO,0.00
5213,"NA",0,0,NO,NO,0.00
5214,"NA",0,0,NO,NO,0.00
5215,"S2CON727",3072,1065,NO,NO,25.00
5216,"NA",0,0,NO,NO,0.00
5217,"S2CON728",3073,1081,NO,NO,33.00
5218,"NA",0,0,NO,NO,0.00

```

Please refer to the following chapter for a detailed discussion of the RSP data file contents.

12. Data File Formats

12.1 RSP Data File

The RspWin program produces files that are directly 'Importable' to most spreadsheet software and easily readable by dedicated software. The following main features accomplish this:

- A comma character separates items.
- Text items are quoted.
- Each line is prefixed (the very first item on the line) by a 'Line-ID-Number', which is the key to the contents of the line.

The data file type is: SEQUENTIAL UASCII Text File (Line lengths vary).

A file consists of "Header" information followed by RSP Profiling Data and optional IMS data.

Numeric items are located within fixed fields indicated by [X, Y, W], which defines the first and last character positions and the width. Numbers are right justified except for the special Nil value ('No use' number), which is stored as "N0", padded with spaces.

Most Text items are fixed width where W indicates the width excluding quotes.

Units	Numeric information is stored in either Metric or English systems.
Stations	Meters, km, feet, yards, miles or miles.feet
Geographic	Degrees. Latitude is positive North. Longitude is positive east. Altitude is meters, always.

Common to ALL lines is the Line ID number [1,4,4].

12.1.1 RSP File Header Information

1. Program Version

```
5001,35.80,1,38,"RspWin 1.0.8"
  [ 6, 10, 5] 35.80 Program Identification
  [ 12, 12, 1] 1 No of Headers (ONE always)
  [ 14, 15, 2] 38 No of Lines in Header
  [ 18, , ] Rsp... Program Comment
```

2. Primary Setup Names

```
5002,"LNN-2SI","EMBEDDED","5051-XXX"
  [ 7, 14, 8] LNN-2SI Data Format
  [ 18, 25, 8] EMBEDDED Hardware system
  [ 29, 36, 8] 5051-XXX Equipment S/N
```

3. Secondary Setup Names

```
5003,"B-JONES","UK-MANCH","S1-L5","RSP"
  [ 7, 14, 8] B-JONES Operator Name
  [ 18, 25, 8] UK-MANCH Test setup name (part of)
  [ 29, , ] S1-L5 Datafile name (the name of this file)
  [ , , 3] RSP Datafile extension
```

4. Units

```

5010,0,0,0,0,0,0,0,0,3,1,0,0,0,0,1,1,0,0,0,0,0
5010,0,0,0,0,0,0,0,0,3,1,0,0,0,0,0,1,0,0,0,0,0
  [ 6, 6, 1] 0 Temperature 0:C° 1:F°
  [ 8, 8, 1] 0 Spare
  [10,10,1] 0 Weight (Mass) 0:kg 1:lb
  [12,12,1] 0 Spare
  [14,14,1] 0 Deflection 0:mu 1:mills
  [16,16,1] 0 Distance 0:mm 1:inches
  [18,18,1] 0 Spare
  [20,20,1] 3 Location 1:StnMeters 2:meters 3:kilometres
                    5:feet 6:yards 7:miles 8:StnFeet 9:ml.feet

  [22,22,1] 1 Angle (GPS) 1:Deg (2:Deg°Min 3:Deg°min'Sec)
  [24,24,1] 0 Force 0:kN 1:lbf
  [26,26,1] 0 Pressure 0:kpa 1:psi
  [28,28,1] 0 Heavy Pres 0:Mpa 1:ksi
  [30,30,1] 0 Spare
  [32,32,1] 0 Spare
  [34,34,1] 1 Angle (0:Radians) 1:Degrees
  [36,36,1] 0 Spare
  [38,38,1] 0 Spare
  [40,40,1] 0 Spare
  [42,42,1] 0 Spare
  [44,44,1] 0 Spare

```

5. Date and Time

```

5011,2,1,28,08,2003,21,45,0,"Non",000
  [ 6, 6, 1] 2 Date style (fixed)
  [ 8, 8, 1] 1 Time style (fixed)
  [10,12,2] 14 Day
  [13,14,2] 07 Month
  [16,19,4] 1999 Year
  [21,22,2] 14 Hour
  [24,25,2] 30 Minute
  [27,27,1] 0 not used
  [30,32,3] Non not used
  [35,37,3] 000 not used

```

6. Operating Parameters

```

5020,0,0.100,0.50,9.820,1,11,1,21,11,21,0,25.5,26.9
  [ 6, 6, 1] 0 0:Normal (1:Bounce)
  [ 8,13,6] 0.100 Filter Wavelength (same unit as Stations)
  [15,18,4] 0.50 Filter Damping
  [20,24,5] 9.820 Gravity (m/s²)
  The following pairs are channel numbers for Left, Full and Right Rutting
  respectively.
  [26,27,2] 1 Leftmost laser for "Left Rutting"
  [29,30,2] 11 Rightmost laser for "Left Rutting"
  [32,33,2] 1 Leftmost laser for "Full Rutting"
  [35,36,2] 21 Rightmost laser for "Full Rutting"
  [38,39,2] 11 Leftmost laser for "Right Rutting"
  [41,42,2] 21 Rightmost laser for "Right Rutting"
  [44,44,1] 0 0:Center line Index (1:Half Car Index)
  [46,50,5] 25.5 Surface Temperature (Manual entry)
  [52,56,5] 26.9 Air Temperature (Manual entry)

```



7, 8. Roughness Index Parameters for IRI (5021) and Ride Number (5022)

```

5021, 250, 80.0, 63.3, 6.0, 653.0, 0.150
  [ 6, 10, 5] 250 Averaging Distance (mm/inches)
  [ 12, 16, 5] 80.0 Simulation Speed (kmh/MPH)
  [ 18, 22, 5] 63.3 Normalized Suspension Stiffness
  [ 24, 27, 4] 6.0 Normalized Suspension Damping
  [ 29, 34, 6] 653.0 Normalized Tire Stiffness
  [ 36, 40, 5] 0.150 Mass Ratio

```

9. DMI and Stationing

```

5023, 1709645, 0, 0.863, 0.000, 0.774
5023, 10000000, 0, 0.000, 0.000, 0.000
  [ 6, 13, 8] 1709645 DMI Calibration Figure
  [ 15, 15, 1] 0 DMI Direction 0:Increasing 1:Decreasing
  [ 17, 24, 8] 0.000 (DMI Reading when the file was created)
  [ 26, 33, 8] 0.000 Minimum Station in file
  [ 35, 42, 8] 0.774 Maximum Station in file

```

10. Name of Driver

```

5029, "Jack"
  [ 7, , ] Jack

```

11. Name of Operator

```

5030, "Jones"
  [ 7, , ] Jones

```

12. Facility Information

```

5031, "Dynatest Boulevard", "A1", "Motorway", "ACC"
  [ 7, , ] Dynatest Boulevard Name
  [ , , ] A1 Code
  [ , , ] Motorway Type
  [ , , ] ACC Class

```

13. Subsection Information

```

5032, "East bound lane one", "A1+1", "Townhall ", " Airport", "Right-1", "1R"
  [ 7, , ] East bound lane one Name
  [ , , ] A1+1 Code
  [ , , ] Townhall Start
  [ , , ] Airport Ending
  [ , , ] Right-1 Lane name
  [ , , ] 1R Lane code

```

14 to 34. Data for each of 21 lasers max. (5201-5221)

```

5201, "20081817", 2724, 1163, 300, 100, -59.49, -63.39
  [ 7, 14, 8] 20081817 Serial Number
  [ 17, 21, 5] 2724 Reading at reference distance 250mm
  [ 23, 27, 5] 1163 Reading at reference distance 350mm
  [ 29, 33, 5] 300 Mean Profile Depth Bias (mu/mill)
  [ 35, 39, 5] 100 RMS Texture Bias (mu/mill)
  [ 41, 46, 6] -59.49 Lateral position (mm/inches)
  [ 48, 53, 6] -63.39 Optional secondary position (for angled lasers)

```

For positions above, centreline is zero, negative to the left, positive right. TWO positions apply to ANGLED lasers only; the first is closest to the centreline (calibration beam closest to lasers) the second is farthest from the centreline.

A spare (not used) laser channel appears like this:

```

5202, "NA", 0, 0, NO, NO, 0

```

35 to 37. Data for each of 3 accelerometers max. (5223-5225).

```

5223, "DDK-LWA", -11936, 12135

```



```

[ 7, 14, 8] DDK-LWA Serial Number
[ 17, 22, 6] -11936 Reading in upright position
[ 24, 29, 6] 12135 Reading in opposite position

```

A spare (not used) Acc channel appears like this:
5224,"NA", 0, 0

38. Inertial Motion Sensor.

```

5228,"WS-0123", 0.3,1.000, 0.1,1.000, 0.1,1.000
[ 7, 14, 8] WS-0123 Serial Number
[ 17, 20, 5] 0.3 Bank Bias (deg)
[ 22, 26, 5] 1.000 Bank Gain
[ 28, 31, 5] 0.1 Grade Bias (deg)
[ 33, 37, 5] 1.000 Grade Gain
[ 39, 42, 5] 0.1 Heading Rate Bias (deg/s)
[ 44, 48, 5] 1.000 Heading Rate Gain

```

12.1.2 RSP Measurement Data

Measurement data is stored chronologically after the header. Most items cover an interval of some size (see "Storage Intervals" in section 8.1, Test Setups), e.g. IRI could be reported every 50 meters, Average Laser Elevations every 25mm. The beginning and ending Stations are the first two items in most lines. Information from the various transducers is always written in sequence with the leftmost laser first and the rightmost farthest to the right. The following examples show data from a typical "Five lasers plus two accelerometers" system.

Common to most lines

```

54XX, 0.000000, 0.000100, .....
[ 6, 15,10] 0.000000 Beginning of interval
[ 17, 26,10] 0.010000 End of interval

```

Laser elevations and raw accelerations.

Distance from the lasers down to the pavement.
5401, 0.000000, 0.000100, 293.1, 298.6, 298.1, 303.9, 316.7, -9.8123, -9.8123
[28, 33, 6] 293.1 Leftmost Laser (mm/inches)
[35, 40, 6] 298.6 Left Wheel path
...
[56, 61, 6] 316.7 Rightmost laser
[63, 70, 8] -9.8123 Left acceleration
[72, 79, 8] -9.8123 Right acceleration

Failures.

Percentage of dropouts/erroneous readings
5402, 0.010000, 0.020000, 1.0, 0.0, 0.0, 0.0, 4.1, 0.0, 0.0
[28, 33, 6] 1.0 Leftmost Laser
[35, 40, 6] 0.0 Left Wheel path
...
[70, 75, 6] 0.0 Right Accelerometer

Velocity and Driving Acceleration.

```

5403, 0.000000, 0.010000, 14.0, 1.3
[ 28, 32, 5] 14.0 Velocity (kmh/MPH)
[ 34, 37, 5] 1.3 Acceleration (m/s2 ft/s2)

```



Longitudinal Profile elevation

```

5405, 0.000000, 0.000100, -0.5, -0.8, 2.1
[ 28, 34, 7] -0.5 Left Wheel path (mm/inches)
[ 36, 42, 7] -0.8 Centreline
[ 44, 50, 7] 2.1 Right Wheel path

```

International Roughness Index (IRI)

```

5406, 0.000000, 0.020000, 4.75, 4.09, 3.69
[ 28, 33, 6] 4.75 Left Wheel path (m/km or in/mile)
[ 35, 40, 6] 4.09 Centreline IRI
[ 42, 47, 6] 3.69 Right Wheel path

```

Ridenummer (RN)

```

5407, 0.000000, 0.020000, 1.73, 2.05, 2.69
[ 28, 33, 6] 1.73 Left Wheel path
[ 35, 40, 6] 2.05 Centreline RN
[ 42, 47, 6] 2.69 Right Wheel path

```

Texture, RMS (Root Mean Square)

```

5408, 0.000000, 0.001000, 812, 845,....., 302.5, 298.4
Texture is reported in either microns or mills
[ 28, 34, 7] 812 First texture capable laser
[ 36, 42, 7] 845 Second texture capable laser
Followed by Laser Elevations (mm or inch) for each texture capable laser

```

Texture, MPD (Mean Profile Depth)

```

5409, 0.000000, 0.001000, 436, 534,.....
Texture is reported in either microns or mills
[ 28, 34, 7] 436 First texture capable laser
[ 36, 42, 7] 534 Second texture capable laser
and so on.

```

Rutting

```

5411, 0.000000, 0.001000, 3.6, 4.5, 4.5, 4.3, 5.2, 5.2
[ 28, 33, 6] 3.6 Left Rutting (mm/inches)
[ 35, 40, 6] 4.5 Full Rutting
[ 42, 47, 6] 4.5 Right Rutting
[ 49, 54, 6] 4.3 Max Left Rutting
[ 56, 61, 6] 5.2 Max Full Rutting
[ 63, 68, 6] 5.2 Max Right Rutting

```

For HDR rutting see next chapter.

Faulting

```

5414, 0.007890, 5.4, 5.6, 5.4, 5.2
[ 6, 15,10] 0.007890 Station (average)
[ 17, 22, 6] 5.4 Average Fault Depth
[ 24, 29, 6] 5.6 Left wheel path
[ 31, 36, 6] 5.4 Centre line
[ 38, 43, 6] 5.2 Right wheel path

```

Photo sensor Status-change

```

5415, 0.007890,"OFF"
[ 6, 15,10] 0.007890 Exact station
[ 18, 20, 3] OFF New Status (ON or OFF)

```

Keyboard 'Events'

```

5416, 0.008823,"K"
[ 6, 15,10] 0.008823 Exact station
[ 18, 18, 1] K Ascii Key

```



'Marks'

5417, 0.008823,"Crossing"
[6, 15,10] 0.008823 Exact station
[18, 18, 1] Crossing Mark text

Time of day

5418, 0.001000, 12345.6
[6, 15,10] 0.001000 Exact station
[17, 24 , 9] 12345.67 HrMnSc.nn

Inertial Motion Sensor data

5420, 0.000000, 0.001000,"I", 0.73, -3.53, 26.9, 2.6, 2.6, 54.6, 26,
-1.24, 0.523, 23.45
[32, 38, 7] 0.73 Bank (deg)
[40, 46, 7] -3.53 Grade (deg)
[48, 53, 6] 26.9 Compass Heading (N=0 E=90 S=180 V=270)
[55, 60, 6] 2.6 Yaw Rate (deg/sec)
[62, 67, 6] 2.6 Heading Rate (deg/sec)
[69, 73, 5] 54.6 Velocity (kmh/MPH)
[75, 77, 3] 26 Temperature (C/F)
[79, 85, 6] -1.24 Crossfall (deg)
[87, 92, 6] 0.523 Radius of Curvature (km/ml)
[94,101, 8] 23.45 Degree of Curve (deg/km or deg/ml)

Macro Profile Elevations (RSPIV only).

Distances from the Left (5421) and Right (5422) lasers down to the pavement.
Each record presents 25 (or less) elevations covering 25 mm (1 inch) of travel.
Elevations are prefixed by the acc and laser contributions to the longitudinal
profile.

5421, 0.000000, 0.000025, 298.1, 298.6, 298.7, 299.3, 300.5 ...
[28, 35, 8] -19.1 Acc part of inertial profile (mm/inches)
[37, 44, 8] 37.7 Laser part of inertial profile
[46, 51, 6] 298.1 First elevation sample (mm/inches)
[53, 58, 6] 298.6 Second elevation sample
...
[] 25th sample (typically)

Geographic Positioning System (GPS)

5280, 0.000000, 0.001000,0,130743.5,+90.0000000,+180.0000000,9999.9, 0, 5,
416, 11
[28, 28, 1] 0 0: No Failure
9: Timeout
[30, 35, 6] 130743.5 Time format hhmss.s
[37, 47,11] +90.0000000 Latitude (degrees, real)
[49, 60,12] +180.0000000 Longitude (degrees, real)
[62, 67, 6] 9999.9 Height (meters, always)
[69, 70, 2] 2 0:No Nav. 1:Std.GPS 2:DGPS
[72, 73, 2] 5 No of satellites
[75, 78, 4] 416 Beacon/Reference ID (DGPS)
[80, 82, 3] 11 Age of differential corrections (seconds)

Stop flag

5429, 0.000, 0.774, 0, 0
[6, 13, 8] 0.000 Lowest Station
[15, 22, 8] 0.774 Highest Station
Additional parameters are for internal use by Dynatest (typ zero).

12.2 HDR Data File

The optional HDR system stores data in a separate ASCII file similar to the RSP file. The header is identical to the RSP file. The HDR file is named as the RSP file with HDR as extension.

The following lines appear in the HDR file.

High Definition Rutting

One or the average of more measurements taken over a short interval

```
5412, 0.000000, 0.005000, 3.6, 4.1, 4.6, 104.3, 4.5, 245.2 ...
[ 28, 33, 6] 3.6 Left Rutting (mm/inches)
[ 35, 40, 6] 4.1 Average of Left and Right Rutting
[ 42, 47, 6] 4.6 Right Rutting
[ 49, 54, 6] 104.3 Width of Left Rutting
[ 56, 61, 6] 174.8 Average Width
[ 63, 68, 6] 245.2 Width of Right Rutting
[ 70, 75, 6] 212 Cross section area of Left Rutting (mm2/in2)
[ 77, 82, 6] 947 Left + Right area
[ 84, 89, 6] 735 Cross section area of Right Rutting
```

High Definition Rutting Summary

Averages and statistics from all measurements taken over a larger segment.

The same layout is used for line 5428, which covers the whole file.

```
5413, 0.000000, 0.100000, 3.6, 4.1, 4.6, 104.3, 4.5, 245.2 ...
[ 28, 33, 6] 3.6 Left Rutting (mm/inches)
[ 35, 40, 6] 4.1 Average of Left and Right Rutting
[ 42, 47, 6] 4.6 Right Rutting
[ 49, 54, 6] 104.3 Width of Left Rutting
[ 56, 61, 6] 174.8 Average Width
[ 63, 68, 6] 245.2 Width of Right Rutting
[ 70, 75, 6] 212 Cross section area of Left Rutting (mm2/in2)
[ 77, 82, 6] 947 Left + Right area
[ 84, 89, 6] 735 Cross section area of Right Rutting
[ 91, 98, 8] 0.02 Left Levelling volume (m3/ft3)
[100,107, 8] 0.10 Left + Right volume
[109,116, 8] 0.07 Right Levelling volume
[118,123, 6] 1.2 Minimum Left Rutting
[125,130, 6] 1.2 Overall Minimum
[132,137, 6] 1.8 Minimum Right Rutting
[139,144, 6] 5.8 Maximum Left Rutting
[146,151, 6] 12.4 Overall Maximum
[153,158, 6] 12.4 Maximum Right Rutting
[160,165, 6] 3.1 STD of Left measurements
[167,172, 6] 4.5 STD of all measurements
[174,179, 6] 5.9 STD of Right measurements
```

High Definition Rutting Totals

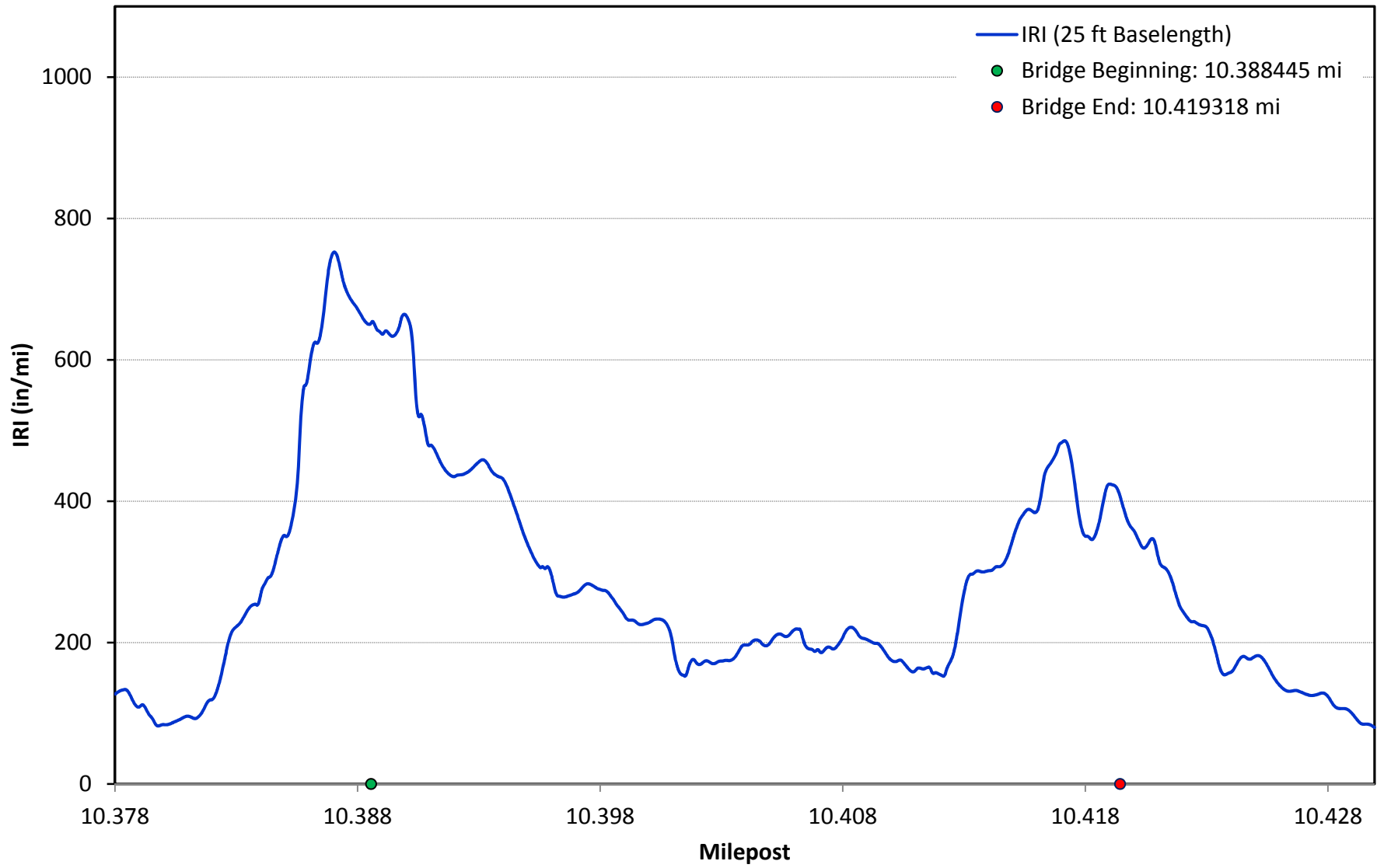
The last line contains averages and statistics from all measurements taken (the whole file)

```
5428, 0.000000, 1.79000, 3.6, 4.1, 4.6, 104.3, 4.5, 245.2 ...
Same layout as lines 5413
```

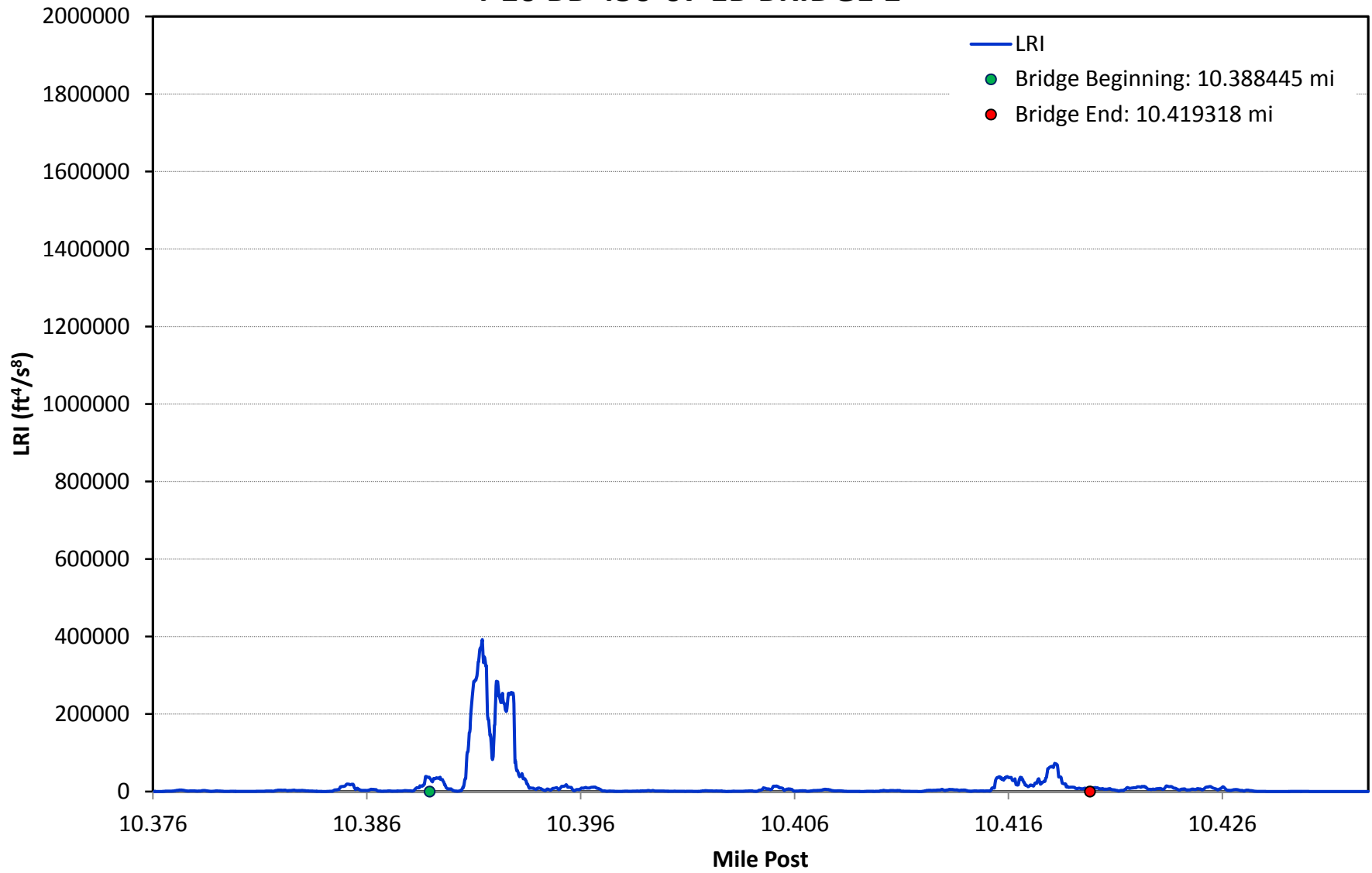

APPENDIX B

IRI_{25-ft} and LRI_{PS} Curve Summaries

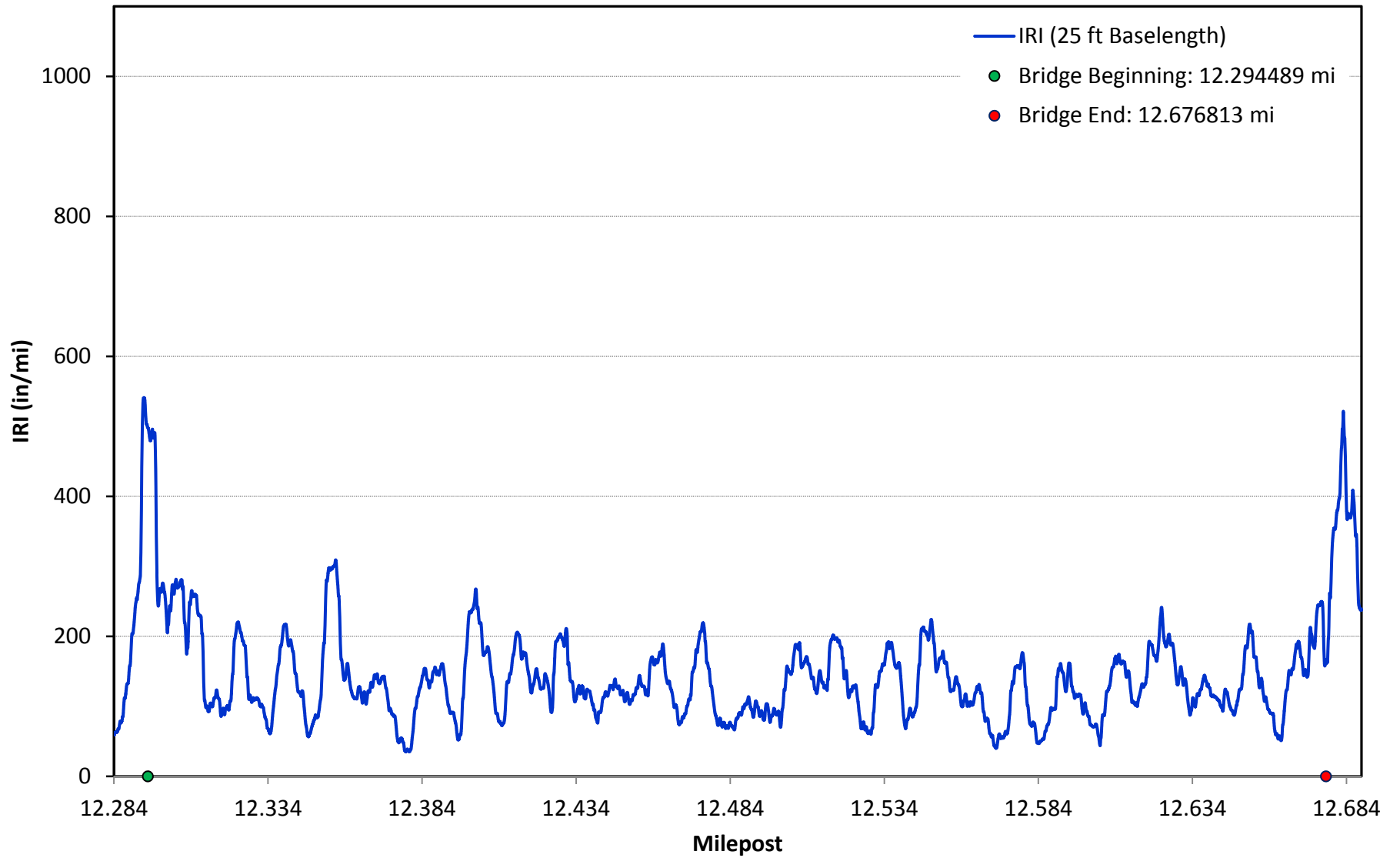
I-10 BB 450-07 EB BRIDGE 1



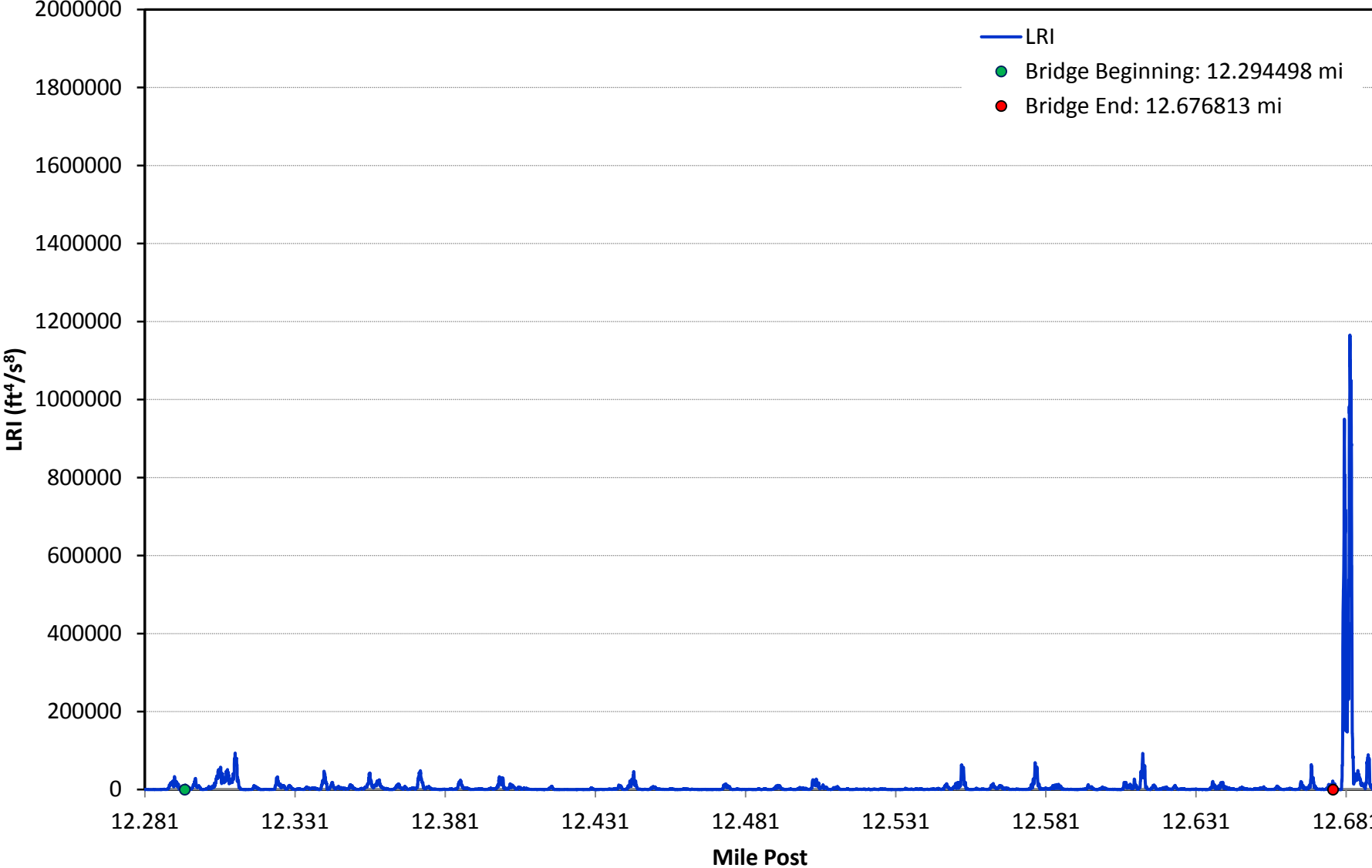
I-10 BB 450-07 EB BRIDGE 1



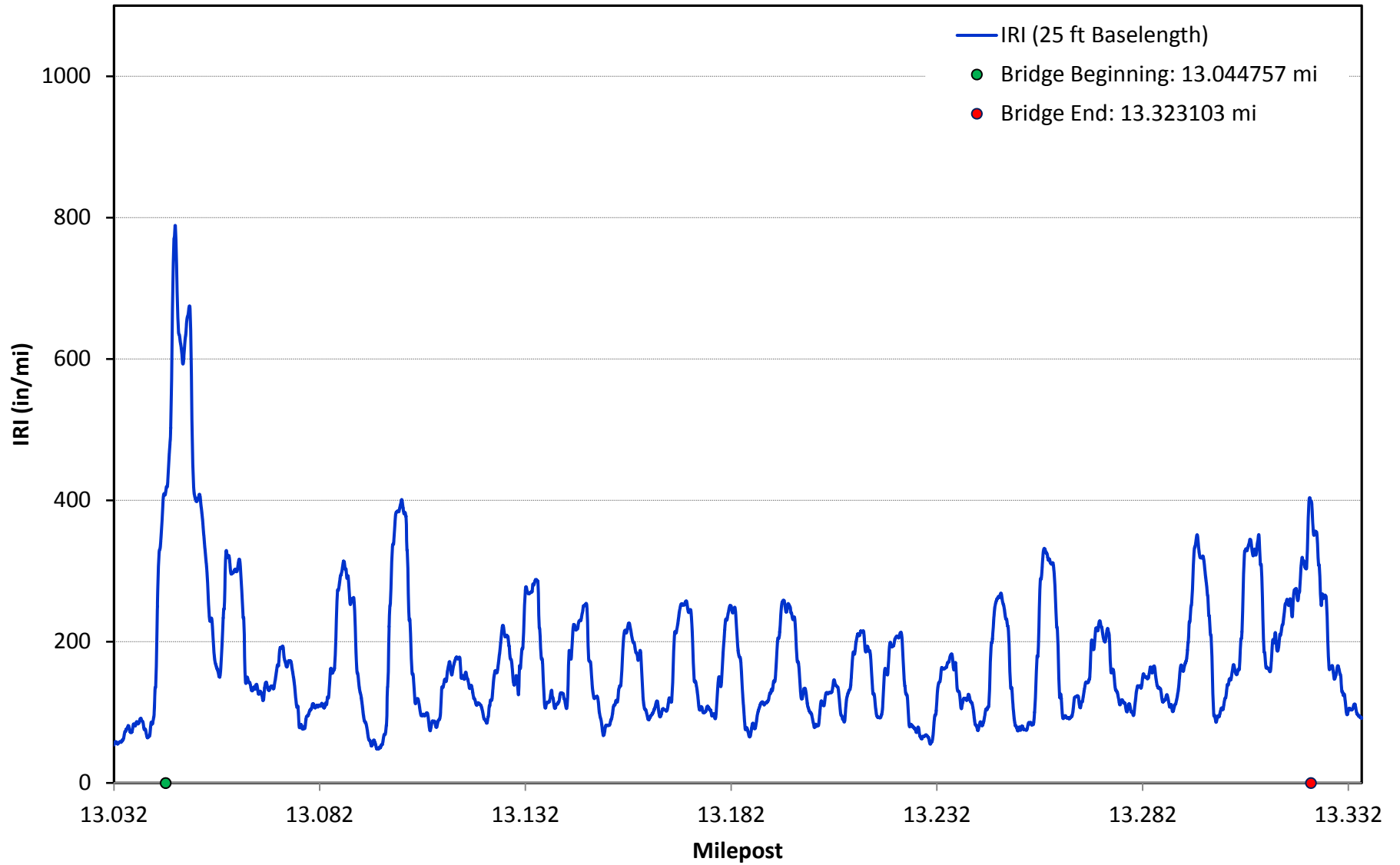
I-10 BB 450-07 EB BRIDGE 2



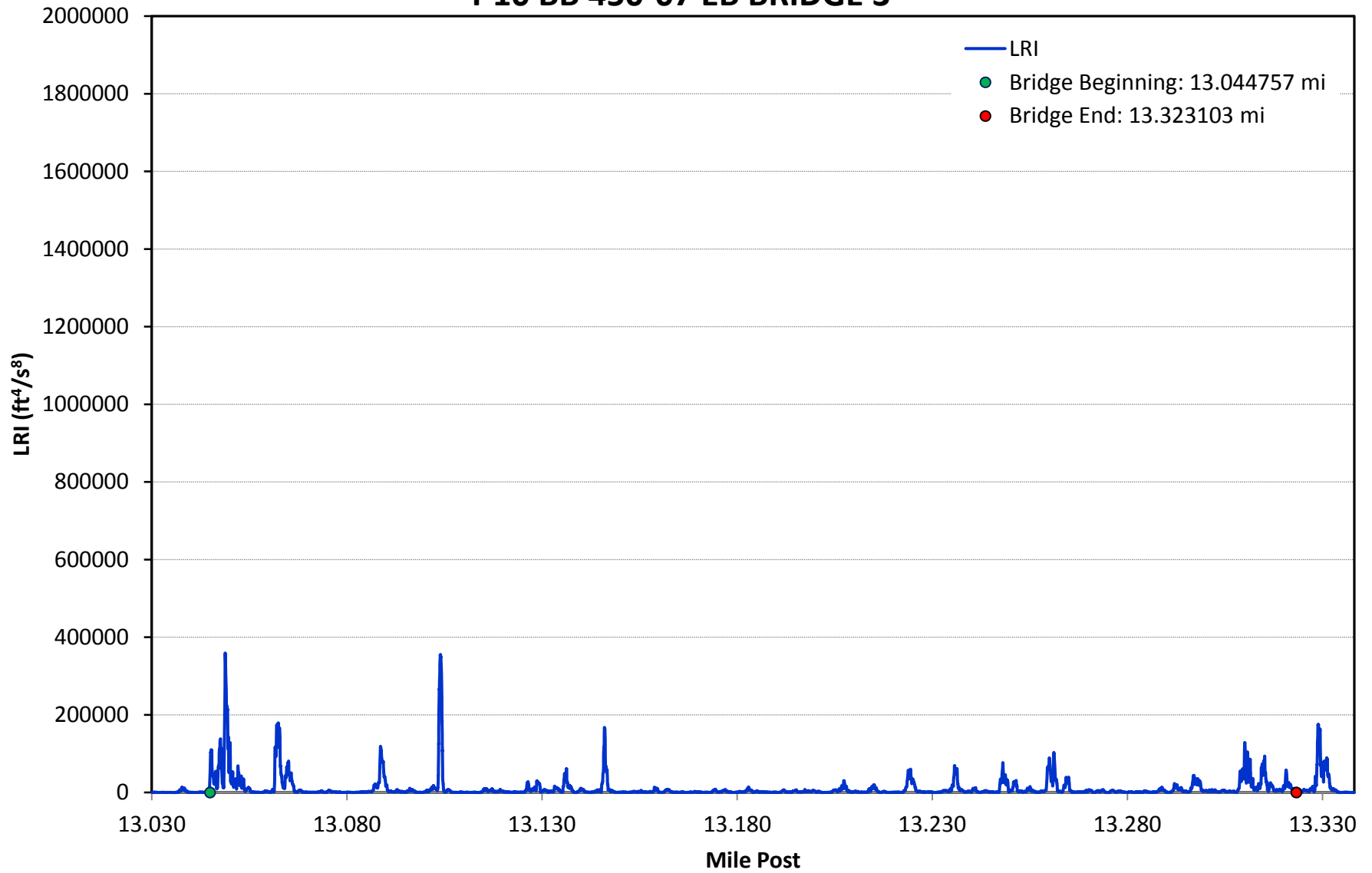
I-10 BB 450-07 EB BRIDGE 2



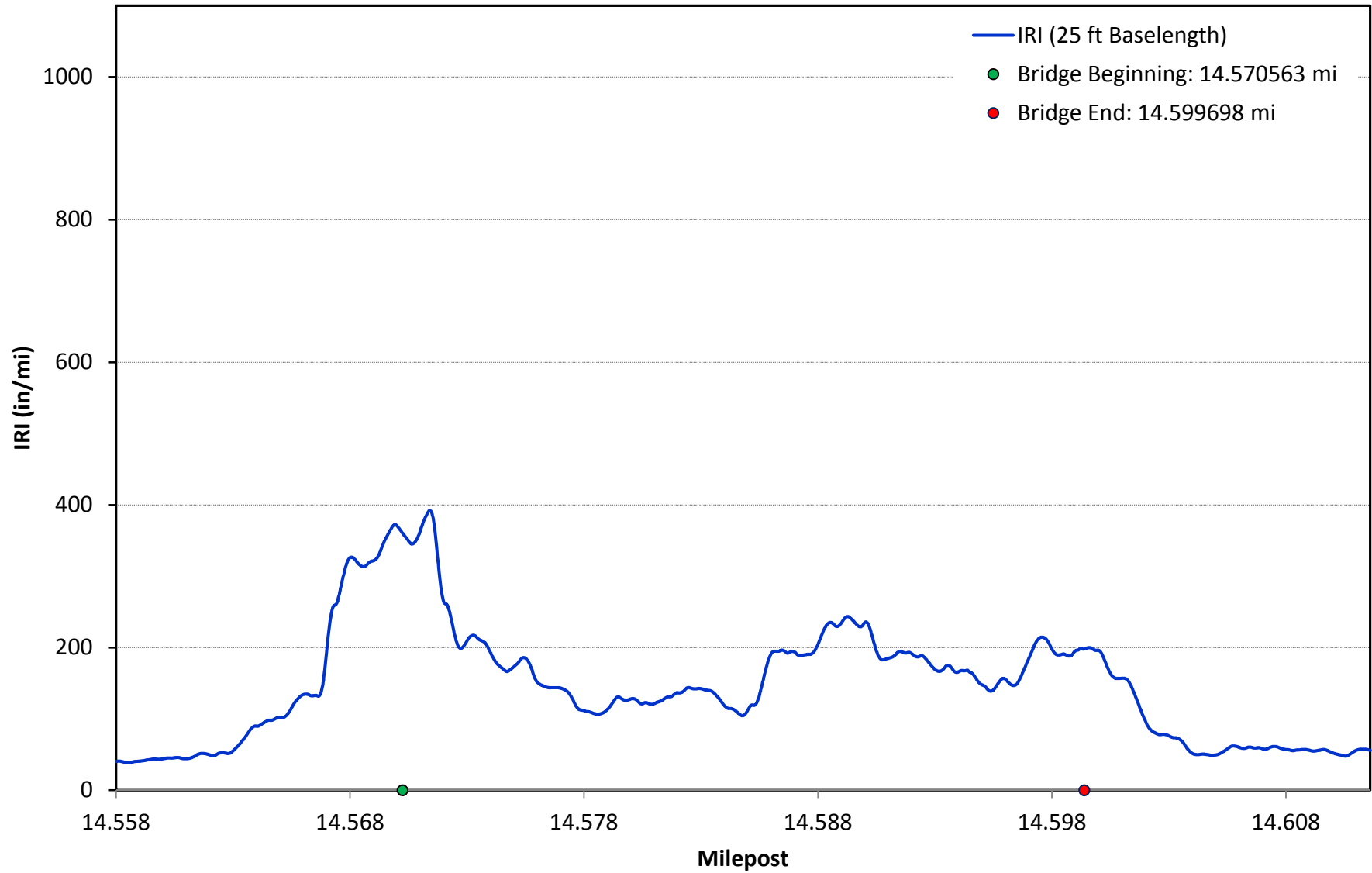
I-10 BB 450-07 EB BRIDGE 3



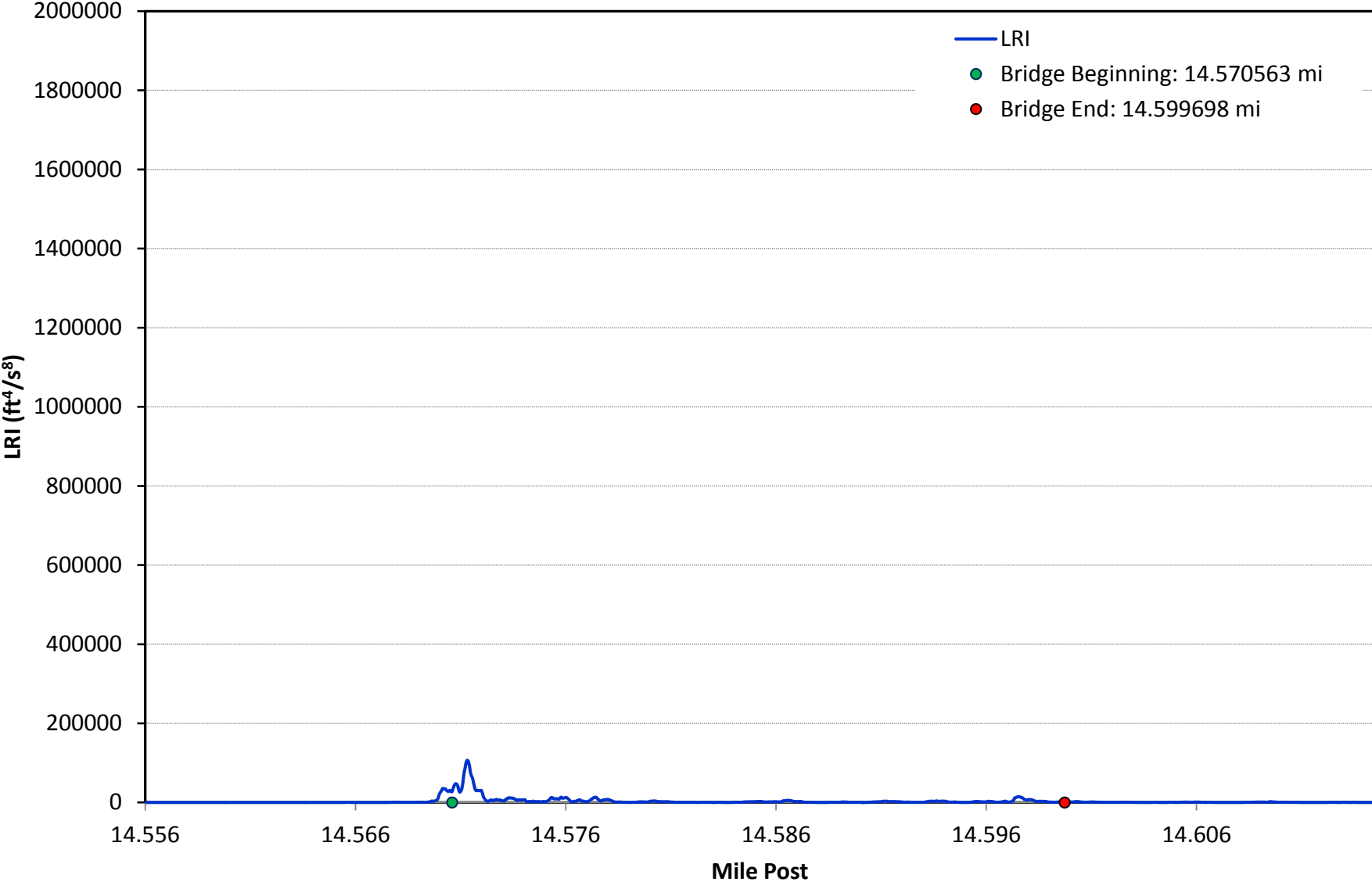
I-10 BB 450-07 EB BRIDGE 3



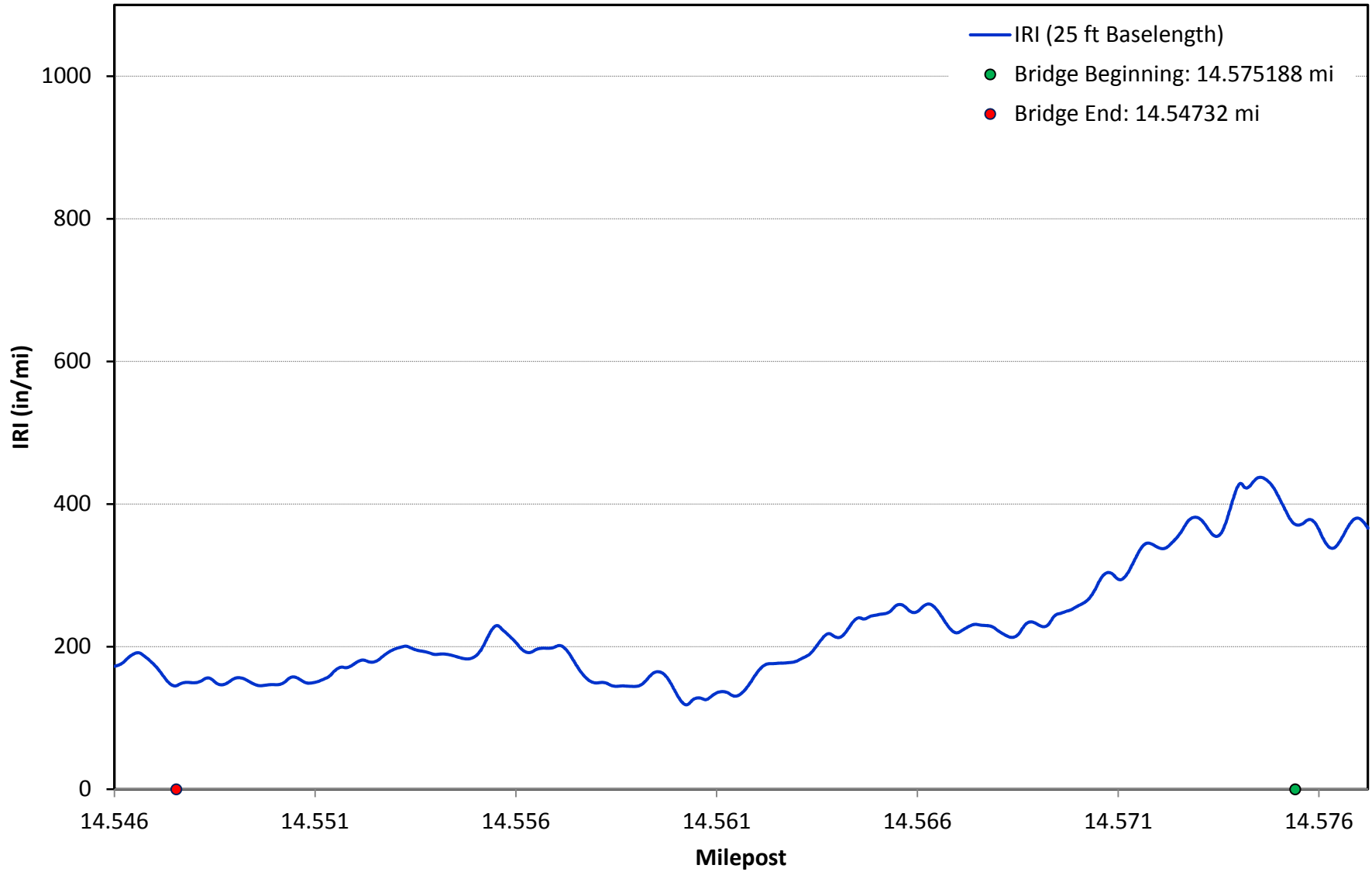
I-10 BB 450-07 EB BRIDGE 4



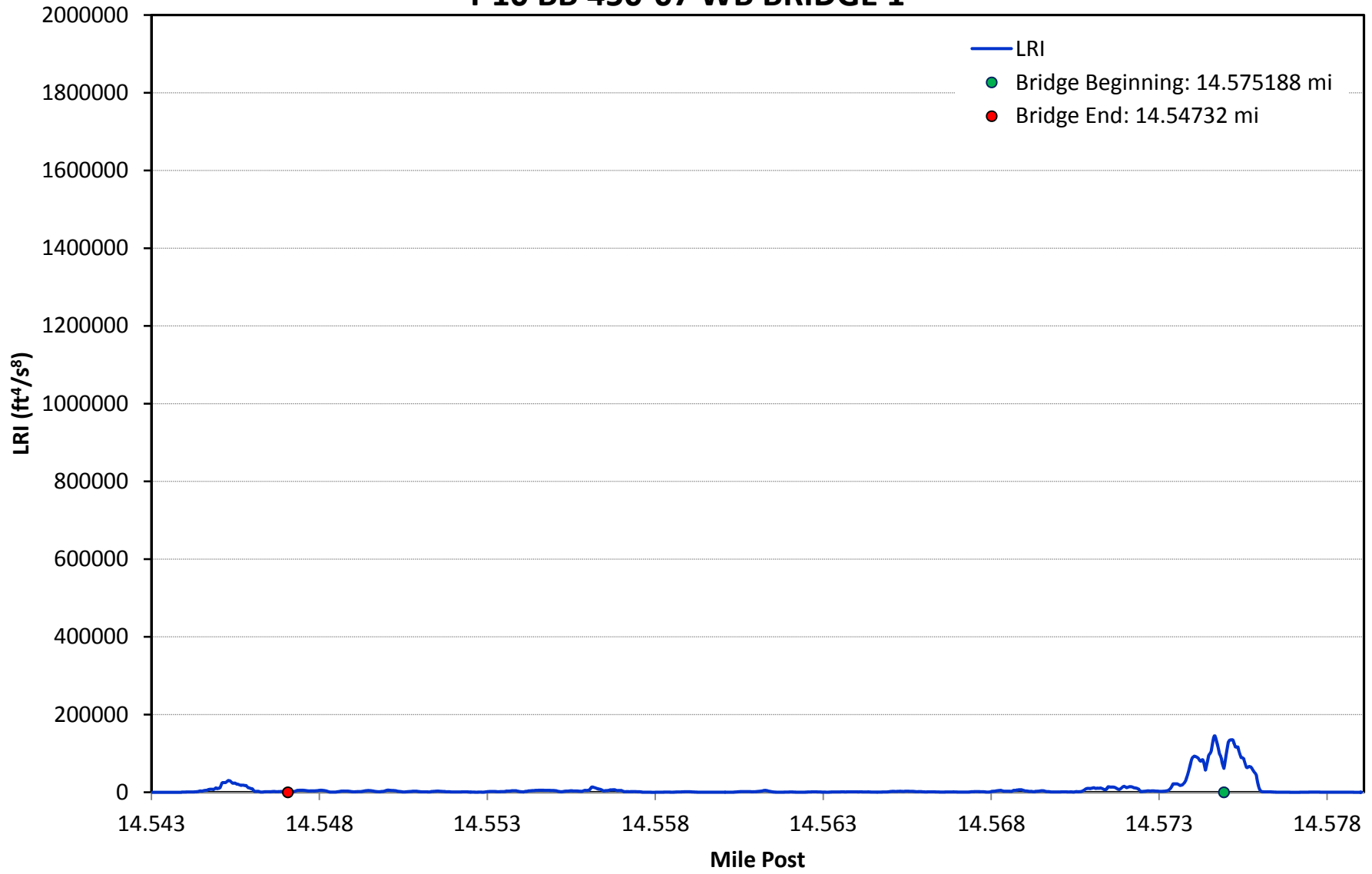
I-10 BB 450-07 EB BRIDGE 4



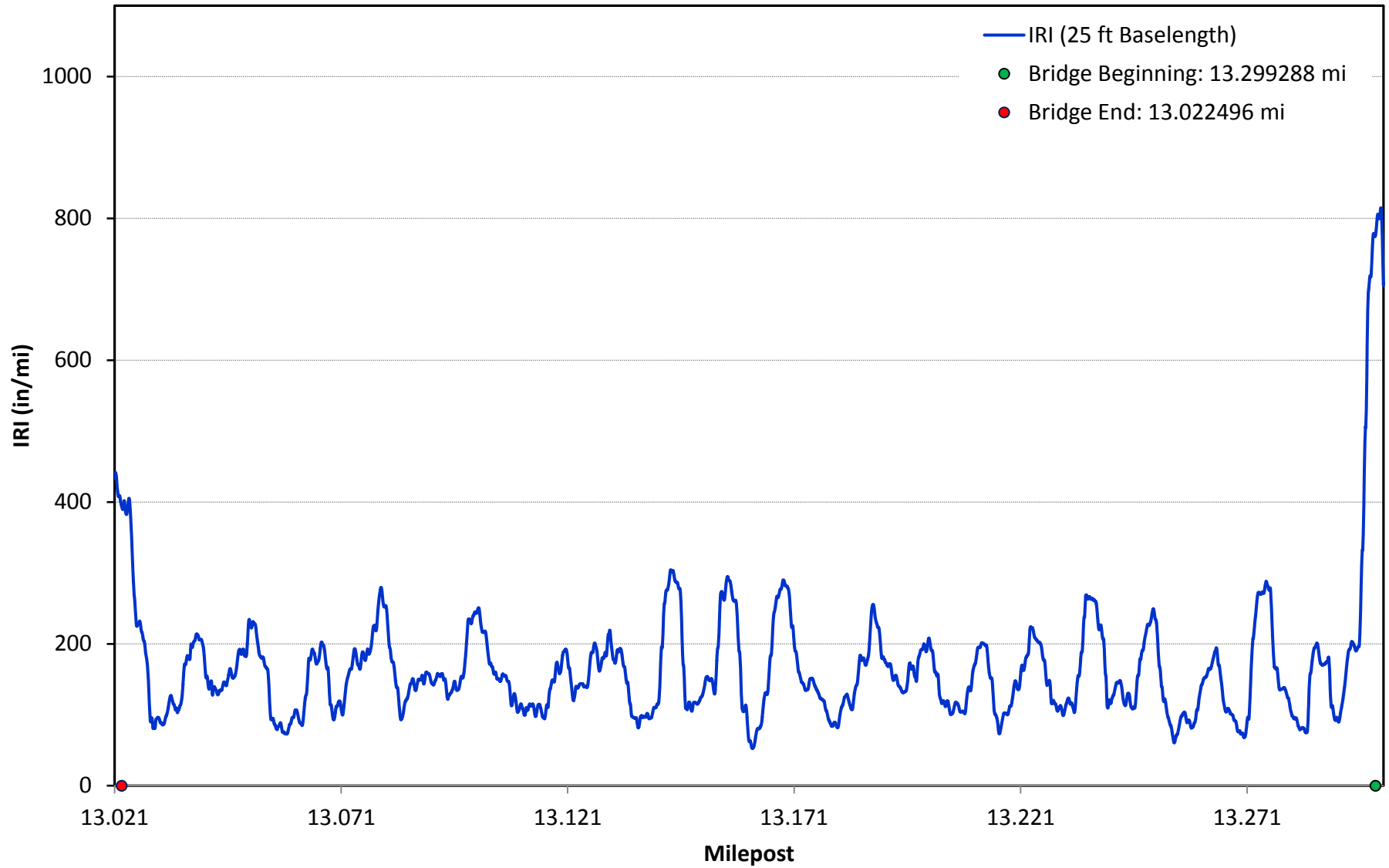
I-10 BB 450-07 WB BRIDGE 1



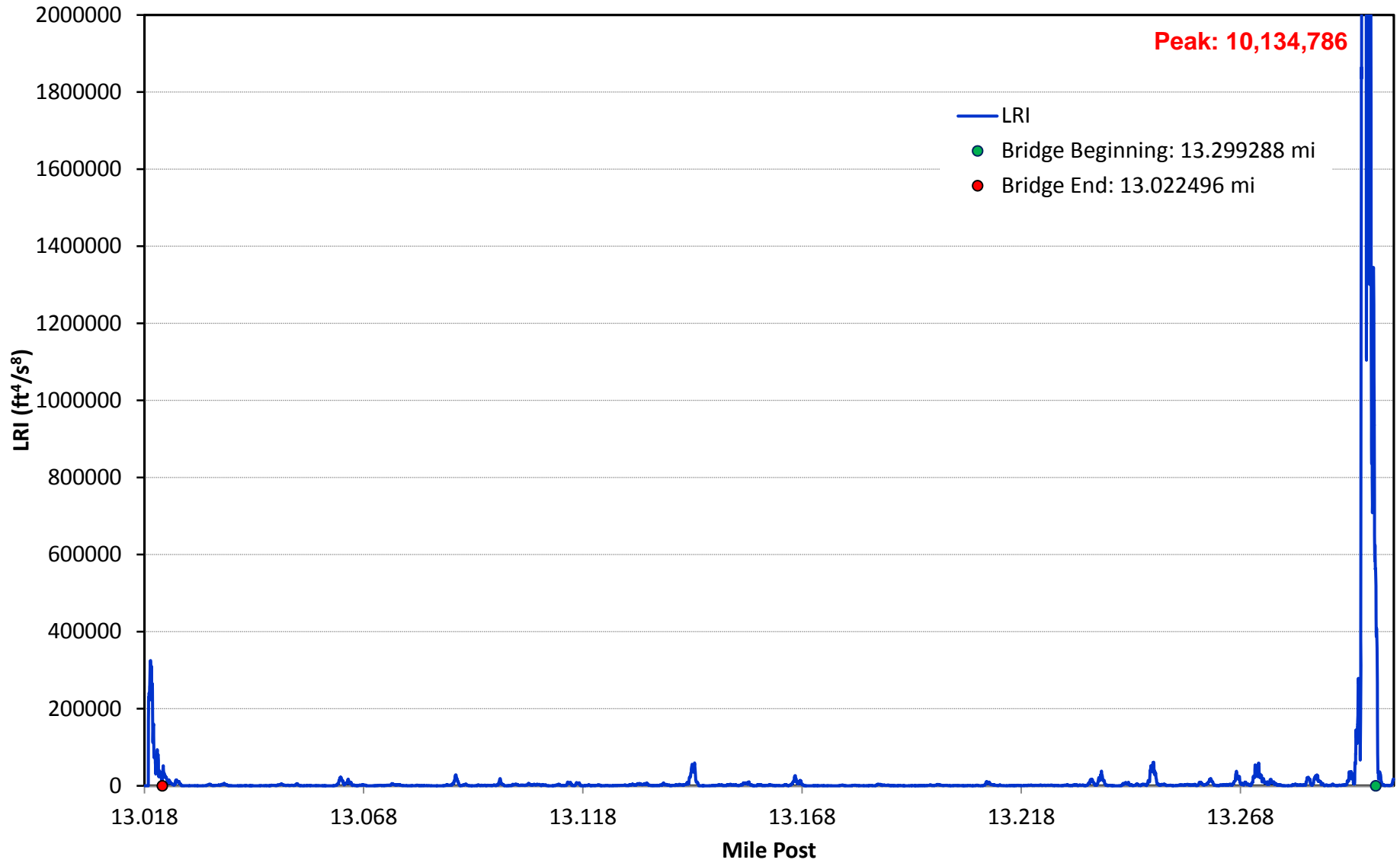
I-10 BB 450-07 WB BRIDGE 1



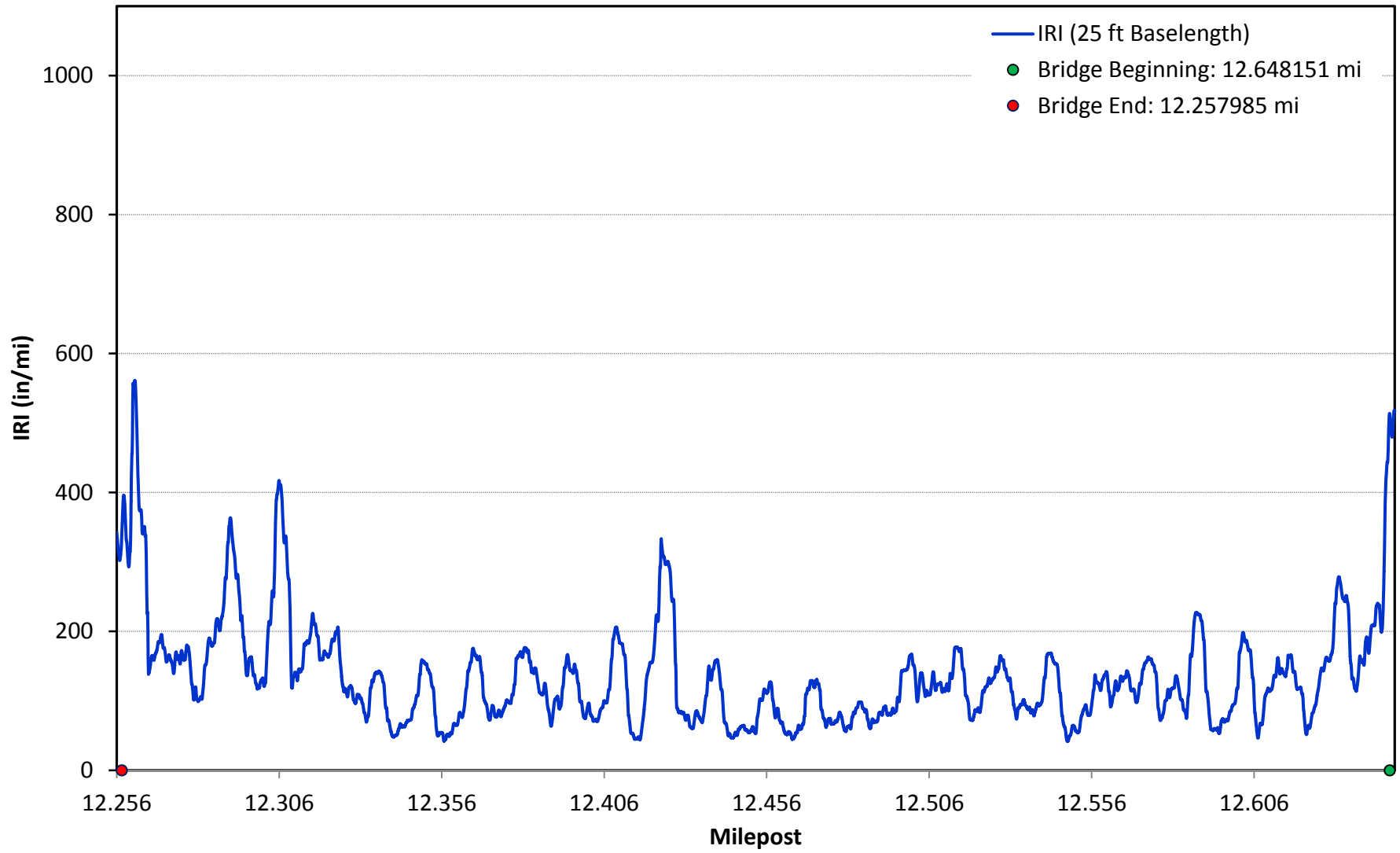
I-10 BB 450-07 WB BRIDGE 2



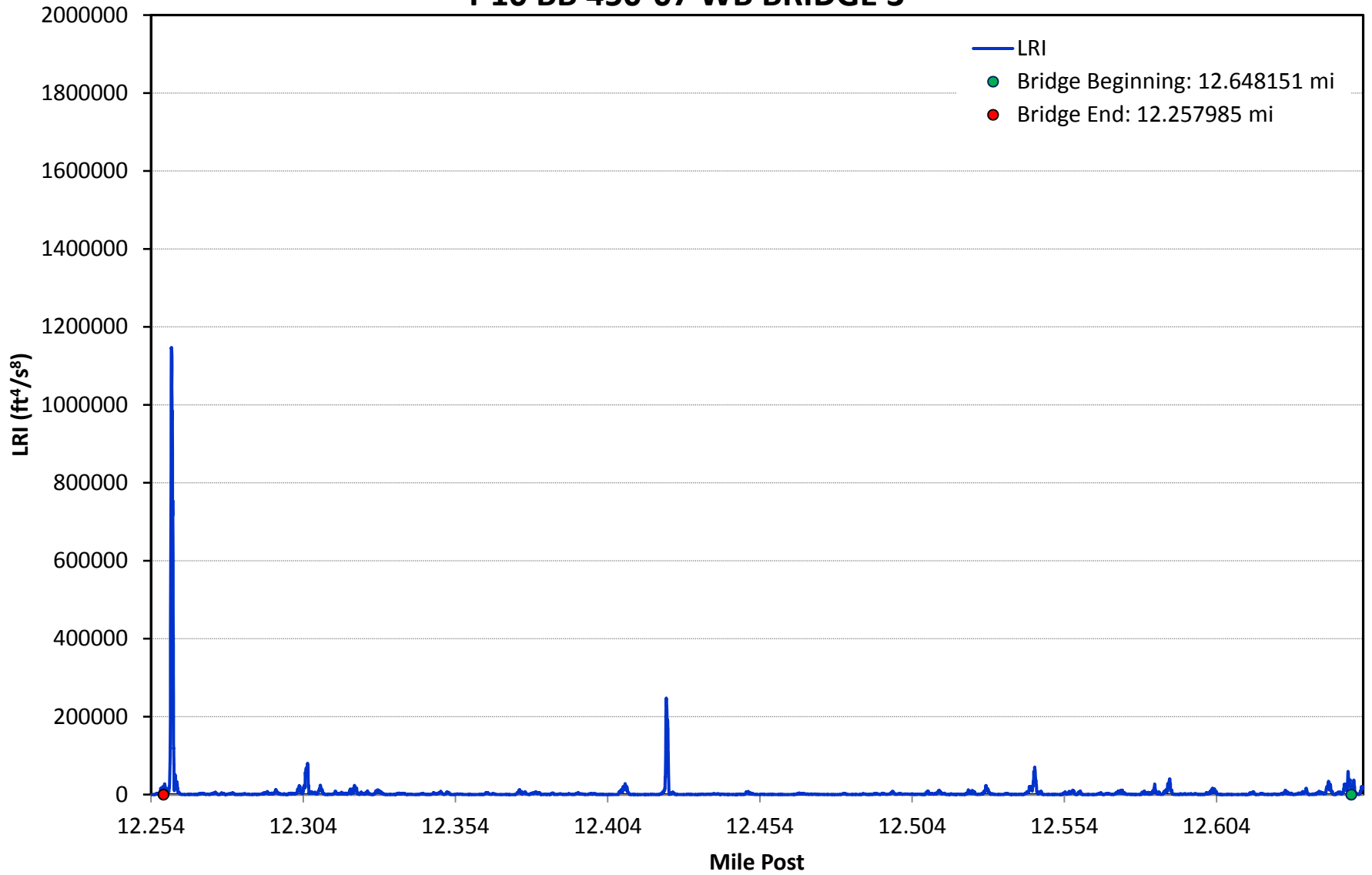
I-10 BB 450-07 WB BRIDGE 2



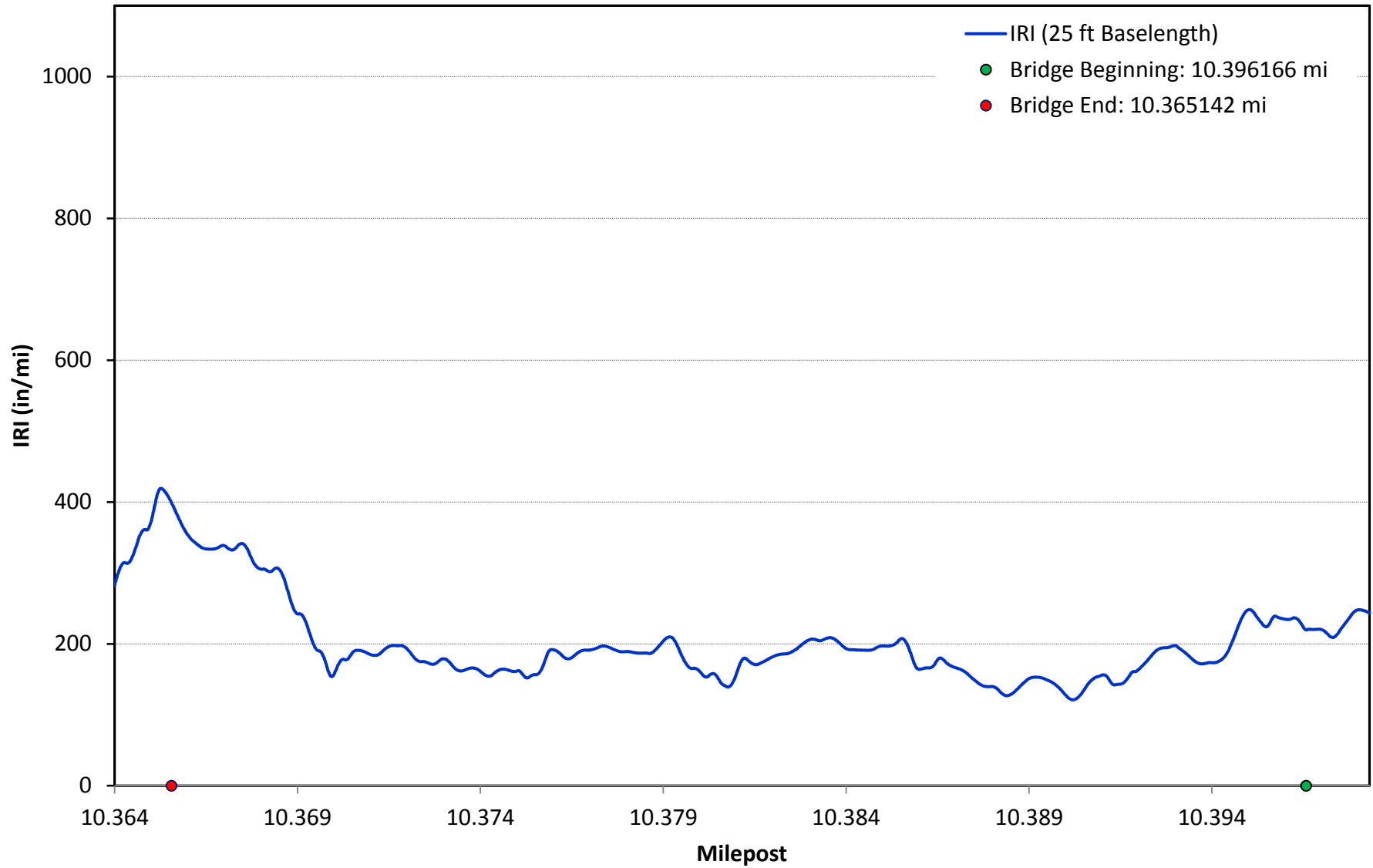
I-10 BB 450-07 WB BRIDGE 3



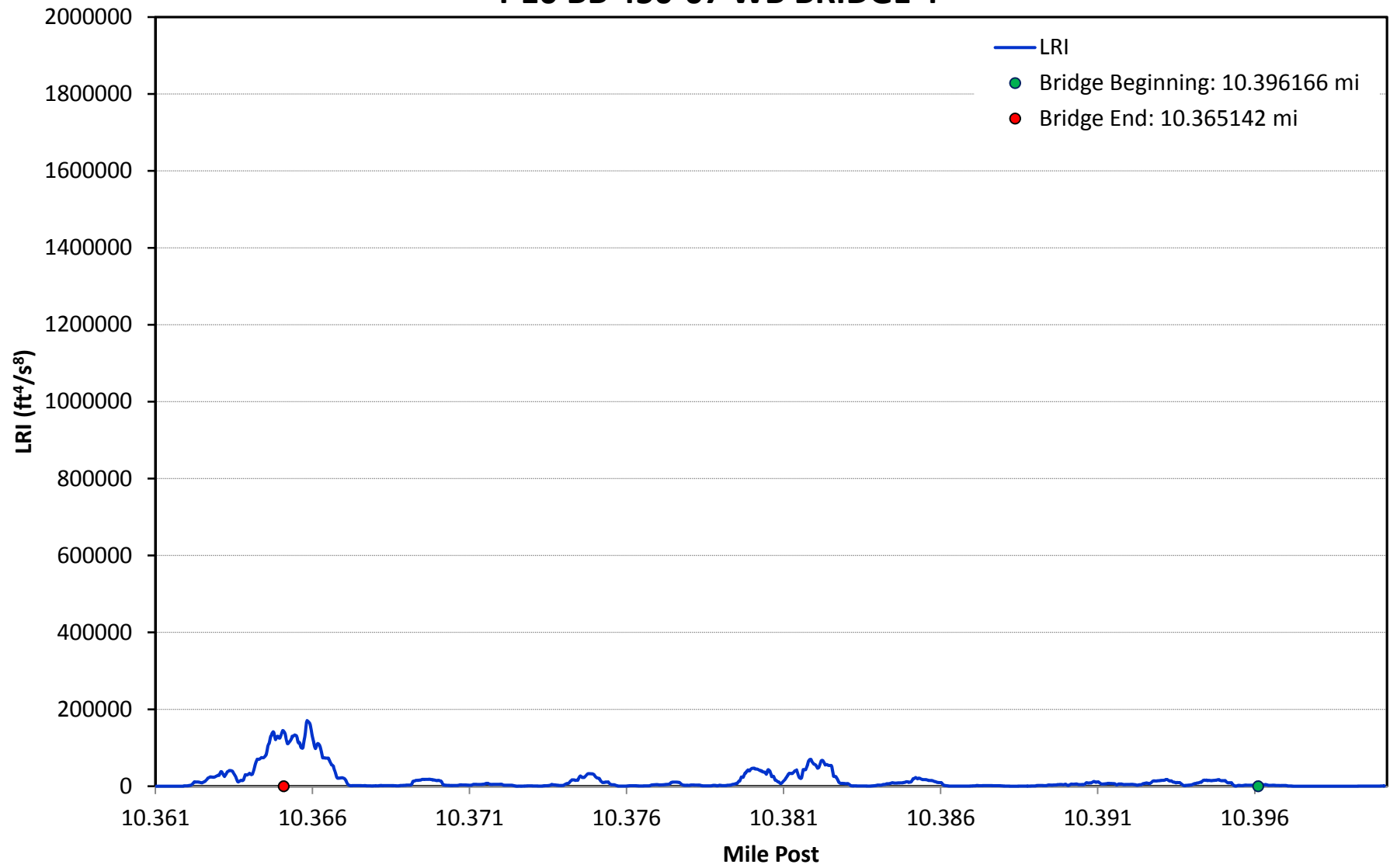
I-10 BB 450-07 WB BRIDGE 3



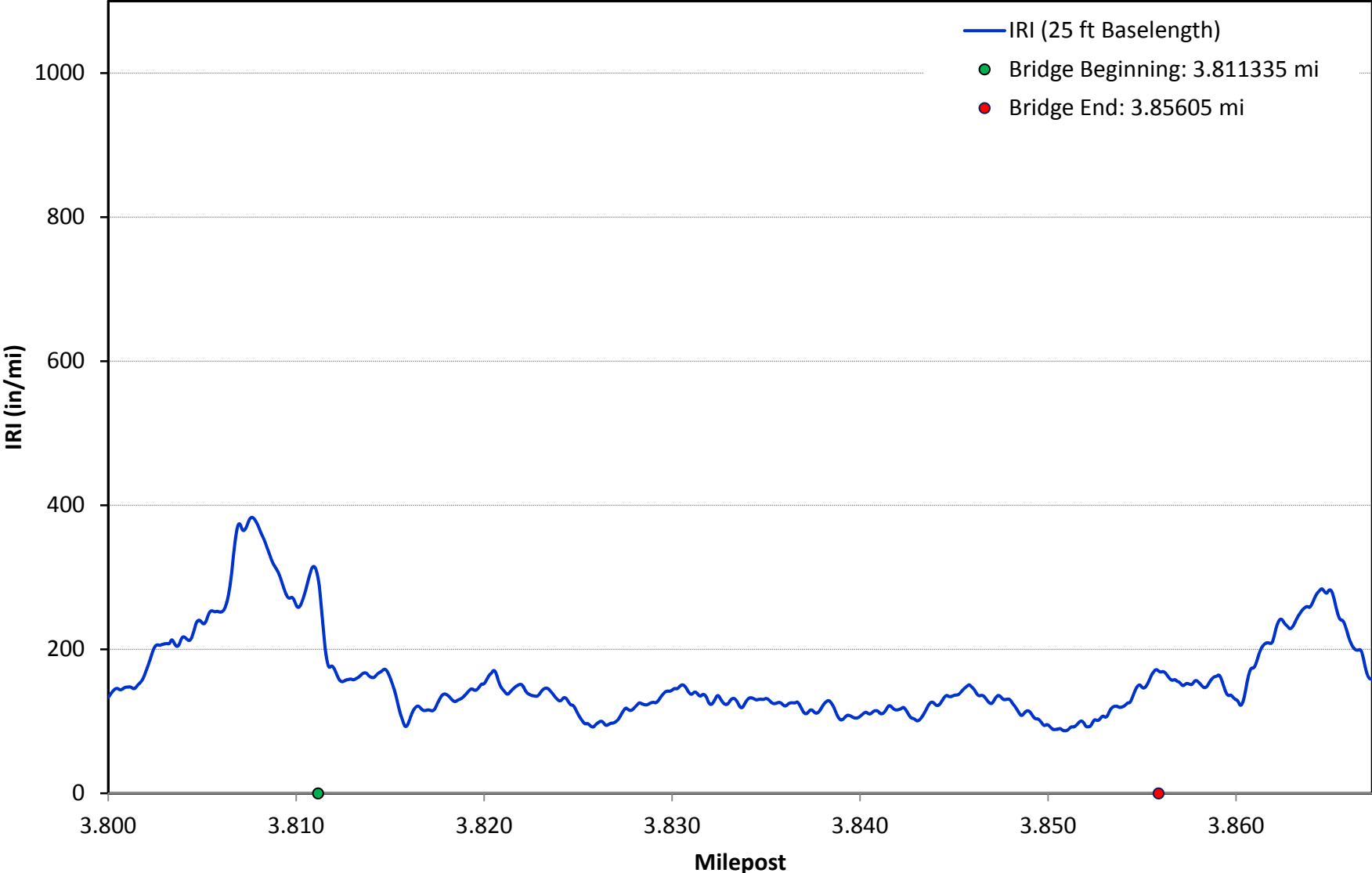
I-10 BB 450-07 WB BRIDGE 4



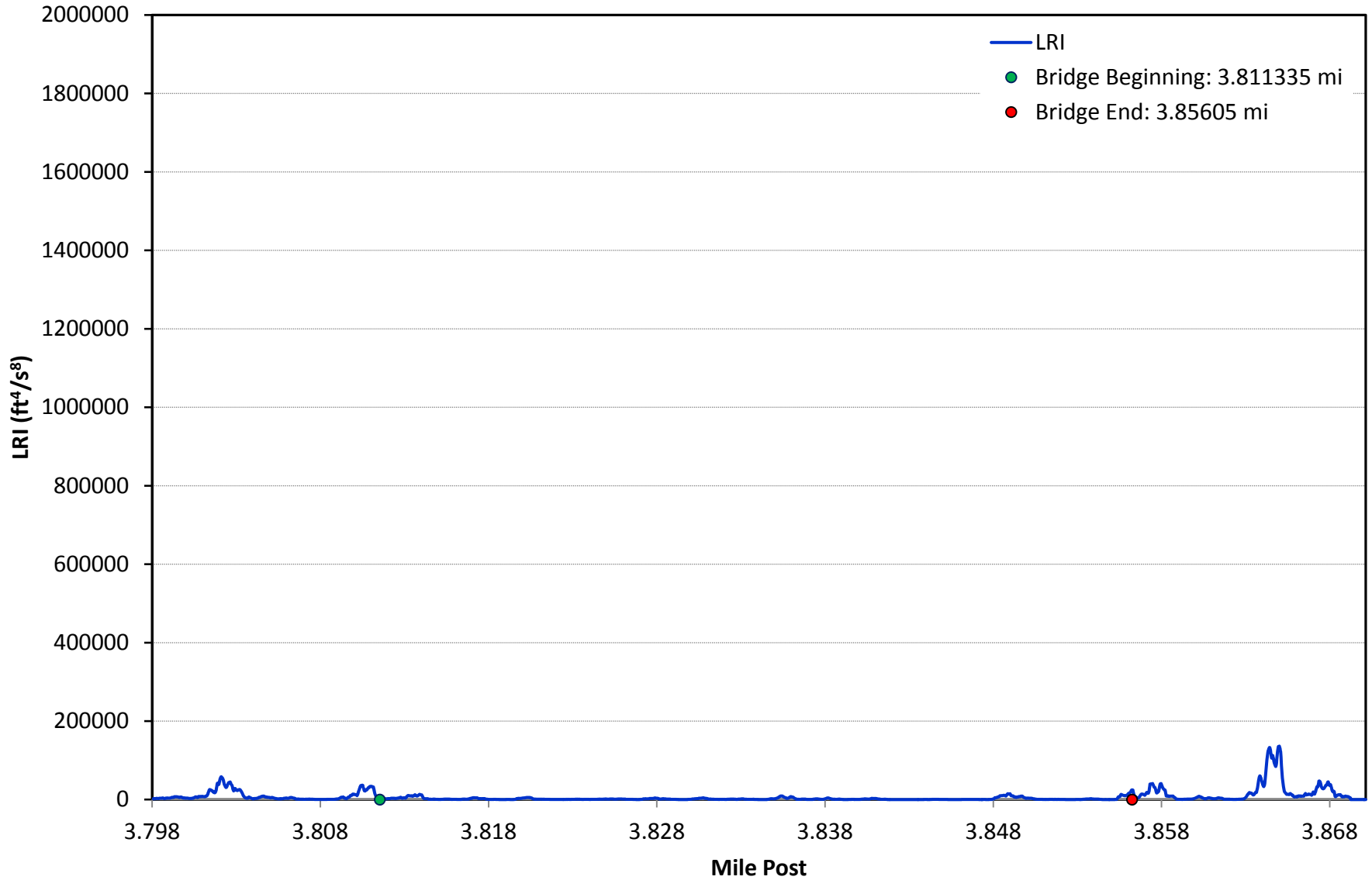
I-10 BB 450-07 WB BRIDGE 4



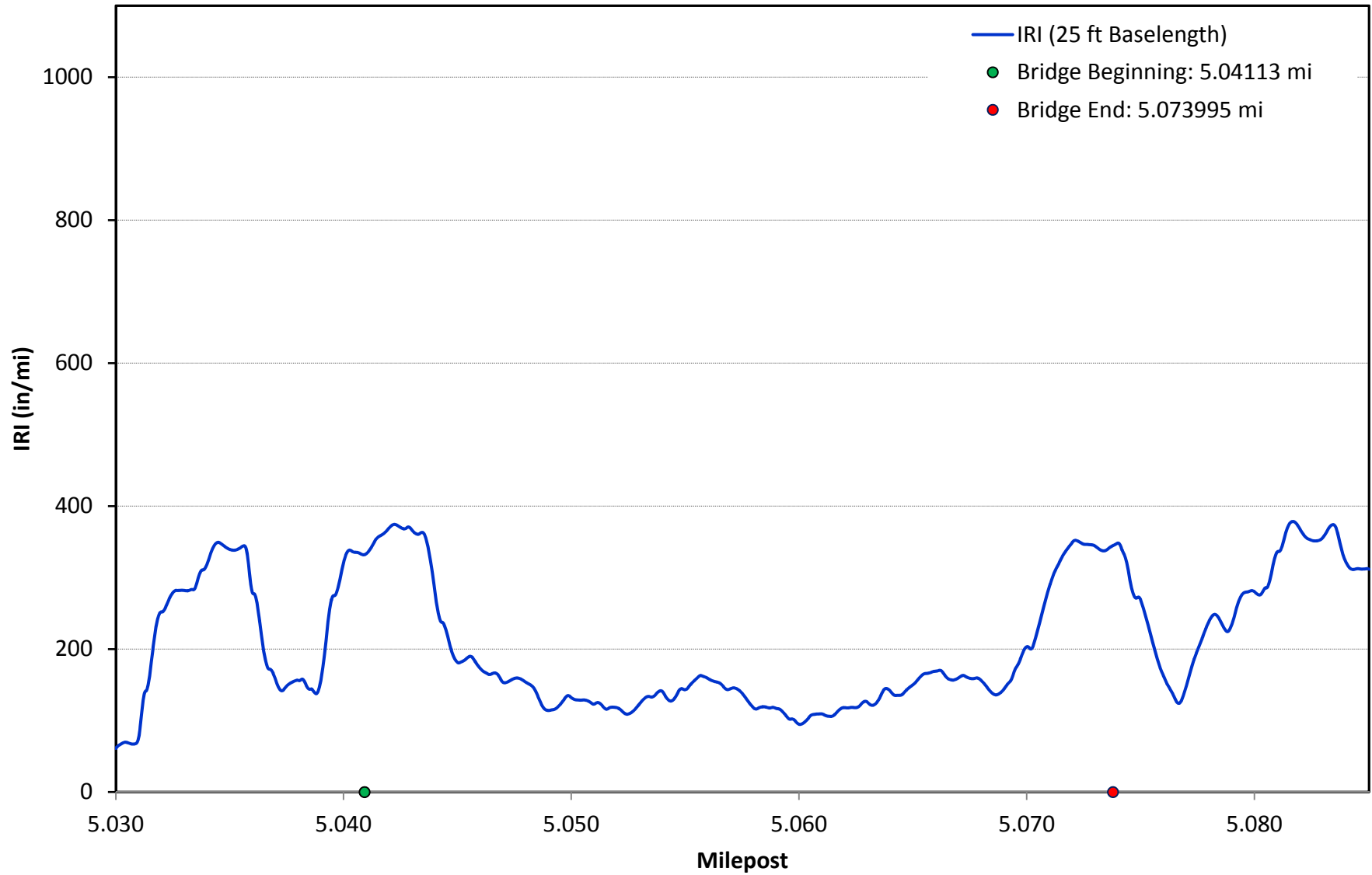
I-10 BB 450-08 EB BRIDGE 1



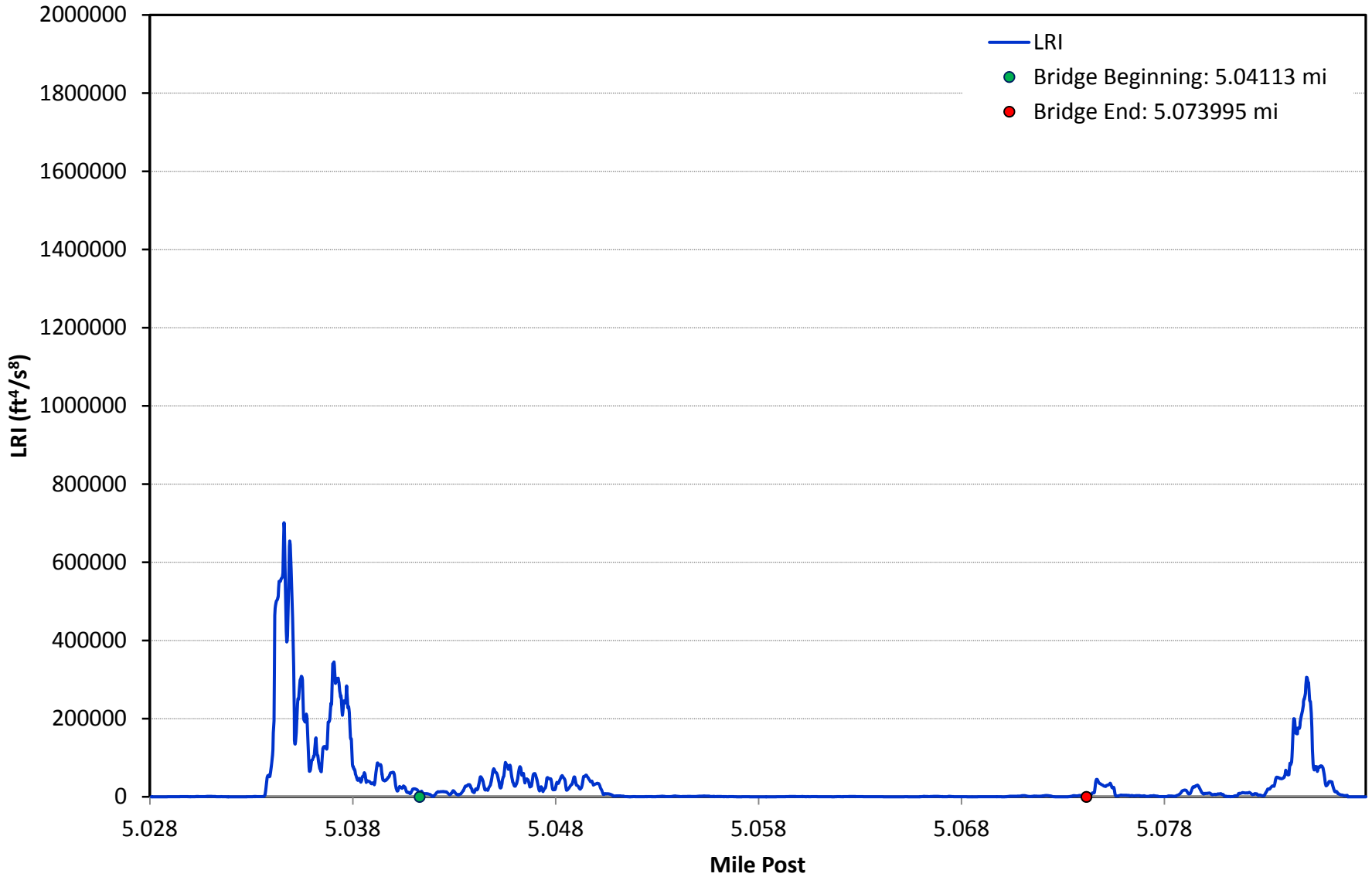
I-10 BB 450-08 EB BRIDGE 1



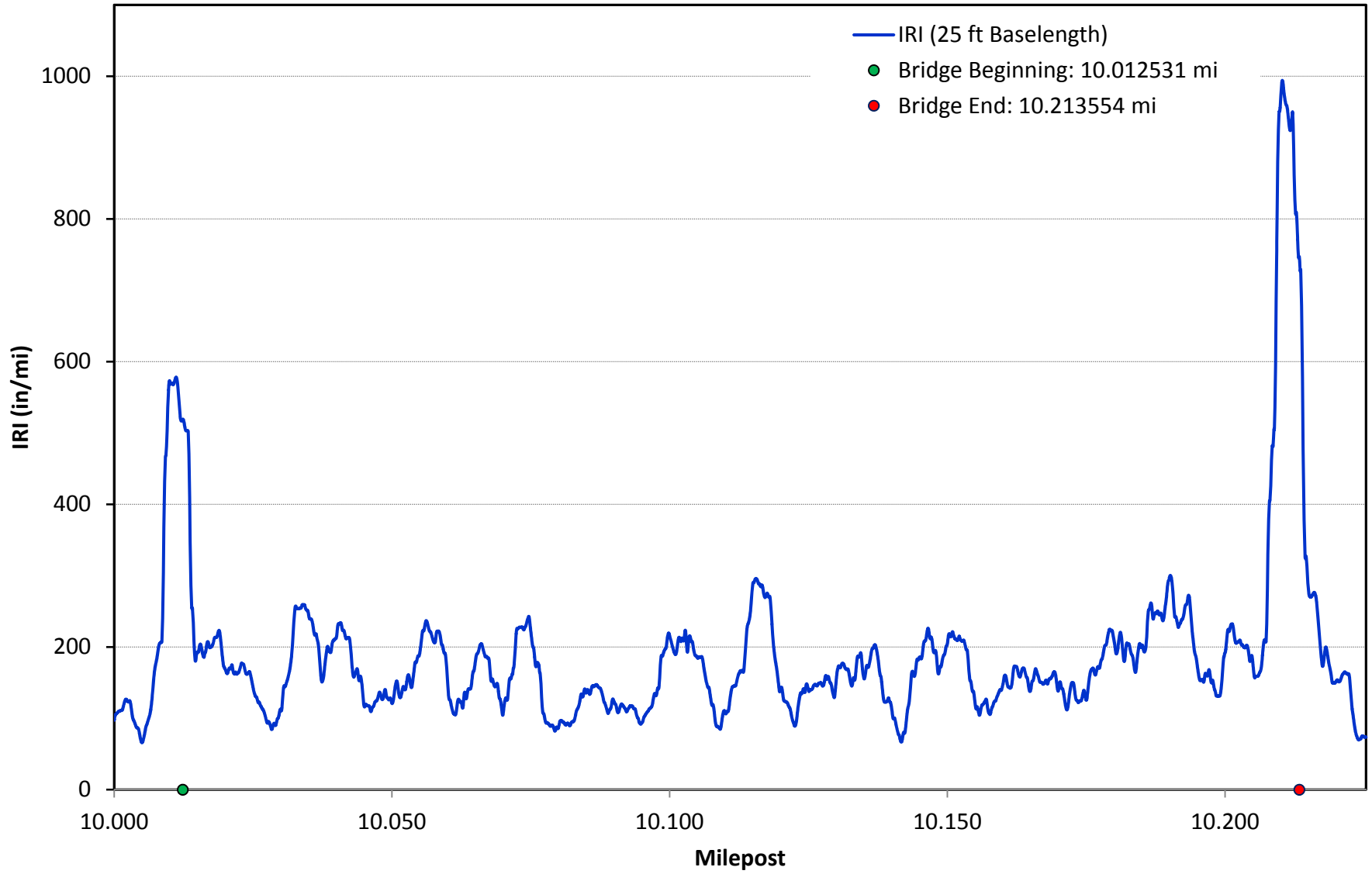
I-10 BB 450-08 EB BRIDGE 2



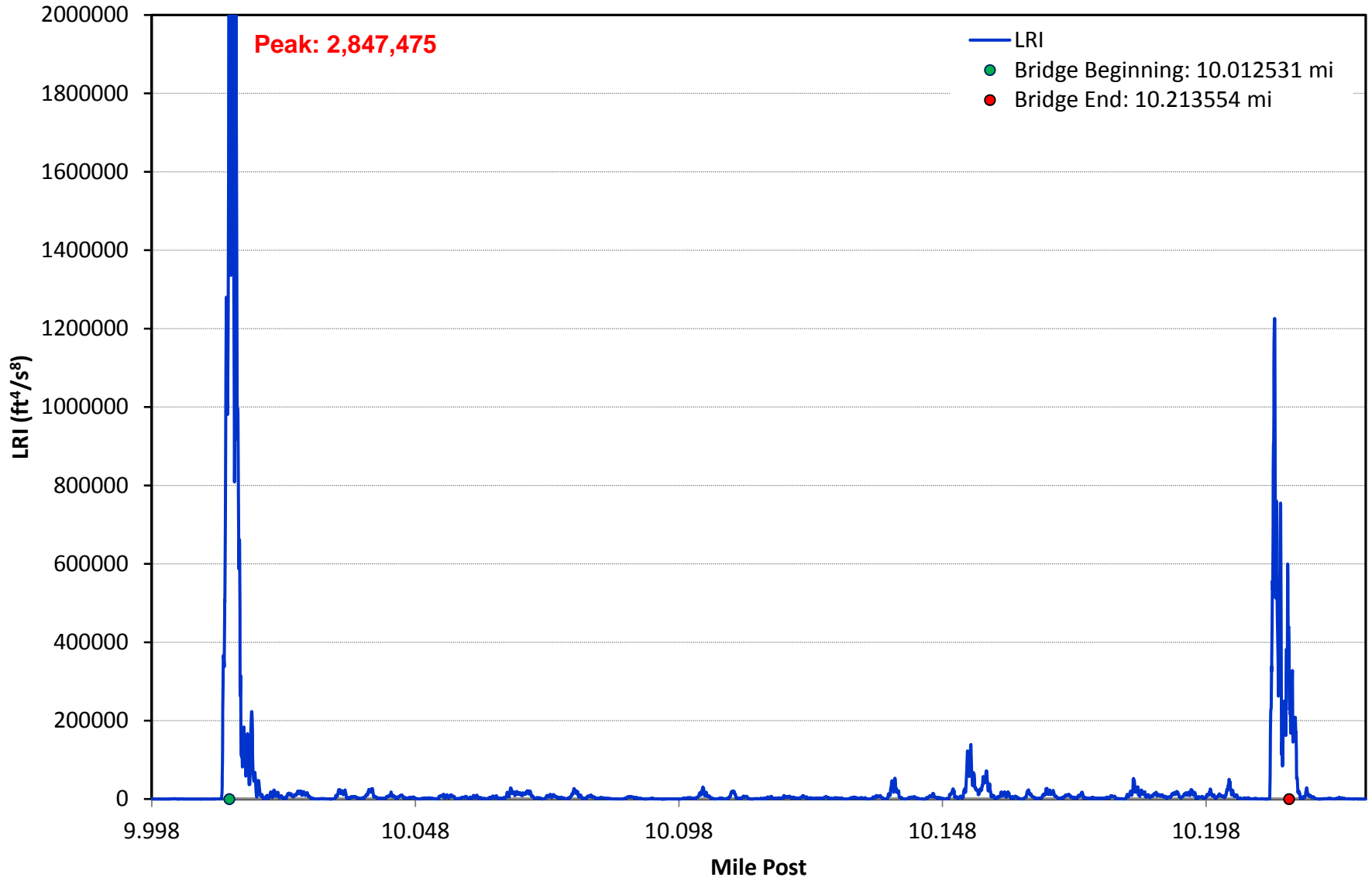
I-10 BB 450-08 EB BRIDGE 2



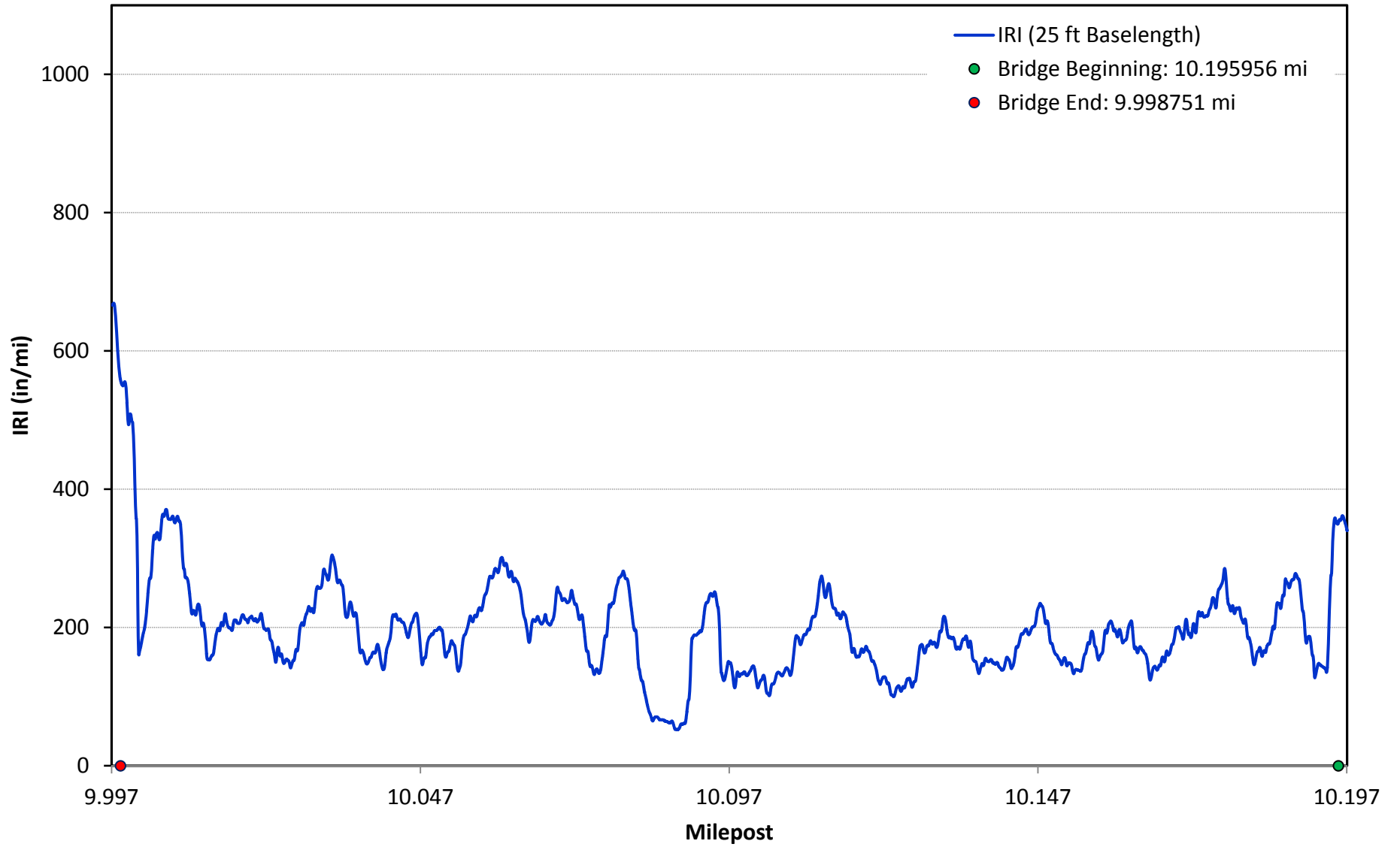
I-10 BB 450-08 EB BRIDGE 3



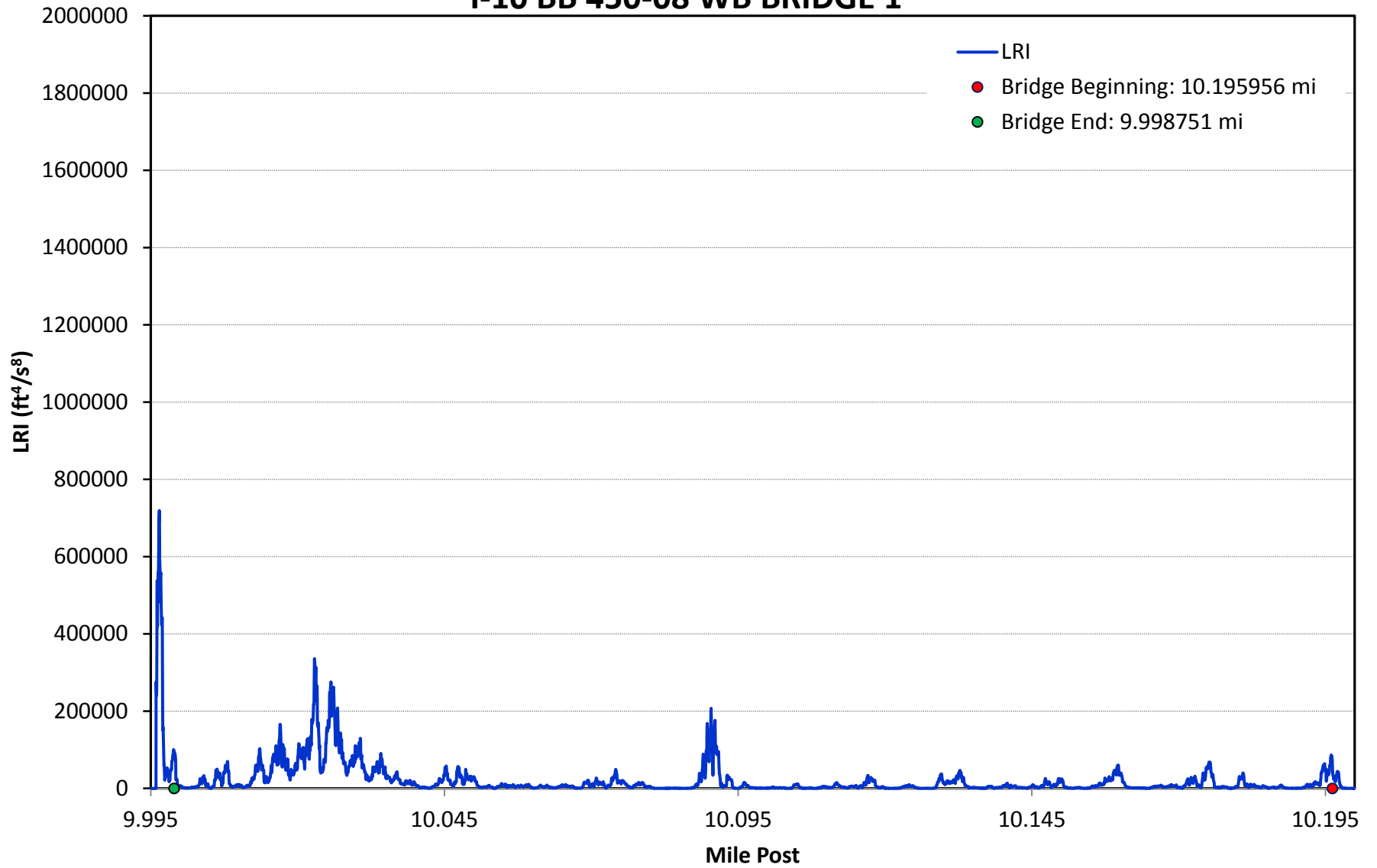
I-10 BB 450-08 EB BRIDGE 3



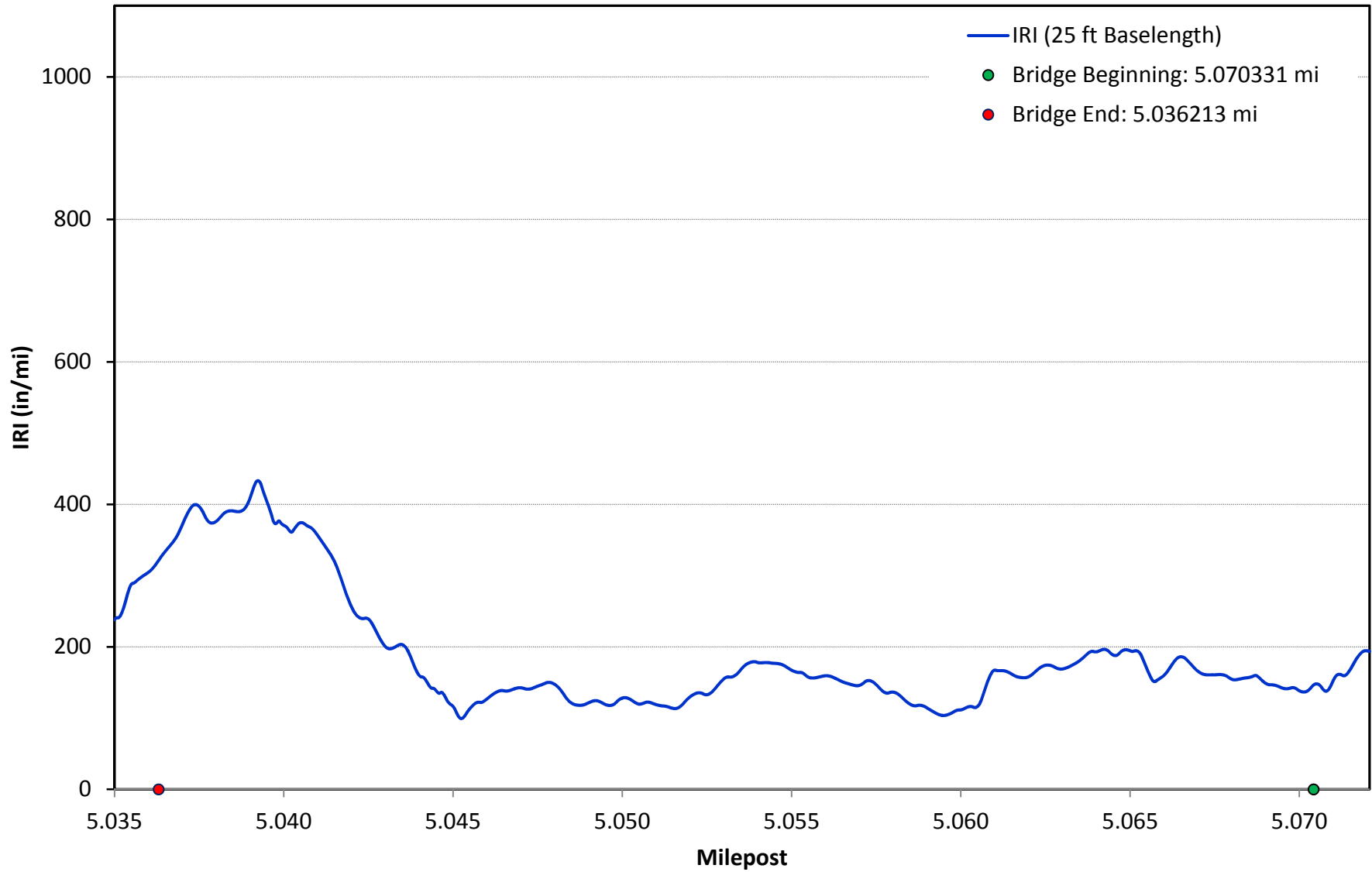
I-10 BB 450-08 WB BRDIGE 1



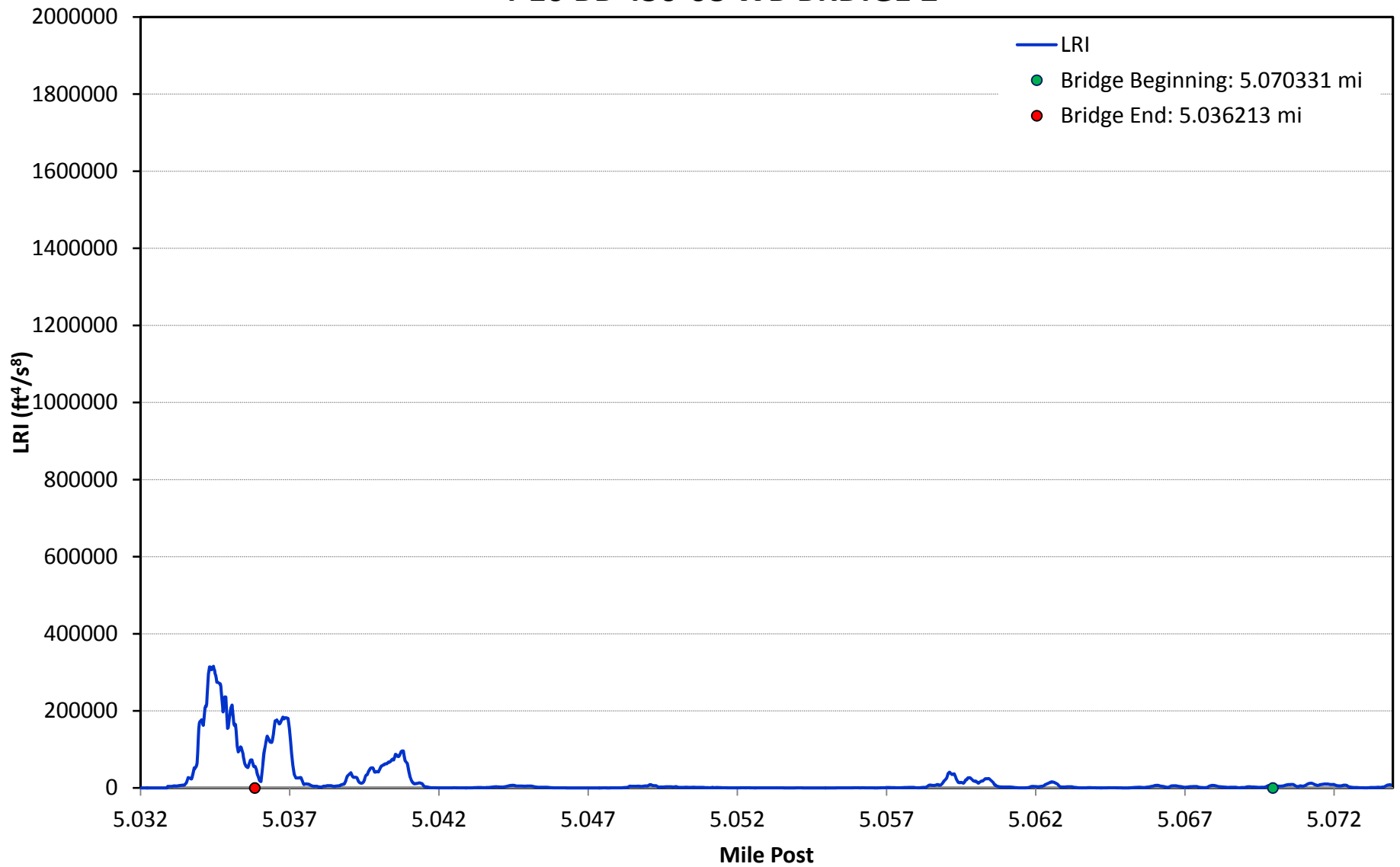
I-10 BB 450-08 WB BRIDGE 1



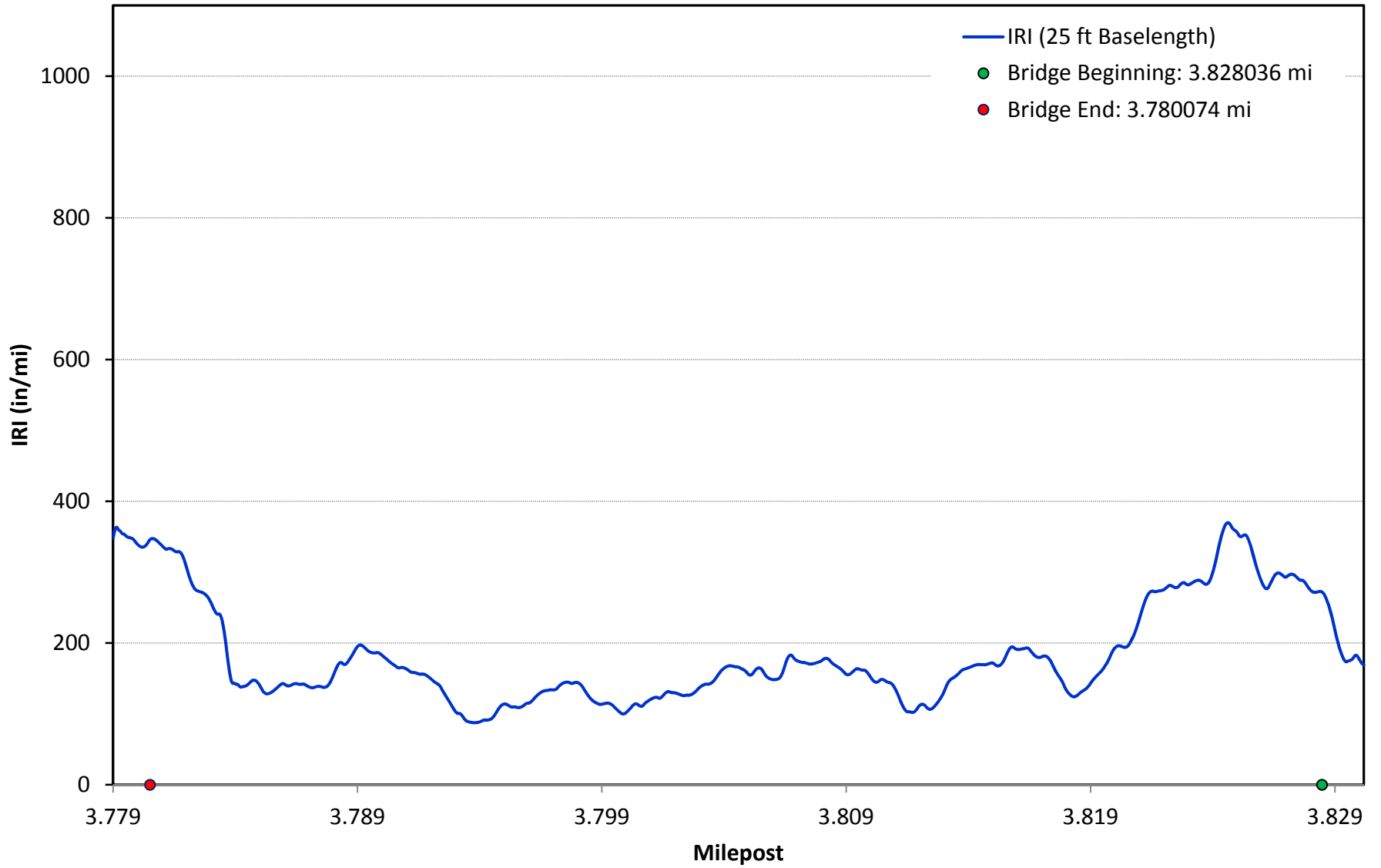
I-10 BB 450-08 WB BRIDGE 2



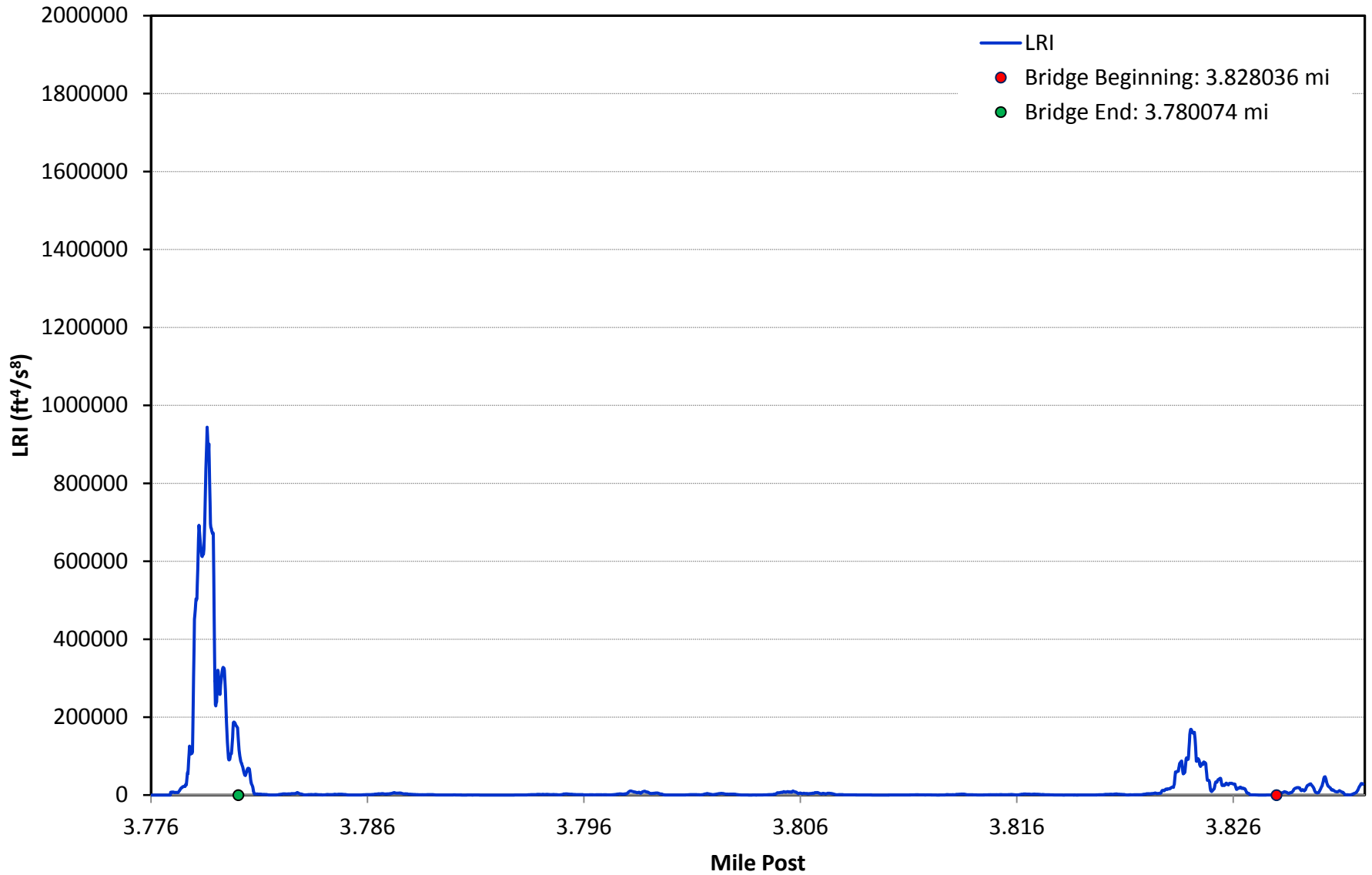
I-10 BB 450-08 WB BRIDGE 2



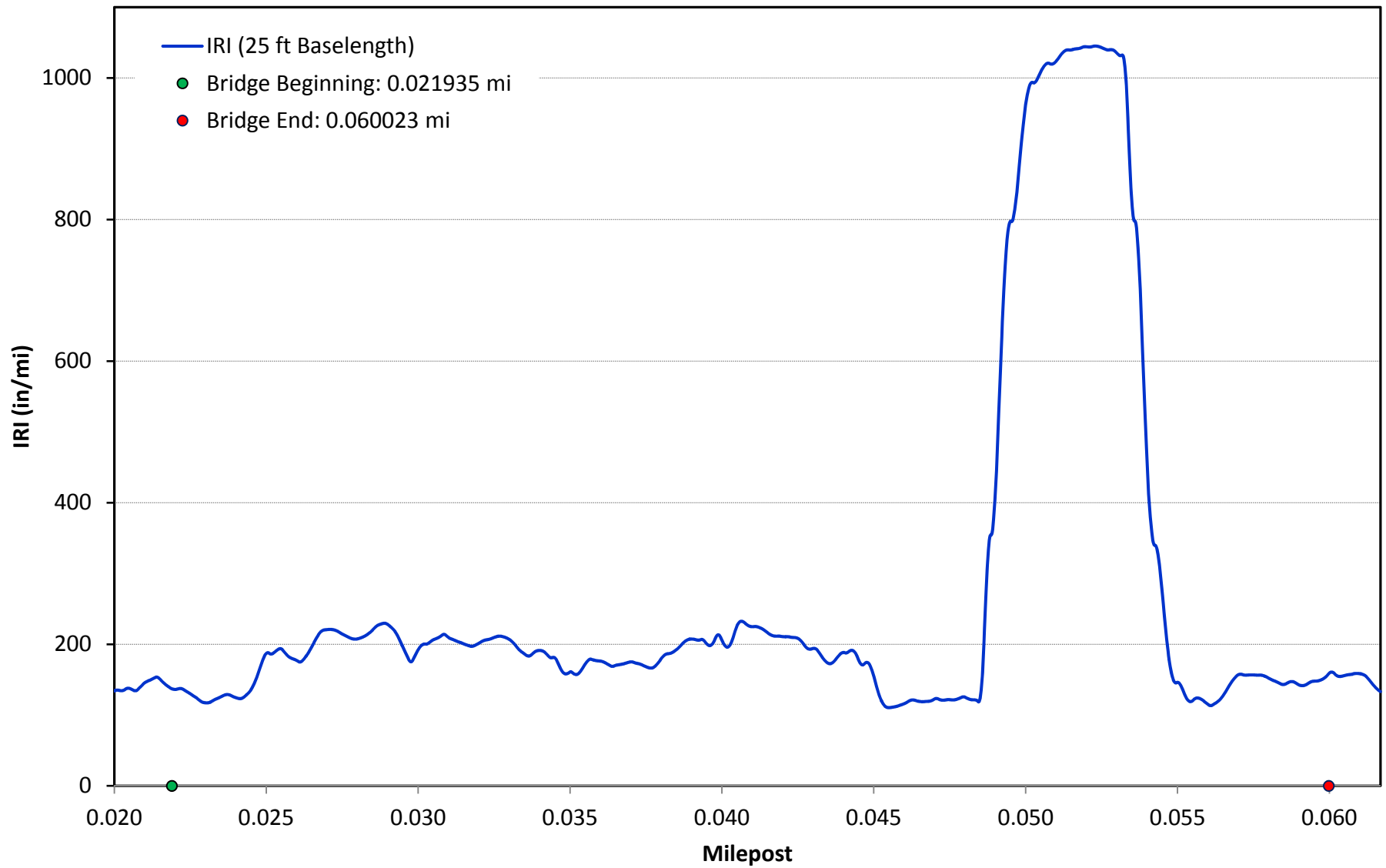
I-10 BB 450-08 WB BRIDGE 3



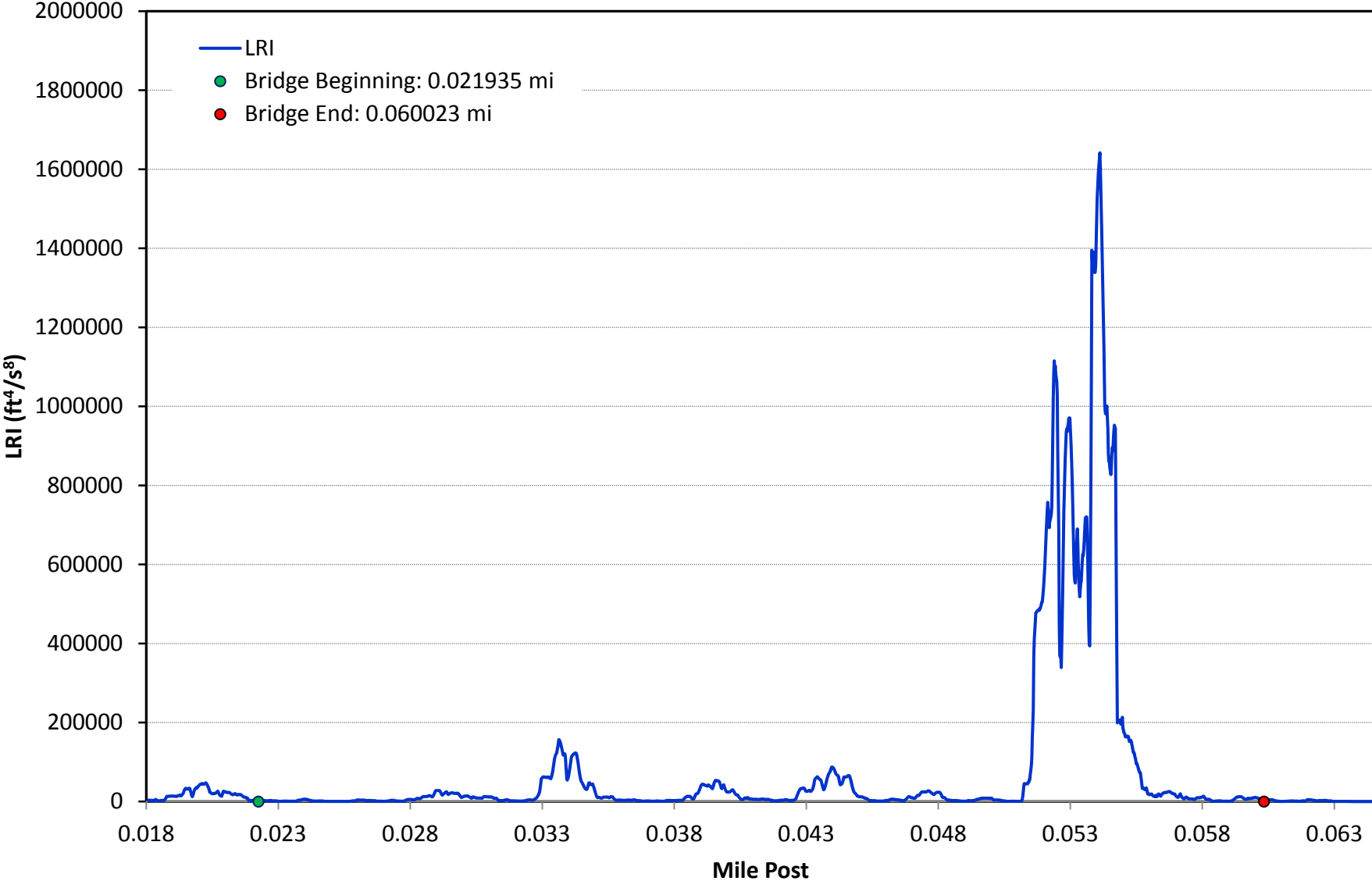
I-10 BB 450-08 WB BRDIGE 3



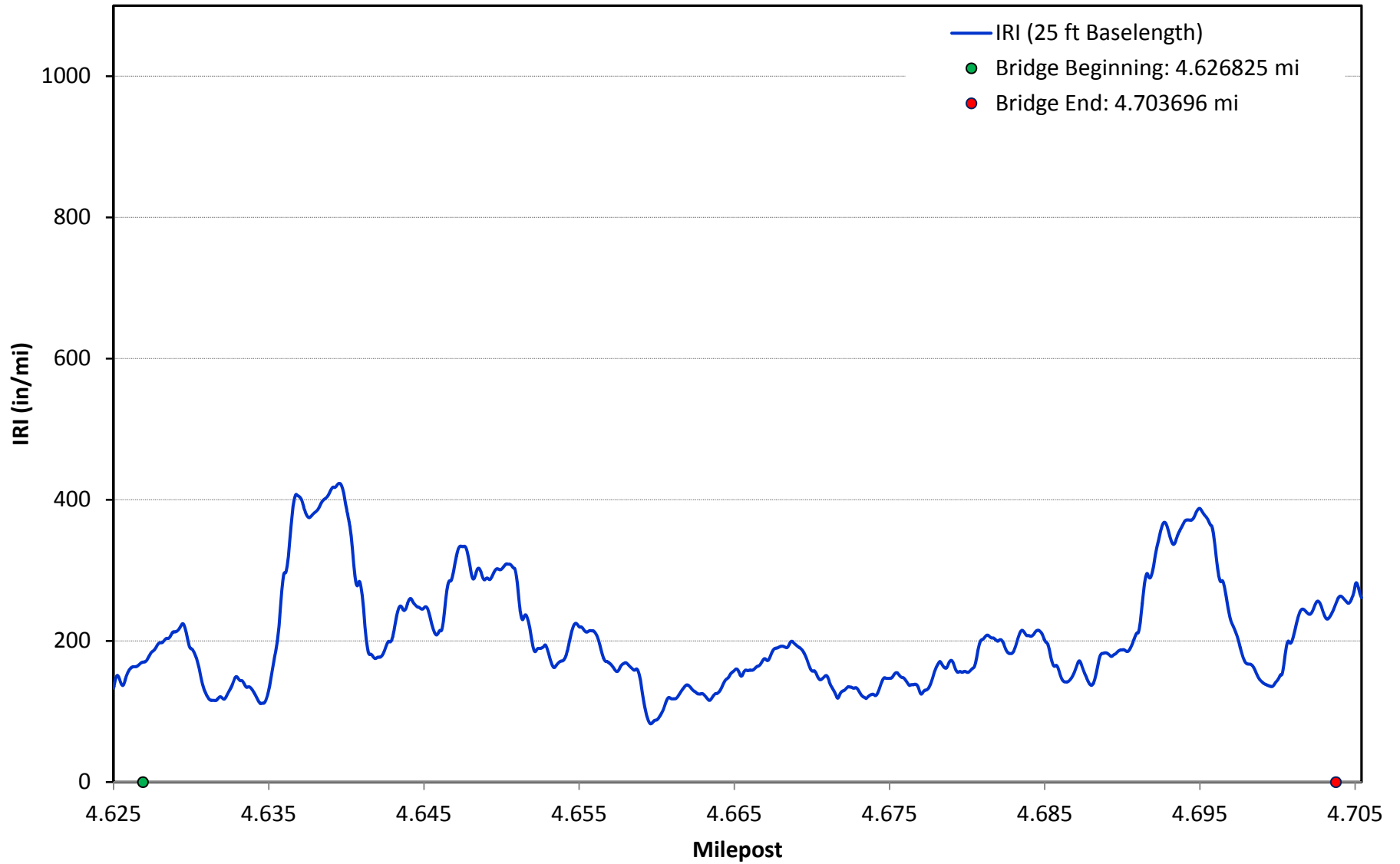
I-10 BB 450-11 EB BRIDGE 1



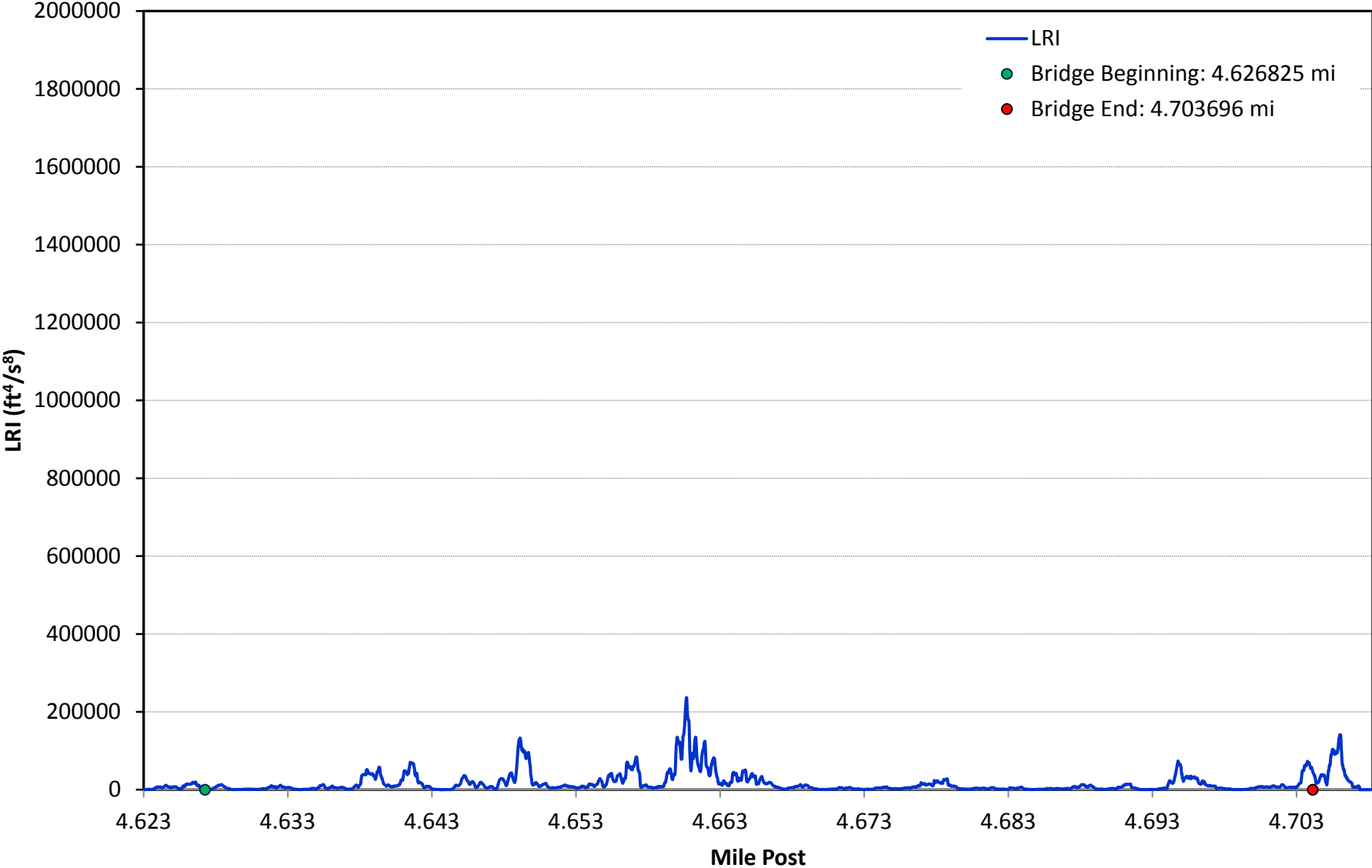
I-10 BB 450-11 EB BRIDGE 1



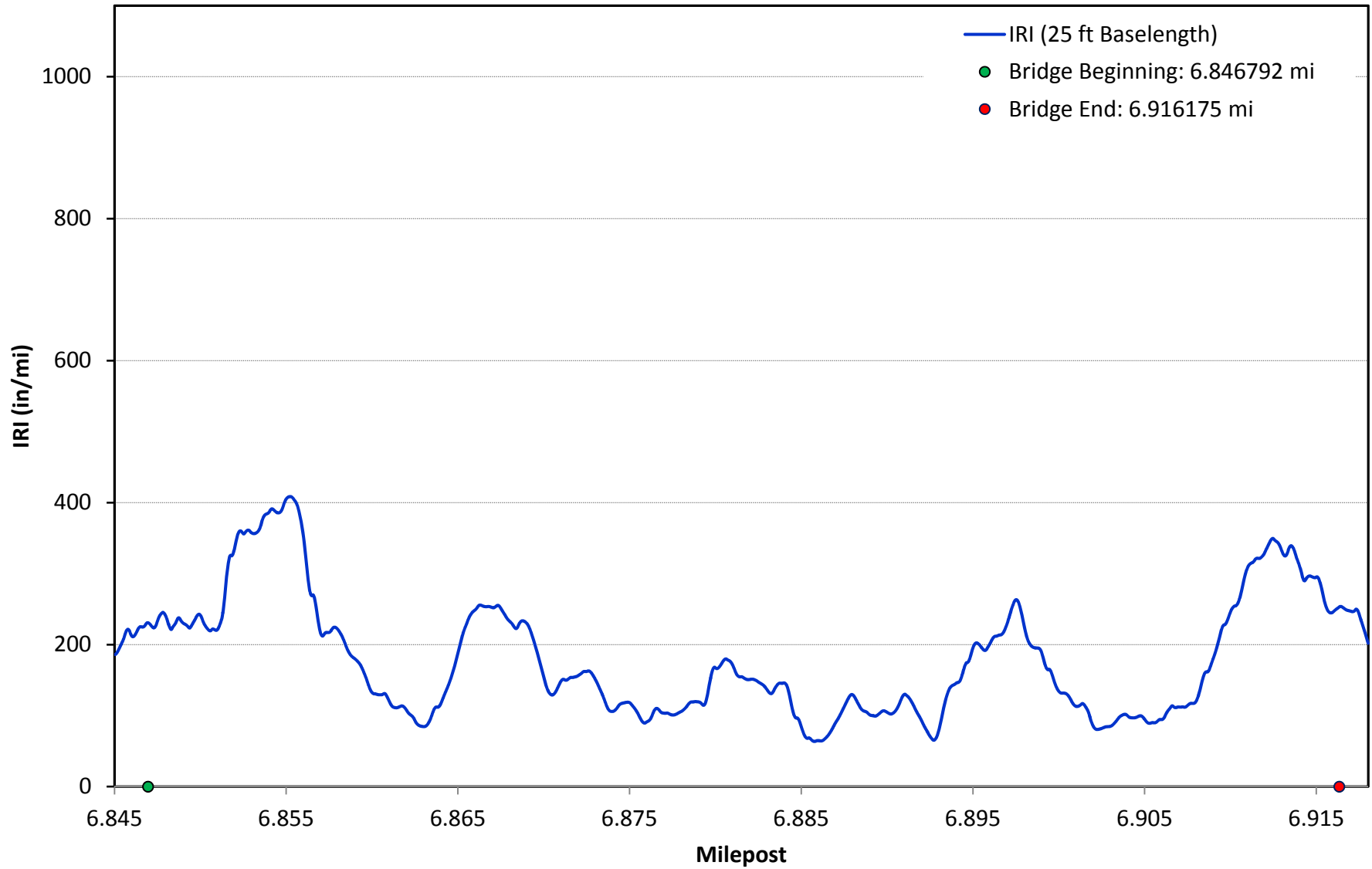
I-10 BB 450-11 EB BRIDGE 2



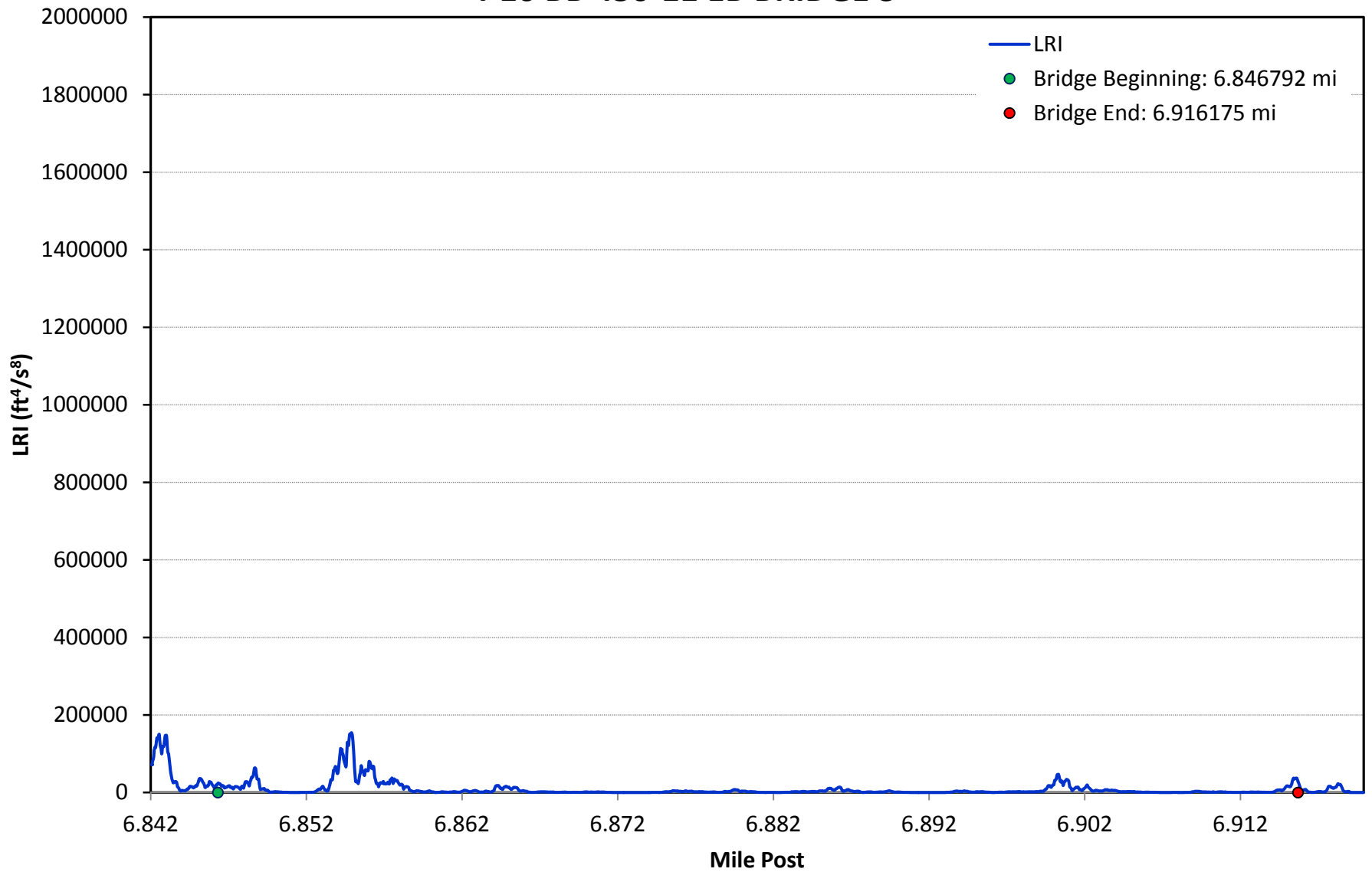
I-10 BB 450-11 EB BRIDGE 2



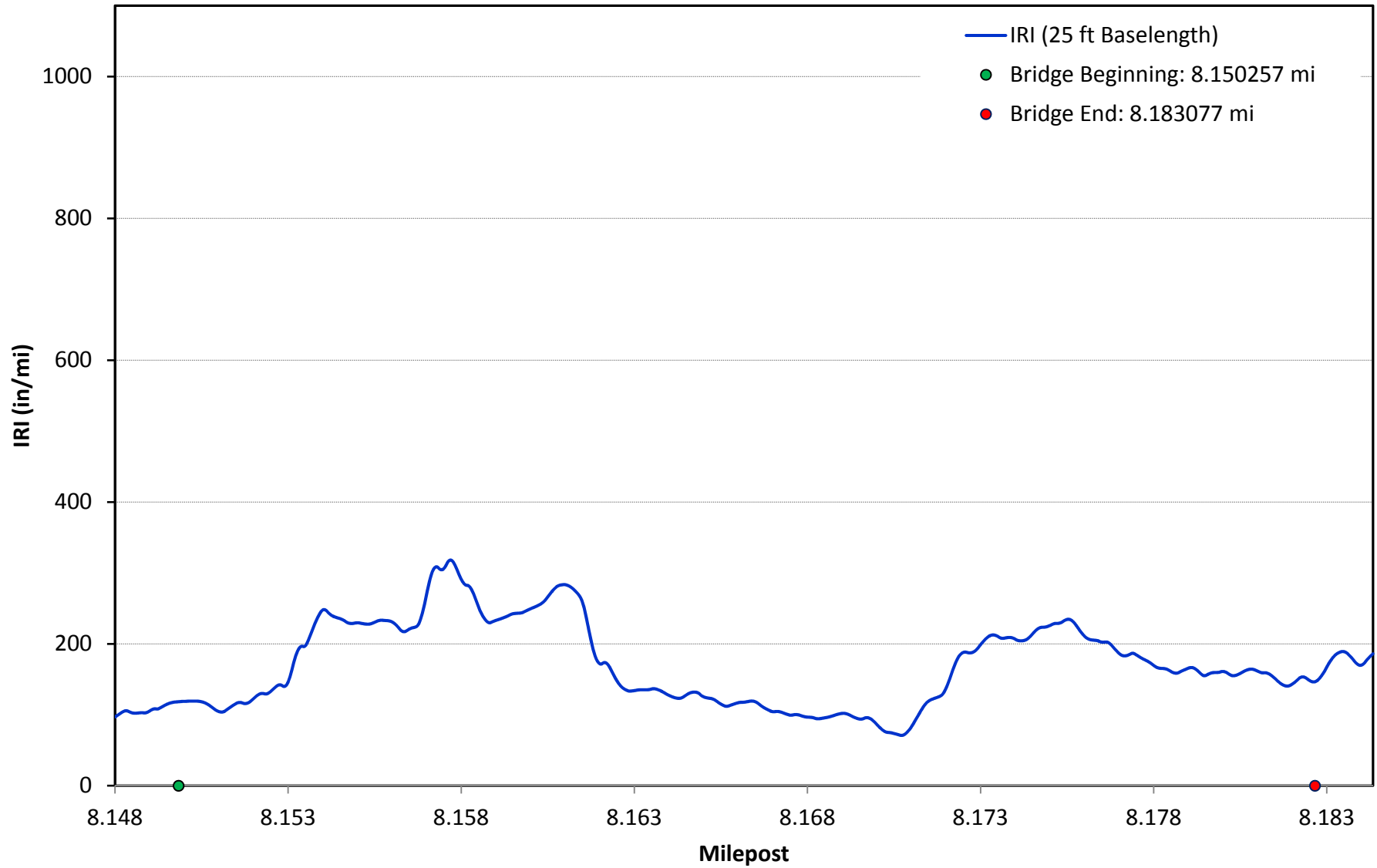
I-10 BB 450-11 EB BRIDGE 3



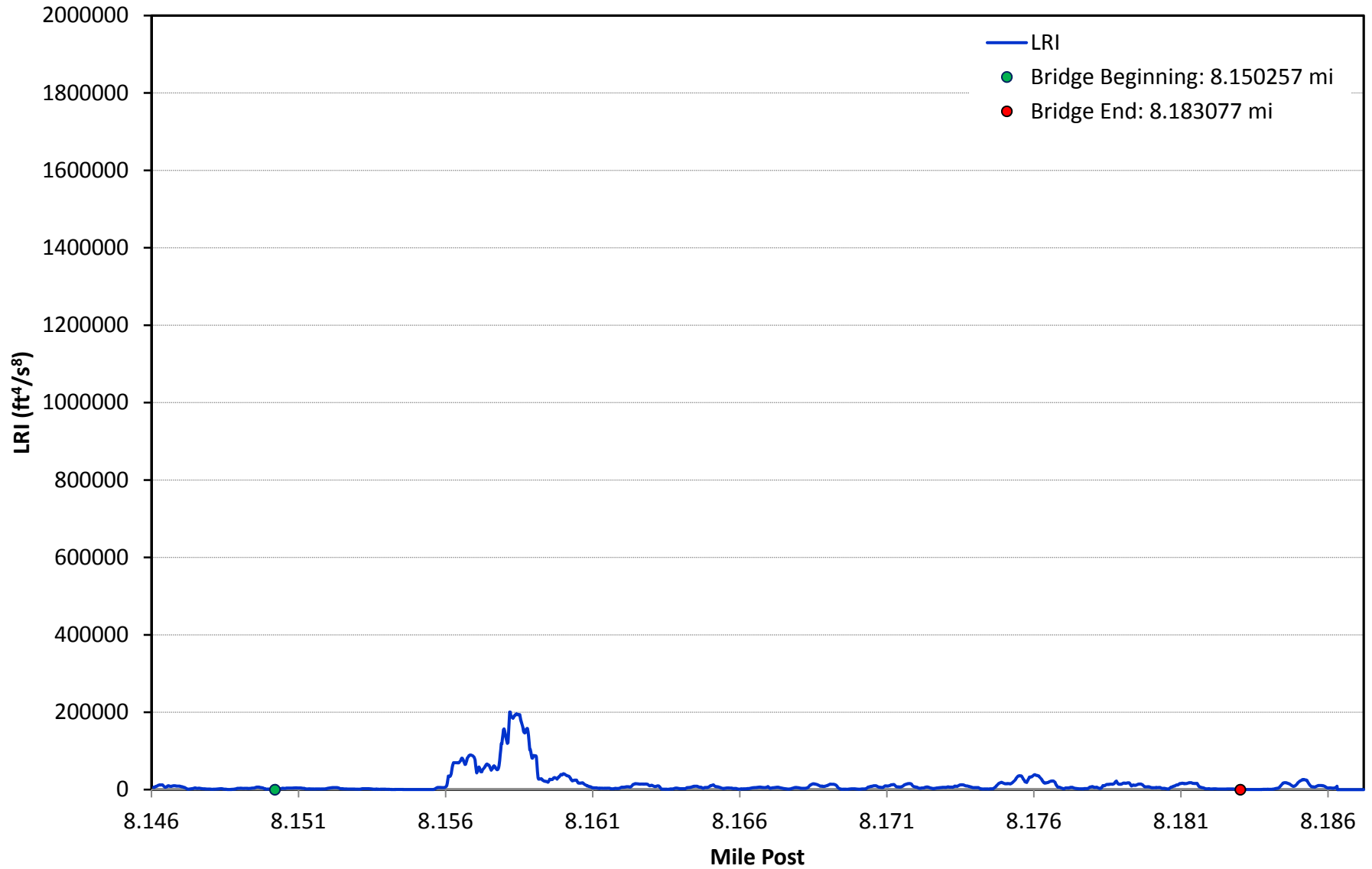
I-10 BB 450-11 EB BRIDGE 3



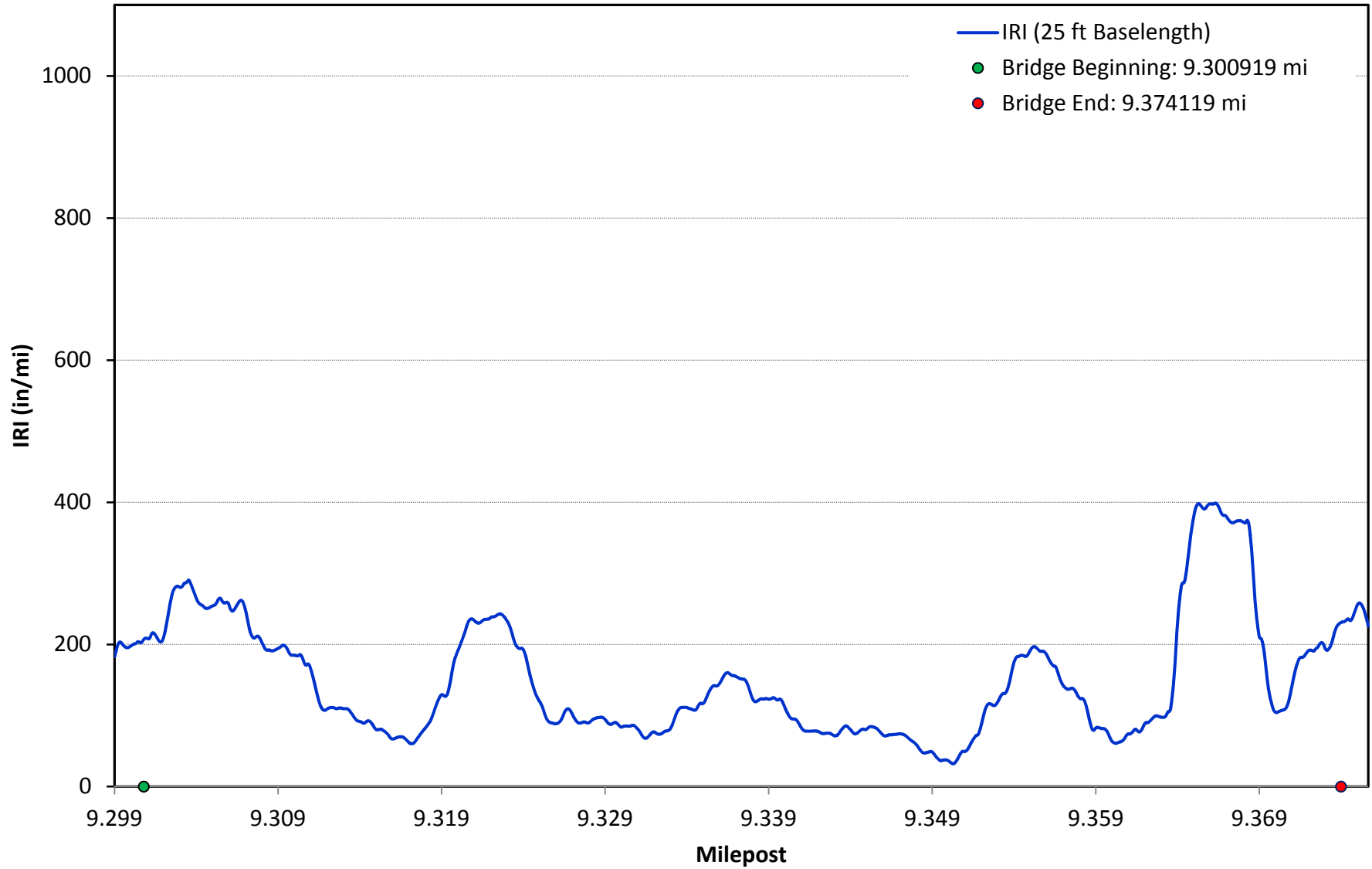
I-10 BB 450-11 EB BRIDGE 4



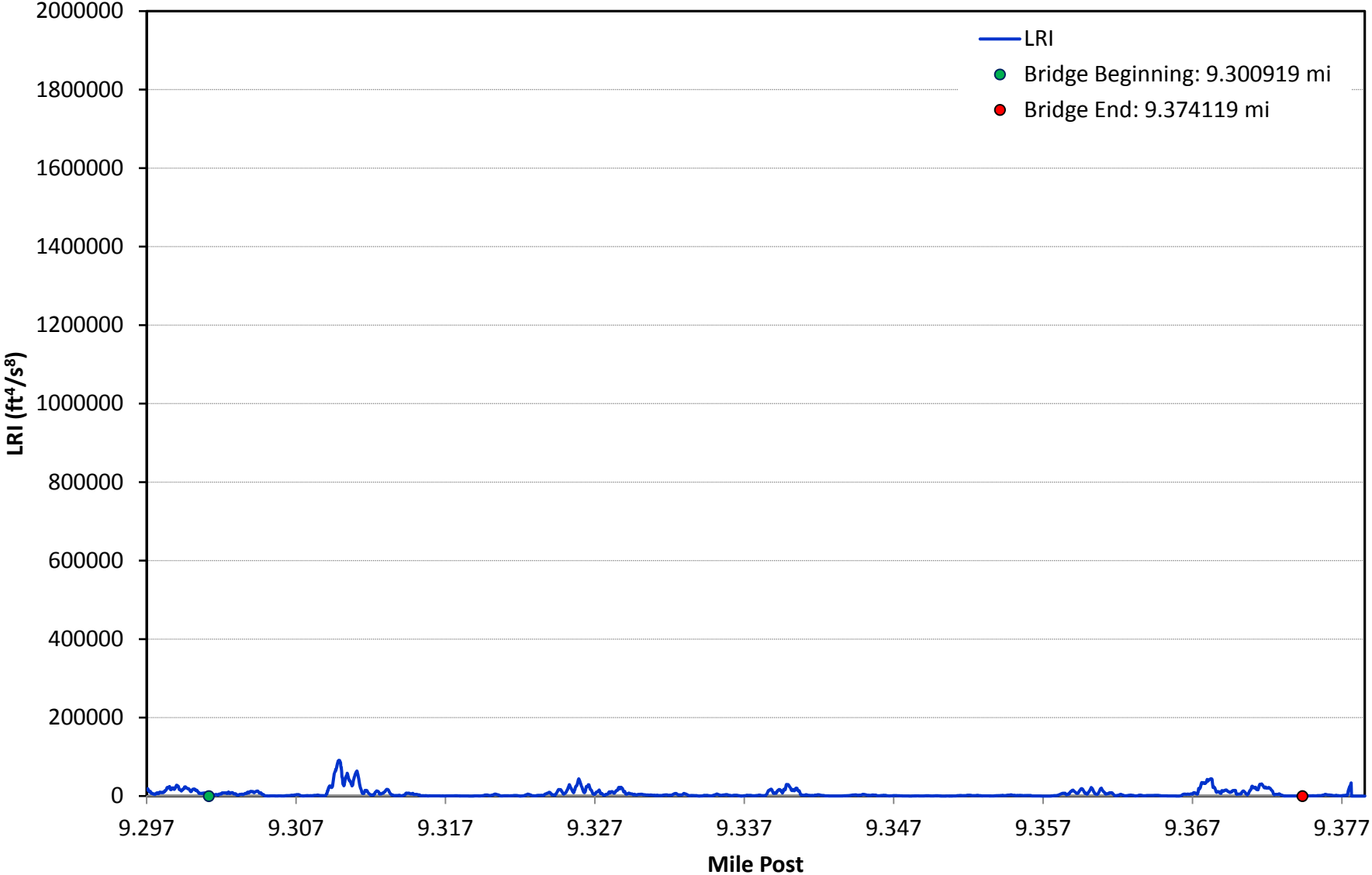
I-10 BB 450-11 EB BRIDGE 4



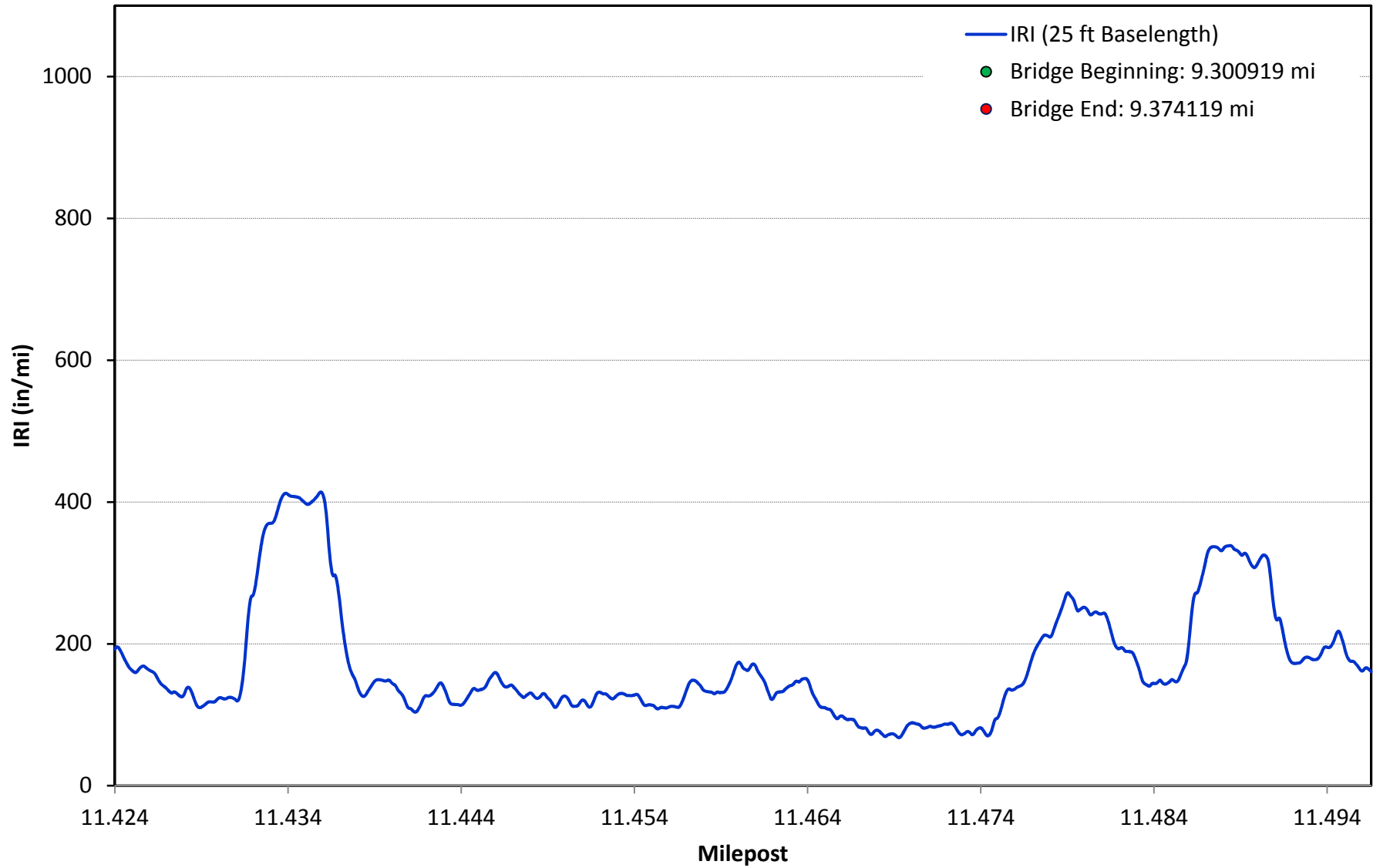
I-10 BB 450-11 EB BRIDGE 5



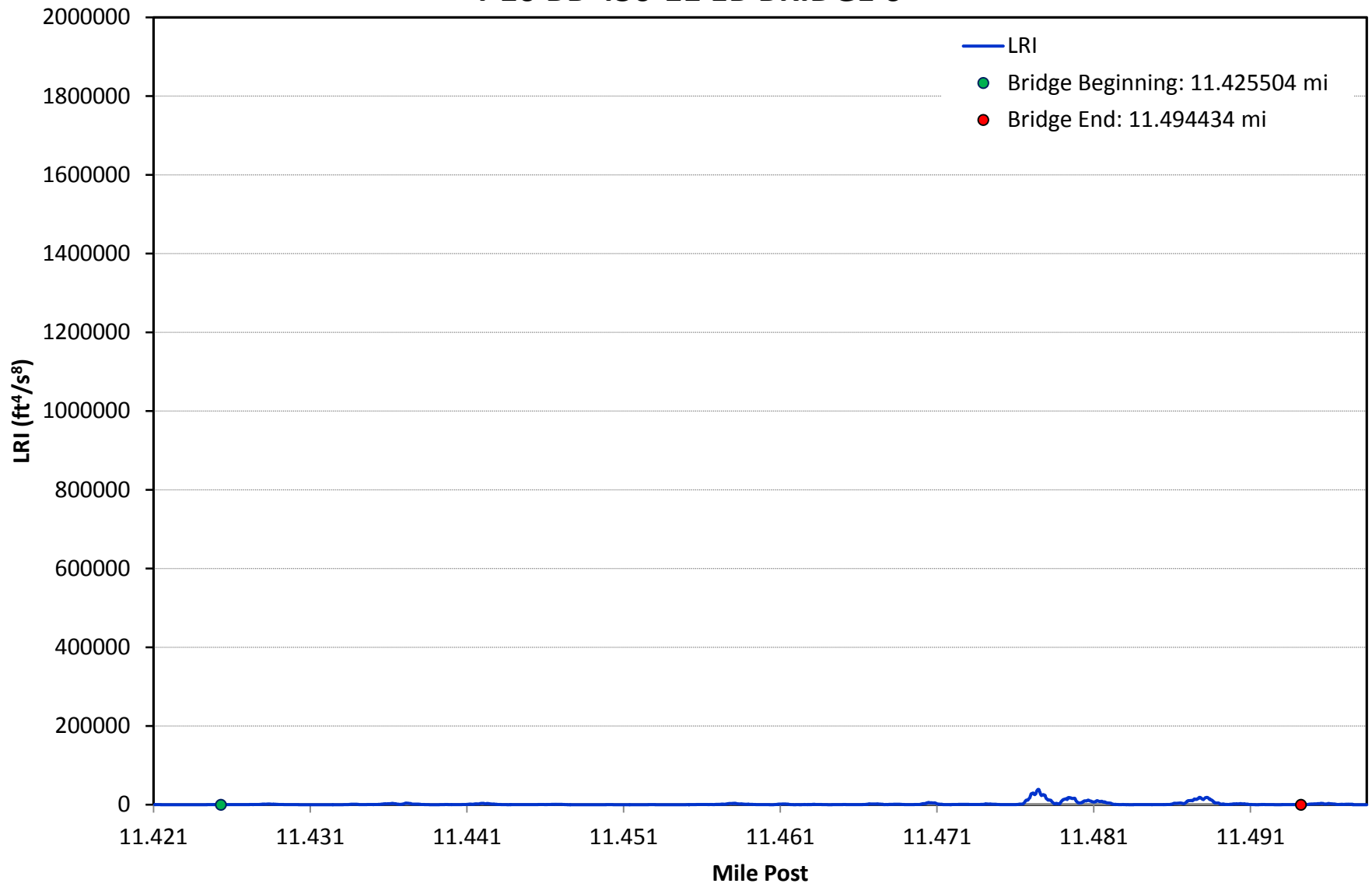
I-10 BB 450-11 EB BRIDGE 5



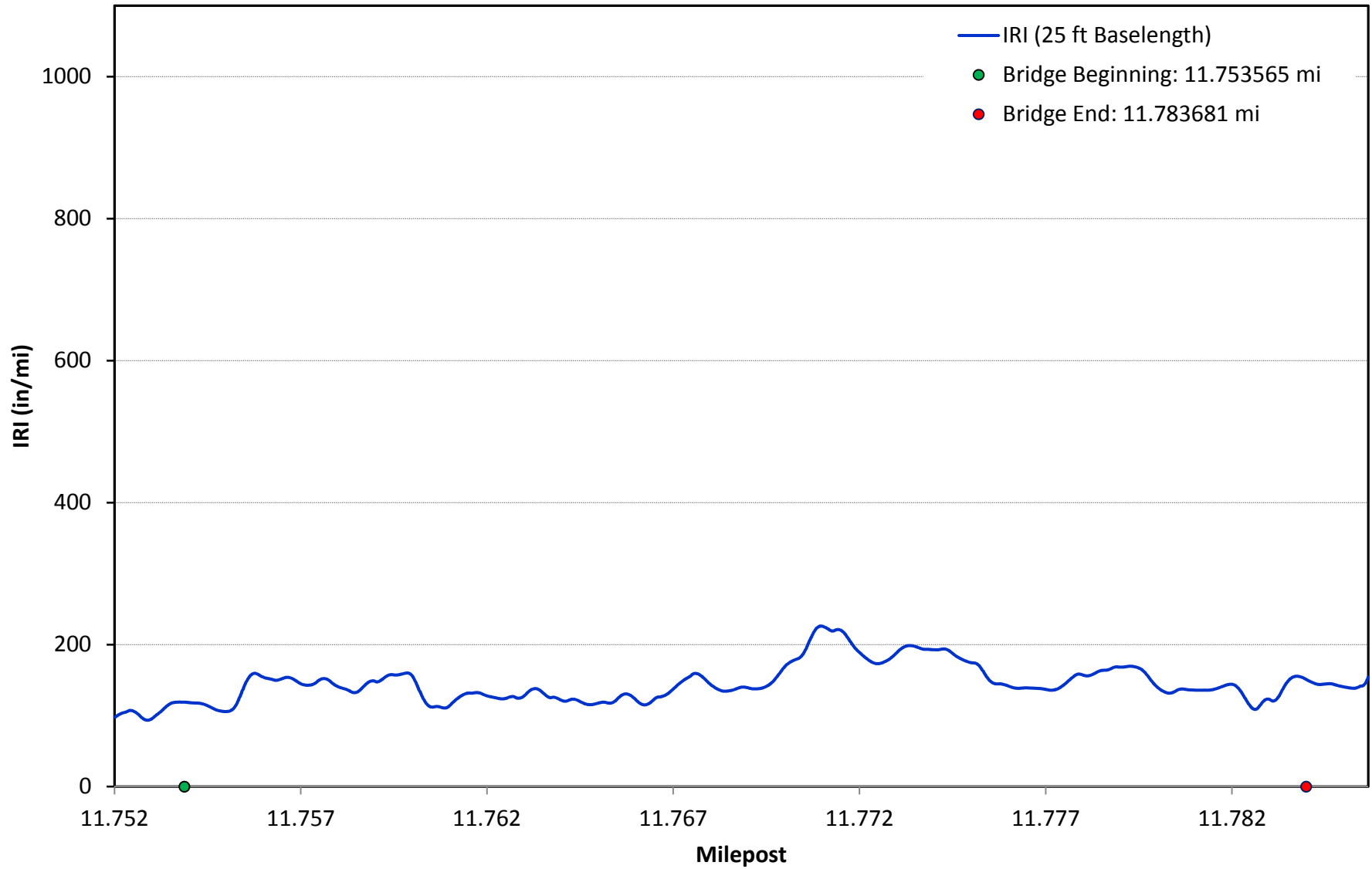
I-10 BB 450-11 EB BRIDGE 6



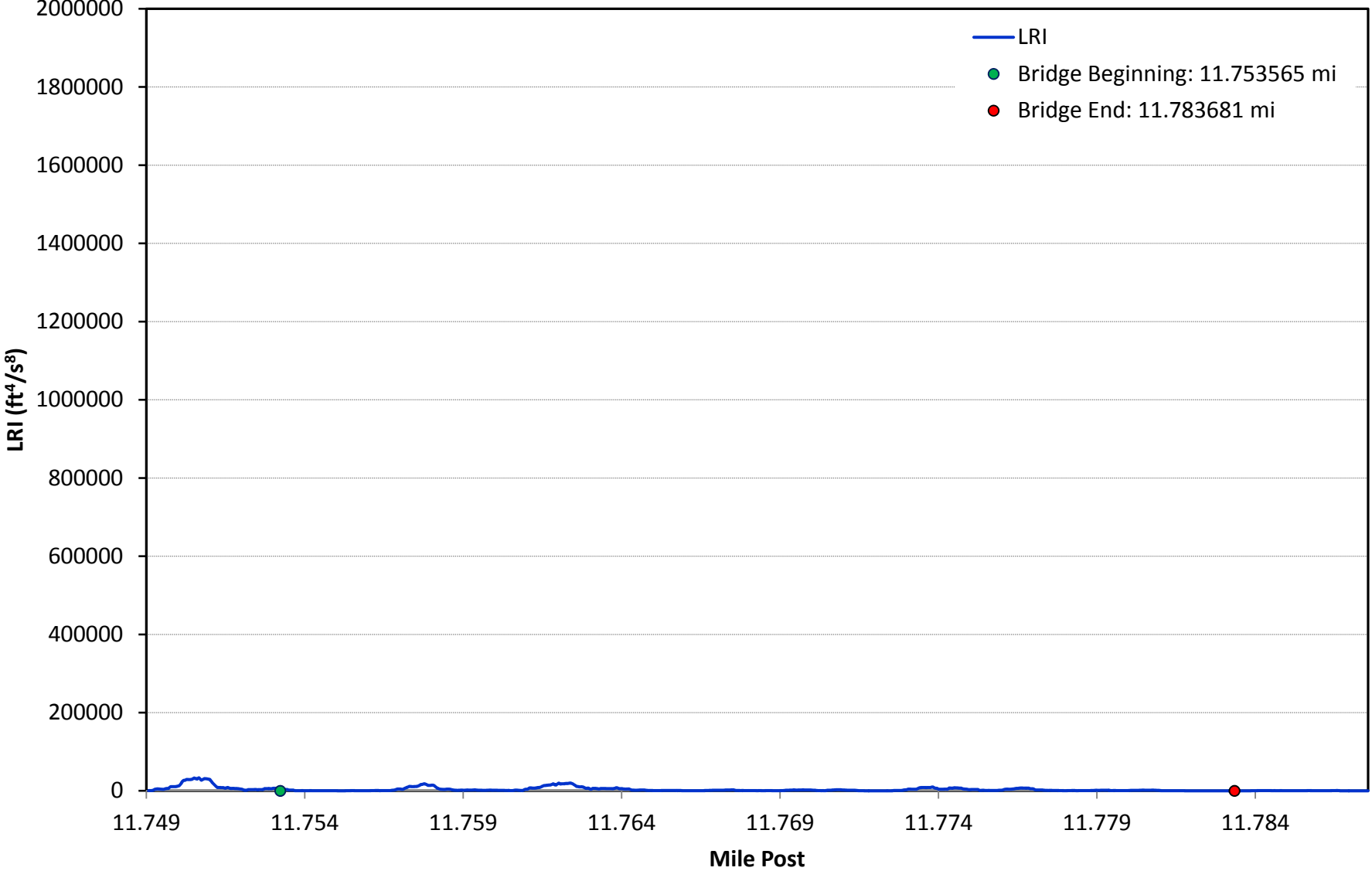
I-10 BB 450-11 EB BRIDGE 6



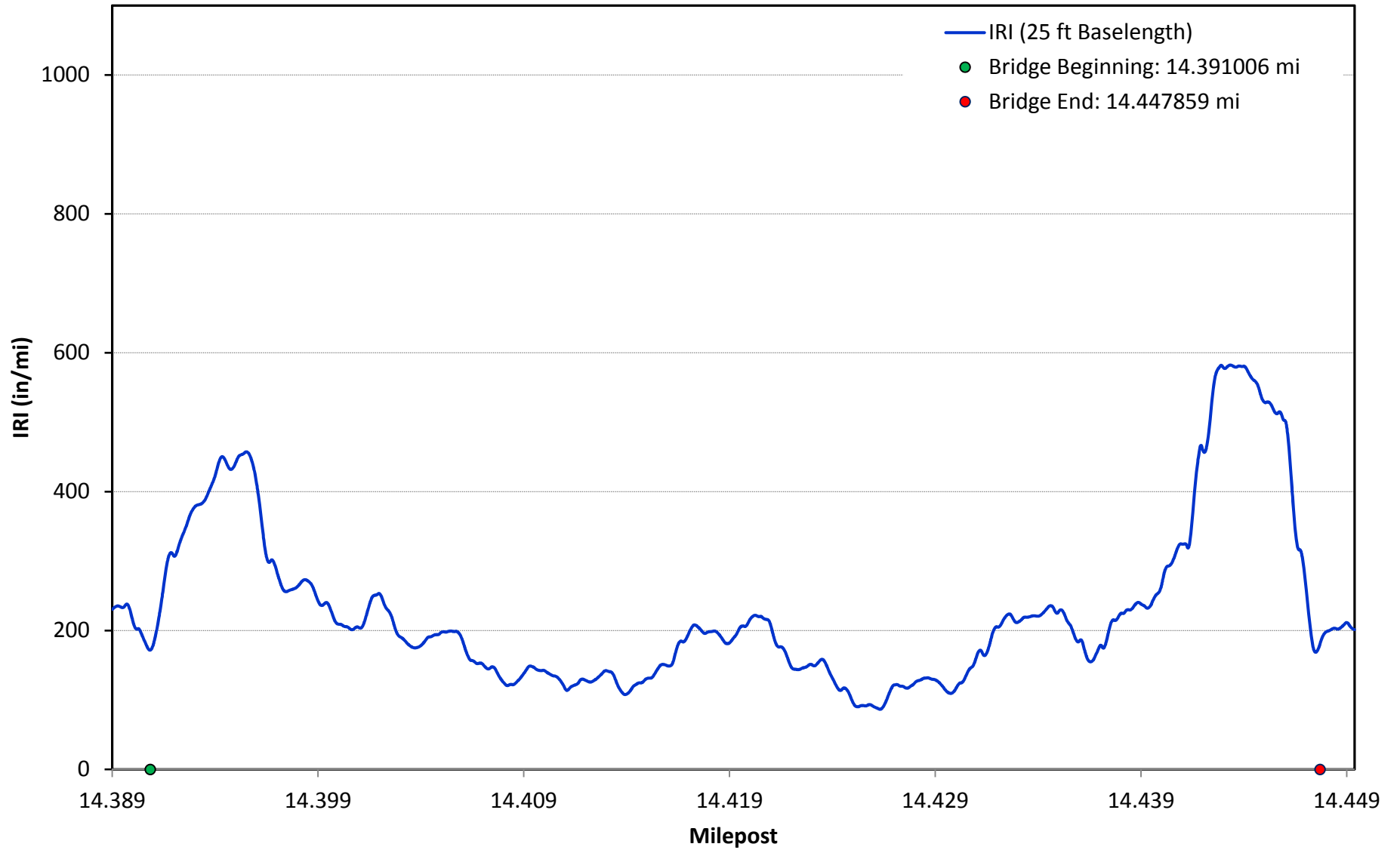
I-10 BB 450-11 EB BRIDGE 7



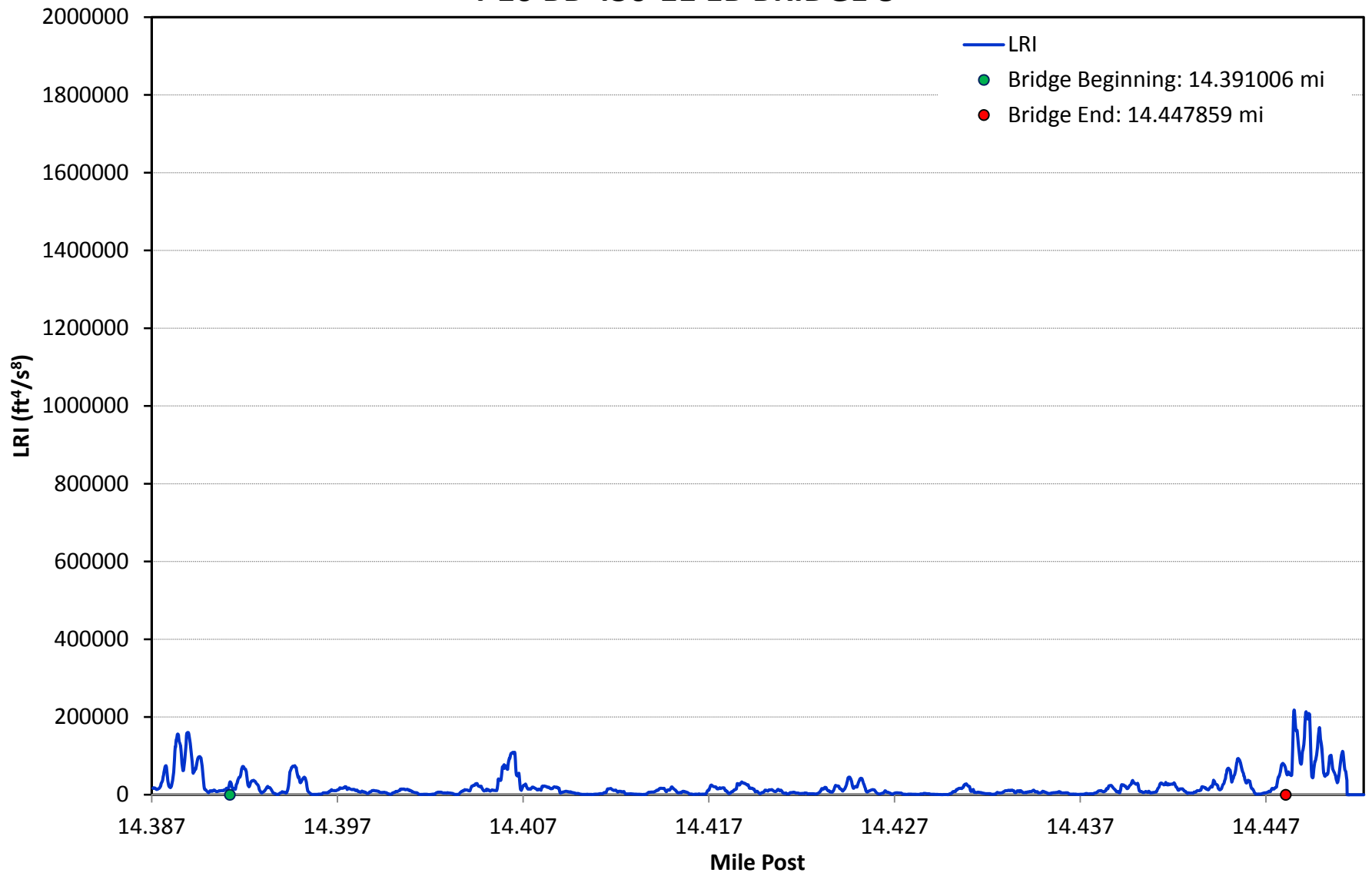
I-10 BB 450-11 EB BRIDGE 7



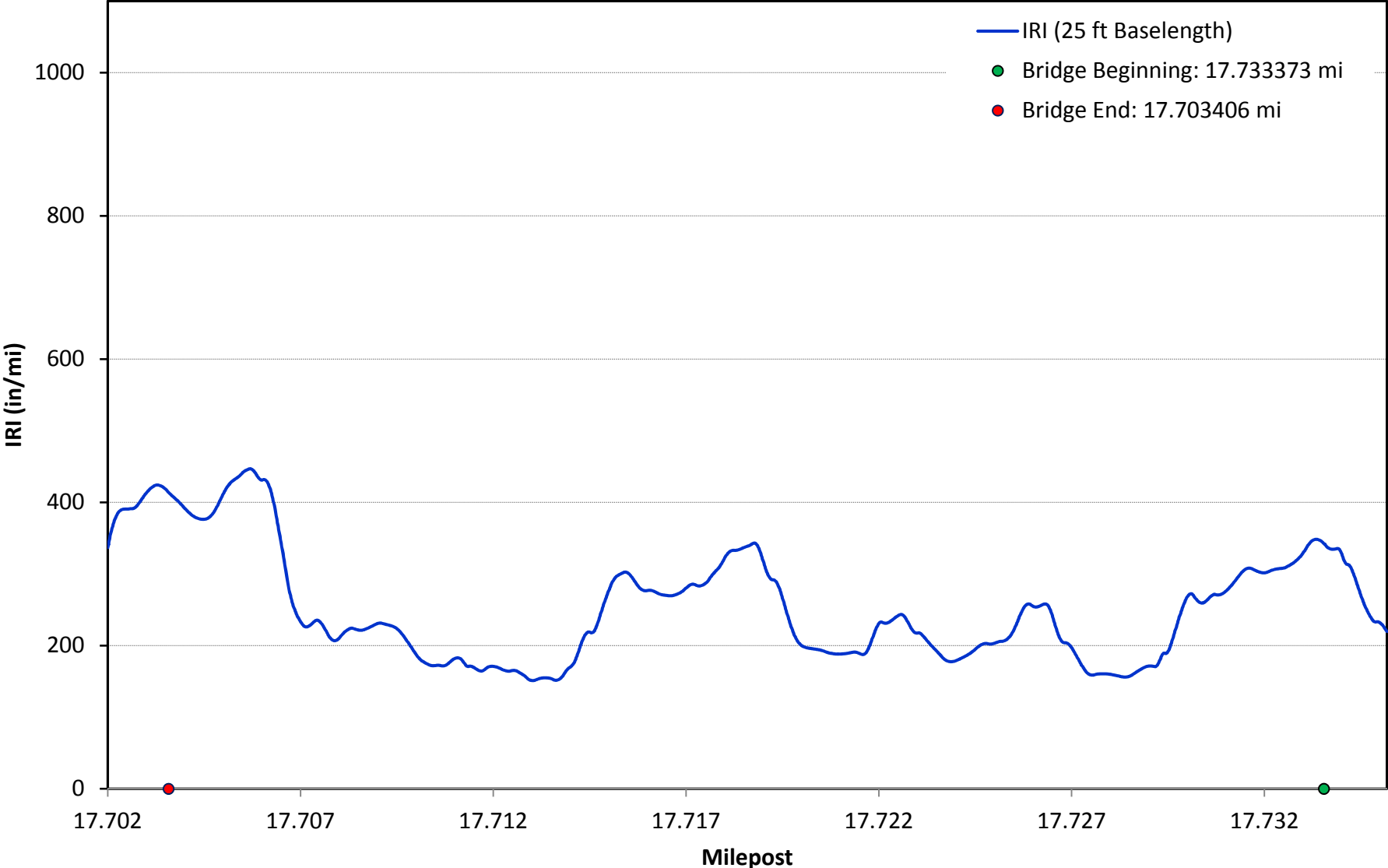
I-10 BB 450-11 EB BRIDGE 8



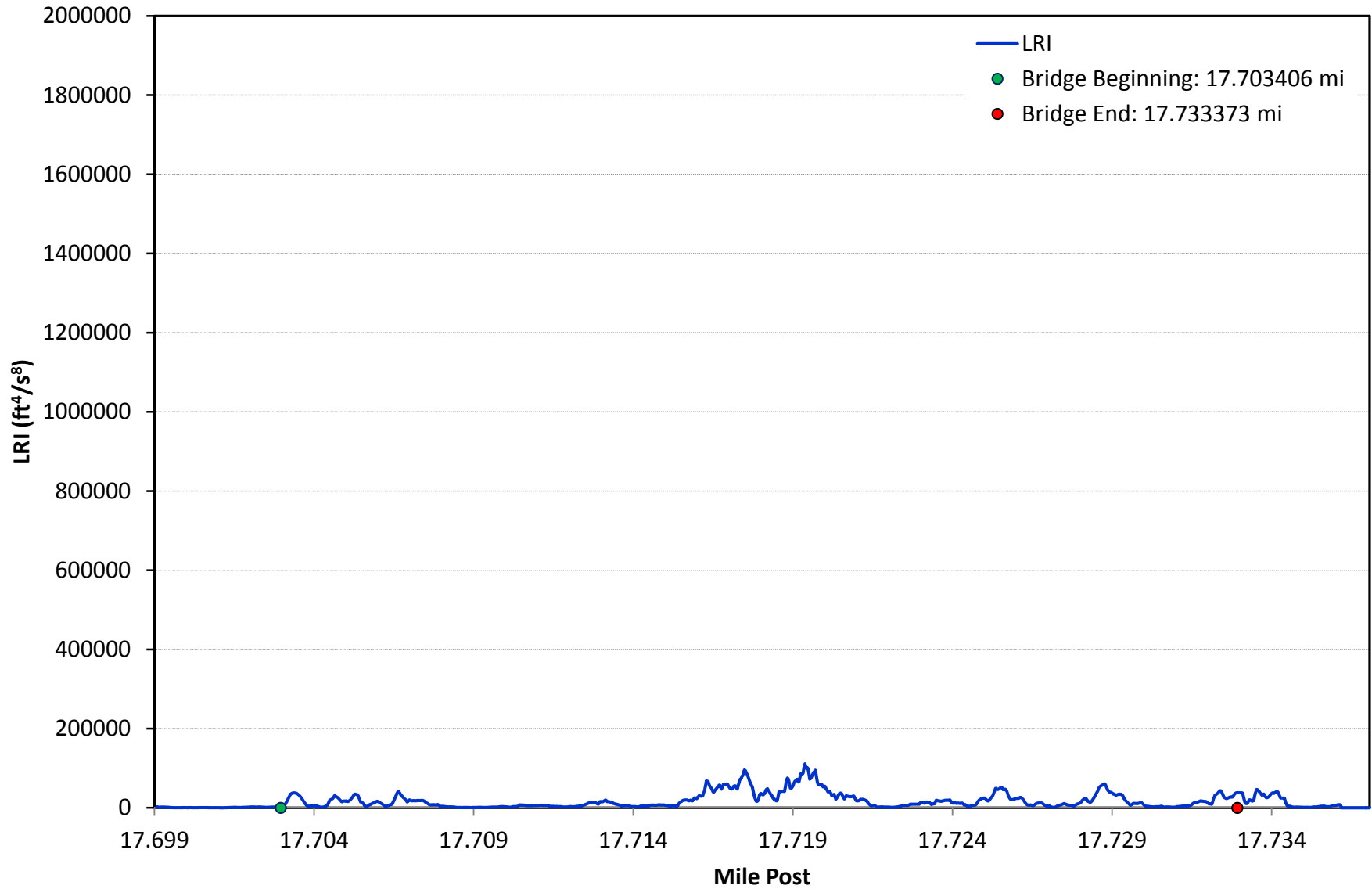
I-10 BB 450-11 EB BRIDGE 8



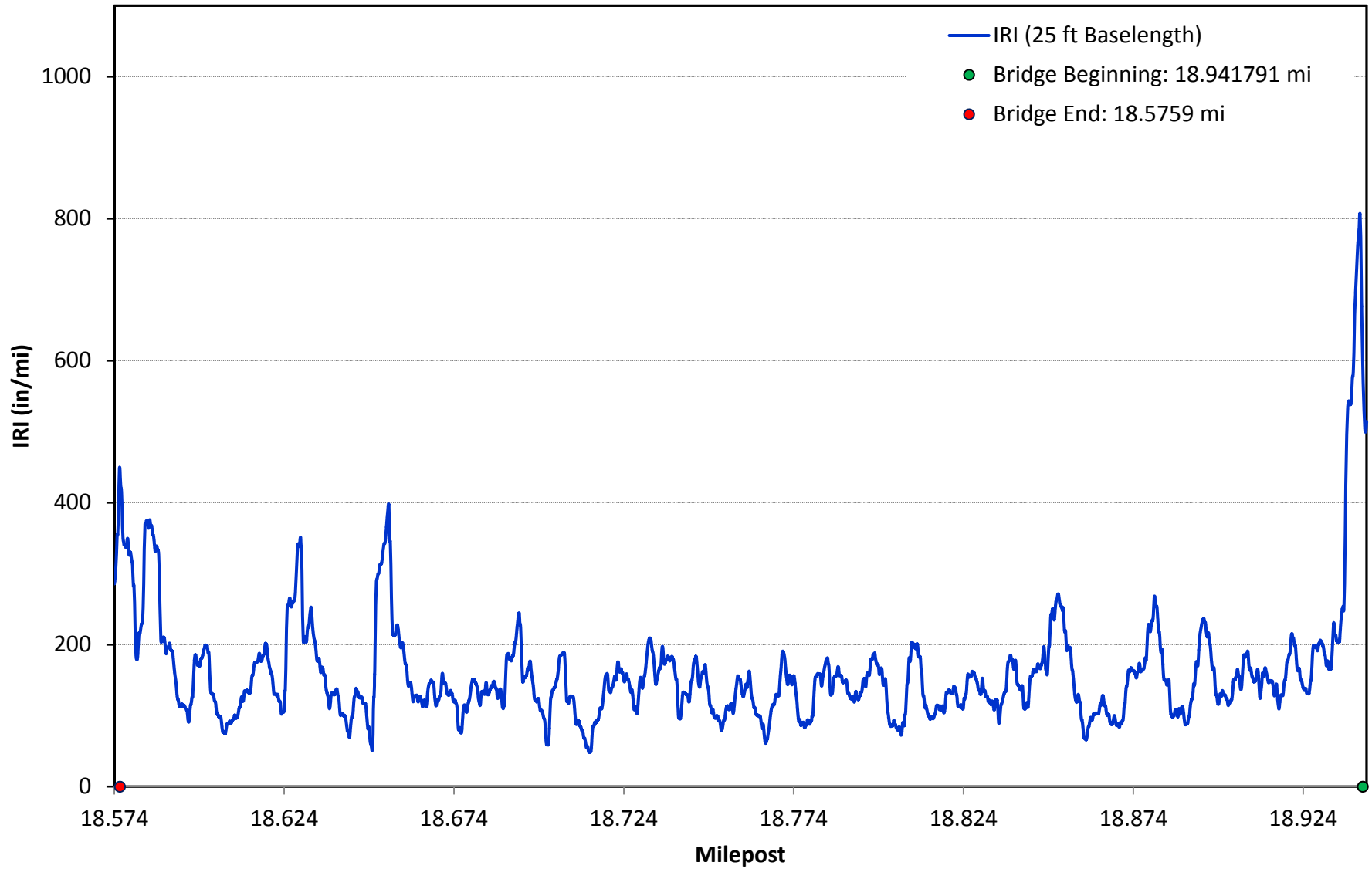
I-10 BB 450-11 EB BRIDGE 9



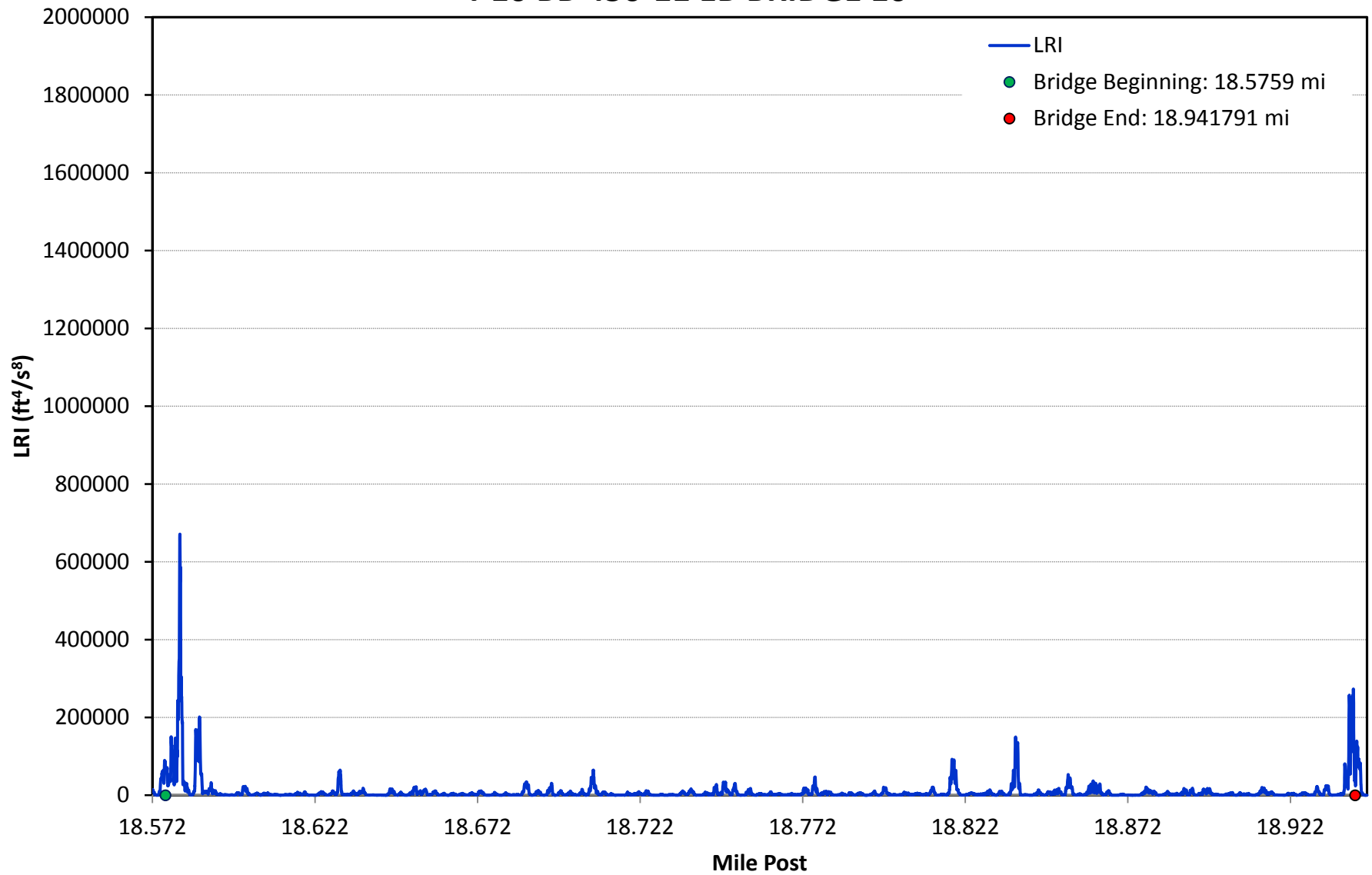
I-10 BB 450-11 EB BRIDGE 9



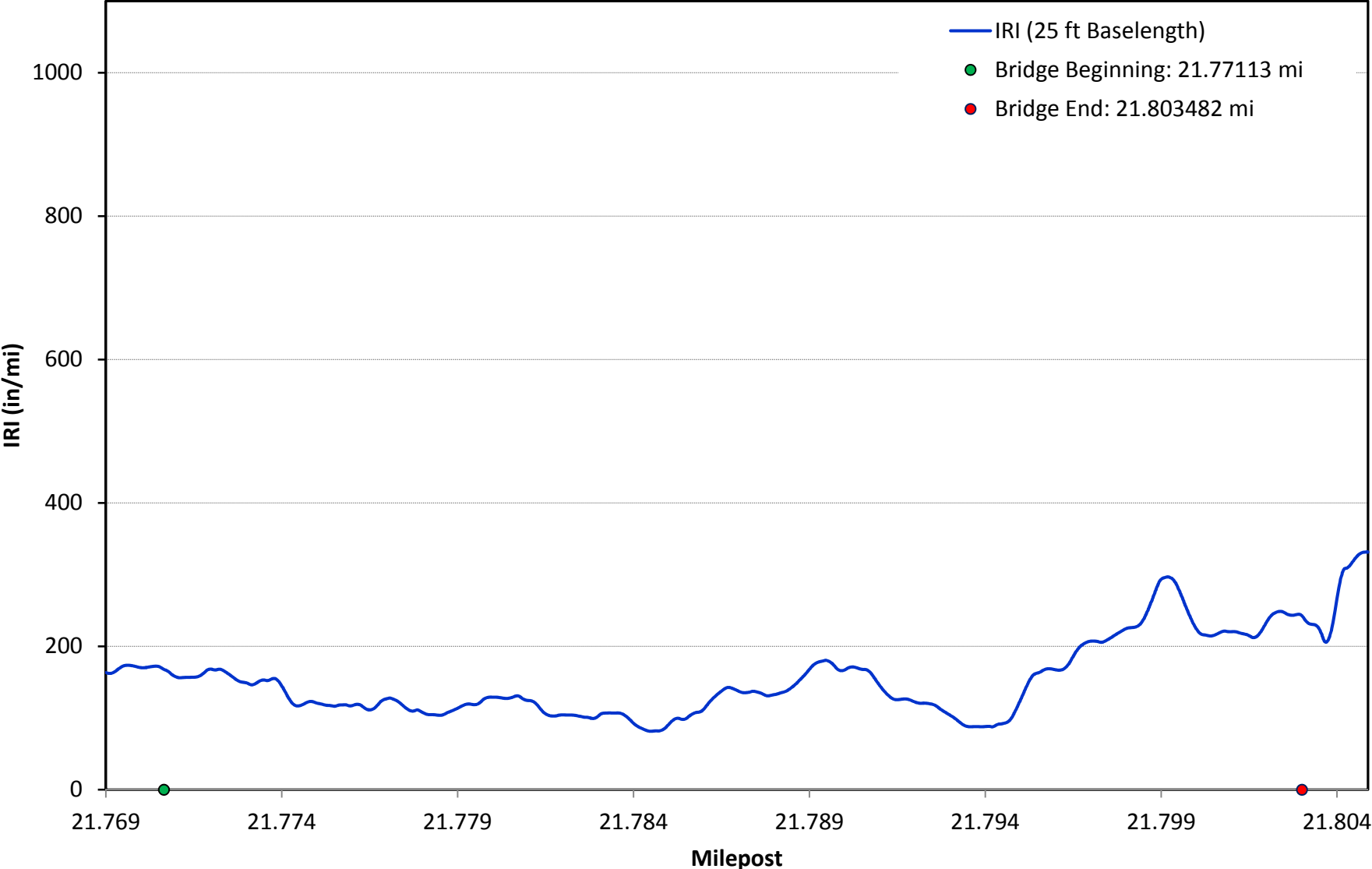
I-10 BB 450-11 EB BRIDGE 10



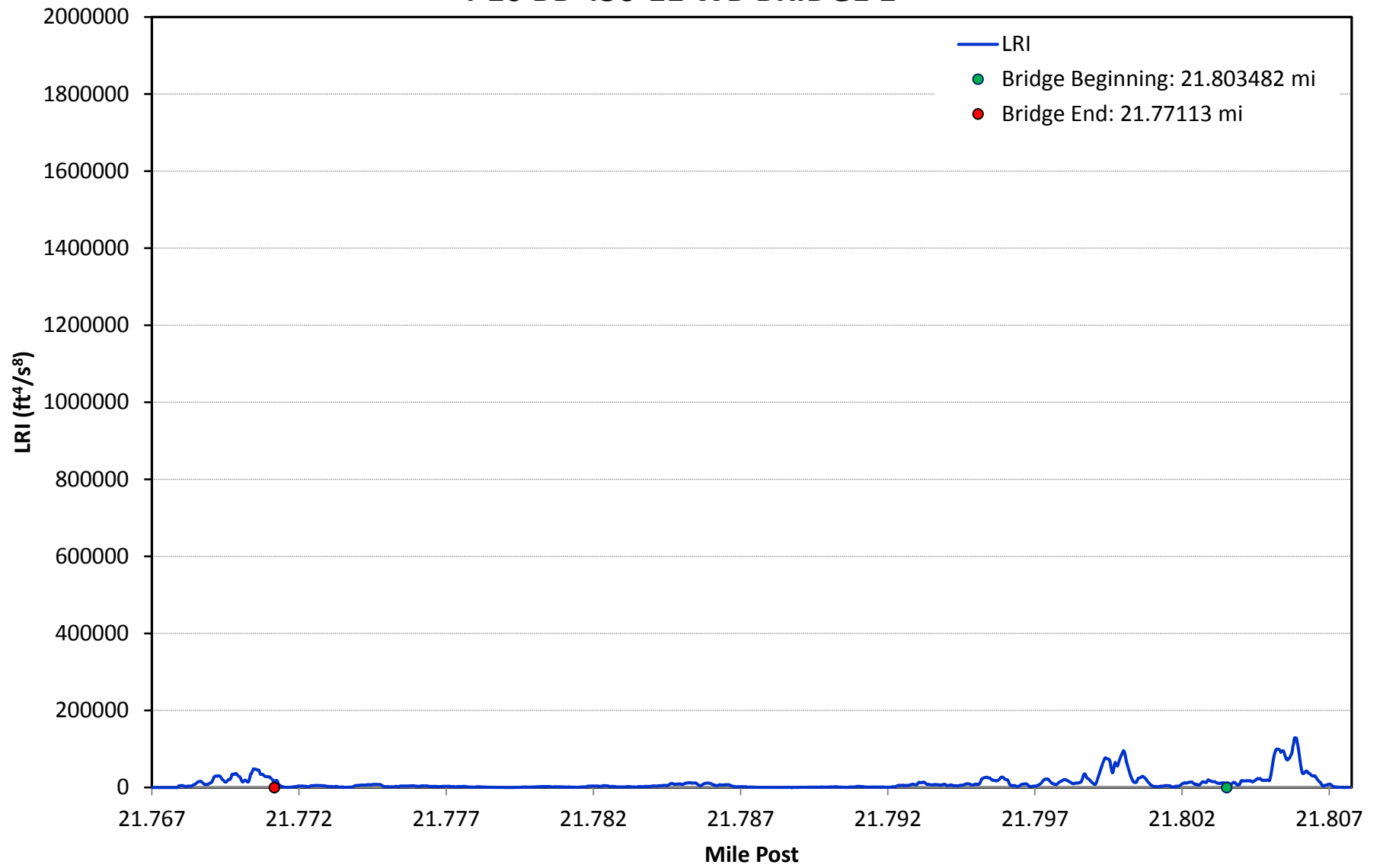
I-10 BB 450-11 EB BRIDGE 10



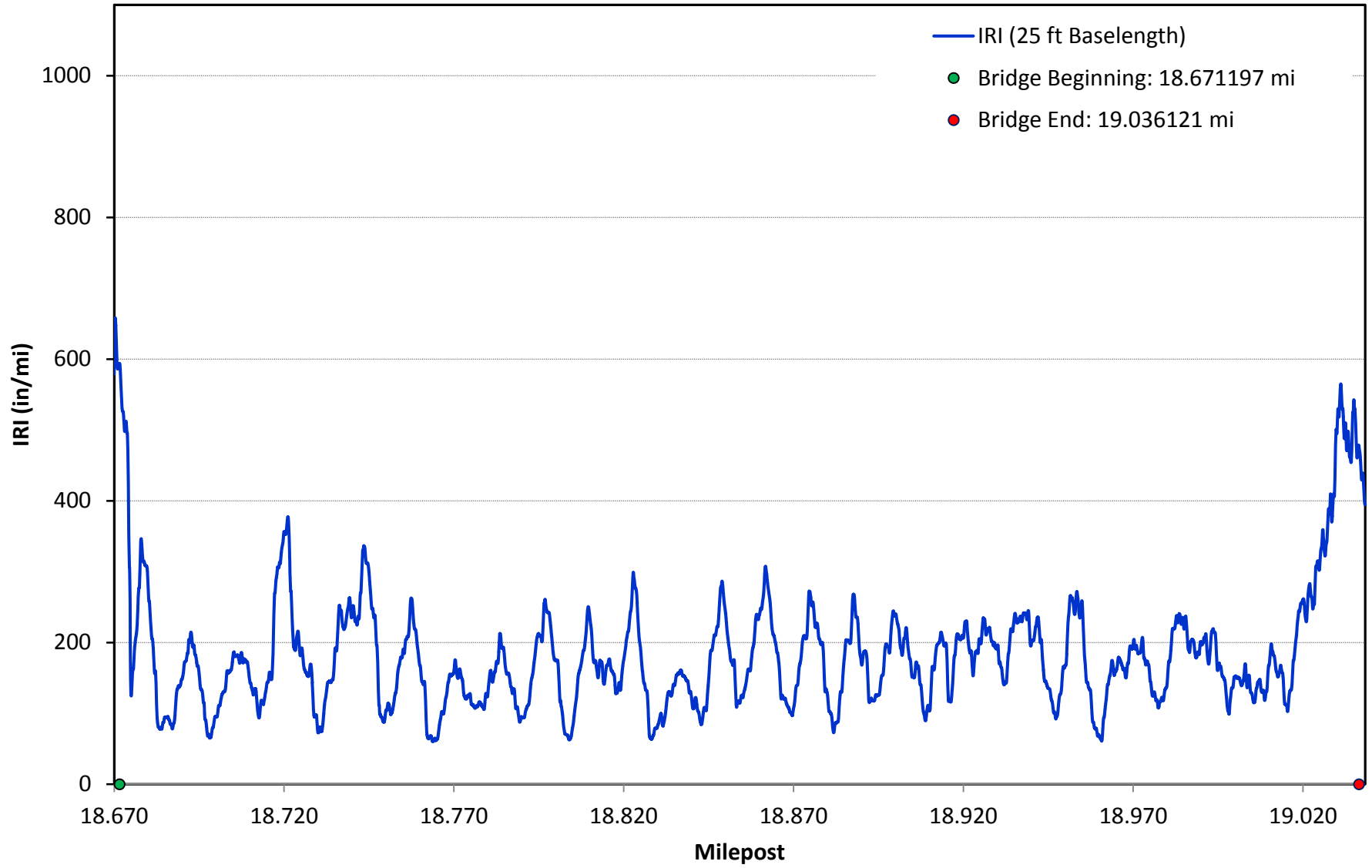
I-10 BB 450-11 WB BRIDGE 1



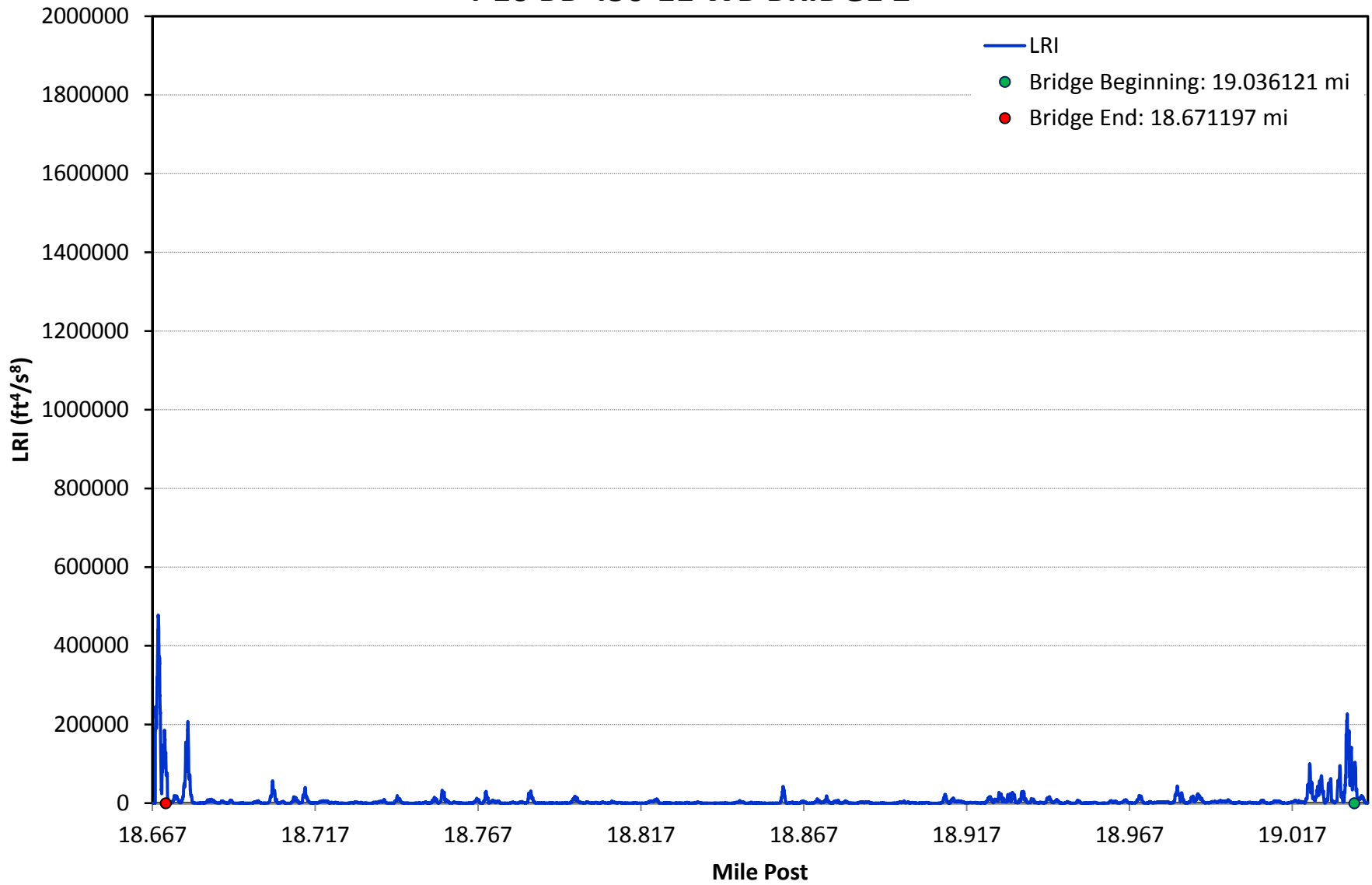
I-10 BB 450-11 WB BRIDGE 1



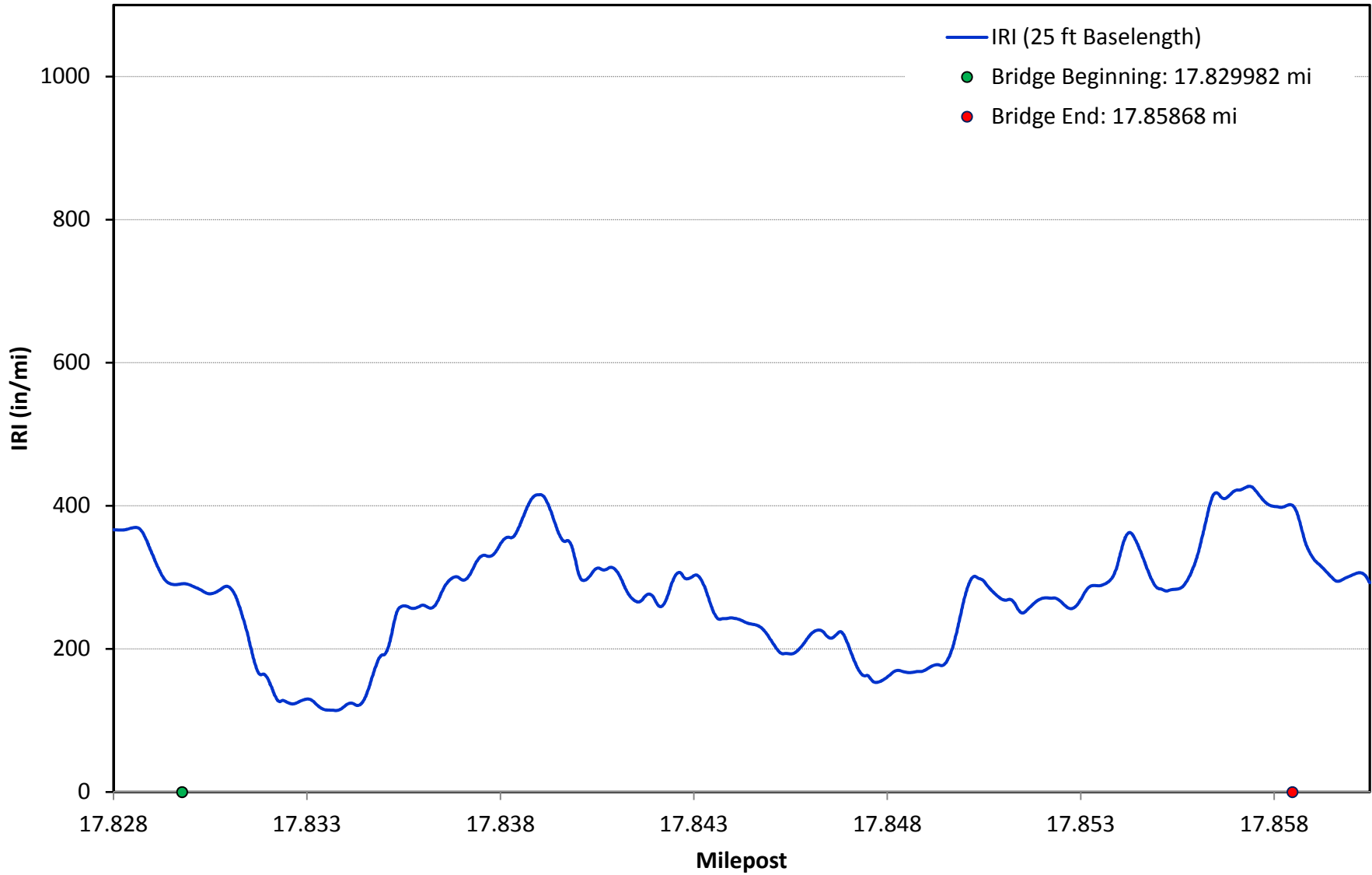
I-10 BB 450-11 WB BRIDGE 2



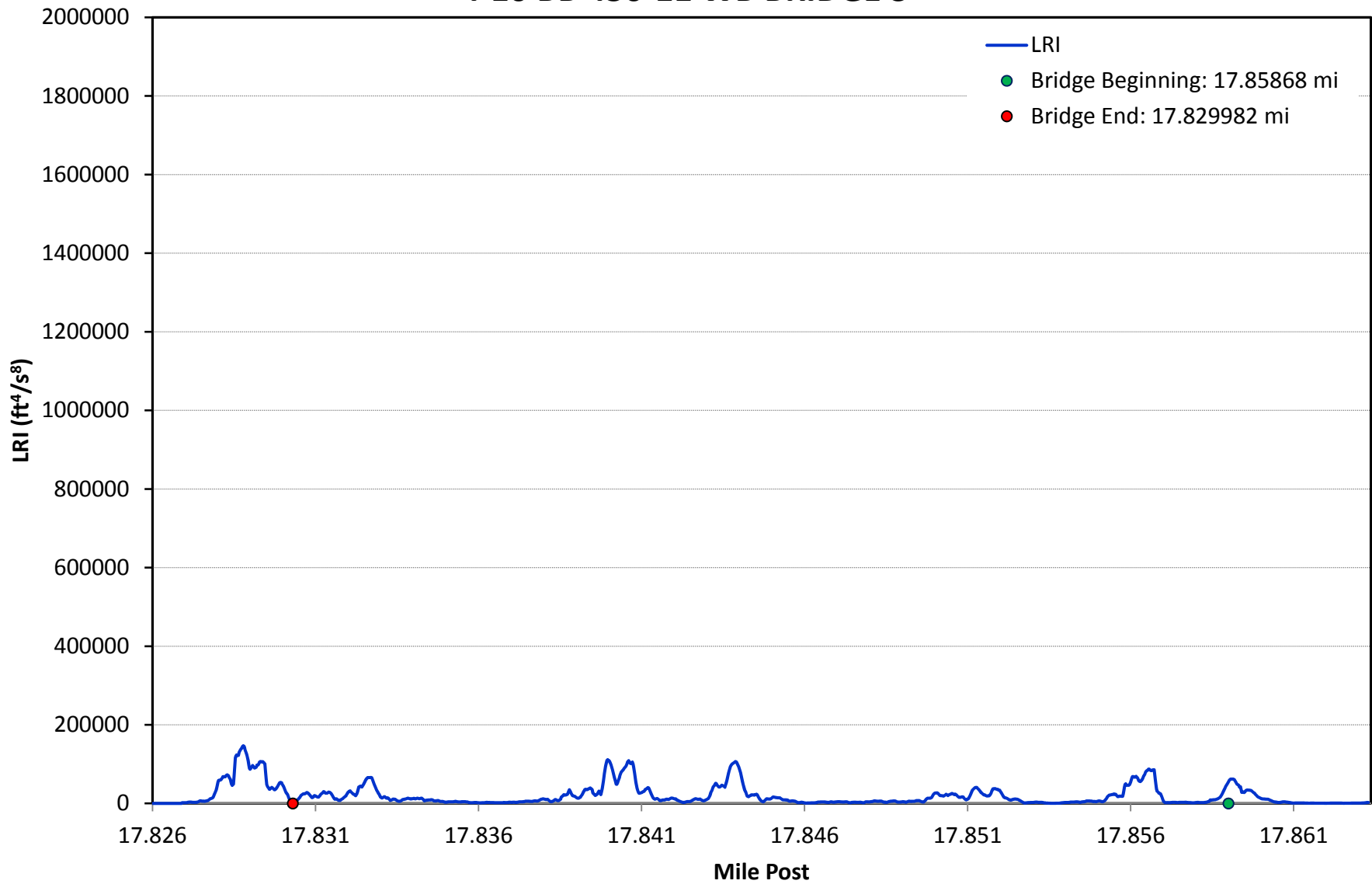
I-10 BB 450-11 WB BRIDGE 2



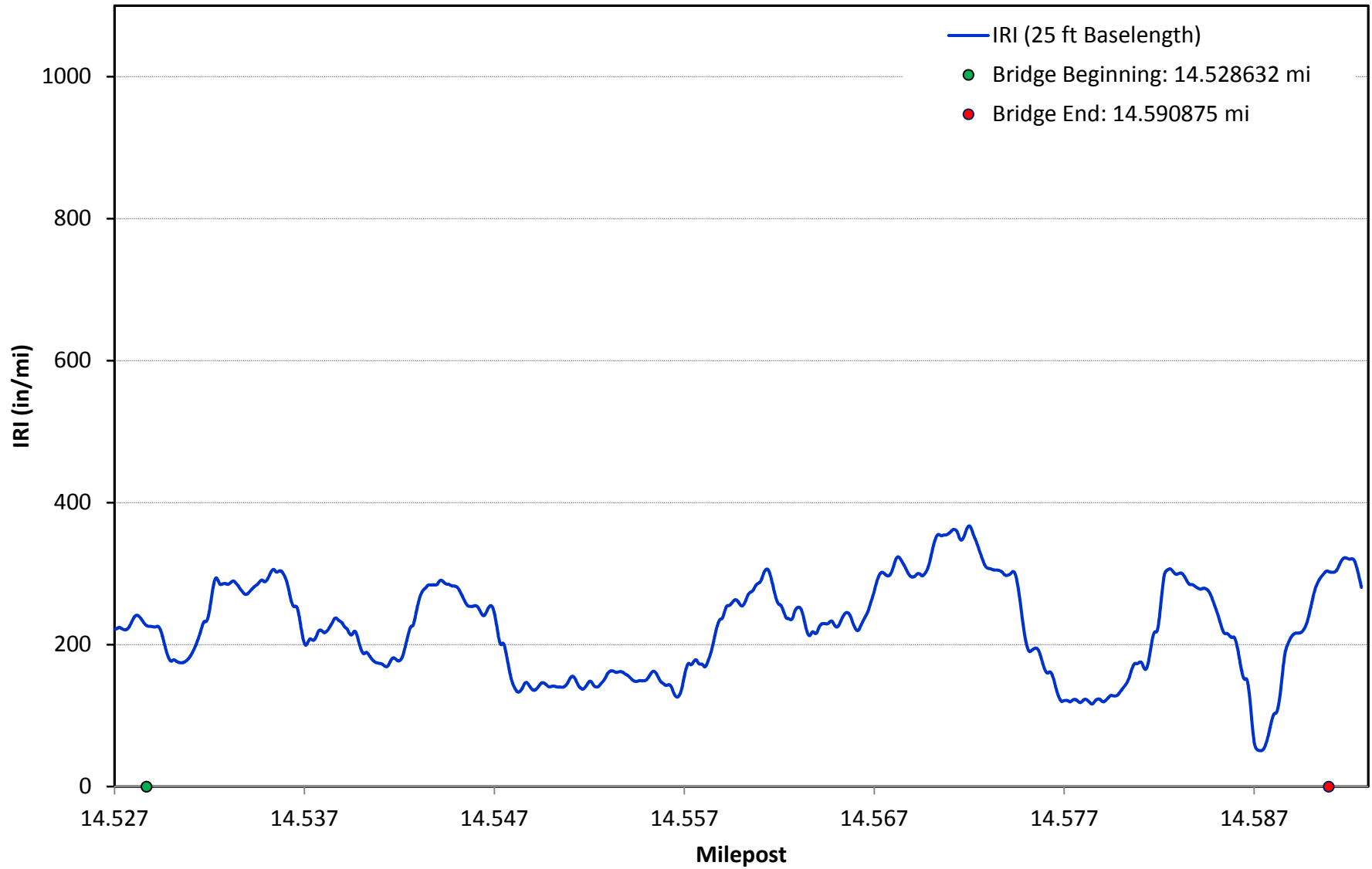
I-10 BB 450-11 WB BRIDGE 3



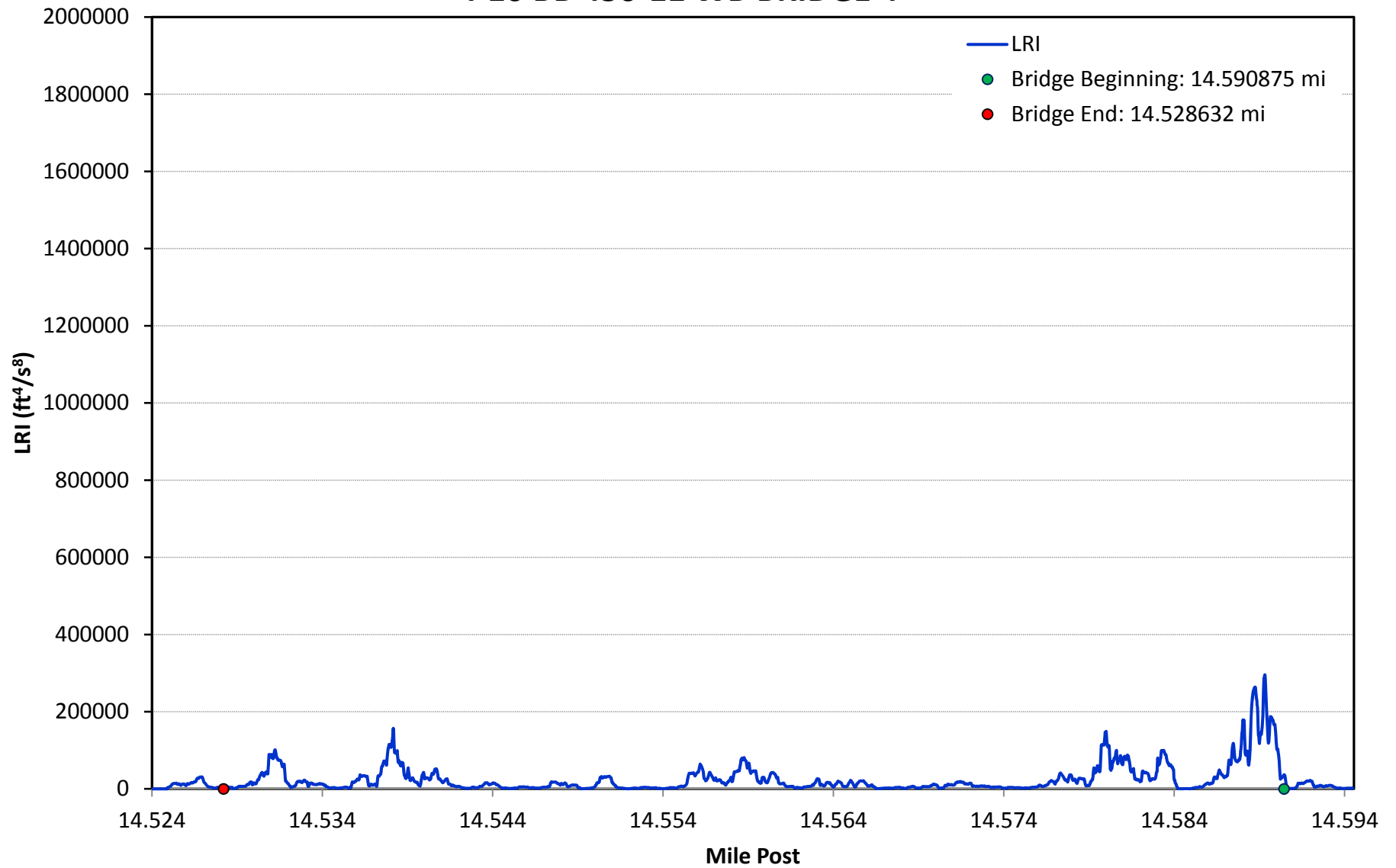
I-10 BB 450-11 WB BRIDGE 3



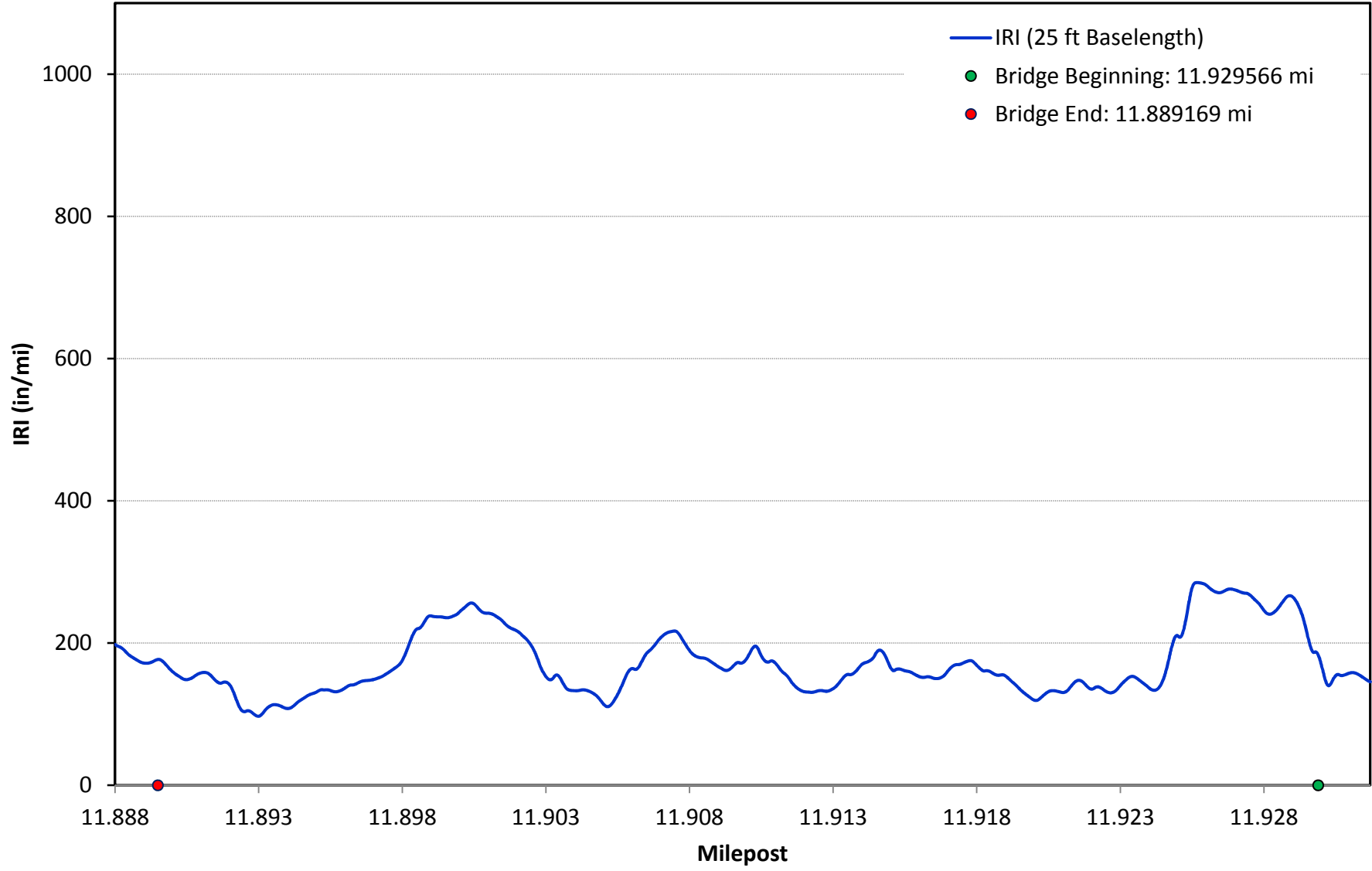
I-10 BB 450-11 WB BRIDGE 4



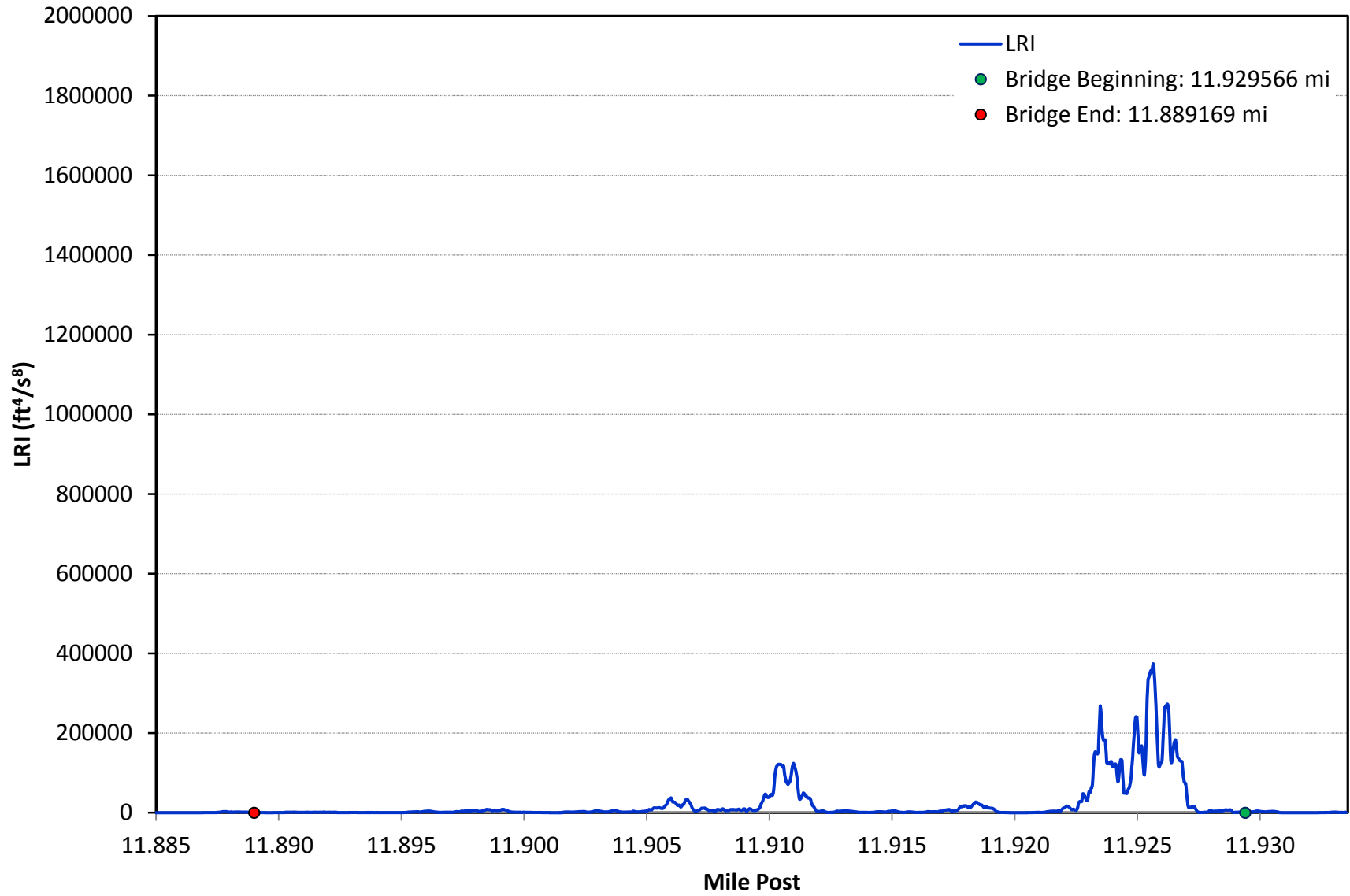
I-10 BB 450-11 WB BRIDGE 4



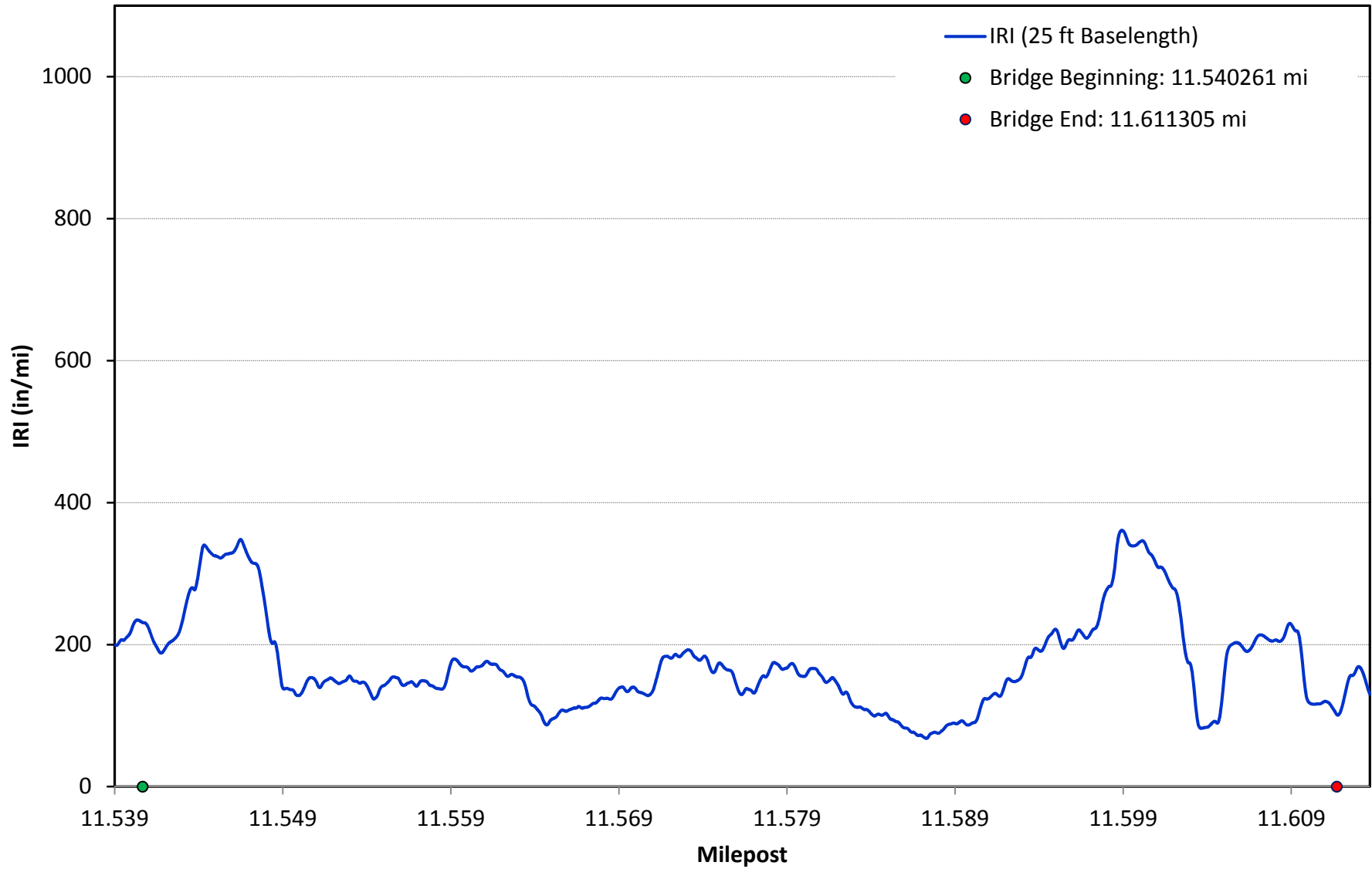
I-10 BB 450-11 WB BRIDGE 5



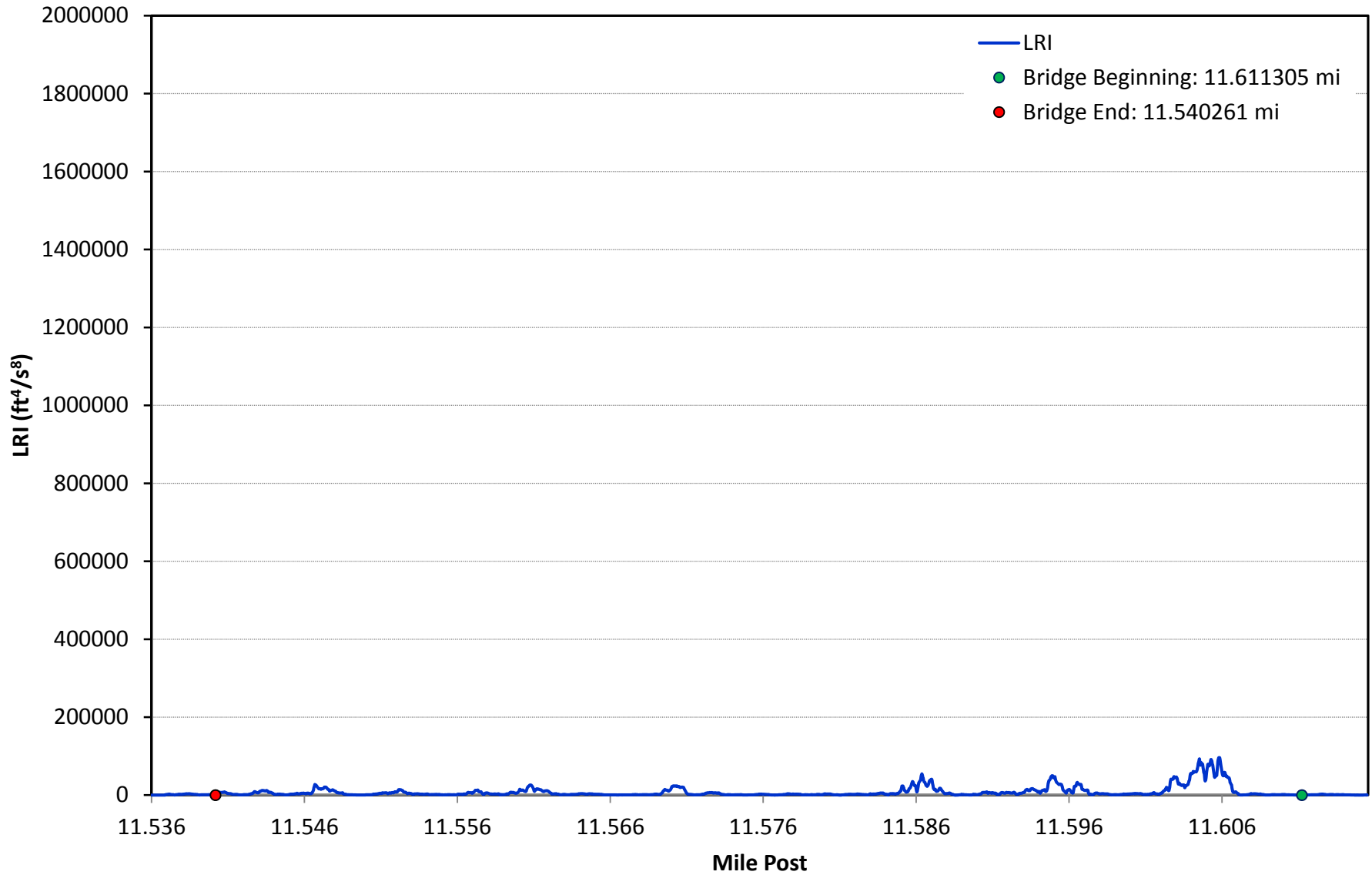
I-10 BB 450-11 WB BRIDGE 5



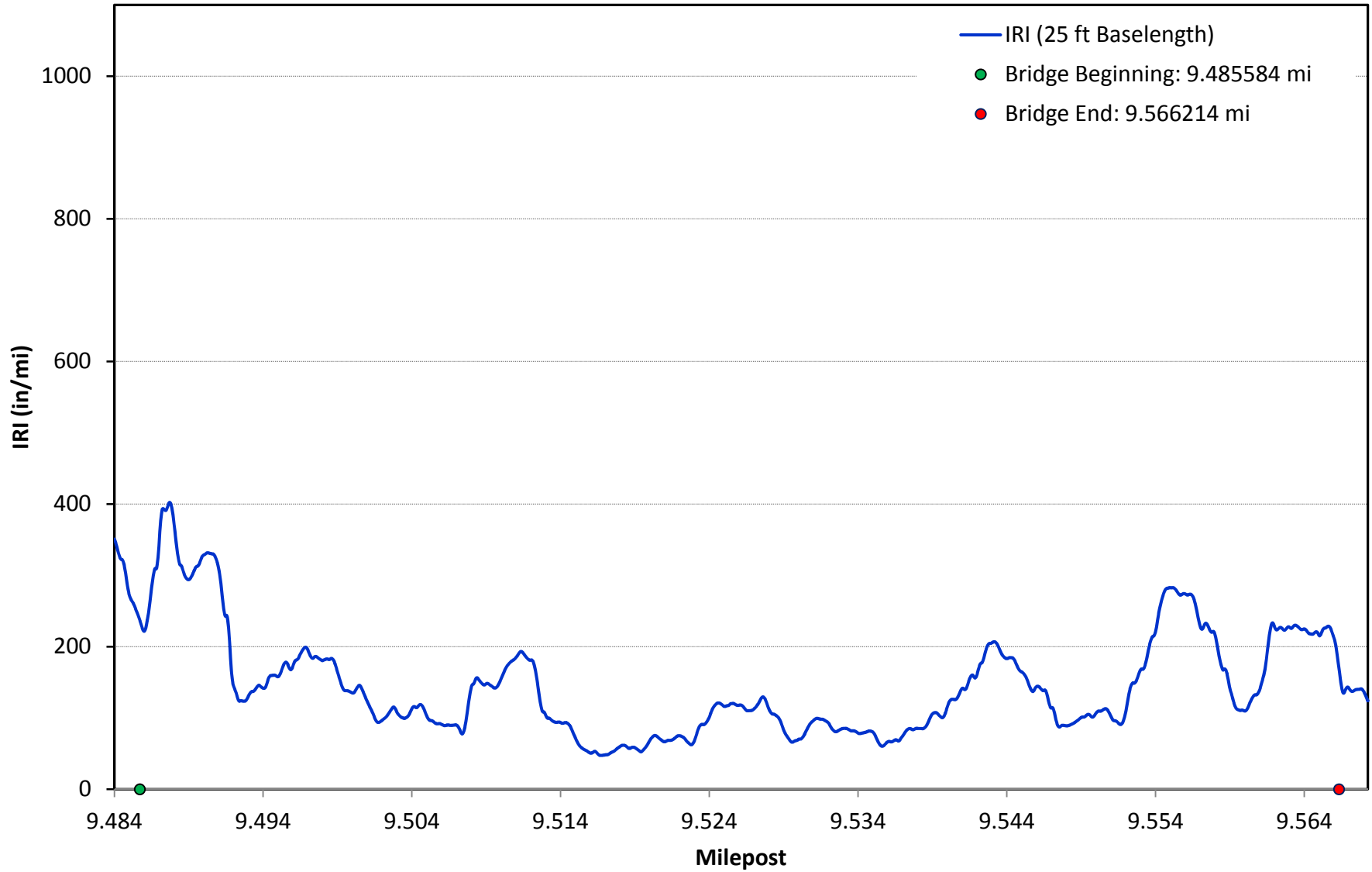
I-10 BB 450-11 WB BRIDGE 6



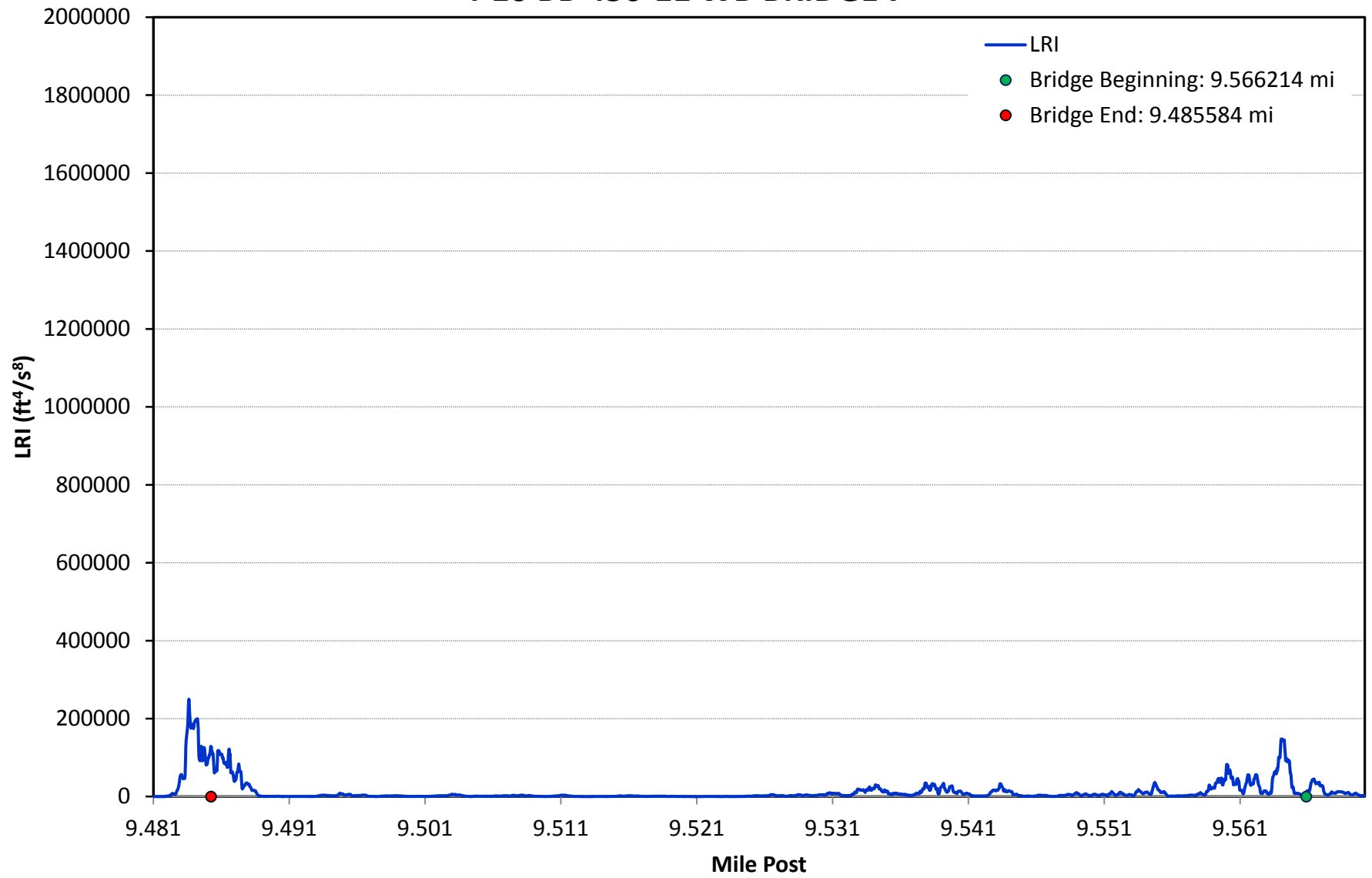
I-10 BB 450-11 WB BRIDGE 6



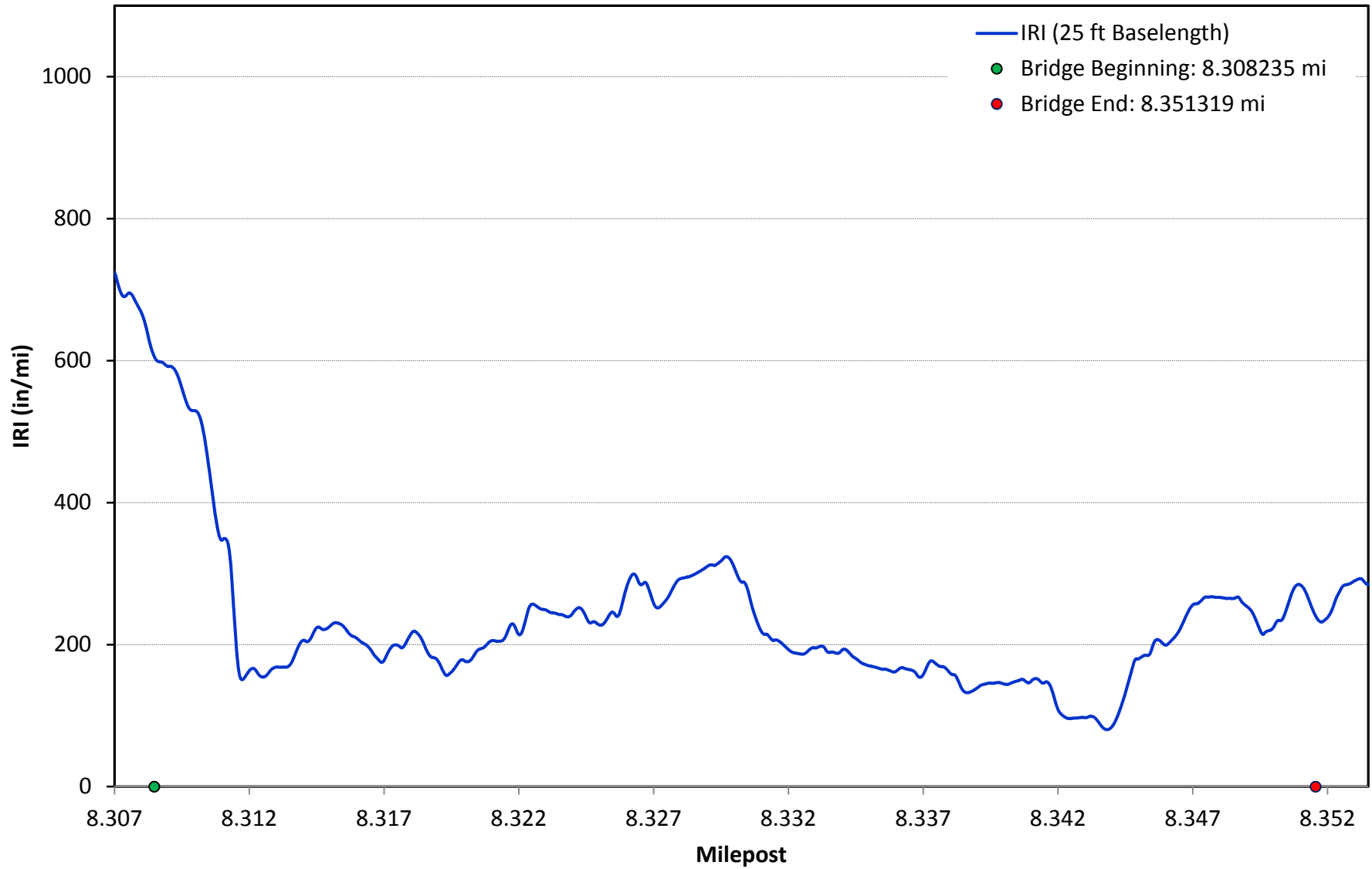
I-10 BB 450-11 WB BRIDGE 7



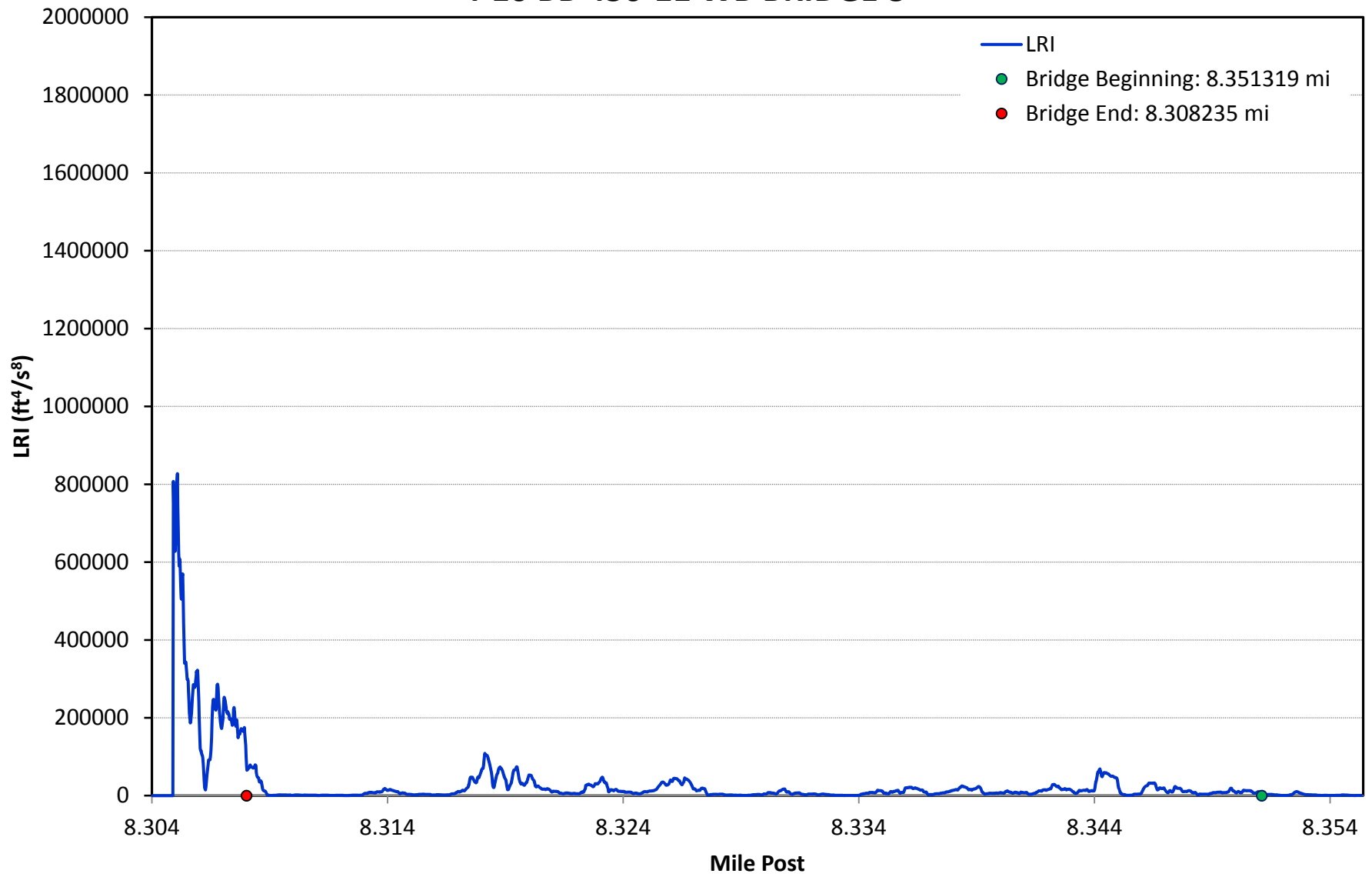
I-10 BB 450-11 WB BRIDGE 7



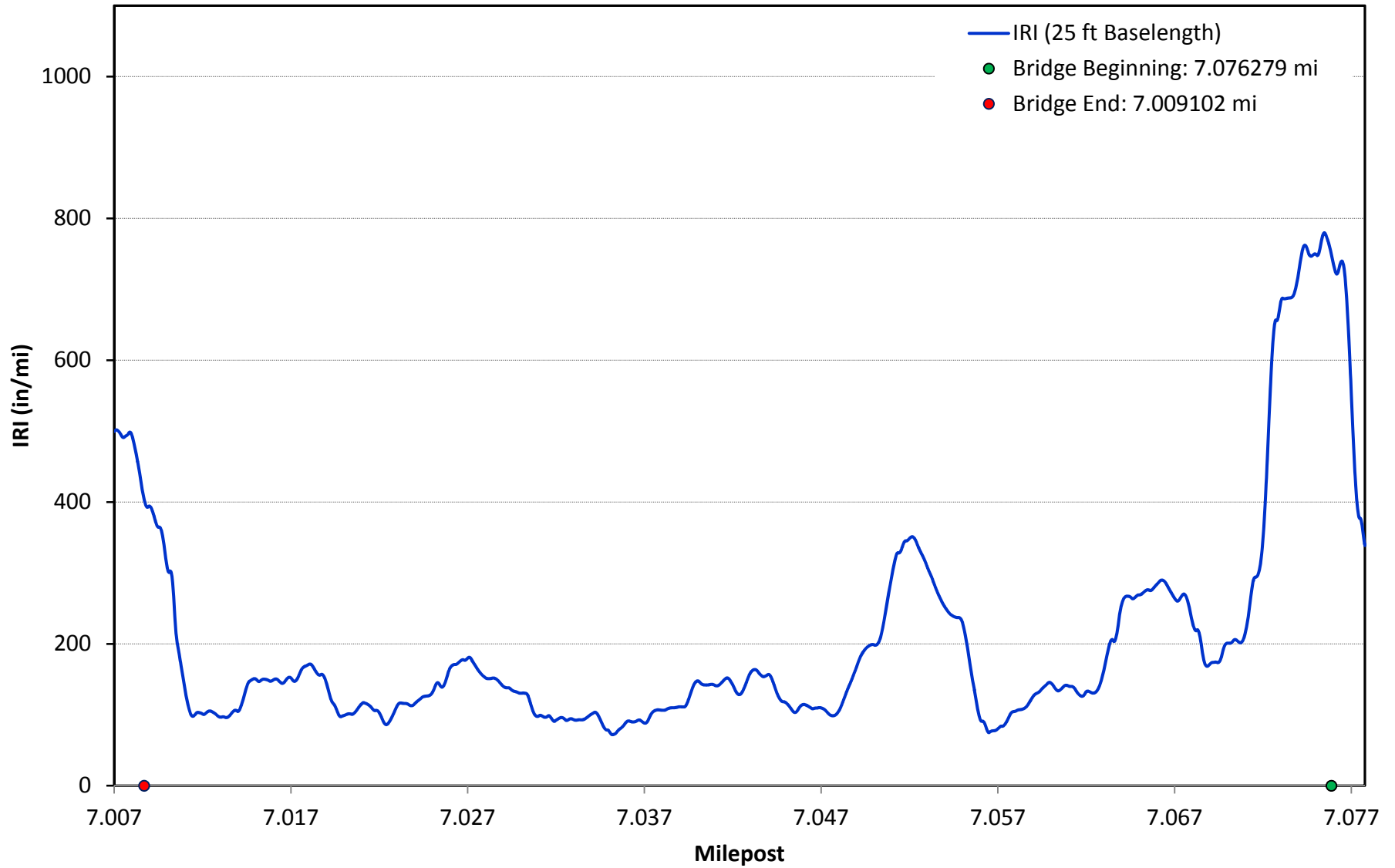
I-10 BB 450-11 WB BRIDGE 8



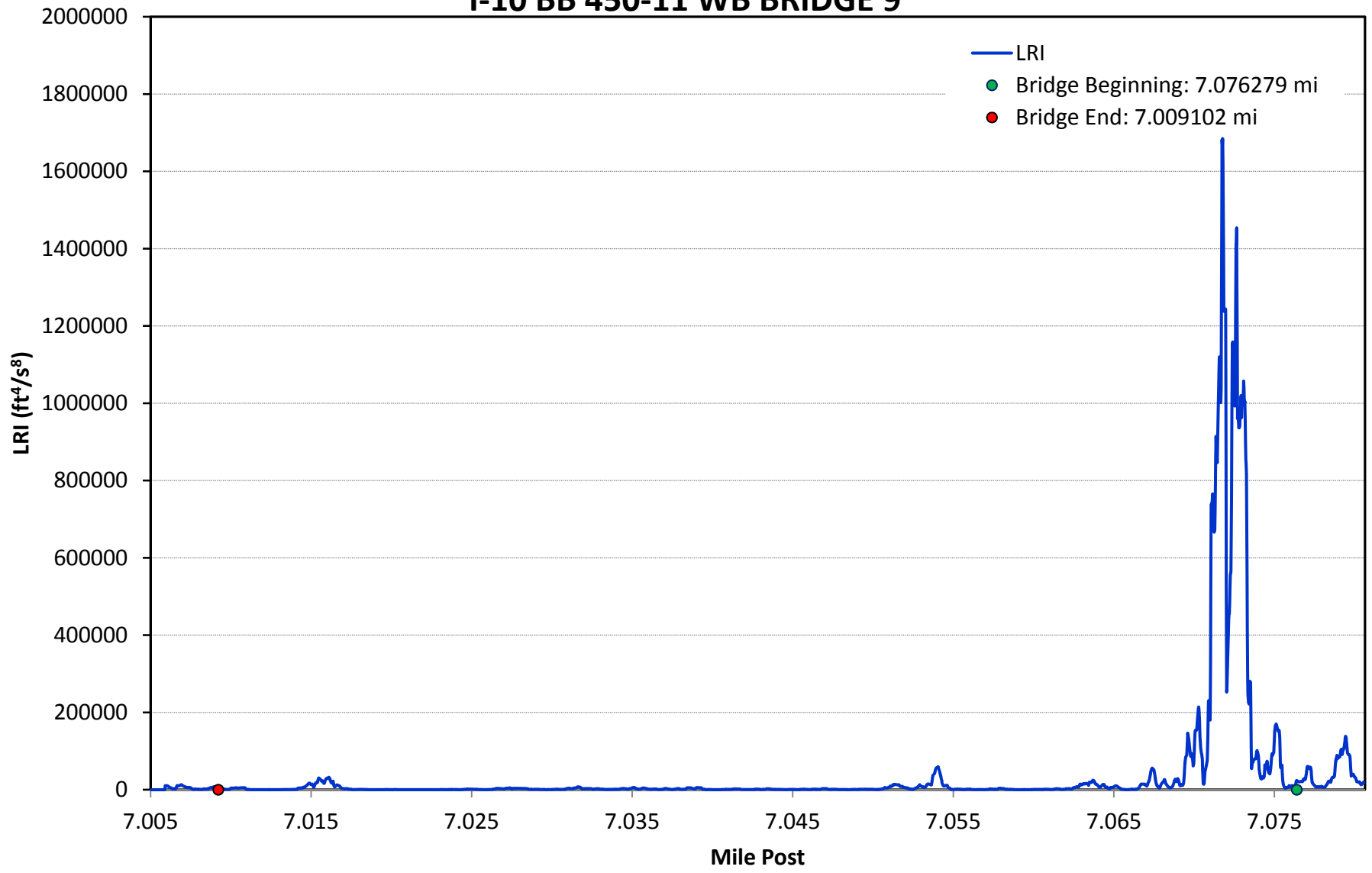
I-10 BB 450-11 WB BRIDGE 8



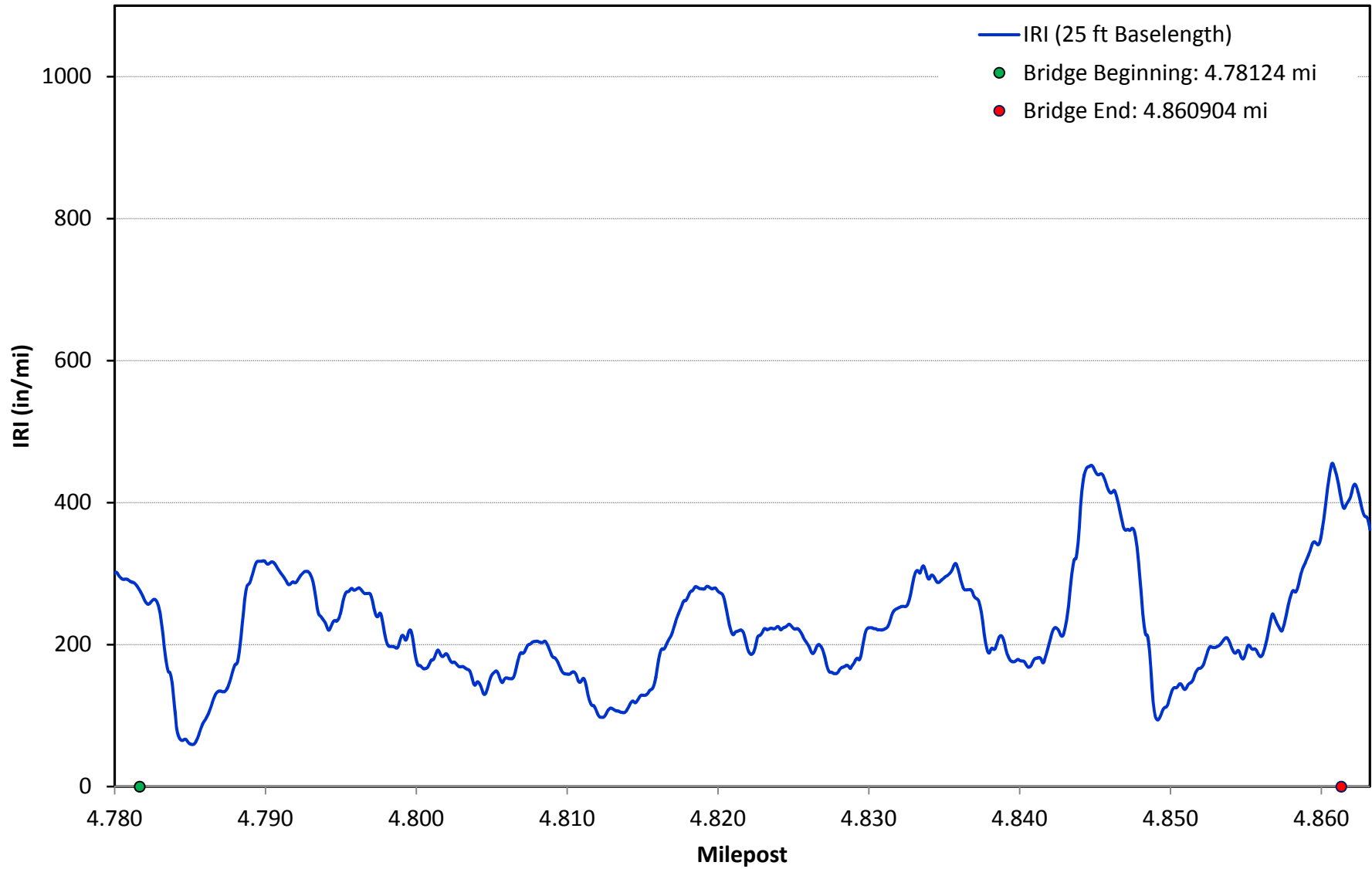
I-10 BB 450-11 WB BRIDGE 9



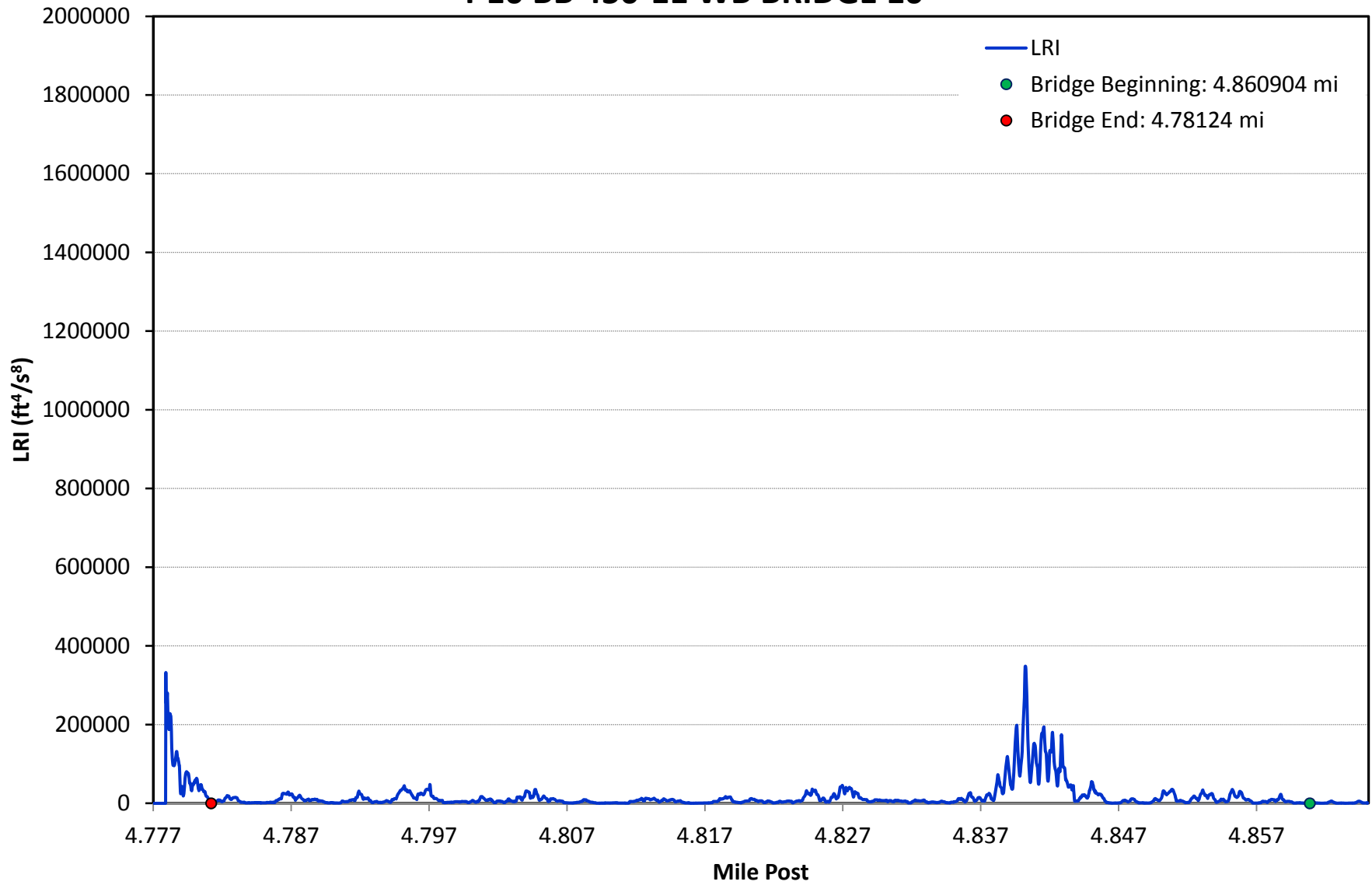
I-10 BB 450-11 WB BRIDGE 9



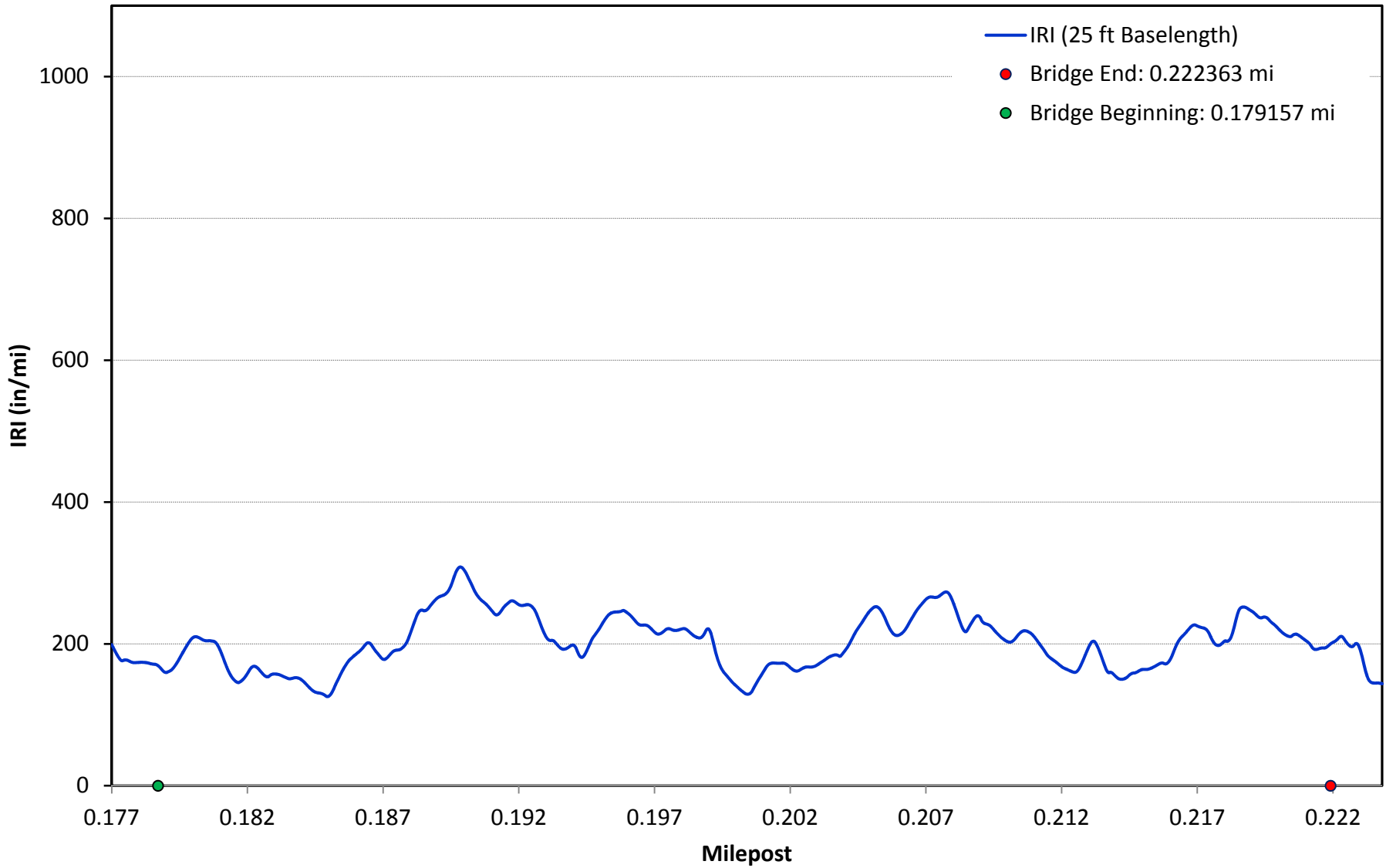
I-10 BB 450-11 WB BRIDGE 10



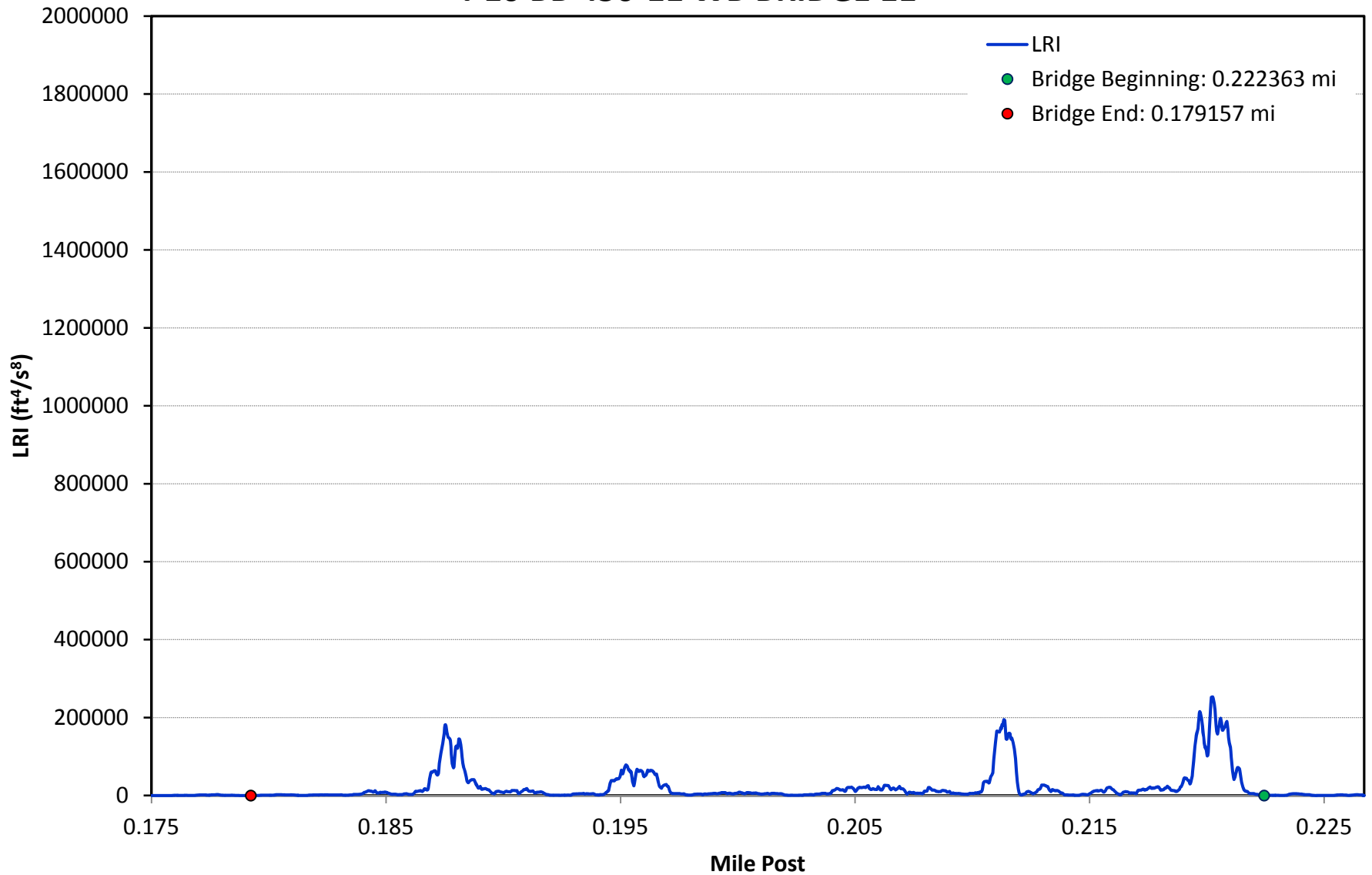
I-10 BB 450-11 WB BRIDGE 10



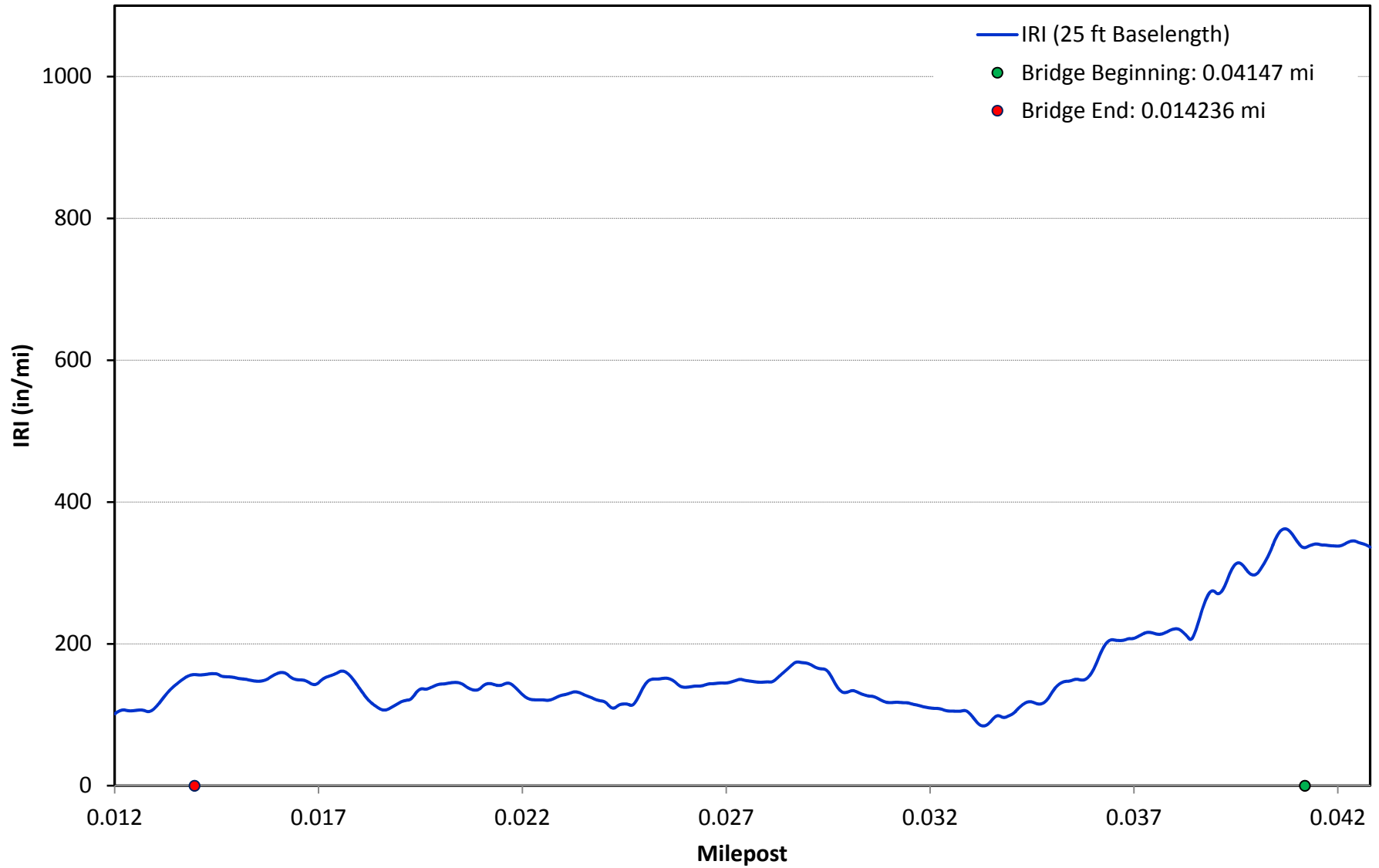
I-10 BB 450-11 WB BRIDGE 11



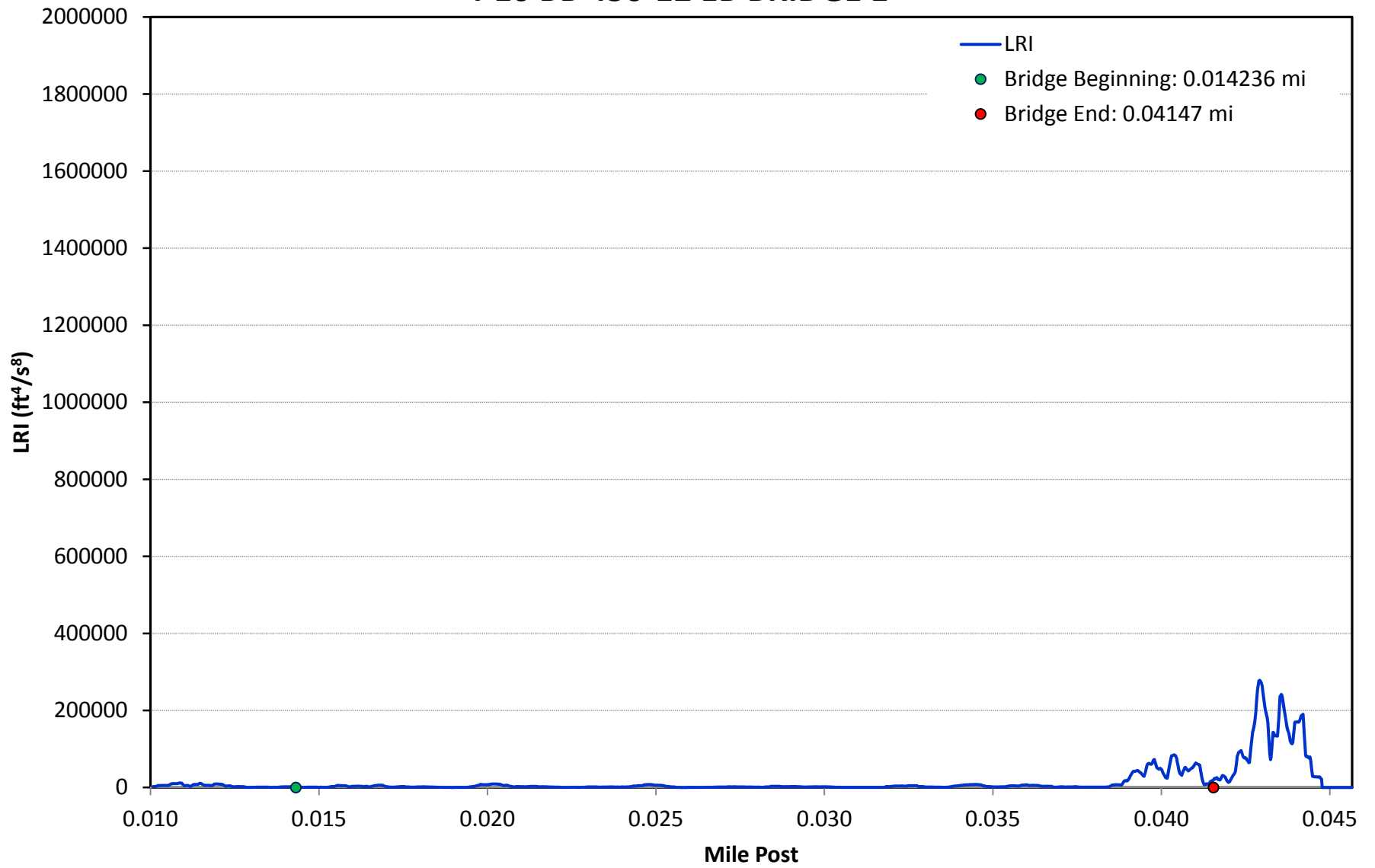
I-10 BB 450-11 WB BRIDGE 11



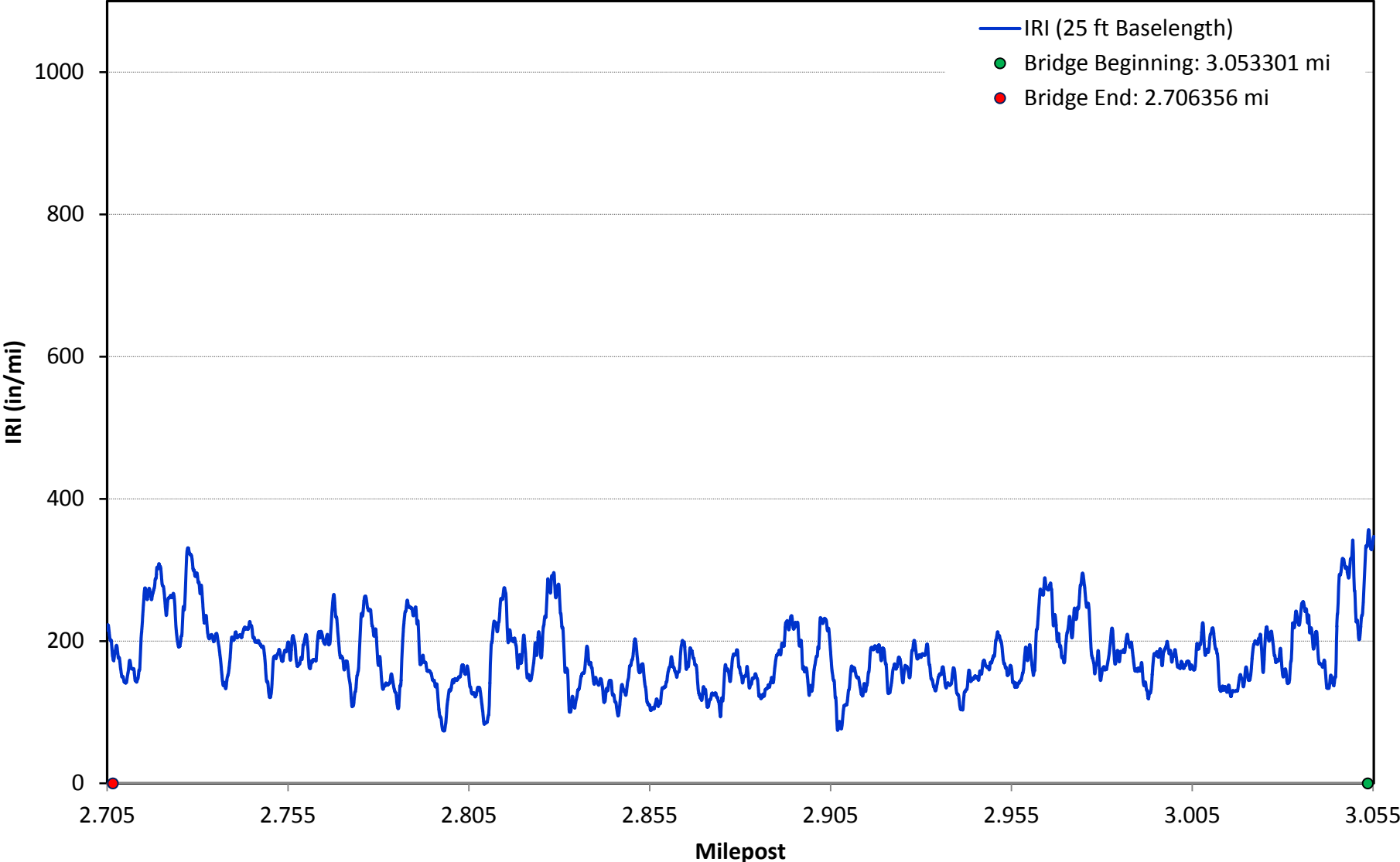
I-10 BB 450-12 EB BRIDGE 1



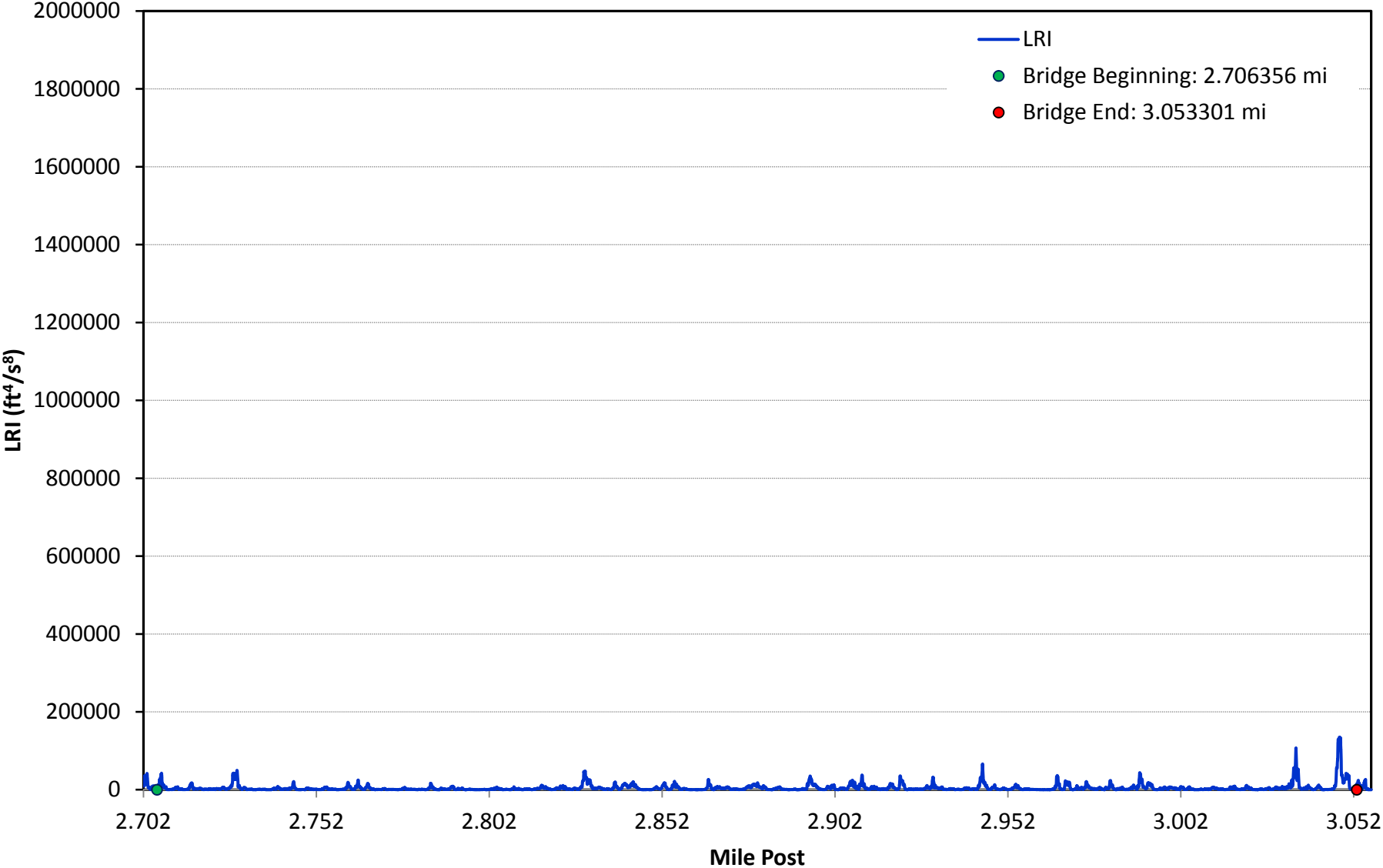
I-10 BB 450-12 EB BRIDGE 1



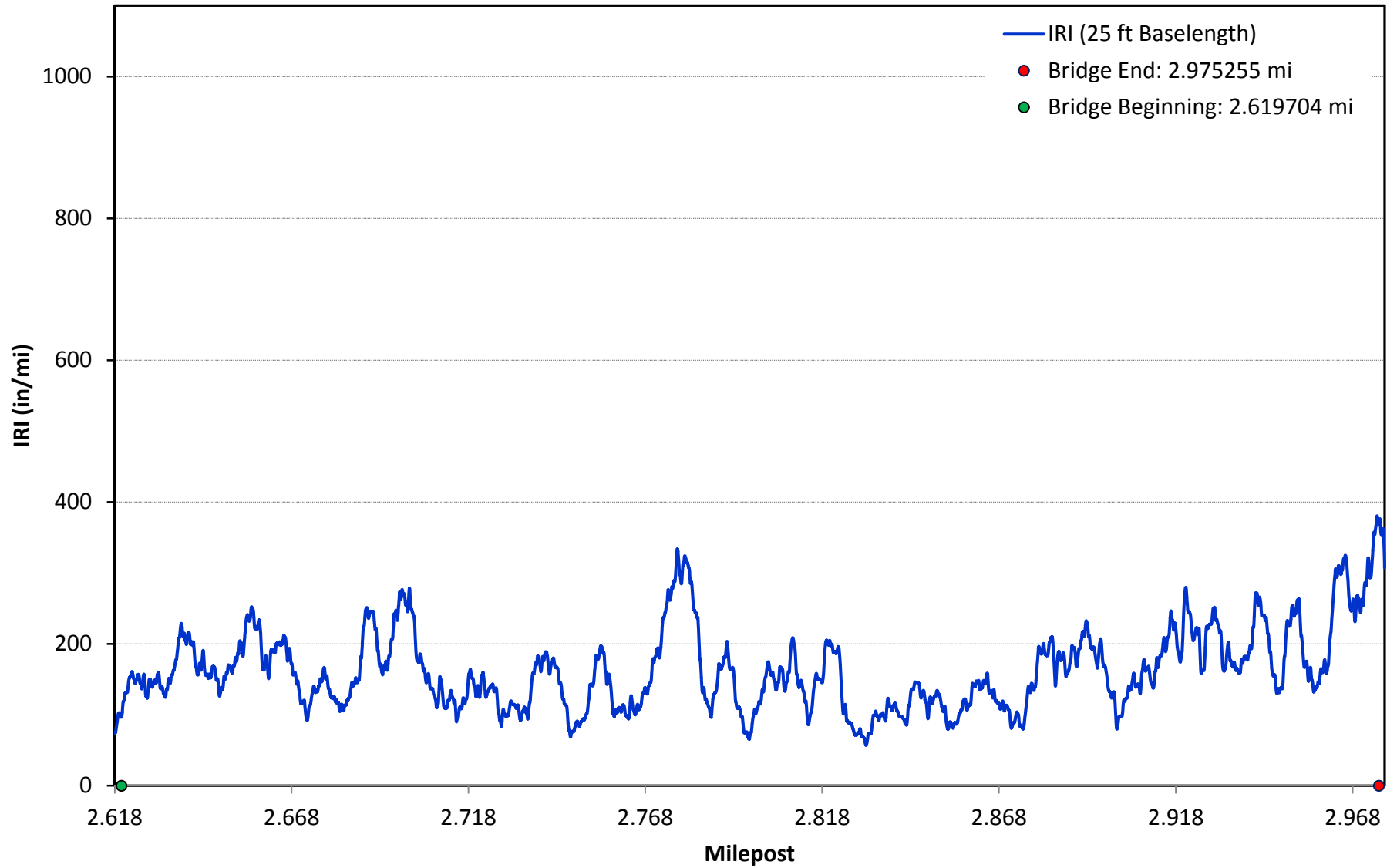
I-10 BB 450-12 EB BRIDGE 2



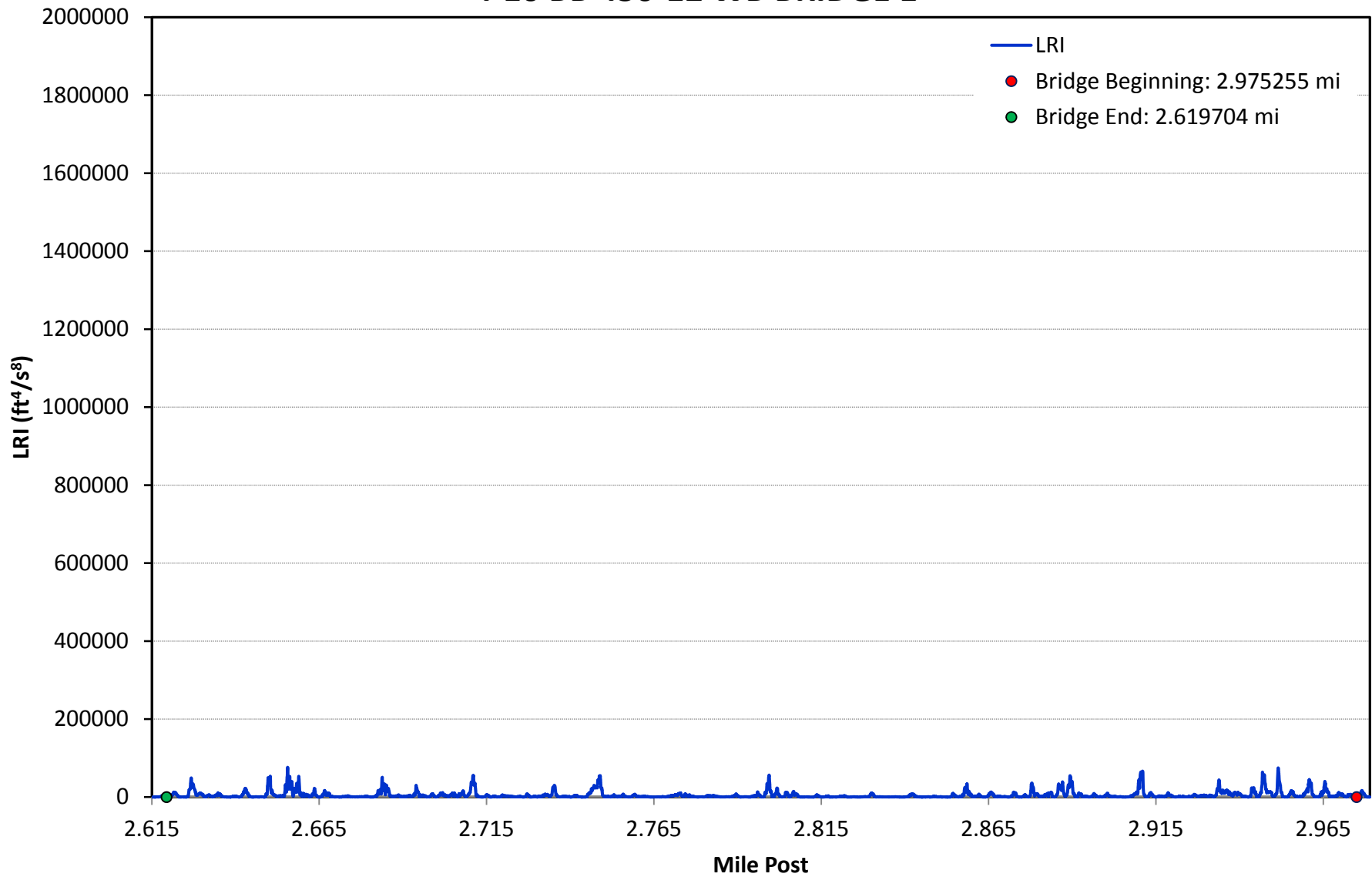
I-10 BB 450-12 EB BRIDGE 2



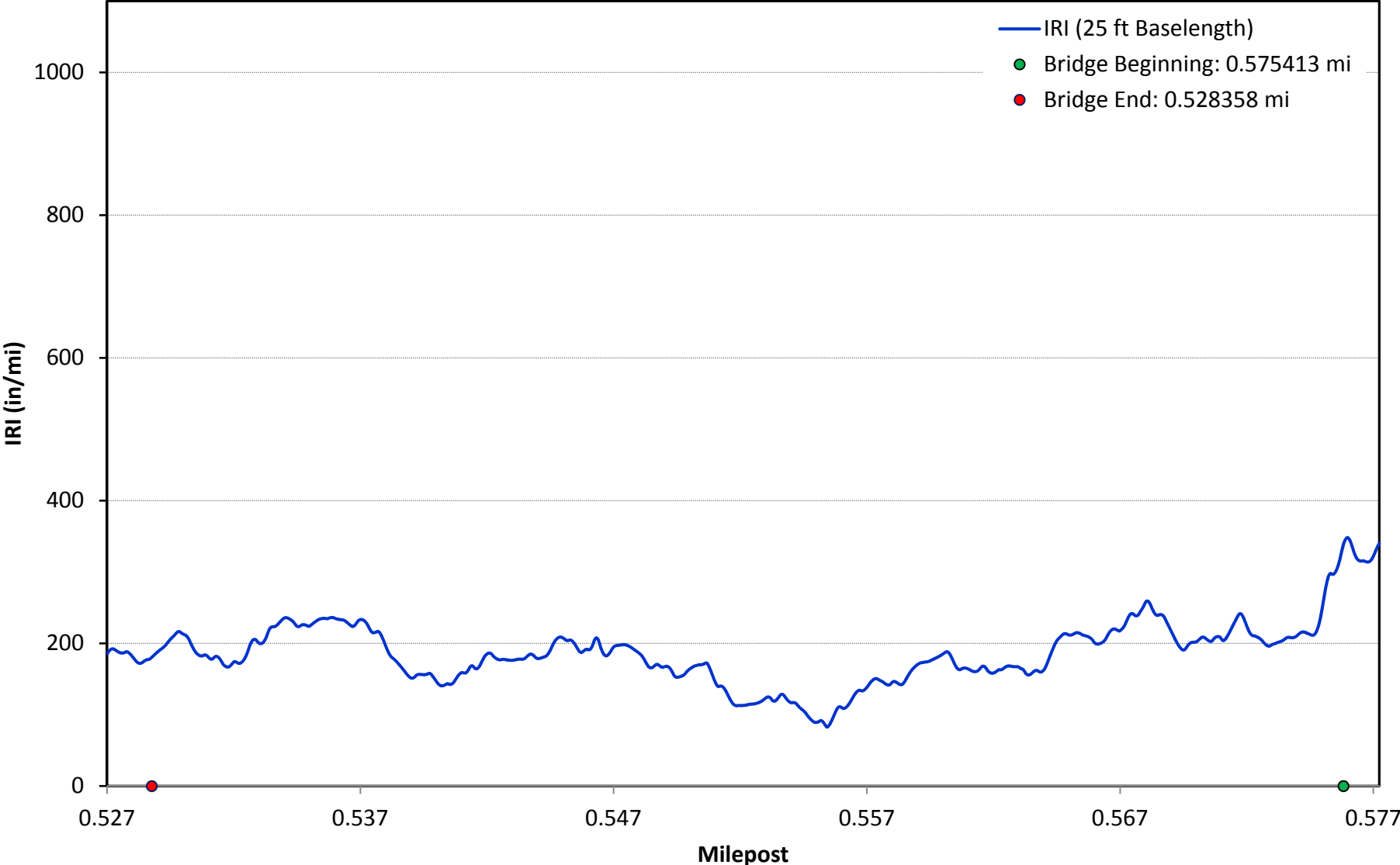
I-10 BB 450-12 WB BRIDGE 1



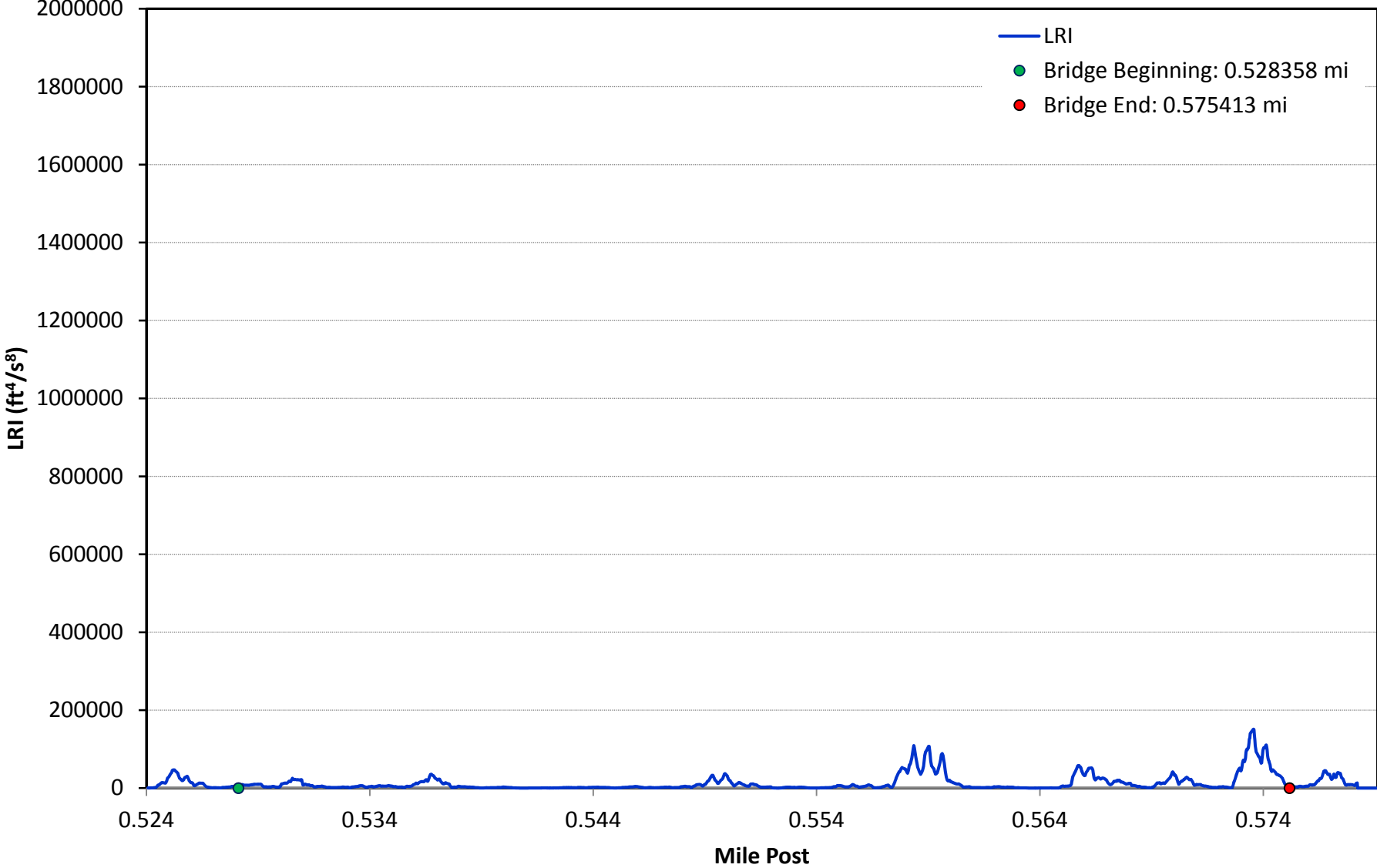
I-10 BB 450-12 WB BRIDGE 1



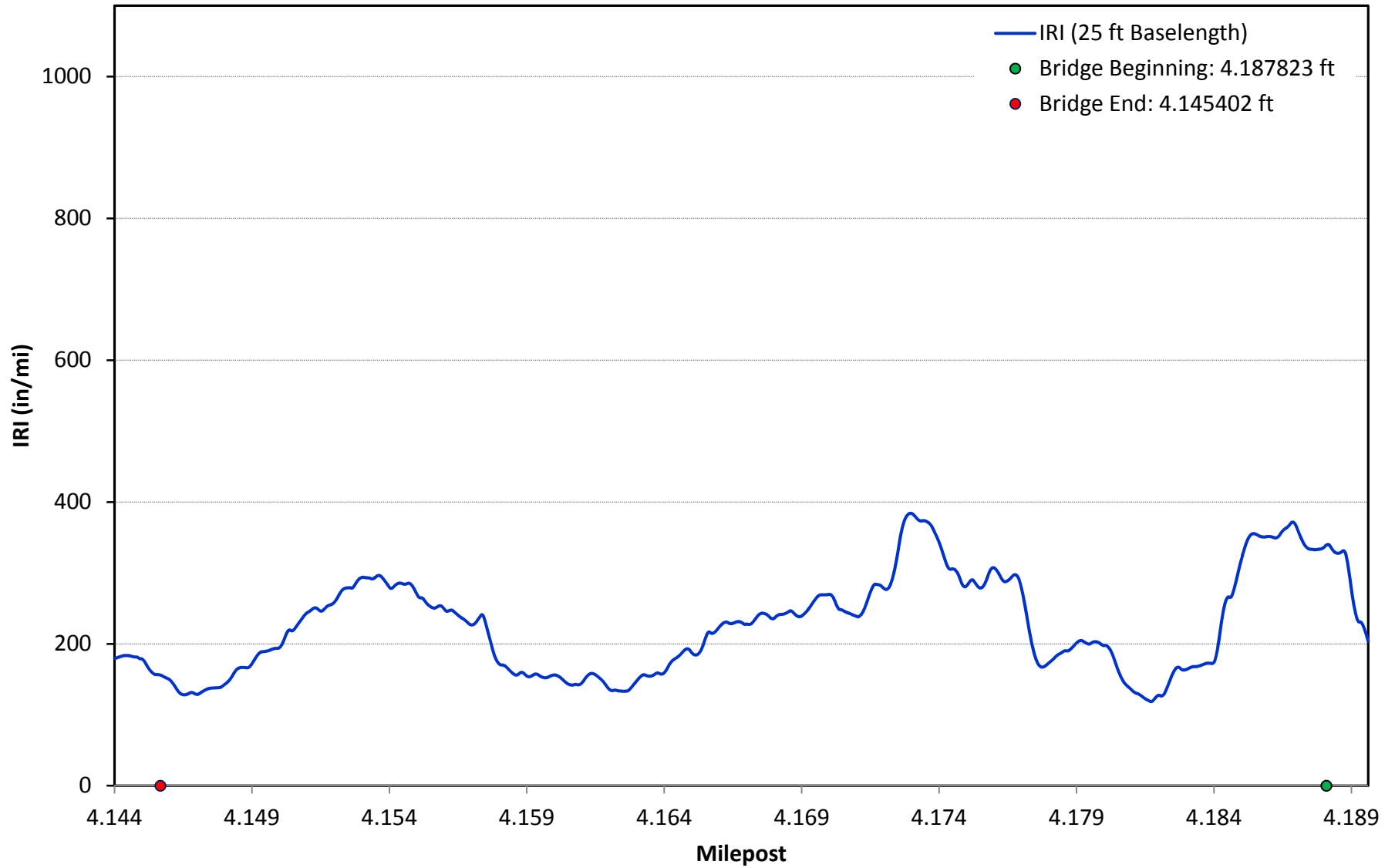
I-10 BB 450-13 EB BRIDGE 1



I-10 BB 450-13 EB BRIDGE 1



I-10 BB 450-13 EB BRIDGE 2



I-10 BB 450-13 EB BRIDGE 2

